UNIVERSITY *of* LIMERICK

OLLSCOIL LUIMNIGH

Design and Characterization of Monoacylglycerol Lipid Cubic Phase Systems for the Effective Delivery of Small Molecule Pharmaceuticals

Michele Dully B.Sc

2021

Candidate Supervisors: Prof. Tewfik Soulimane, University of Limerick
Dr Sarah Hudson, University of Limerick
Candidate Industry Mentors: John Neilan, David Murray, Jim Butler

Thesis submitted in fulfilment of the requirements for the Degree of Doctor of Philosophy at the Faculty of Science and Engineering, University of Limerick

Submitted to the University of Limerick 2021

Declaration

I declare that this thesis is entirely my own work and has not been previously submitted to this or to any other university. Where the work of others is utilised, this is acknowledged and cited in the proper manner.

Candidate: Date: 10th February 2021

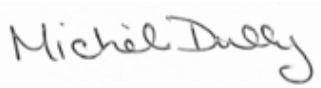

Ms. Michele Dully

Dedication

For my lovely family….

A wise father told me to
"Always remember two important things:
Never sweat the small stuff, and
It's *all* small stuff "

A wise mother always reminded me
"To accept the things I cannot change, have courage to change the things I can and the wisdom to know the difference"

A kind brother always looked out for me and brought me back down to earth when things got tough.

Your support and encouragement kept me motivated.

Acknowledgments

I would like to acknowledge and express my appreciation to all those who helped me and guided me throughout this project, with special thanks to:

My wonderful supervisors, Prof. Tewfik Soulimane and Dr Sarah Hudson, whose knowledge and constructive suggestions during the planning and development of this research proved invaluable. For the guidance and opportunities I am very grateful. Thank you for your willingness to give time and support, especially emotional support through negative results and for guiding me when I was unsure.

COOK Medical and my industry mentors, John Neilan, David Murray and Jim Butler, for offering their advice and suggestions throughout this project and for always making time to meet us. Their support and encouragement and endless ideas have greatly assisted me in the work carried out in this thesis. Getting a different perspective on my results helped me see the bigger picture of the work we carried out. And of course for all of the coffees before early meetings!!

To all of the members of the Bernal Institute, for all of the training and access to equipment. With special thanks to Wynnette Reddington for the lunchtime pep talks and Ajay Kumar for help with PXRD.

My friends, and members of our research group, Miriama, Hannah and Sally for always being there. For all of the laughs and words of wisdom during our time in UL, from cell culture to dissolution testing, you have been mentors and friends and for that I will always be grateful.

To my one-in-a-million family. My lovely parents Anne and Tom, whose unending moral support and encouragement over the course of this project has kept me motivated and enthusiastic about my work, especially when the pressure was on. Thank you mom for all of the lasagnes and spaghetti Bolognese you sent back to Limerick with me - fuel for the mind! Thank you dad for your jokes and hugs when the research was getting the better of me. Cian, my little brother, thank you for the fun and laughs – my personal thesaurus.

Finally, to my lovely David, the most patient man in Ireland. Thank you for listening to my woes and for always being there for me. For the adventures and for reminding me that there is life outside of the lab throughout my PhD.

This research was funded in part by The Irish Research Council under the Enterprise Partnership Scheme in association with Cook Medical Ireland Ltd.

Abstract

To be effective, a drug must be efficiently delivered in sufficient quantities over a period of time long enough for it to carry out its desired effect. A major challenge in this sense is poor retention and bioavailability of drugs, particularly those that display poor solubility. The number of newly discovered drugs is disproportionate to the number that make it to market because of less than desirable solubility and permeability profiles, but smart drug delivery systems, such as lipid-based systems, are capable of overcoming these challenges. One particular system, the amphiphilic, biocompatible, and biodegradable lipid cubic phase, has shown promise as an effective carrier system for the controlled release of drugs varying in solubility. This work explores the behaviour of a variety of industrially relevant small molecule pharmaceuticals in lipid cubic phases formulated with different host lipids for potential controlled delivery applications. An understanding of the molecular mechanisms underlying the process of dissolution/diffusion from these phases was elucidated to support the field of controlled drug delivery using *in silico* molecular dynamic modelling and empirical approaches. A comprehensive characterization approach was taken both macroscopically and microscopically using small-angle X-ray scattering and polarized light to ascertain the mesophase accessed upon incorporation of molecules of varying solubilities and size.

In the first instance, the influence of environmental conditions on the release profile of four antihistamine molecules was studied to establish *in vitro* models that might assist in predicting the dissolution behaviour of a given pharmaceutical with known physicochemical properties. Two model first-generation and two model second-generation H_1 antagonist antihistamine drugs were selected and formulated in two separate monoacyglycerol-derived matrices. The impact of encapsulating the molecules in the lipid cubic systems on their mucoadhesive properties was demonstrated using multi-parametric surface plasmon resonance (MP-SPR). With a potential application in developing therapies for the treatment of allergic reactions, the ability of the formulations to inhibit mediator release utilizing RBL-2H3 mast cells with the propensity to release histamine upon induction was presented.

Lipid cubic formulations can enhance the intestinal solubility and subsequent bioavailability of notoriously hydrophobic drug entities by reducing drug precipitation and facilitating mass

transport to the intestinal surface for absorption. In this context, the aims of the second study were twofold: to evaluate an approach to regulate the rate of degradation of lipid cubic phase drug delivery systems by targeting the enzyme interactions responsible for their demise; and to study the subsequent drug release profiles from bulk lipid cubic gels using model drugs of contrasting hydrophobicity. In a novel approach, monoacylglycerol cubic phases were formulated with a potent lipase inhibitor tetrahydrolipstatin displaying controlled degradation with at least a 4-fold longer release compared to the blank systems. Sustained release of a model hydrophobic pharmaceutical (a clofazimine salt) was studied over 30 days to highlight the advantage of incorporating an inhibitor into the cubic network to achieve tunable lipid release systems.

The final aspect of this thesis deals with the interplay between the lipolysis rate and the interfacial interaction of porcine pancreatic lipase with lipid cubic substrates encapsulating the THL. In the final chapter, inhibitor-modified monoolein lipid cubic formulations designed to encapsulate and control the release of a model BCS class IV drug paclitaxel (PTX) were examined under simulated lipolysis in the presence of lipase and its cofactors colipase and calcium. We present a combination of thermodynamic and molecular dynamics simulations of the competitive inhibition with experimental dynamic digestion studies to reveal the role and mode of action of the studied lipase effectors in designing a degradation-controlled release system for the poorly soluble drug PTX. These studies facilitated a deeper understanding of the approach described in the previous chapter, expanding the study to open new important possibilities in the field of pharmaceutical transport especially where difficult-to-formulate drugs are concerned.

Key words

Liquid crystals, lipid cubic phase, cubosomes, lipolysis, controlled delivery, poorly soluble drugs

Contributions

JOURNAL CONTRIBUTIONS

i. Dully, M., Brasnett, C., Djeghader, A., Seddon, A., Neilan, J., Murray, D., Butler, J., Soulimane, T. and Hudson, S.P., 2020. Modulating the release of pharmaceuticals from lipid cubic phases using a lipase inhibitor. *Journal of Colloid and Interface Science*.
ii. Dully, M., Ceresnakova, M., Soulimane, T. and Hudson, S.P. A Lipid Cubic System for prolonged delivery of antihistamine drugs. *Under review*
iii. Dully, M., Bhattacharya, S., Verma, V., Murray, D., Thompson, D., Soulimane, T. and Hudson, S.P. Probing the mechanism behind inhibitor-controlled degradation of lipid cubic formulations. *In progress*
iv. Ceresnakova, M., Dully, M., Soulimane, T. and Hudson, S.P. Stent conditioned media for in vitro evaluation of hydrophobic stent coatings. *In progress*
v. Ryan, S. M., Dully, M., Soulimane, T. and Hudson, S.P. *In progress*

AWARDS

i. Outside front cover artwork for Journal of Colloid and Interface Science Volume 574 August 2020 (Appendix D)
ii. BOC gases bursary for outstanding researcher recipient 2019
iii. Published Case study "Modulating API release with a tuneable lipid carrier" for Diamond Light Source, Didcot, United Kingdom (Appendix E)
iv. Bernal Research Day Illustration award 1st place
v. YESBernal Writing competition First place for article titled "Teaching reimagined – An Educational Revolution", available at: https://bernalinstitute.com/2020/07/23/teaching-reimagined-an-educational-revolution/

WORKSHOPS & CONFERENCES

i. Dissolution workshop at the School of Pharmacy and Pharmaceutical Sciences, TCD
ii. Poster presentation at COST Imaging School at the Hamburg Centre for Ultrafast Imaging, Universität Hamburg

List of Acronyms and Abbreviations

ACRONYM/ABBREVIATION	FULL NAME
ACN	Acetonitrile
API	Active pharmaceutical ingredient
AZL	Azelastine hydrochloride
BCS	Biopharmaceutical classification system
$CaCl_2$	Calcium Chloride
CBX	Carbinoxamine Maleate
CCS	Cell Cycle Specific
CFZ	Clofazimine
CNS	Central nervous system
Conc	Concentration
CPP	Critical packing parameter
Cryo-TEM	Cryogenic transmission electron microscopy
CZH	Cetirizine dihydrochloride
DBS	Double-barrelled syringe
DDS	Drug delivery system
DI	Deionized
DLS	Dynamic light scattering
DMEM	Dulbeccos modified Eagle's media
DMSO	Dimethyl sulfoxide
DPH	Diphenhydramine hydrochloride
EB	Ethidium bromide
ESI-MS	Electrospray ionization mass spectroscopy
EthD-1	Ethidium homodimer-1
EtOH	Ethanol
ER	Endoplasmic reticulum
FaSSGF	Fasted state simulated gastro fluid
FBS	Fetal bovine serum
FDA	Food and Drug Administration
FFA	Free fatty acids
GRAS	Generally regarded as safe
H_{II}	Reversed hexagonal phase
HCD	Hydroxylpropyl-β-cyclodextrin
HCl	Hydrochloric acid
L_{α}	Lamellar phase
LC-MS	Liquid chromatography - mass spectroscopy
LCP	Lipid cubic phase
LLC	Lyotropic liquid crystal

ACRONYM/ABBREVIATION	FULL NAME
LN_2	Liquid nitrogen
MAG	Monoacylglycerol
MCEC	Mouse cardiac endothelial cells
MeOH	Methanol
MO	Monoolein (9.9 MAG)
MPL	Monopalmitolein (9.7 MAG)
MP-SPR	Multi-parametric surface plasmon resonance
MTT	3-(4,5-Dimethylthiazol-2-yl)-2,5-Diphenyltetrazolium Bromide
MV	Monovaccenin (11.7 MAG)
NCE	New chemical entities
NLC	Nanostructures lipid carrier
NMR	Nuclear magnetic resonance
ORL	Orlistat (Xenical)
PBS	Phosphate-buffered saline
PDI	Polydispersity index
PEG	Polyethylene glycol
PHY	Phytantriol
PTX	Paclitaxel (Taxol)
Q	Cubic
Q_{II}^{P}	Primitive (Im3m)
Q_{II}^{G}	Gyroid (Ia3d)
Q_{II}^{D}	Double Diamond (Pn3m)
rpm	Rotations per minute
SASA	Solvent accessible surface area
SAXS	Small-angle X-ray scattering
SD	Standard deviation
SIF	Simulated intestinal fluid
SLN	Solid lipid nanoparticles
SNF	Simulated nasal fluid
THL	Tetrahydrolipstatin (Orlistat)
UV	Ultra-violet
VLDL	Very low Density lipoproteins
XRD	X-ray Diffraction
ZP	Zeta potential

Nomenclature

SYMBOL	DESCRIPTION
g_{tot}	The calculated free energy of a given system
g_p	The packing frustration of a given system
g_c	The curvature of a system calculated using CPP
l_{max}	The maximum lipid chain length
v	Volume
$\emptyset_{aq}$	The volume fraction of the aqueous portion of a liquid crystalline phase
$\emptyset_{MAG}$	The lipid volume fraction
c_{aq}	The water weight fraction
ρ_{aq}	The density of water (0.997 g cm^{-3})
ρ_{MAG}	The density of the MAG host lipid (0.942 g cm^{-3}[1, 2] for monoolein and 0.982 g cm^{-3} for monopalmitolein)
A_o	A surface area constant specific to the type of bicontinuous cubic phase related to the minimal surface area
χ	The Euler characteristic constant specific to the type of bicontinuous cubic phase related to the minimal surface area
r_{aq}	The radius of the congruent aqueous channels of a liquid crystalline mesophase
a_i	The area at the interface per lipid molecule in the unit cell of a liquid crystalline mesophase
a_{cs}	The cross sectional area of a lipid head group
v_{MAG}	The lipid molecular volume of MAG lipid
MW_{MAG}	The molecular weight (g.mol^{-1}) of a MAG lipid
Å	Unit of size, Angstrom
E_{A-B}	The single point energy of a given dimer
E_A **and** E_B	The respective single point energies of isolated monomers
ps	Pico second
ns	Nano second
$\Delta E_{binding}$	The total binding energy of a ligand-receptor complex
$\Delta E_{binding,\ vacuum}$	$\Delta E_{binding,\ vacuum} = \Delta E_{MM}$ (molecular mechanics energy = electrostatic energy + vdW energy in vacuum)
$\Delta G_{solv,\ complex}$	The free energy of solvation of a given ligand-receptor complex
$\Delta G_{solv,\ ligand}$	The solvation energy of a given ligand
$\Delta G_{solv,\ protein}$	The solvation free energy of a given enzyme receptor
°C	Degrees Celsius, a measure of temperature

SYMBOL	DESCRIPTION
ΔG_{polar}	The polar solvation free energy or electrostatic component of solvation free energy
$\Delta G_{nonpolar}$	The nonpolar solvation free energy approximated by the solvent accessible surface area (SASA) times a constant factor
W_0	The initial gel weight before immersion in media
W_1	The weight of the submerged gel at a measured time point
wt%	The weight of a component of a system as a % of the total weight of the system
Λ_{max}	Maximum absorption wavelength
cP	Measure of viscosity
px	Pixel
kV	Kilo Volts
VdW	Van der Waals force

Table of Contents

Declaration ***2***

Dedication ***3***

Acknowledgments ***4***

Abstract ***6***

Key words ***7***

Contributions ***8***

JOURNAL CONTRIBUTIONS **8**

AWARDS **8**

WORKSHOPS & CONFERENCES **8**

List of Acronyms and Abbreviations ***9***

Nomenclature ***11***

Chapter I: Introduction & Scientific Background ***17***

1.1 Introduction to Drug delivery strategies **17**

1.2 Lipid based drug delivery systems **23**

1.3 Self-assembled Lipid Liquid Crystalline Phases **29**

1.4 The Cubic Phase: Structure and properties **33**

1.5 LCP for Drug delivery **39**

Lipid nanosystems in solution 45

1.6 Lipid Digestion and its role in drug absorption **47**

Digestion of MAGs by biological enzymes 47

Improving oral bioavailability of lipophilic drugs 49

1.7 Concluding Remarks and Identified Research objectives **51**

1.8 Thesis outline **53**

Chapter II: Lipid Cubic System for the controlled delivery of pharmaceuticals of varied solubility. A Case Study: Antihistamine delivery ***54***

2.1 Introduction **54**

2.2 Background **54**

2.3 Materials and Methods **60**

2.3.1 Materials 60

2.3.2 Preparation of bulk Antihistamine-LCP matrix formulations 60

2.3.3 Preparation of cubic dispersions (cubosomes) 61

2.3.4 Mesophase characterization 61

SAXS data collection 61

SAXS data processing and analysis 62

Lipid cubic phase structural dimensions calculations 62

Mucoadhesion studies 64

2.3.5 Particle size estimation and zeta-potential studies [348] 65
2.3.6 Drug release studies 65
PXRD 65
Encapsulation efficacy 66
2.3.7 Cell culture methods 68
2.3.8 Cell viability study: Cytotoxicity 68
2.3.9 Cellular uptake of cubosomal formulations 69
2.3.10 Anti immunoglobulin E- (IgE-) induced histamine release studies 69

2.4 Results and Discussion 70
2.4.1 Mesophase characterization 70
2.4.2 Properties of Cubic dispersions: Zetasizer Studies, encapsulation efficacies 74
2.4.3 Cellular uptake of cubosomes [375] 76
2.4.4 Cytotoxicity study 78
2.4.5 Mucoadhesion studies 79
2.4.6 Drug release studies 83
2.4.7 RBL-2H3 inhibitory effect study 94

2.5 Conclusion and leading research questions 97

Chapter III: Modulating the Release of Pharmaceuticals from Lipid Cubic Phases using a Lipase Inhibitor 99

3.1 Introduction 99

3.2 Background 99

3.4 Materials and Methods 103
3.4.1 Materials 103
3.4.2 Preparation of MAG LCP matrix formulations 104
3.4.3 Mesophase characterization 104
3.4.4 Enzyme stock preparation 106
3.4.5 Swelling and degradation Behaviour 106
3.4.6 Drug release studies 107
3.4.7 High Performance Liquid Chromatography 108
3.4.8 UV-visible Spectroscopy 108
3.4.9 Drug release kinetics 108

3.5 Results and Discussion 109
3.5.1 Mesophase characterization 109
3.5.2 Swelling and degradation 119
3.5.3 Drug release studies 128

3.6 Conclusions and Leading Research Questions 136

Chapter IV: Probing the mechanism behind the inhibitor-controlled degradation of lipid cubic formulations 138
4.1 Introduction 138
4.2 Background 139

4.3 Materials and Methods 143
4.3.1 Materials 143
4.3.2 Mesophase characterization 143
4.3.3 Preparation of PTX-LCP matrix formulations 143
4.3.4 Mesophase characterization 144
4.3.5 PTX binding energy with lipid and lipase inhibitor using DFT calculations 146

4.3.6 In silico predictive modelling of enzyme, lipid substrate, and inhibitor interactions 146
4.3.7 Digestion Studies 149
4.3.8 Solubility study of PTX to facilitate in vitro drug release studies 150
4.3.9 Degradation controlled in vitro drug release studies 150

4.4 Results and Discussion 151
4.4.1 PTX-LCP matrix formulation and characterization 151
4.4.2 PTX binding energy with lipid and lipase inhibitor using DFT calculations 158
4.4.3 Modelling of interactions and binding affinities between the components of lipid cubic formulation *via* atomistic molecular dynamics simulations 161
4.4.4 Enzyme-driven degradation behaviour 168
4.4.5 *In vitro* drug release studies 172

4.5 Conclusions 175

Chapter V: Formulation strategies for the lipid cubic phase 177

5.1 Introduction 177

5.2 Background 177

5.3 Materials & Methods 180
5.3.1 Materials 180
5.3.2 Double-barrelled syringe method 180
5.3.3 'In situ' forming cubic phases: studying the effect of swelling buffer 181
5.3.4 SAXS for mesophase assignment 182

5.4 Results & Discussion 182
5.4.1 Double-barrelled syringe method 182
5.4.2 'In situ' forming cubic phases: studying the effect of swelling buffer 184

5.5 Conclusions 187

Chapter VI Conclusions & Future directions 189

6.1 Conclusions 189

6.2 Final words and future directions 195

References 197

Appendices 226

Appendix A 227

Appendix A 228

A.1. Calibration Curves 228

A.2. Host lipid selection 230

A.3. Cell Culture 233

A.4. Mucoadhesion Studies: MP-SPR investigation 233

A.5. PXRD of antihistamine drugs 236

A.6. SAXS patterns of antihistamine-loaded LCP 237

Appendix B 239

Appendix B *240*
Appendix C *263*
Appendix C *264*
Appendix D *272*
Appendix E *274*

Chapter I: Introduction & Scientific Background

1.1 Introduction to Drug delivery strategies

The *in vivo* effectiveness and efficiency of pharmaceuticals in the treatment of a wide range of disease states is often related to, or limited by, the administration route and the chosen dosage form for a particular therapy. To attain the desired therapeutic effect, the drug must first reach the target site of action following administration. Despite the enormous amount of new chemical entities discovered yearly with therapeutic potential, the vast majority, even with strategic formulation, are unable to localize at the target disease site (especially Class IV drugs, figure 1.1). The result is a distinct imbalance between those entities that gain regulatory approval, and those that do not because of below par efficacy and poor clinical safety data [3].

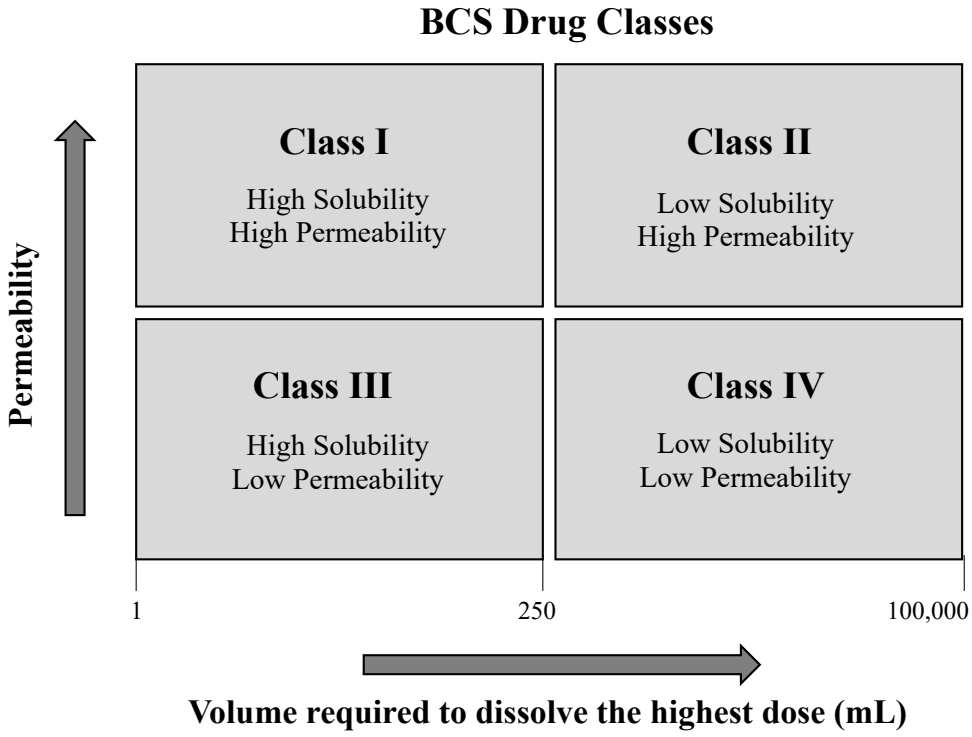

Figure 1.1. Four classes of pharmaceuticals according to the Biopharmaceutical Classification System (BCS) recreated from [4]

In overcoming this imbalance, the design of a drug delivery strategy may first look at the selection of the most suitable route of administration, a decision that is limited by the nature of the target disease site. Several routes of administration exist. In this context, the benefits and

challenges associated with each route are laid out in figure 1.2 and careful consideration should be given in assessing these aspects. For one, obtaining and maintaining optimal drug plasma concentrations after administration (through oral, intravenous, intramuscular routes) is problematic due to rapid normal body metabolism. Dilution of the administered dose to concentrations below the therapeutically effective concentration can induce drug resistance in target cells [5]. Variations in drug absorption and concentration related to individual administration routes mean that more concentrated dosages or multiple dosages over the treatment period may be required to compensate for these inconsistencies, bringing with it a plethora of other complications (including a risk of toxicity). Further, the site-specific bioavailability of drugs is also severely limited by the presence of physical barriers *in vivo* that must be passed. The extent of the restrictive barricade varies between tissues and the therapies given, which govern the suitability of potential approaches to overcome the obstacles. Such physical barriers may include tissues and/or the materials they produce (including enzymes). While those such as the skin and the blood-brain barrier present more distinct barriers to flux, others such as connective tissue surrounding a nerve or plaque deposits may be less obvious in their ability to impede the exchange of pharmaceutical material [6-8].

Parenteral Delivery (Intravenous (IV))

✓ Overcome oral delivery issues.

✗ Risk of infection and invasive.

Transdermal Delivery

✓ Non-invasive, painless, possibility of patient self-administration.

✗ Favours low MW, low dosage (mg), lipophilic drugs [9-11], drugs must be capable of crossing the impermeable barrier at low flux [12].

Vaginal Delivery

✓ Local delivery to infection site, mucosal membrane [13], convenient access, high permeation area and vascularization, relatively low enzymatic activity, avoidance of first-pass metabolism.

✗ Low retention time, mucociliary clearance.

Parenteral Delivery (Intramuscular)

✓ Reduced infection risk vs IV [14, 15], delivery of poorly soluble drugs in solvent.

✗ Pain, aqueous solubility issue when contacts body fluid.

Subcutaneous Delivery

✓ Local delivery to infection site [16], possible self-administration

✗ Localized pain, volume restrictions, tissue backpressure, leakages [17].

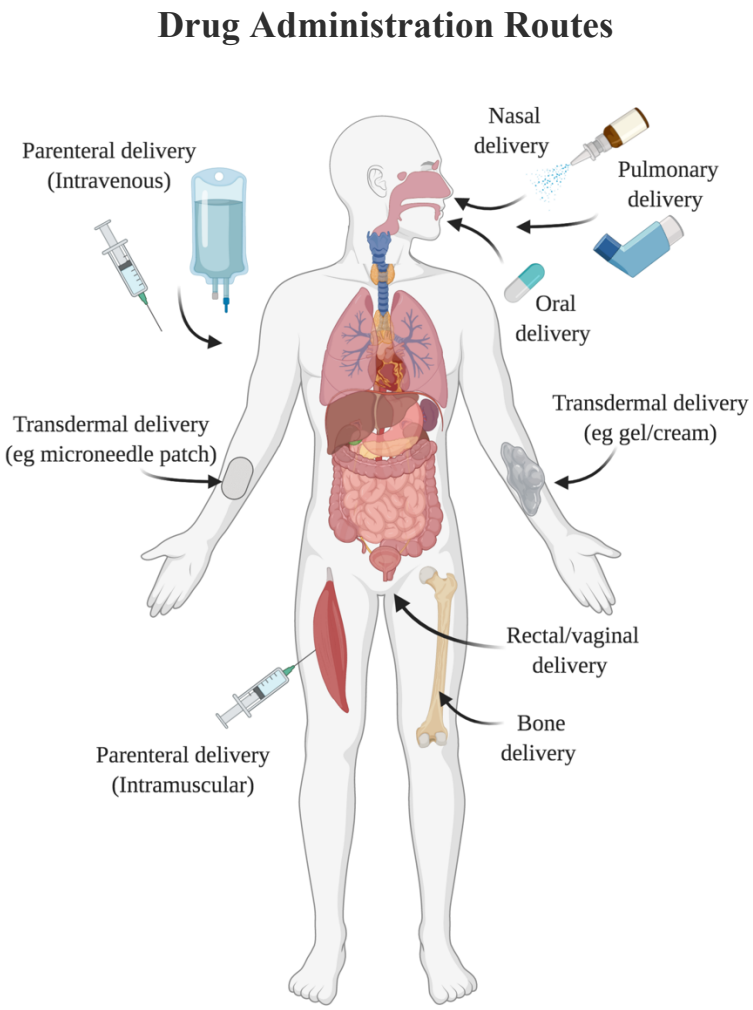

Figure 1.2 Drug administration routes and their associated benefits and challenges

Nasal Delivery

✓ Readily accessible, large surface area, porous endothelial membrane and high blood flow, access to blood brain barrier [18].

✗ Mucociliary clearance and filtration mechanisms [19, 20], low deliverable volumes (<200 µl) and molecular weight cut off (~1 kDa) [21].

Oral Delivery

✓ Economical benefits, patient compliance, flexibility and reduced sterility concerns, variations in pH for responsive delivery.

✗ pH and enzymes directly influence the behaviours of drugs within the gastrointestinal tract [12].

Pulmonary Delivery

✓ Large surface area, plentiful alveoli, thin tissue lining [22], low hydrolytic enzyme concentration [23-26].

✗ Inefficient drug delivery, requirement for frequent administration, liquid formulations include environmentally unfriendly chlorofluorocarbons [27].

Bone Delivery

✓ Local delivery, concomitant scaffold and drug delivery [28-30].

✗ Bisphosphonates colloids or calcium salt/complex precipitates of in plasma [31].

Following administration, it is necessary for the drug to reach the desired site of action in order to achieve a favourable therapeutic index, while preferably having minimal interaction with healthy tissue along the way. Localized or 'smart' targeted delivery alleviates unwanted side effects often seen in non-specific systemic and conventional delivery such as with intravenous or oral routes, and serves to maximise the drug's efficacy at the desired organ or tissue. Here, the design of tailored drug delivery systems (DDS) is an attractive approach to improve the pharmaceutical biodistribution, retention time [32], tissue uptake, pharmacokinetics and therapeutic index of existing drug entities [33-36] and conventional free dosage forms [37]. Further, many DDS have the added advantages of impeding early metabolism and elimination of the drug by shielding it from digestive enzymes and *in vivo* environments and also lend themselves to the possibility of associating the drug moieties with a specific intracellular component.

For the numerous routes of administration that exist, matching the drug formulation strategy with the preferred route of administration must be considered. Here, 'formulation' applies not only to the inputs and processes of the drug manufacturing process, but also the final form of the dosage product, which is ultimately what a patient receives. This encapsulates all dosage forms and DDS; from tablets to capsules, ointments and liquids, reservoir and matrix type systems, sustained release drug delivery systems to emulsions, solid dispersions, drug conjugates and organic, inorganic and metal organic frameworks among countless others [38, 39]. Currently, the vast majority of research in this field is directed towards polymeric systems, ceramics, plastics, and inorganic materials. In that context, drug molecules can be incorporated into a DDS by simple mixing approaches, chemically through covalent attachment, or through encapsulation of the drug in the final formulation. Depending on the ultimate aim and desired site of action, countless materials for DDS exist, and the selection of the most suitable in terms of chemical characteristics, geometry and release properties as well as biocompatibility and immunogenicity is an important stage in the design process [40, 41]. These will be looked at these in more detail to highlight the relationship between the design of a drug delivery strategy and the challenging properties of (i) the drug molecule (either chemical or physical properties), (ii) the target site in the body and (iii) the preferred route of administration.

Polymeric systems (including biodegradable and nondegradable polymers) are non-corrosive and can demonstrate density values close to those of natural tissue such as collagen and hyaluronic

acid making them attractive materials in drug delivery applications [42]. The benefits of these systems are related to the properties of the materials selected which could be of natural origin (chitosan, dextran [43], etc.) or synthetic (block co-polymers, etc.). Commonly used synthetic polymers include polymethylmethacrylate, polyvinyl alcohol, polylactides, polyanhydrides among many others [42] and are easily fabricated into many forms. Polymeric nanoparticles such as PLGA nanoparticle systems have been studied for the delivery of drugs in managing infection [44]. These systems offer a number of advantages in: overcoming the biological barriers and transport drugs at high local concentrations [45, 46] within a desirable time [47, 48]; enhancing pharmacological activity and overcoming issues of solubility and toxicity, for example with plant bioactive compounds in curcuminoids [49, 50]. Although synthetic polymer systems constitute a large range of DDS, the requirement for essential fabrication additives such as anti-discolouring agents, plasticizers and antioxidants in many cases pose a toxic risk if additive leaching was to occur [42]. Further, the low modulus of elasticity and viscoelastic characteristics of these polymer make them unsuitable for load bearing applications. Not only that, but the acidic nature of the degradative products of certain polymers such as poly(glyco1ic acid) (PGA) and poly(L-lactic acid) (PLA) can induce unwanted side effects *in vivo* [51]. Certain polymers such as polylactides and glycolides are highly susceptible to harsh environmental conditions such as low pH, high temperature and radiation which can dramatically alter the mode of degradation and action potentially ruling them out for certain applications [52].

Other polymeric DDS, including naturally occurring polymers, can be designed such that physicochemical modifications of the formulation can provide stimuli-responsive systems [53-58], garnering tighter control of the release kinetics under certain conditions of pH [59], hydration or temperature [60], or through the use of external stimuli such as light [61, 62]. The DDS may be present as free-flowing liquids at room temperature, that swell or gelate at physiological pH and temperature, increasing their mesh size to facilitate drug release [63]. The most widely studied class of swellable delivery systems are hydrogels, hydrophilic networks that swell rapidly in aqueous solvents [64-66]. An in situ swelling hydrogel with a polyelectrolyte complex, was shown to sustain the release of proteins (insulin and Avidin) over two weeks [67]. The natural polymer xyloglucan (1.5% w/w) has also been used to formulate in situ gels, specifically for ocular delivery in a rabbit model [68]. Various other polymers such as alginic acid [69], chitosan [70] and

Carbopol [71] have also been investigated in these applications. Hydrogel nanoparticles combine the advantages of both hydrogels and nanoparticles [72-76]. They comprise 3D crosslinked polymeric networks that are formed upon self-assembly of amphiphilic copolymers, giving rise to nanostructures with a hydrophilic exterior and hydrophobic core. The minimal associated toxicity and serum stability [77, 78], and their small size makes them injectable and easily internalized by cells [64, 79, 80]. Mucoadhesive polymeric systems have been designed to improved drug retention [81], including hydrogels, microspheres (including those formulated from alginate for the delivery of hypertension drug carvedilol [82] and dextran [83], albumin and degradable starch for the delivery of insulin [84]); and in situ gelling formulations [85-87]. The advantage of naturally occurring polymer systems over other polymer type DDS is that they usually do not require the use of organic solvents or chemical crosslinking agents, reducing associated toxicity. However, the hydrated systems usually exhibit poor mechanical properties and stiffness. Further, the high hydration capacity of the hydrophilic polymers, such as Carbopol®, sodium alginate, Poloxamer®, hydroxypropylmethylcellulose, and hydroxyethylcellulose, accelerate erosion of the system in aqueous media leading to rapid drug release [88-90].

Composite materials [91, 92] such as composite nanofibers [93], and ceramics [94] are also utilized as DDS. While they can be hard and brittle, they can also demonstrate high compressive strength which may be more attractive for load bearing applications [94, 95]. Commonly used ceramic materials include hydroxyapatite ceramics [96] and tricalciumphosphate ceramics [97, 98]. In recent years, “bone-seeking” agents with osteotropic properties such as bisphosphonates [31] have been investigated to enhance and prolong pharmacological effects in osteo-applications to deliver gentamicin and other antibiotics to combat osteomyelitis, as well as anti-inflammatory drugs and bisphosphonates, and growth factors [99]. However, these bisphosphonate conjugates can form colloids or calcium salt/complex precipitates in plasma that cause a major pharmacokinetic drawback sometimes leading to renal or hepatosplenic accumulation [31]. Magnetic nanoparticles have also demonstrated potential for different biomedical applications, including oncology [100]. The small magnetic particles can be modulated to react to certain magnetic field gradients to elicit a controllable desired effect in the body. The versatile systems have been used in therapies such as drug delivery, magnetic hyperthermia, photodynamic and photothermal therapy [101-103]. Fe_3O_4 nanoparticles combined with PEG-based hydrogel

magnetic nanoparticles have demonstrated efficient delivery of paclitaxel to glioma cells [100], however, toxicity of other magnetic nanoparticles, such as manganese nanoparticles, may be an issue [104] in the clinical applicability of these systems.

1.2 Lipid based drug delivery systems

Several commonly studied DDS have now been introduced, and in doing so a number of challenges associated with them have been highlighted, including: associated toxicity (of the material itself or of solvents in their manufacture), rapid release, environmental factors and mechanical properties among others. A final group of DDS that are the topic of this thesis, are biocompatible and biodegradable lipid systems. Lipid-based DDS have gained interest from the pharmaceutical industry due to their potential to enhance the bioavailability and therapeutic index of otherwise problematic formulations. A resurgence over the last number of years in the interest in these materials is owed to the proven commercial success of lipid systems in the delivery of HIV protease inhibitor ritonavir (Table 1.1).

Table 1.1. Commercially available lipid-based products for oral administration [105] with additional information. Most are formulated in gelatin capsules or coated tablets.

Trade name	Company	Molecule	Therapeutic use	Formulation
Rocaltrol®	Roche	Calcitriol	Calcium regulator	triglyceride of coconut/palm oil
Neoral®	Novartis	Cyclosporin A/I	Immuno-suppressant	corn oil mono-di-triglycerides
Gengraf®	Abott	Cyclosporin A/III	Immuno-suppressant	Sorbitan monooleate
Accutane®	Roche	Isotretinoin	Anti-comedogenic	triglycerideS
Kaletra®	Abott	Lopinavir and Ritonavir	HIV antiviral	Sorbitan monolaurate
Norvir®	Abott	Ritonavir	HIV antiviral	Sorbitan monolaurate
Lamprene®	Alliance laboratories	Clofazamine	Treatment of Leprosy	oil-wax base
Restandol®	Organon laboratories	Testosterone undecanoate	Hormone replacement therapy	propylene glycol monolaurate
Convulex®	Pharmacia	Valproic acid	Anti-epileptic	glycerol monostearate 44-55 Type II

Current trends in the pharmaceutical industry are moving towards an increasing number of new potent, lipophilic chemical entities emerging as potential drug candidates [106, 107]. Not only that, but as the discovery and clinical approval of new drug candidates is a lengthy and expensive process, the pharmaceutical industry now put a greater emphasis on directing research toward the resolution of previously abandoned and problematic candidates through the use of biocompatible carrier systems that enhance the bioavailability and biodistribution of difficult drug molecules [108]. Lipid based systems may serve to improve gastrointestinal solubilization and absorption through selective lymphatic uptake of these problematic drugs [109-112] to improve bioavailability and reduce associated toxicity.

In terms of selecting the lipid excipient itself, there exists a wide range of options; from mono-, di- or triglycerides to oils constituting a combination of any of them, and phospholipids to sphingolipids, and ever emerging novel and modified oils and tailorable lipids. Selection of a suitable excipient can lead to the development of novel biomaterials useful in drug delivery applications. Further, various types of formulations/lipid assemblies can be implemented in improving the bioavailability of drugs, most of which are delivered orally. Table 1.2 outlines a working model of lipid formulation classification that facilitates the prediction of a formulations *in vivo* behaviour [113, 114]. Most of the marketed products are Type III systems, which are diverse with a wide range of oil- and water-soluble substances [115].

Table 1.2. The lipid formulation classification system: characteristic features, advantages, and disadvantages of the four essential types of "lipid" formulations [114]

Type	Material	Characteristics	Particle size dispersion	Digestion	Advantages	Disadvantages
I	Oils without surfactants (e.g., tri-, di-, and monoglycerides)	Non-dispersing	Coarse	Crucial	GRAS status; simple; and excellent capsule compatibility	Formulation has poor solvent capacity unless drug is highly lipophilic
II	Oils and water insoluble surfactants	SEDDS formed without water-soluble components	100–250 nm	Not crucial, but likely to occur	Unlikely to lose solvent capacity on dispersion	Turbid o/w dispersion (particle size 0.25–2 μm)
III	Oils, surfactants, and cosolvents (both water-insoluble and water-soluble excipients)	SEDDS/SMEDDS* formed with water-soluble components	100–250 nm	Not crucial, but may be inhibited	Clear or almost clear dispersion, drug absorption without digestion	Possible loss of solvent capacity on dispersion, less easily digested
IV	Water-soluble surfactants and cosolvents	Formulation disperses typically to form a micellar solution	50–100 nm	Not required and not likely to occur	Formulation has good solvent capacity for many drugs	Likely loss of solvent capacity on dispersion may not be digestible

*SEDDS is self-emulsifying drug delivery system; SMEDDS is self micro-emulsifying drug delivery system

Numerous formulation approaches exist producing different types of lipid based drug delivery systems and assemblies. In general these can be categorized into three different types of systems: Emulsions, vesicular systems, and lipid particulate systems.

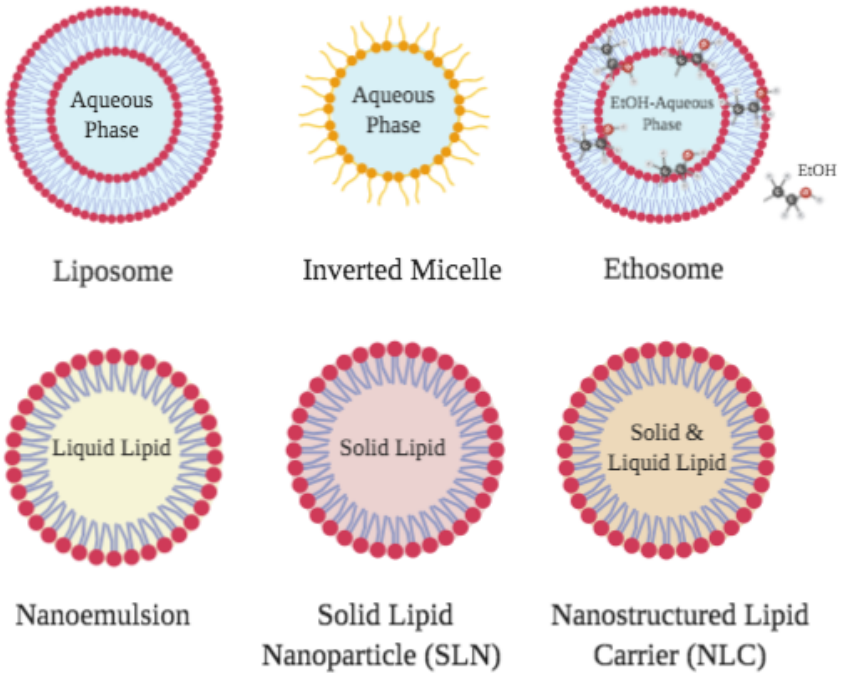

Figure 1.2. Representation of different lipid carrier systems

Traditionally, emulsion systems are formulated from a blend of oil, surfactant and co-surfactant that is dispersed in aqueous phase. They can be designed to meet the specifications of the physicochemical properties of drug substances [116]. SEDDS are the most advanced approach of emulsion based drug delivery systems and relies on physiological fluids for the in situ formation of the micro/nanoemulsion. This formulation strategy comprises the drug dissolved in oils and stabilized by surfactants and co-surfactants, which upon exposure to the aqueous environment under gentle agitation leads to the spontaneous formation of an emulsion [117].

Solid lipid nanoparticles (SLNs) are an alternative version to emulsions in which the liquid oil is replaced by solid lipids. Nanostructured lipid carriers (NLCs) are the advanced generation of SLNs with increased drug loading capacity and stability (oil versus solid lipid) [118]. Both SLNs and NLCs have proven themselves to be effective drug delivery systems incorporating a host of biologically active ingredients [119]. Enhanced oral paclitaxel bioavailability was

reported after encapsulation and administration in loaded lipid nanocapsules as a suspension in saline solution. This eliminates the need for harmful castor oils used in intravenous delivery of this highly water-insoluble drug [120].

Vesicular systems can be classified into two categories: Rigid vesicles (liposomes and niosomes) and elastic or ultra-deformable vesicles (transferosomes and ethosomes) [121]. Liposomes are spherical shaped vesicles produced from non-toxic phospholipids. The nanocarriers have exhibited extensive potential for use in the delivery of drugs, proteins and even genetic material [122]. The response of the amphiphilic lipids when placed in aqueous solution is to rearrange themselves into a sealed, circular lipid bilayer encapsulating an aqueous phase [123] where bio-/pharmaceuticals may be transported. In other cases however, different three dimensional phases can result after this lipid reorganization [123-126]. They are often utilized in reducing systemic toxicity and stabilization of the encapsulation drugs which might otherwise be rapidly degraded. A number of routes have been explored to improve their blood circulation time by introducing polymers such as PEG into the system. One of the major drawbacks with liposomes as drug carriers is their inherent physical instability [127], as liposomes are composed of biodegradable materials that are easily metabolized *in vivo*. Additionally, with the exception of transferosomes, liposomal formulations are generally unsuitable for transdermal delivery as they become trapped in the superior layers of stratum corneum preventing them reaching the deeper layers of the skin [128-130].

Examples of each of these different systems and the advantages they hold are described in table 1.3.

Table 1.3. Examples of implemented lipid based drug delivery formulations

Lipid-Based Drug Delivery Systems					
System	**Advantages**	**Examples**			
		Formulation	**Drug**	**Delivery**	**Result**
Emulsions SEDDS SMEDDS SNEDDS Microemulsions Nanoemulsion	Thermodynamic (microemulsions) or kinetic (nanoemulsions) Stability Supersolvency, Small droplet size, High industrial scalability - low energy requirements for manufacturing	Microemulsion of dimethyl isosorbide, Tween 80 and D, L-α-tocopherol [131]	Paclitaxel	Oral	bioavailability increased from 4.6% to 41%
		Microemulsion [132]	Amphotericin B	Skin	2-fold higher drug permeation & higher antifungal properties
		SEDDS [133]	DTX & curcumin	Oral	3.2-fold increase in the oral bioavailability
		Solid self-nanoemulsifying oily formulations (S-SNEOFs) [134]	Lopinavir	Oral	Significant enhancement in absorptivity
		Miglylol 812 lipid nanoemulsions [112]	Primaquine	Oral	Improved bioavailability & liver uptake (+>45%)
Vesicular systems Liposomes Transferosomes Ethosomes Vesosomes Colloidosomes	Liposomes most sophisticated Capable of accommodating both hydrophilic and lipophilic drug substances within them [135, 136]	Mannosylated liposomes [137]	Amphotericin B	Oral	Improvement in anti-parasitic activity (+35%)
		Chitosan coated liposomes [138]	Furosemide	Oral	Eight-fold increase in FUR permeability
		Phospholipid based ethosomes [121]	Zidovudine	Skin	Increased transdermal flux (15-fold), prolonged drug release
		Transferosomes (soya lecithin and cholesterol) [139]	Risperidone	Skin	Increased transdermal permeation
Lipid particulate systems Lipospheres Solid lipid nanoparticles (SLN) Nanostructure lipid carriers Lipid Drug conjugates (LDC)	Modulation of drug release, increased drug stability, exclusion of organic solvents from the manufacturing process, manufacturing scalability and industrial adaptability [140] Higher solubility of drugs in oils as compared to solid lipids	Glyceryl behenate SLN [141]	Lopinavir	Oral	3.56-fold increase in oral bioavailability
		SLN [120]	Paclitaxel	Oral	Enhanced bioavailability
		Stearic acid-based SLN [142]	Lopinavir	Oral	5-fold increase in oral bioavailability
		NLC [118]	Saquinavir	Oral	3.5-fold enhancement of SQV transport across Caco-2 monolayers
		Squalene-based LDC	Nucleoside analogue	Oral/ intravenous	Increased potency *in vitro* and *in vivo* (murine)

Other examples of lipid based systems include novel hybrid systems, such as one that relies on the use of a commercially available methoxyPEG-liposome encapsulated doxorubicin (DOX) to produce a thermoreversible hydrogel for the treatment of glioma [143]. Another example is the innovative hydrogel formed by lipid nanocapsules (LNC) and lauroyl-gemcitabine (GemC12), intended to be injected inside the tumour or in the tumour resection cavity [144].

In more recent years, an intriguing family of self-assembled lipid systems known as liquid crystalline mesophases have emerged as potential drug delivery systems. Originally developed to facilitate the crystallisation of difficult to crystallize membrane proteins, these mesophase systems mimic those of naturally existing membranes and present a means for effectively delivering drugs and therapeutic proteins [145]. The versatility of these systems in the encapsulation and delivery of drugs and biopharmaceuticals of different size, charge and solubility has been extensively studied and may provide a means to overcoming issues seen with other lipid based systems such as poor stability, and toxicity [123]. The remainder of this chapter will present a detailed description of these interesting systems and aims to highlight the reasons for selecting this family of carrier systems for the delivery of industrially relevant drugs within this thesis.

1.3 Self-assembled Lipid Liquid Crystalline Phases

Amphiphilic lipids, in their solid state, exhibit a defined architecture that comprises a bundle of planar molecular bilayers stacked to form the lipid framework. The polar lipid heads surround the outer surface of the tightly packed hydrocarbon chains [146]. It is the hydrophobic effect, acting to reduce the interface between the aqueous phase and the hydrocarbon tails of the amphiphilic lipid that drives the instinctive self-assembly of these lipids in water [147]. Exclusive to a certain subset of lipid molecules is a physical or structural property that drives a spontaneous association in aqueous environments to form highly organized structural units which exhibit long-range order. A number of polymorphs exist for each of these lipids in aqueous media, whereby, under defined environmental conditions of pH, pressure, temperature, and water content, different complex liquid-crystalline phases of defined geometries can be accessed [1, 148]. These highly viscous mesophases are so named lyotropic “liquid crystals” due to their short-range disorder despite the fact that they are considered to be plastic crystals [146]. The lipid molecules are dynamic in these liquid crystalline systems, behaving like a viscous lipid while still maintaining a global degree of

order characteristic of a crystalline solid, owing to the unique rheological properties of these interesting systems.

The influence of the key environmental conditions on the lipid mesophase formed is demonstrated on corresponding phase diagrams, which have been defined for a number of functional lipids. The three most understood phases on these diagrams are the lamellar, hexagonal and cubic phases:

Lamellar (L_α) phase – This liquid-crystalline phase displays one dimensional long range order, where the lipid molecules can diffuse laterally. A linear arrangement of interchanging lipid bilayers and aqueous channels make up the three dimensional structure of the phase [123, 146]. This phase demonstrates relatively low viscosity compared to phases observed through an increase in water content and is commonly formed in an aqueous environment above the associate hydrocarbon chain Tm. Above that temperature the water can penetrate the polar portion of the lipid and form the L_α phase which displays higher mobility than the other corresponding mesophases [146]. By raising the temperature or hydration of a system, the hydrocarbon chain disorder becomes more apparent and geometrical reorganization ensues causing a transition from the lamellar phase to the three dimensional cubic phase.

The cubic phase (Q) – This interesting phase is commonly seen sandwiched between the lamellar and reversed hexagonal phase on the phase diagram. It is observed as the water content is raised [123]. A further increase in the influential environmental factors sees a collapse of the mesophase geometry and a transition beyond the cubic phase to the highly curved hexagonal phase.

Reversed Hexagonal (H_{II}) phase – An arrangement of limitless water rods divided by lipid bilayers in a two dimensional lattice comprises the reversed hexagonal phase [146].

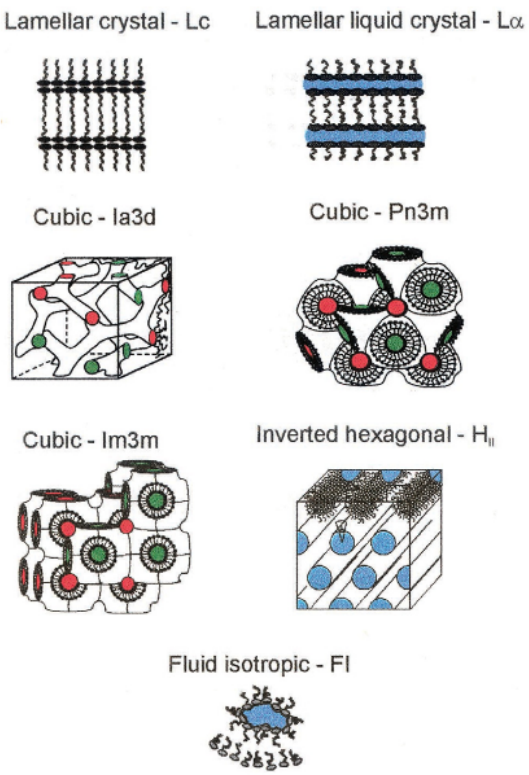

Figure 1.3. Schematic representation of the various lyotropic liquid crystalline phases including: solid (lamellar), mesophase (lamellar phase; cubic- Pn3, -Ia3d and -Im3m phases; inverted hexagonal phase), and liquid (fluid isotropic phase) states spontaneously formed upon contact with an aqueous environment. Water is represented by the coloured regions [149].

The formation of an additional phase was also noted during the course of mesophase compatibility studies, and is now referred to as the 'sponge phase'. This phase was observed when test components caused swelling of the cubic phase under particular conditions. It is said to evolve from the LCP possibly as a result of the added component reducing the structures bending rigidity and lowering the bilayer interfacial curvature and thus allowing the mesophase to absorb more of the aqueous solution [150]. The sponge phase still maintains its bicontinuity despite this phase transition [145] and may be advantageous for applications with large proteins or pharmaceuticals, as the aqueous channels in the swelled phase are dilated and have the capacity to incorporate larger molecules [145].

The free energy of the system is a critical factor in the assembly of inverse mesophases. It is reported that both the instinctive formation of the phase and the thermodynamic stability of the

liquid crystalline phases are driven by an opposition between a pair of free energy terms. When this competition between the curvature energy of the individual monolayers and stretching energy of the lipid chains exists in its least frustrated state, it is suggested to be responsible for the nature of the solid state phase and its position on the phase diagram (equation 1.1) [151-153].

$$\textbf{\textit{Equation}}\ \mathbf{1.1}: \qquad g_{tot} = g_c + g_p$$

Where g_{tot} is the calculated total free energy of the system, which is defined as the sum of the free energies associated with the system curvature, (g_c, calculated for each lipid using critical packing parameter (CPP)) and, that of the packing frustration (g_p).

As the free energy of curved geometries is always in the frustrated state, changes in environmental conditions or additional stresses imposed by factors including temperature, pH, pressure or the addition of additives may induce global changes in the curvature of the system or result in a phase transition in a bid to compensate and relive the frustration. While these environmental factors greatly govern the behaviour of amphiphilic lipids in aqueous media, various other structural and chemical factors such as lipid chain length, molecular shape, and lipid concentration dictate the polymorph accessible for a particular lipid system under these conditions [148, 154]. The molecular shape of the lipid is one of the most influential factors in determining whether a lipid system favours lamellar or non-lamellar structures. The literature utilizes the relationship between the contribution of the hydrophobic and hydrophilic moieties. Here, the shape of the lipid components are considered, where the ratio of the volume (v) and maximum chain length (l_{max}) of the incompressible hydrocarbon chain to the effective cross-sectional area the head group can assume (a_{cs}) defines the phase behaviour of a lipid. This theoretical ratio is referred to as the critical packing parameter (CPP), and is described in equation 1.2 [155].

$$\textbf{\textit{Equation}}\ \mathbf{1.2}: \mathrm{CPP} = \frac{\mathrm{v}}{(a_{cs} l_{max})}$$

When the contribution of the two different moieties reaches near equal, the value of the CPP approaches 1. In this case, a normal type (type I) self-assembled structure is preferred, where the surfactant molecules favour the formation of planar membranes with a cylindrical critical packing

shape. When the CPP value is less than 1, micellar structures are favoured, with an interface of convex curvature. For these assemblies, water content greatly influences the stability of the structures and their geometry is highly sensitive to dilution rendering them rather unsuitable for biological applications. On the other hand, for inverted type structures (type II), the CPP value exceeds 1 and the self-assembled structures bear an interface that is concave with respect to their hydrophilic domains, favouring non-lamellar structures such as the inverted hexagonal and micelle phases, as well as the cubic phase [156, 157].

While CPP values are considered semi-quantitative at best, estimating this parameter provides a means for predicting the mesophase accessible in a particular sample, and may serve in qualitatively studying phase transitions when laying out a phase diagram. If one were to increase the temperature of a cubic lipid-water system for example, the cross-sectional area of the head group is reduced due to a dehydration of the polar domain, in turn increasing the value of the associated CPP and transitioning out of the cubic phase toward the inverted hexagonal or micellar architectures [154, 156]. The complex architecture of the liquid crystalline phases involves numerous energies and interactions, and for this reason calculation of the CPP value alone would not be sufficient in determining the phase behaviour of these amphiphilic lipid systems. To provide a detailed description of the complex systems and how they behave in aqueous environments requires high resolution techniques combined with mathematical modelling.

1.4 The Cubic Phase: Structure and properties

The intrigue around the lipid cubic phase (LCP) in recent decades can be owed to its unique microstructure [158] which has been defined after extensive study by means of different spectroscopic approaches including X-ray diffraction [1], freeze-fracture electron microscopy [159], resonance Raman spectroscopy [160] and NMR [161]. The microstructure agreeably resembles that of the naturally occurring physiological lipid bilayer [125, 146] displaying flawless long-range three dimensional periodicity [146]. Two different classes of cubic phases are known to exist, both of which are macroscopically stable, completely transparent and solid-like viscous materials [162, 163]. The first of these is the micellar cubic phase which comprises a cubic lattice of lipids which are packed into micelles. These micelles assemble when the critical micellar temperature (Krafft temperature) is less than or equal to the experimental temperature [164]. The

second class, of interest in this thesis, is the bicontinuous cubic phase which comprises a curved, extended bilayer which spreads in three dimensions [165] and is accessed upon hydration of the system upon which the lamellar phase undergoes structural reorganization.

These bicontinuous phases can assume architectures of varying surface symmetry, forming different cubic structures of primitive (Im3m or Q_{II}^{P}), gyroid or (Ia3d or Q_{II}^{G}), or double-diamond (Pn3m or Q_{II}^{D}) symmetry with associated values of 229, 230, and 224 respectively. The latter two symmetries, listed in order of increasing hydration, are of particular interest in the areas of drug delivery and applied sciences as they are inherently thermodynamically stable even in excess water [148, 166, 167]. Despite these differences in space group geometry, they share distinct structural features of a set of identical interpenetrating, congruent aqueous channels which never intersect, delineated by a lone, uninterrupted, and highly curved lipid bilayer [123, 165, 168]. The size of the aqueous pores in a fully swollen cubic phase is said to range from approximately 4-5 nm in diameter and forms the diffusion space [123, 169].

The cubic phases themselves are distinguishable by their discrete crystallographic space groups, optical isotropy and its non-birefringent refraction. A range of characterization techniques can be applied in the distinction and characterization of these systems outside of the cell environment. In the first instance, characterization of the structural properties of the lipid cubic formulations is carried out using techniques such as polarized light microscopy (PLM). Small angle X-ray-scattering (SAXS) is applied in distinguishing between cubic space groups and is utilized in dimensional analysis. Lipid cubic phases typically give rise to diffraction patterns similar to those of powder X-ray diffraction; characterized by a series of sharp, clearly defined concentric rings owing to their randomly orientated domains of cubic symmetry [170]. More traditionally, DSC, NMR and fluorescence microscopy were applied in the characterization of the formulations. Beyond that, electron microscopy approaches are utilized to study the topography of the formulations, specifically cryo-TEM is utilized to visualize the structural organization of the cubic systems [171].

A wide range of lipids have the ability to form different cubic and other mesophases including: monoacylglycerols (MAGs); phospholipids; alkyl glycerates; PEGylated phospholipids; and

glycolipids, [161, 167, 172-175] and the selection of a suitable host is key in developing the cubic phase for drug delivery applications.

Monoacylglycerols, are a class of esters of the trihydric alcohol glycerol with one of the hydroxyl groups esterified with a long-chain fatty acid. They are commonly used as surfactants (emulsifiers) and in the food and cosmetic industries to prevent oil-water mixtures from separating and also as antistaling agents [176]. Two different monoglycerides can be formed depending on the alcohol group attached to the fatty acid. Glycerols may provide both primary (1-monoacylglycerols) and secondary alcohols (2-monoacylglycerols) (Figure 1.4). 2-monoacylglycerols are one of the primary digestive products of dietary fats (triacylglycerols and diacylglycerols).

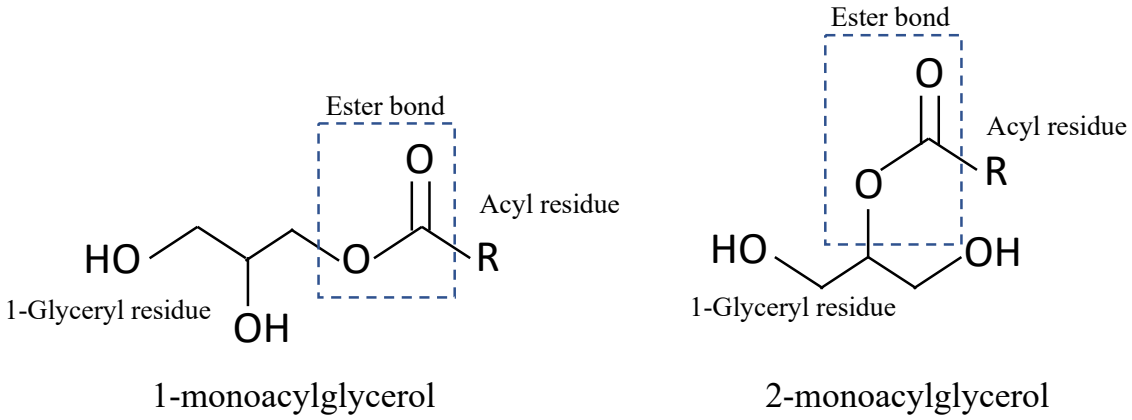

Figure 1.4. Chemical structures of 1- and 2-monoacylglycerols stereoisomers

In this context, cis-monoacylglycerols (MAGs) are a widely studied class of amphiphilic lipids that demonstrate anomalous polymorphism favourable for drug delivery and fundamental applications. Arguably the most extensively studied polar lipid in lyotropic liquid crystal applications is Monoolein (MO) for its rich and unique polymorphism [177]. Other monoacylglycerides of interest in this study are monopalmitolein (MPL) and monovaccenin (MV) (Figure 1.5), while others such as monoelaidin [172], monoeicosenoin [158], and various phospholipids [161, 178] have also demonstrated the ability to form biocompatible cubic phases under different conditions of temperature and water content [174]. All of the cis-monoacylglycerols exhibit differences in hydrocarbon chain length, location of unsaturation and in cis double bond count. Synthesis of these lipids follows an enzymatic hydrolysis of naturally occurring triglycerides, yielding an amphiphilic product comprising the characteristic glycerol

head and a cis unsaturated fatty acid chain bridged together via an ester bond that is critical in assuming the correct curvature and rotational and translational motions crucial in the formation of the inverse cubic symmetries [179-181].

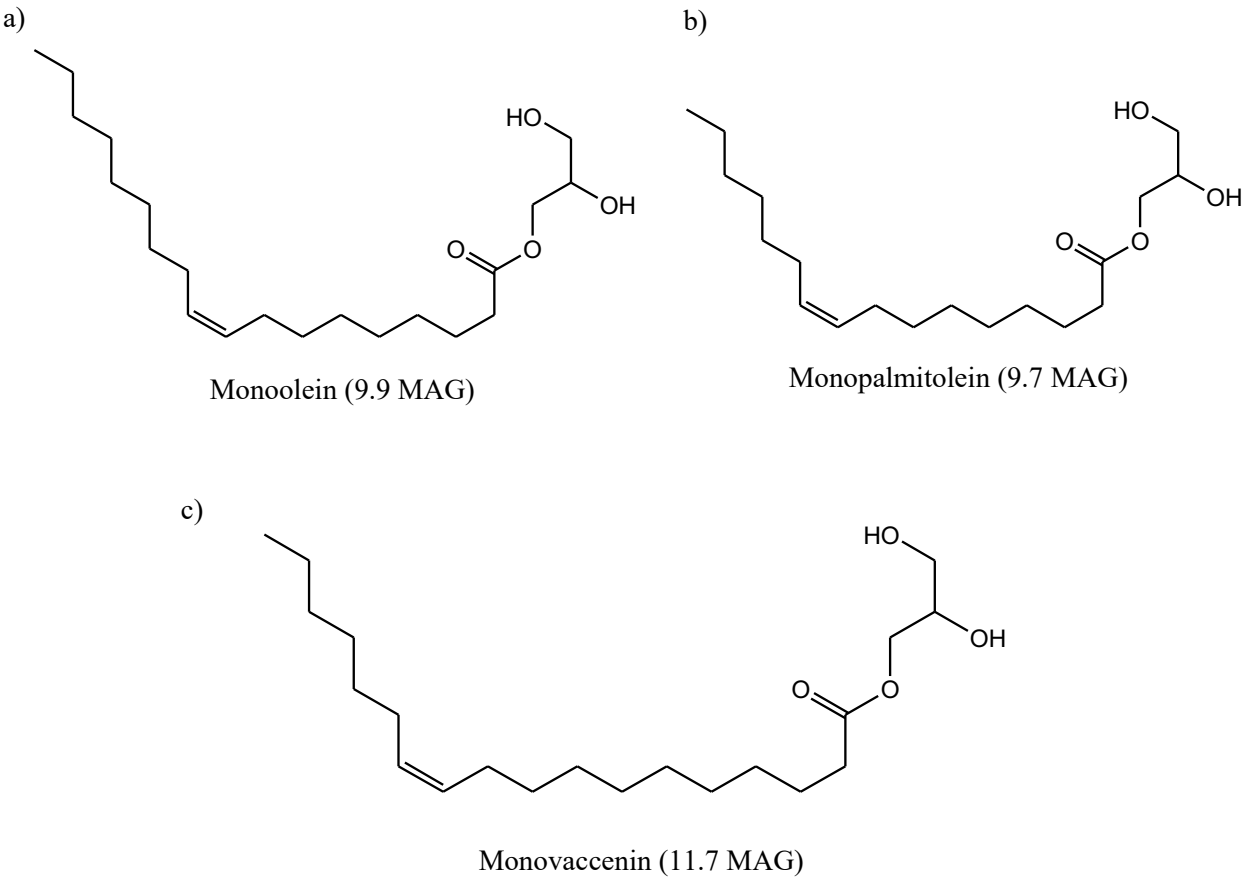

Figure 1.5. Chemical structures of the cis-monoacylglycerols used in this investigation: monoolein (a); monopalmitolein (b); and monovaccenin (c).

Monoolein was introduced into the food industry in the 1950s as an emulsifying agent and a food additive and is also a commonly used ingredient in the cosmetic industry today. It has since exploded into the pharmaceutical world as a biocompatible transporter for various drugs [180] as it is a non-toxic, biodegradable and shows biocompatibility (GRAS listed) [123].

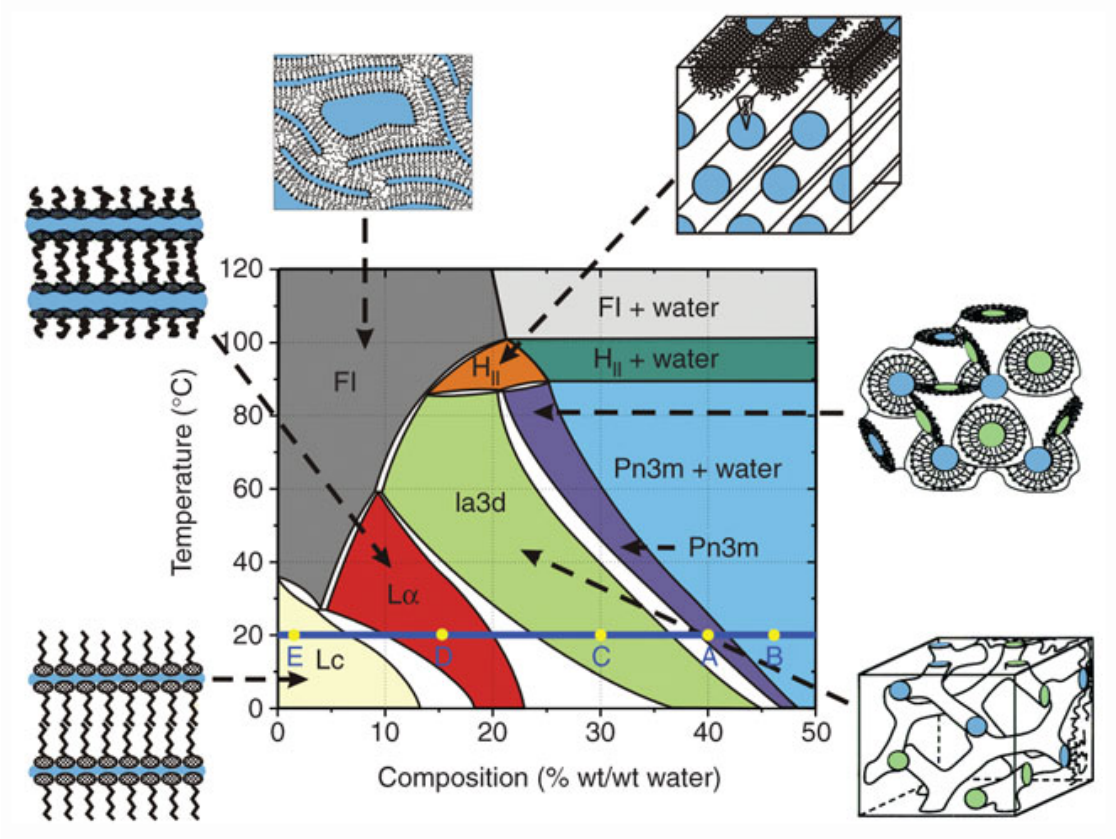

Figure 1.6. Temperature-composition Liquid crystalline phase diagram for Monoolein [182].

The amphiphilic molecule displays spontaneous self-assembly into the various thermostable lyotropic and thermotropic phases with different rheological properties in environments of varying water content and temperature. MO is insoluble in water, however the cubic liquid crystalline phase formed with MO above 17°C with 40% hydration and has the ability to co-exist in equilibrium with excess water [1, 123, 146, 183, 184]. These cubic symmetries are metastable and collapse at temperatures below 17°C [177]. The cubic region of the Monoolein-water phase diagram (Shown in Figure 1.6) comprises two different cubic phases - Ia3d and Pn3m phases [182]. The fact that the Monoolein cubic phase can be prepared at water concentrations from 55 to 85% with 15%-45% MO lipid, means that drugs with very different polar nature and different dosages can be incorporated [123]. The phase has demonstrated the ability to protect drugs, such as peptide drugs, from enzymatic cleavage making it an attractive carrier for easily degraded molecules [126]

and is itself subject to biodegradation (lipolysis) by the various esterases and lipases in biological tissues [1].

The lipid-water phase diagrams of the other monoacylglycerols of interest in this study share similarities with that of monoolein. Diffraction patterns from monopalmitolein samples prepared at hydration levels of 50 wt% exhibited a distinct cubic region of pure Pn3m symmetry [173]. Again, the phase diagram of monovaccenin is comparable with that of MO. Here, the pure Pn3m phase is identified between 48% and 52% (w/w) hydration at 20°C [185] while the less hydrated Ia3d phase precedes the Pn3m at 48% hydration under room temperature. Increasing the temperature reduces the water content necessary to access this mesophase to between 23 and 38%. Although the phase diagrams are relatively similar in terms of the location of the cubic region, their slight differences highlight how the lipid molecular shape influences the polymorph behaviour of the systems. Lipid chain length, and shape, governed by the position of the ester bond, control the microstructure of the associated mesophases. The importance of the location of the ester bond is best highlighted when comparing the MO and MV systems, both of which possess hydrophobic chains 18 carbon atoms in length. The shift in cis double bond location further away from the polar headgroup to position 11 from 8 in the MO increases the hydration capacity of the system, reported to be influenced by a stabilizing effect on a less curved interface at the polar-nonpolar boundary [185]. Not only does the location of this bond greatly influence the layout of the mesophase phase boundaries, structural parameters such as water channel diameter are affected. This may become relevant when matching up APIs to the most appropriate system, where, for example, molecular size or concentration is an issue.

Additionally there are sugar-phytane lipids which enter the cubic phase within a wide range of temperatures. A fully hydrated cubic phase is achieved with the right ratios of water and lipid from 10°C to 70°C [175]. Phytantriol (3,7,11,15-tetramethyl-1,2,3-hexadecanetriol), is a biocompatible surfactant which finds frequent application as an ingredient in the cosmetic industry [186, 187]. It is a small, non-ionic amphiphile which undergoes self-assembly into inverse micellar, lamellar, cubic phase Ia3d, and cubic phase Pn3m and an inverse hexagonal phase under certain conditions of water content and temperature [167].

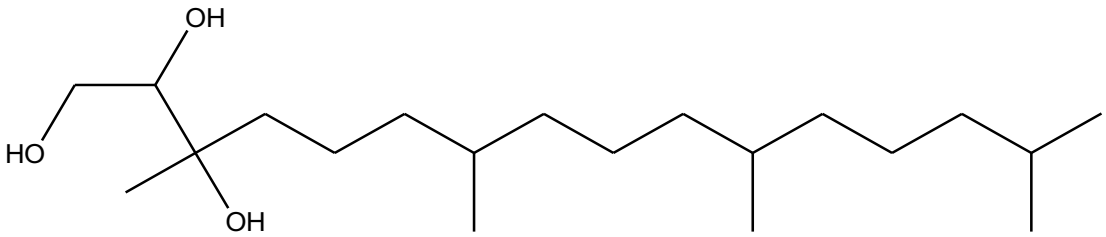

Figure 1.7. Chemical structure of Phytantriol

The phase transitions undergone by phytantriol are qualitatively similar to those observed in monoolein [127, 167]. Importantly, the cubic phase again exists in equilibrium with excess water [127]. Unlike MAGs, phytantriol does not possess a hydrolysable ester bond on its backbone [127, 167] and so is not susceptible to hydrolysis *in vivo*. While this may be more useful for drug delivery to degradative environments such as tumours, as exemplified in a comparative study for the delivery of oridonin, this may result in incomplete release of encapsulated drugs [188]. Additionally, the phases differ in water channel diameter; 3 nm versus 4-5 nm in PHY and MAGs respectively [189]. This feature may become important when selecting the most appropriate lipid system for the API of interest, as size may dictate. As a key focus of this thesis was on the delivery of hydrophobic drugs whose release is controlled by the degradation of the lipid cubic phase, phytantriol was ruled out in the early stages of the investigation.

1.5 LCP for Drug delivery

The use of LCP in controlled drug release applications is owed to its unique microstructure and physio-chemical properties as well as its amphiphilic character and the biodegradable, biocompatible nature of the lipids used [167, 168]. The phase geometry and symmetry can be manipulated at nanoscale to design compatible systems for a given application [190]. Not only that, but the inherent ability of the system to transition between phases by ramping up temperature and hydration, subsequently modifying the structural properties of the system, and in turn its diffusion coefficient. It is well studied that the release kinetics of the mesophases phase are governed by the phase identity (3D LCP>> 2D Lamellar >> 1D Hexagonal phase) [191, 192] and the capacity of the aqueous channels [191, 192]. In terms of commercialization, the uncomplicated manufacturing requirements of the systems, which generally do not necessitate the use of organic solvents [193, 194], mean production costs may be reduced. These features, coupled with its

thermostability and resistance against dilution, make the cubic phase and its dispersions appealing for drug delivery applications [195, 196].

In order to serve as a functional delivery system, a matrix is required to have the ability to dissolve or disperse drugs of different concentrations and solubility. LCP possesses both hydrophilic and hydrophobic areas which aid its function [168] and serve to modulate the release of actives from its network by different phenomena [197]. There are a number of different mechanisms by which sequestration of pharmaceutical moieties from DDS can occur, often related to the nature of the DDS, but also the properties of the drugs themselves (size, charge, hydrophilicity etc.). These mechanisms include: 1) diffusion of the drug either through or from the carrier; 2) liberation of the drug through the degradation of the carrier system by chemical (hydrolytic) or enzymatic digestion; 3) solvent activation (through swelling of the system or osmotic effect); and 4) more obscure activation by externally applied forces such as magnetic fields or ultrasonic technology. Various mathematical models are used to study the complex and often multifactorial kinetics of release for a particular system for comparative reasons and in their design to better predict the behaviour of a system *in vivo*. The relationship studied in each model is shown in table 1.4:

Table 1.4 Summary of commonly used mathematical models for studying release kinetics

Model	Relationship	System kinetics and limitations
Zero-order [198]	$\frac{M_t}{M_\infty} = kt$	Drug release rate is independent of the analyte concentration. Same amount of drug is released per unit of time [199].
First order [200]	$ln(\frac{M_t}{M_\infty}) = kt$	Drug release rate is dependent on analyte concentration. The same percentage of drug cargo is released per unit of time [199]
Hixson-Crowell order [201]	$W_0^{1/3} - W_t^{1/3} = kt$	Drug release by dissolution not diffusion, combined with changes in matrix surface area and inner diameter [199]. Not suitable for hydrogel systems as dependent on changes in structural dimensions of the system.
Higuchi order [202]	$\frac{M_t}{M_\infty} = kt^{1/2}$	Drug release follows diffusive mechanisms. Release kinetics from ointments, films, and planar transdermal systems and three-dimensional dosage forms. Suitable only where release is solely diffusion-controlled.
Korsmeyer-Peppas order [203-205]	$\frac{M_t}{M_\infty} = kt^n$	Drug release is erosion and diffusion controlled. For $n<0.49$ Quasi Fickian diffusion, $n=0.49$ drug smaller than mesh size and rapid Fickian diffusion, $0.49 >n<0.89$ non-Fickian diffusion and swelling controlled release [206, 207]

Where M_t is the total amount of drug released at a time t, M_∞ is the total amount of loaded drug, n is the diffusivity exponent, W_0 is the initial drugload in the DDS, W_t is the unreleased drug in the DDS at time t, and k is the kinetics constant [199, 208].

Since drug release is complex and often governed by more than one factor (eg. diffusion, swelling, erosion etc.) fitting distinct models to more sophisticated systems is not always possible. However, several of these mathematical models are applied in defining the release kinetics from LCP, the most commonly referred to model is the Higuchi square root of time release kinetics, which defines the release of pharmaceuticals from the cubic phase as diffusion controlled in the case of hydrophilic drugs [123]. The Higuchi equation is based on a pseudo-steady-state and it provides a mathematical means of demonstrating a direct proportionality between the total quantity of released drug and the square root of time, allowing one to understand the release mechanism of a material [202]. The lipid cubic phase's aqueous nanochannels exhibit regular structure and

repetition enabling the carriage of hydrophilic drugs and proteins with suitable dimensions [209]. Here, their release is diffusion controlled where an exchange of water from the media into the internal matrix and simultaneous transfer of incorporated drug and water from the matrix to the external environment are the proposed events occurring during hydrophilic drug release from the cubic phase [123].

Hydrophobic molecules on the other hand are embedded in, or loosely bound to, the lipid bilayer portion of LCP as solid dispersions meaning that their liberation is limited by the breakdown of the lipid envelope surround them. Owing to the highly viscous and mucoadhesive nature of the LCP [210] the formulations encapsulating the hydrophobic agents can be retained at the site for a greater length of time compared to the free drug which are often rapidly washed away. There they are protected against the aqueous environment thus limiting their exposure to oxidative and degradative processes and their dissolution is slowed down. In a study using hydrophobic model drug cinnarizine the solubility of the drug was increased by 2 x 10^5 fold over the drug in aqueous buffer, and the same study demonstrated a prolonged release of the drug from the cubic phase compared to a lamellar system over a 4 hour testing period [211]. Further, comparison of *in vivo* plasma profiles after administration highlighted significantly slower absorption from the cubic phase compared to a lipid suspension of the drug (~10 times slower) proving the system as an improved lipid based sustained-release delivery systems for lipophilic drugs [211]. Other mathematical models such as the Korsemeyers Peppas model relate matrix degradation and erosion to the release kinetics of hydrophobic APIs in these cases.

In addition to the effect the structure and properties of the matrix itself have on the diffusion of the drug, both the physical and chemical properties of the drug being incorporated into the cubic phase, including the shape and molecular size of the drug itself, also influence the transport properties of the matrix [168, 212]. It is also imperative to ensure that the incorporated drug does not disrupt the assembly of the cubic phase lattice structure which may in turn affect its function. In some cases this may limit the use of the cubic phase as a drug delivery matrix. The location and effect of an incorporated active agent can be distinguished by monitoring induced changes in the structure of the mesophase upon the additives introduction. More traditionally, DSC, NMR and fluorescence microscopy were applied in the characterization of the formulations. Beyond that, electron microscopy approaches are utilized to study the topography of the formulations,

specifically cryo-TEM is utilized to visualize the structural organization of the cubic systems [171].

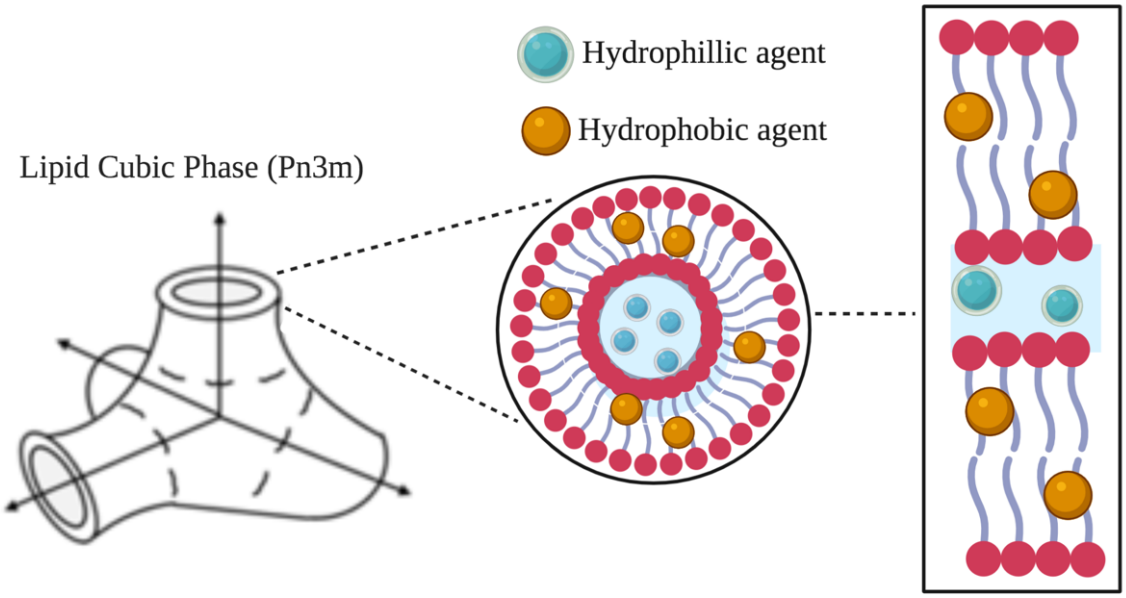

Figure 1.8. Schematic representation of a bicontinuous lipid cubic phase of generic single chain lipid, water and encapsulated drugs. The magnified image on the right demonstrated the matrix lipid bilayer which is the insertion site for the hydrophobic drugs and envelopes a water conduit where hydrophilic drugs can be encapsulated.

Lipid cubic-based formulations have been investigated in the literature for use in numerous drug delivery applications [123, 181], including topical [209, 213], oral routes [214], and parenteral routes for a range of pharmaceutical agents of different aqueous solubilities [169, 174, 197, 215-217]. The literature reports how the cubic phase maintains its nanostructure and controlled release capabilities when subcutaneously injected [218] or orally dosed [219] *in vivo*. Bicontinuous lipid cubic phases are said to exist within numerous biological systems, where their presence may be related to the cell's pathological state and health [220]. For this reason, they have been applied as transporters of both small molecules and larger proteins through both oral and parenteral routes as well as in local delivery applications including subcutaneous and intramuscular routes [123, 158]. Sustained release of hydrophilic drugs from medical implants has been achieved primarily through

the use of comparably hydrophilic lipids in their solid state [123]. The lipid cubic system's applicability as a sustained release system has been investigated for a range of pharmaceutical agents of different aqueous solubilities [169, 174, 197, 215-217], the majority of which demonstrate diffusion-controlled release that follows first order kinetics, with total release observed within 24 hours. These studies have shown the system's ability to sustain a controlled release of various antibiotics including: Clindamycin phosphate [221]; Cefuroxime [222]; Benzylpenicillin [223]. Sustained release has also been demonstrated for a range of pharmaceutical agents such as acetyl salicylic acid (aspirin) [169], antihistamine chlorpheniramine maleate [215], corticosteroid budesonide [223], pyrimethamine [216] and decongestant pseudoephedrine [217], all of which demonstrate diffusion-controlled release that is follows first order kinetics.

Moreover, the stabilizing effect of the cubic phase on incorporated drugs makes it an attractive vehicle for use in drug delivery. It has demonstrated its ability to stabilize small molecule labile drugs from the destabilizing effects of reactions such as hydrolysis and oxidation, thus slowing down their degradation [222]. Its applications are however somewhat limited as a consequence of the matrix's shorter release profile which is often less than 24 hours for hydrophilic agents [123] and its highly viscous consistency which has been likened to thick sticky toothpaste [145]. It is this viscous and mucoadhesive nature however that makes the lipid cubic phase suitable for the delivery of poorly soluble, lipophilic molecules that would otherwise be washed away before they could elicit a response [210].

The selection of a suitable host lipid is key in developing the cubic phase for drug delivery applications [145]. Significant research has been directed towards synthesising novel lipid cubic systems capable of forming the lipid cubic phase for drug delivery [224, 225]. Additionally, it is useful to highlight research carried out in the way of manipulating the cubic phase rheology and phase behaviour through the addition of additives such as ethanol , PG, PEG [150], cholesterol and fatty acids [145] to name a few. In addition, several groups have reported success in incorporating other lipids and lipid derivatives into a host lipid system to achieve modified, tailored cubic phase matrices. Nazaruk and colleagues recently reported the incorporation of charged monoolein derivatives to modulate the control of a positively charged chemotherapeutic agent based on electrostatic interactions between the drug and the negatively charged modified LCP [226]. Wadsten-Hindrichsen *et al.* in the Swedish Chalmers University of Technology described

the addition of Monoolein lipid as an additive to Phytantriol LCP to create cubic phase gels with modified properties for topical drug delivery [189].

Lipid nanosystems in solution

Bulk liquid crystalline mesophases lend themselves to dispersion, allowing for the formulation of nano-sized drug delivery systems. In the case of lamellar, hexagonal, and cubic phases, researchers have coined the terms liposomes, hexosomes, and cubosomes to describe these nanoparticles. Importantly, the nanostructured lipid systems maintain the internal structures of the bulk mesophases and present an opportunity to deliver a variety of drugs with reduced system viscosity compared to their bulk counterparts.

Lipid cubic nanostructures, cubosomes, can be readily produced from the bulk lipid system when a suitable stabilizer is present to support the internal structure of the liquid crystal [190, 227, 228]. All of the physicochemical features of the cubic phase that control the drug release kinetics are retained and preserved in these dispersions [227, 229], eliminating issues associated with handling and injecting the sticky bulk formulation. By fragmenting the bulk cubic phase through high-shear mechanical approaches or chemical techniques, liquid-crystalline nanodispersions ranging in size from 100-140 nm are formed in solution [230, 231]. Such fragmentation approaches include high pressure homogenization and sonication of bulk gel [232-234] or chemical approaches which involve use of a solvent precursor and dilution of an isotropic lipid-ethanol mixture [235, 236].

Typically, drugs are added prior to dispersion of the phase (pre-loaded cubosomes), either in the molten lipid, or the water phase depending on their solubility properties. However, the harsh fragmentation methods are often unsuitable for sensitive proteins and peptides such as those discussed above. In the case of these delicate bioactives, other formulation methods that employ a post-loading approach are favoured [237]. For example, growth hormone-inhibiting hormone (GHIH) somatostatin was post-loaded to liquid crystalline nanoparticles to improve its otherwise short half-life *in vivo* [238]. The common strategy takes advantage of the slightly negative zeta-potential of the cubosomes to attract and adsorb water soluble drugs onto their surface by electrostatic and hydrophobic interactions.

Cubosomes are a widely studied and utilized for the delivery of hydrophilic active agents. Their structure differs from that of liposomes as it can encapsulate hydrophilic, lipophilic and amphiphilic molecules all at once [239]. Cubosomes have been employed to stabilize numerous biologically active substances through their encapsulation in the particles [219]. Some examples include vitamins [239], anti-inflammatory agent Indomethacin [240], insulin [241], ocular treatment [213], and a variety of peptides and proteins [152, 236, 238, 242-244] all of which showed promising results in terms of bioavailability, sustained release compared to free drug and improved half-life. Furthermore, nanosized carrier systems (smaller than 200 nm) have demonstrated their efficient accumulation and retention in tumorous tissue compared to healthy tissues due to the pathological architecture of the diseased state tissues [245-247]. The system's proven ability in sustained release and in protecting the molecules it encapsulates from degradation demonstrate the potential of these cubosomes as versatile drug delivery vehicles for various active pharmaceutical agents. However it should be considered that, as the surface area of these cubosomes is much too high to maintain the controlled delivery that the bulk phase can, these nanosystems may be better suited to rapid release applications as they often exhibit burst release [248].

Although not the topic of this thesis, hexosomes should not be disregarded as promising drug delivery systems. Owed to the closed nature of the water channels in the hexagonal phase, that are shielded from the external environment [249, 250], hexosomes have the potential to slow the of release of hydrophilic drugs compared to cubosomes. The release of hydrophilic drugs takes place through these discontinuous water rod-like compartments [251] and generally follows Higuchi order diffusion kinetics. Despite their promise, the limited number of lipids capable of forming hexagonal mesophases, coupled with the harsh preparation conditions required (eg. high temperatures), means hexosomes are historically less frequently reported in a drug delivery capacity. In more recent years however, groups have focused on synthesising a new class of materials with glycerate headgroups to form the hexagonal lyotropic liquid crystal. Among these materials, oleyl glycerate and phytanyl glycerate were found to form hexagonal phase in excess water at physiological temperature [252]. The dispersed matrices were applied as delivery systems for a range of model hydrophobic and hydrophilic drugs, such as paclitaxel, doxorubicin,

irinotecan, glucose, histidine, and octreotide [214, 253-256] where the distribution of the drugs within the system was not dissimilar to that of the cubic systems.

1.6 Lipid Digestion and its role in drug absorption

The amphiphilic nature of the lipid cubic phase, and its ability to deliver active ingredients of varied solubility has been presented. While the release of hydrophilic drugs that are incorporated into the cubic network has been shown to be a diffusive process, the release of hydrophobic agents is regulated by the digestion of the lipid bilayer envelope that encapsulates the drug. For this reason, and the significant impact digestion of the lipid carrier will have on the performance of lipid-based drug delivery systems, understanding the digestion behaviour of the system is pivotal in predicting the dissolution behaviour of this class of drugs *in vivo*.

Digestion of MAGs by biological enzymes

The importance of the ester bond on the backbone of MAG lipids in the self-assembly of liquid crystalline mesophases [179-181] has already been discussed, however these bonds render mesophases formulated with this class of lipid highly susceptible to the lipolysis by biological enzymes *in vivo* [257]. These MAG lipid systems are subject to slow hydrolysis at the ester linkage connecting the acyl chain (oleic acid) to the glycerol backbone by a family of enzymes, lipases, that are found in the body, often accompanied by other offending abettors such as esterases [257-259]. Lipases are water-soluble and act at an oil-water interface during lipolysis of glycerides in any aqueous system through a series of intricate steps [257], with the surface area being the rate limiting factor [258, 260]. Briefly, pancreatic lipases employ a surface loop system that controls access of its various substrates to its serine active site [261]. In the presence of lipid substrates and other amphiphiles, the surface loop, or ‘lid’, undergoes a conformational change thus exposing the enzyme’s putative catalytic site [262]. The adapted schematic in figure 1.9 summarizes the action of pancreatic lipase on MAGs [263].

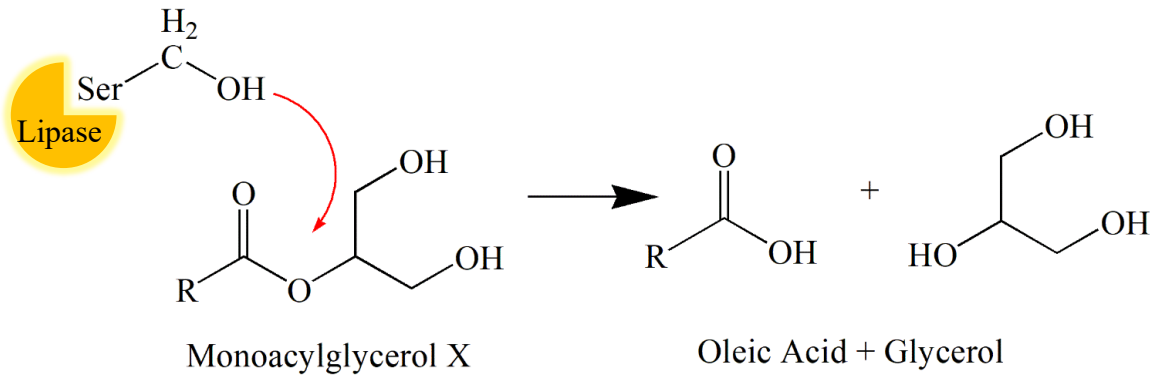

Figure 1.9. Lipase attack on the ester bond present on the Monoacylglycerol lipid chain bridging the oleic acid component to the glycerol backbone breaking the lipid down into its constituents. Adapted from [263].

Colipase is an important non-enzymatic lipase cofactor that is secreted by the pancreas in an inactive form to be activated by trypsin cleavage [264, 265]. It facilitates the action of the enzyme by first binding at the oil-water interface to anchor the lipase to the substrate [266]. Furthermore, colipase stabilises the enzyme in its active conformation through hydrogen bonding with the over-laid polypeptide chain 'lid' sealing the active site [264, 265]. Upon binding at the oil-water interface, the α-helical surface loop is opened to expose the serine-histidine-aspartic acid triad active site [267] and the co-factor serves to maintain this conformation thus facilitating catalysis. Unlike the majority digestive lipases however, gastric lipases' hydrolytic function is independent of cofactors or bile salts [268-270].

It is reasonable to assume that the action of these enzymes and cofactors [174, 257, 258] is likely to influence the *in vivo* release kinetics of any membrane-embedded reconstituted hydrophobic drug as has been described for numerous hydrogel systems [271]. These release of these poorly soluble drugs is limited by their portioning into the aqueous channels of the phase, and issues with solubility mean they cannot be transported by simple diffusive processes. As such, they are liberated only when the lipid network surrounding it is disassembled. Within this thesis we delve further into understanding this mechanism of lipolytic action on our MAG cubic phase systems (Chapters 3 & 4) and explore methods for controlling the digestions as a means of establishing control of the stability of the system to modulate the release of highly hydrophobic drugs.

Improving oral bioavailability of lipophilic drugs

Lipids are assimilated in the body through a multi-step process that beings in the stomach [268, 269, 272]. However, the upper intestine is the major site for the lipolysis and absorption of lipid excipients (and the drugs they carry). The mixtures have been homogenized in the stomach and are then delivered to the duodenum that contains a mixture of bile and pancreatic juice containing an enzyme cocktail of trypsinogen, chymotrypsinogen, elastase, carboxypeptidase, α-amylase, phospho-lipase A, pancreatic lipase, and colipase [273, 274]. In combination with these, a complex mixture of amphiphilic species, including bile salts, phospholipids, lipolytic and other digestive products from the stomach facilitates further emulsification in the upper small intestine [275-277].

To be absorbed, lipid transporters delivered orally must overcome the intestinal diffusion barrier (aka the unstirred water layer) that separates the enterocytes' apical membrane from the bulk aqueous fluid in the intestinal lumen. Micellar solubilisation is said to increase the uptake of molecules by the enterocytes, in comparison to the poorly soluble fatty acids which struggle to overcome the barrier [273, 276, 278-280]. Although the mechanism of lipid molecule uptake is not completely understood, it has been suggested that the micelles are broken down by the acidic environment of the barrier in the process [279, 281] allowing the lipolytic molecules to be absorbed across the membrane; either by means of a carrier system when extracellular lipid concentrations are lower than inside the cell or by straight-forward passive diffusion at higher fatty acid concentrations outside the cell [109, 277, 278, 282]. The transport from micelles to the membrane may also be driven by vesicular-mediated uptake or alternatively, it may be driven directly by a collisional mechanism [109]. Several transporters of the ATP binding cassette family of proteins (ABC proteins) have been identified as being responsible for the efflux of material back in to the intestinal lumen post-absorption. Arguably the most widely studied of this family is p-glycoprotein (P-gp), whose action is notoriously linked to challenges in the bioavailability of drug compounds. There are many reports in the literature on the use of lipid and polymeric excipients to modulate the activity of P-gp in a bid to increase gastrointestinal absorption and oral bioavailability of a variety of drugs [283-287]. In these studies, the lipid excipients decreased or inhibited P-gp protein expression, thus impeding and reducing PGP-mediated efflux of target molecules [283, 288]. Once the lipid molecules have been taken up by the intestinal absorptive cells enterocytes, they may

simply diffuse across the cytosol independently or through interactions with intracellular lipid-binding proteins [289-292] for further processing.

An important step in the way of lipid secretion is their transport to the endoplasmic reticulum (ER). Following their transport to the ER, monoacylglycerols are esterified with FFAs by monoacylglycerol acyltransferases to re-synthesize diacylglycerols, which may then be converted to triacylglycerols by a group of proteins called diacylglycerol acyltransferases [277, 293] or combined with choline and ethanolamine to synthesize phospholipids by choline and ethanolamine transferases. The re-synthesis of triacylglycerols is achieved through one of a pair of two pathways: 1) within the smooth endoplasmic reticulum by means of the 2- monoglyceride (2-MG) pathway; or 2) the α–glycerol-3-phosphate pathway (G3P) associated with the rough endoplasmic reticulum. The reassembled lipids face two possible fates: they may become part of lipid droplets for storage, accumulating ER lumen or in the cytosol of enterocytes to be mobilized and secreted during fasting state in enterocytes [294, 295]; or transported to the ER to be secreted. The lipids are packaged into large, spherical triacylglycerol-rich lipoproteins (LP) called chylomicrons or into *very* low density lipoproteins (VLDLs). The enterocytes export the lipoproteins into the lamina propria containing capillaries and central lacteal (lymph vessel) via exocytosis. Chylomicrons are released and enter systemic circulation at the thoracic duct. The LP cross the highly permeable lymphatic endothelium [109, 110]. In a similar way, drug molecules can also enter the general circulation through uptake into the portal vein or via the mesenteric lymphatic system. Highly lipophilic drugs with log P values that exceed 5 are said to partition into the LPs during their assembly which facilitates their access to the intestinal lymph [109] dodging first pass metabolism in the process. On the other hand, drug entities with lower lipophilicity tend to access general circulation via the liver through the portal vein in a similar manner to medium to short-chain fatty acids [273, 276].

In this way, lipids can influence oral drug absorption in numerous ways. Lipids present in the GI tract stimulate the gall bladder to secrete bile into the small intestine which aids the solubilization of poorly water soluble drugs. Further, the digestive products of lipids produce a variety of amphiphilic colloidal species including micelles, mixed micelles and vesicles increase the solubilisation capacity of the intestinal milieu [109, 296]. Drugs that are pre-solubilized in amphiphilic colloidal species demonstrate a higher mass transport across the unstirred water layer

compared to solute drug molecules who's diffusion is retarded by their unfavourable aqueous solubility. The lipid excipients influence the enterocyte-based transport of drug molecules through the apical brush border membrane through a number of mechanisms including: increasing membrane fluidity enabling transcellular absorption; facilitating paracellular transport by opening of the tight junction and; through the previously discussed targeted inhibition of P-gp and/or CYP450 efflux to increase intracellular residence time and concentration [109, 110]. Lipophilic drug absorption through the lymphatic pathway can also be influence by co-administering lipid molecules which may trigger the assembly of LPs in the duodenal cell facilitating drug absorption; entering systemic circulation by bypassing the liver in the intestinal lymph and subsequently dodging first pass metabolism to improve bioavailability. The incorporation of lipophilic drug molecules into lipid-based delivery formulations has been shown to improve oral bioavailability [120, 297-301].

1.7 Concluding Remarks and Identified Research objectives

The ever-increasing number of drugs emerging from discovery posing challenges of poor solubility and permeability present a need for the development of bio-enabling formulation approaches to tackle the issue of reduced bioavailability akin to these troublesome drugs. Emerging trends in lipid-based formulation design focus on the structure and stability of these systems, and on their ability to overcome these complications. As discussed, lipid-based delivery formulations have been shown to improve the oral bioavailability of otherwise problematic drugs (Table 1.3) by increasing solubilization and facilitating the mass transport of these drugs to the intestinal surface for absorption [120, 297-301]. There, the lipid excipients have the ability to maximise intestinal drug solubilization and have been explored as a vehicle for improving enterocyte-based transport [109, 110]. The sustained release of poorly soluble drugs from the lipid cubic network compared to other lipid-based drug delivery systems has already been discussed, a process that is driven by the breakdown of the lipid matrix. Understanding these lipolytic processes may present opportunities for modulating the degradation of the systems for local delivery applications, where different lipases are present *in vivo*. This would be particularly for those systems derived from biocompatible MAG lipids, to extend the associated dissolution profiles even further.

Within this work, liquid crystalline lipid formulations of bicontinuous cubic symmetry have been selected and explored as potential drug delivery systems. Their resemblance to biological membrane structures [220, 302], biocompatibility and amphiphilic nature makes these cubic phases attractive contenders in the race to optimise bio-enabling formulations. Additionally, the fully swollen bicontinuous cubic phases studied here are resistant to dilution lending themselves to dispersion into nanoparticles (cubosomes) that maintain the unique internal microstructure of the bulk phase. In this context, the effect of loading a selection of drug molecules differing in solubility properties on the internal structure of bulk and dispersed cubic formulations was evaluated through high resolution approaches such as small-angle X-ray scattering and cryo-TEM, and assess the feasibility of both bulk and dispersed (cubosomes) cubic systems to encapsulate and deliver a range of small molecule drugs.

This work aimed to investigate the impact of active pharmaceutical ingredients with contrasting physicochemical and solubility properties on the application of the lipid cubic phase as a controlled release drug delivery system. In this context, the following four research questions have been addressed:

1. What influence do the physicochemical properties, specifically solubility and size, of the passenger drug loaded into the lipid phase, have on the stability and liquid crystalline structure of the phase? and what are their implications on its subsequent release kinetics?
2. Do environmental factors of the body, including pH and ionic composition, impact the internal structure of the phase or influence the kinetics and duration of loaded drug release from the phase and its dispersions relevant in potential local drug delivery applications?
3. Can the rate of release of hydrophobic or hydrophilic drug molecules be tuned beyond the rate of degradation of the lipid cubic phase through lipolysis by naturally occurring lipases?
4. Could predictions on the rate of release, and degradation of the lipid phase, *in vivo* be made based on relative binding energies of the lipid, drug and lipase and inhibitor molecules to facilitate the design of effective drug delivery systems?

1.8 Thesis outline

The research outlined within this thesis is presented as four distinct experimental chapters, each outlining contributions that have led to published or compiled research manuscripts with additional results included for clarity.

In the interest of transparency, it is declared that all experimental data was collected by the author unless otherwise specified. Specifically, molecular dynamics simulations in Chapter IV were carried out by Dr Shayon Bhattacharya and Dr Damien Thompson at the University of Limerick to compliment the experimental results and used in support of hypotheses presented in relation to the lipolysis of the system. DFT calculations were facilitated by Dr Vivek Verma, University of Limerick. MP-SPR data was collected by Radek Bombera at BioNavis, Tampere, Finland. Cryo-TEM data was collected by Pasi Laurinmaki at the University of Helsinki, Finland.

Chapter II: Lipid Cubic System for the controlled delivery of pharmaceuticals of varied solubility. A Case Study: Antihistamine delivery

2.1 Introduction

The work outlined in this chapter has been compiled into a research manuscript to be submitted for publication titled "*Lipid Cubic System for nasal/topical delivery of antihistamine drugs*". The aim of this initial study was to establish the controlled release properties of the Q_{II}^{D}-type lipid cubic system and its dispersions by studying the dissolution properties of a selection of small molecule antihistamine drugs differing in physicochemical properties in release media of varying pH and ionic composition. Here, the MP-SPR data was collected by Radek Bombera at BioNavis, Tampere, Finland. The author wished to acknowledge Miriama Ceresnakova at the University of Limerick for her assistance in cell culturing to facilitate the study of cellular uptake of cubosomes.

2.2 Background

Histamine, a biogenic amine whose synthesis in tissue mast cells is driven by the decarboxylation of the free amino acid histidine [303], is released in mammals in an inflammatory response to tissue injury or allergic reactions through a complex cascade of mediator release and interactions [303]. Should an imbalance between accumulated histamine and the rate of its degradation occur, histamine intolerance induces a number of unwelcome side effects [304, 305]. In the case of dermatological conditions such as urticaria and atopic/contact dermatitis exorbitant accumulations of histamine induce skin wheals and itchy flare-ups through direct contact, ingestion, or inhalation of allergens [306-308]. In allergic rhinitis, which is purported to affect over 1/3 of the world's population [309, 310], histamine imbalance induces symptoms such as itching, watery eyes, and rhinorrhoea (nasal discharge).

Currently, the primary course of treatment for managing such allergies is oral dosage forms of antihistamines which target the histamine receptors present on the various cells in the body, of which four have been identified; $H_{1\text{-}4}$. Of the four, H_1 and H_2 receptors are currently the most clinically relevant when it comes to treating histamine related disorders. H_1 is a receptor present on endothelial and smooth muscle cells that is the target of the majority of marketed and identified

antihistamine molecules. More than 45 H_1-antihistamines are commercially available worldwide [311]. They are referred to as inverse agonists [312] which bind these receptors without effecting a response, thus inhibiting the action of histamine through competitive or pharmacological antagonism [313]. However, more recent research has shown that they also exert their effect through transcription factor nuclear factor-kB to decrease antigen presentation, reduce proinflammatory cytokine expression, and downregulate cell adhesion molecules and chemotaxis. They have also proven their ability to inhibit mast cell activation and subsequent histamine release, likely through the downregulation of calcium ions in the cell, although the mechanism is still not fully understood [311, 314-316]. All function in a concentration-dependent manner, where the concentration of the antihistamine molecule must be maintained at sufficient levels over the required time to effectively compete with histamine. The use of a controlled-release drug delivery system is therefore an attractive approach to improving the efficacy of these molecules.

These H_1-antihistamines are further classified into 2 groups based on their ability to cross the blood-brain barrier. First-generation antihistamines refer to the group of molecules that because of their lipophilic nature, relatively low molecular weight and lack of recognition by the P-glycoprotein efflux pump, readily cross this barrier and readily interact with H_1 receptors through the central nervous system (CNS) [314, 317-319]. As a result of their lack of selectivity, this class of molecules may also induce deleterious effects such as sedation and reduced psychomotor performance [320]. To overcome these unwanted side-effects, second-generation antihistamines have been developed. These molecules are poorly lipophilic, bind more specifically to H_1 receptors and display a strong affinity for surface P-glycoprotein expressed on vascular endothelial cells reducing the likelihood of their penetration into the CNS [320, 321] thus cause less side-effects. Having said that, second generation antihistamine cetirizine used in this study has been shown to occupy CNS H_1 receptors to a certain extent [322]. Due to their clinical relevance H_1 receptor blockers varying in structure and solubility have been chosen for investigation. Table 2.1 summarises the key physicochemical properties, indications and delivery routes associated with the four selected antihistamines investigated and their chemical structures are shown in figure 2.1.

Table 2.1. Antihistamines investigated in this study

Antihistamine			Mol. weight (g/mol)	LogP value	BCS class*	Trade name	Indication	Dosage	Administration	Formulation
Decreasing aqueous solubility →	1st generation	Diphenhydramine Hydrochloride (DPH)	291.8	3.65	I	Benadryl	Wide spectrum allergy, cough	6.25 - 50 mg orally every 4 to 6 hours [323]	Oral; sterile, pyrogen-free solution in water for injection for intramuscular or intravenous use [324]	Chewable or dissolvable tab; as a cream (containing propyl hydroxybenzoate, liquid paraffin, emulsifying wax and purified water); a gel (sometimes includes skin protectants such as allantoin, zinc acetate as well as inactive ingredients camphor, citric acid, ethanol, glycerin, methylparaben, propylene glycol, propylparaben, sodium citrate); or pill [325].
		Carbinoxamine maleate (CBX)	406.9	3.23	I	Arbinoxa; Karbinal ER	Allergic/ vasomotor rhinitis, conjuntivitis, urticaria, angioedema.	4 - 8 mg 3 to 4 times daily [326]	Oral	Drug-polistirex complex oral suspension under the trade name Karbinal ER [327], or as a tablet under trade name Arbinoxa [328]. The antihistamine is also formulated with decongestant pseudoephedrine HCl as oral treatment Rondec to treat hayfever, allergies and other breathing difficulties.
	2nd generation	Cetirizine Dihydrochloride (CZH)	461.89	2.98	III	Zyrtec	hay fever, allergic rhinitis, chronic urticaria and asthma	10 mg once daily [329]	Oral; Transdermal [330]	Formulated and supplied as a syrup, chewable tab or pill [325] but has also been explored for used in transdermal applications in the form of a cream containing propylene glycol as an emulsifying solvent [330].
		Azelastine Hydrochloride (AZL)	418.4	4.04	IV	Astelin; Asterpro	allergic rhinitis	0.28 mg once daily [331]	Nasal spray; eye drops	Racemic mixture intranasal spray [332]. Aqueous solution containing surfactant benzalkonium chloride [333].

*See Figure 1.1 for BCS classification system

For the most part, these inverse agonists are delivered through oral dosage forms, however, a major drawback of administering required dosages of antihistamines through the oral route are a list of unwanted side effects [334, 335]; including nausea, dry mouth, and drowsiness and sedation. To overcome these effects, other delivery routes can be used. Local delivery to the skin or nasal passage for atopic/contact allergic reactions would confine the effect to the delivery area, eliminating the adverse side effects induced upon non-specific systemic delivery and absorption while still delivering effective concentrations to the affected organ for sustained action.

Numerous formulation approaches have been investigated and described in the literature in the realm of effective antihistamine delivery including [308, 336, 337]: nasal delivery through chitosan-derived microspheres [329, 338-342]; delivery by ethosomes [329], liposomes [340], poly(4-methyl-1-pentene), ethylene-vinyl acetate membranes and matrices [341]; and surfactants [343]. While these systems demonstrated desirable therapeutic effects, the formulations demonstrated rapid release within the first 24 hours, with some reporting the highest concentration after only 2 hours [340]. Further, the requirement for harmful and carcinogenic excipients such as plasticizers in the formulation approach [341], poor stability [127-130], and the low encapsulation efficacy, sometimes as low as 33% [329] reported for these formulations, leaves room for the development of sustained and more biocompatible delivery systems. Given what has already been discussed in section 1.5 of this thesis, the lipid cubic phase (LCP) systems may present an advantageous approach over traditional non-specific systemic delivery of such antihistamine molecules, especially those first generation and poorly soluble H_1 antagonists that are highly lipophilic in nature and can induce unwanted side-effects. The amphiphilic nature of the lipid cubic phase and its dispersions means it has the potential to encapsulate and release organic drugs and bioactives of different solubilities. Ibuprofen-loaded phytantriol systems demonstrated a relative oral bioavailability increase of 222% compared to the free drug with evidence of a longer half-life [344]. The mucoadhesive nature of the system should serve to improve the local retention time of the formulation to allow for sustained release [210]. Not only that, but LCP systems have been shown to enhance transdermal permeation of drugs [345], while the precursor lipids display inherent biocompatibility [1, 346]. The formulations are themselves non-allergenic with low toxicity of their digestive products [123]. Further, the uncomplicated manufacturing requirements of the systems, which generally do not necessitate the use of organic solvents [193, 194], mean

production costs may be reduced. These features, coupled with its thermostability and resistance against dilution, make the cubic phase and its dispersions appealing for drug delivery applications [195, 196].

The cubic phase has previously been investigated for its capabilities in transdermal and ocular delivery of active ingredients as a topically applied formulation [209, 213, 347] and have been shown to enhance transdermal permeation of drugs such as diclofenac sodium formulated in cubic systems of glyceryl monooleate [345]. This may be particularly relevant for CZH as it has proven effective in dermatological and nasal aspects [313, 348]. The nose has previously been investigated as an entry route for delivery of odorranalectin-loaded cubosomes, as a more direct route to the blood-brain barrier demonstrating an enhanced therapeutic effect [349]. However, little has been done in the way of a topical lipid delivery system to be applied on the mucosal lining on the surface of the inner nasal cavity. The aim of this investigation was to study the potential of the cubic phase, in its bulk and dispersed form, for use in the controlled delivery of various commercially available antihistamine molecules for potential use as a topical/local delivery system. *In vitro* drug dissolution was applied to study the extent and release rate of two model first-generation and two model second-generation H_1 antagonist antihistamine drugs from two monoacyglycerol-derived models (Figure 2.1). To optimize the formulation approach, the systems were characterized macroscopically and microscopically by small-angle X-ray scattering and polarized light to ascertain the mesophase accessed upon incorporation of the antihistamines of varying solubilities and size. The impact of encapsulating the antihistamine molecules in the lipid cubic systems on their mucoadhesion was also investigated using multi-parametric surface plasmon resonance (MP-SPR). Facilitated by a model cell system, the internalization and associated cytotoxicity of the dispersed cubic forms are discussed. With the ultimate goal of developing therapies for the treatment of allergic reactions, the ability of the formulations to inhibit histamine release from RBL-2H3 mast cells was explored.

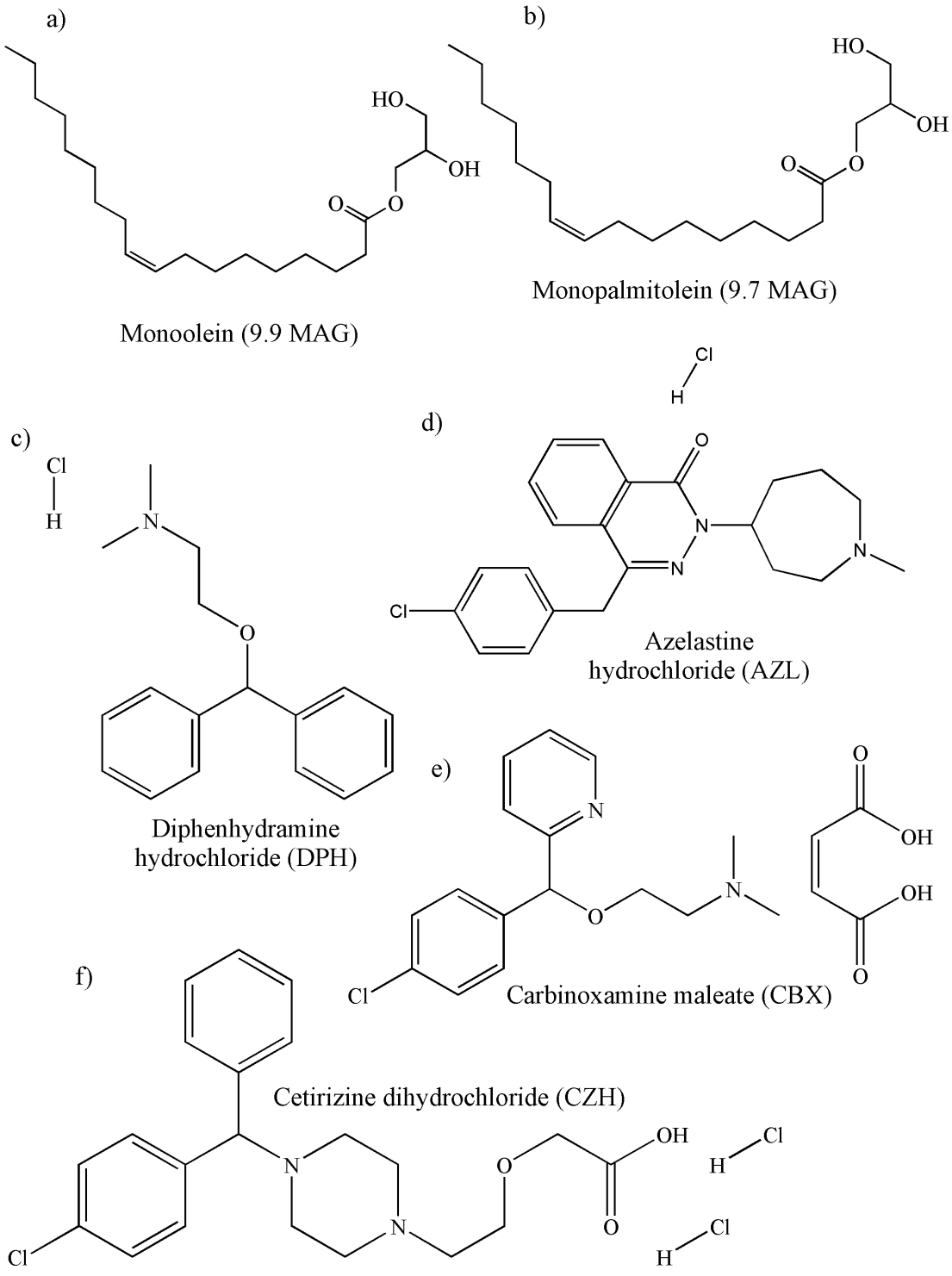

Figure 2.1. Chemical structures of: a) monoolein (9.9 MAG) and b) monopalmitolein (9.7 MAG) both possessing an ester linkage linking the oleic acid chain to the glycerol backbone; antihistamines c) diphenhydramine hydrochloride (DPH); d) azelastine hydrochloride (AZL); e) carbinoxamine maleate (CBX) and, f) cetirizine dihydrochloride (CZH)

2.3 Materials and Methods

2.3.1 Materials

All solvents were analytical grade and purchased from FisherScientific; Monoolein 9.9 MAG (1-(9Z-octadecenoyl)-rac-glycerol) and Monopalmitolein 9.7 MAG (1-(9Z-hexadecenoyl)-rac-glycerol) were acquired from JenaBioscience, Germany at >99% purity; Phosphate buffered saline (PBS) tablets were purchased from Merk (Saint Louis, MO); FaSSGF (Fasted state simulated gastric fluid) powder was purchased from Biorelevant.com Ltd; Water was purified in the lab using a Milli-Q Water System (Millipore Corporation, Bedford, MA); Lipase isolated from porcine pancreas was purchased from Merck, Germany (Type II, 100-500 units/mg protein (using olive oil (30 min incubation)); cetirizine dihydrochloride, azelastine hydrochloride, carbinoxamine maleate and, diphenhydramine hydrochloride were purchased from Merck, Germany at ≥98 % purity; Rabbit monoclonal [RM122] to IgE, rabbit IgG monoclonal [EPR25A] – isotype control, native human IgE protein (Azide free) and, the Histamine ELISA kit used were purchased from Abcam (Netherlands); RBL-2H3 rat basophilic leukemia cells (ATCC-CRL-2256) and Eagle's minimum essential medium (EMEM) were purchased from ATCC (United Kingdom).

2.3.2 Preparation of bulk Antihistamine-LCP matrix formulations

For preparation of LCP containing the water-soluble antihistamines (DPH, and CBX), the APIs were first dissolved in water with sonication to ensure complete dissolution. Fusion of dry lipid crystals to the melt was achieved between 40 - 45 °C in an oven to allow for more facile delivery of the lipid to sample vials. Appropriate volumes of molten lipid (Monoolein (MO) 60 mg/sample or Monopalmitolein (MPL) 50 mg/sample) were added to glass vials. The API-water mixture was then added to molten lipid in appropriate concentrations to access the lipid cubic phase and to deliver API at a concentration of 1 mg per 100 mg hydrated gel. The API-water mixture acted as the aqueous phase (≥40 wt% and ≥50 wt% for MO and MPL LCP respectively) according to their respective phase diagrams [1-3]. The more hydrophobic antihistamine molecules AZL and CZH (1 wt%) were added to the molten lipid prior to addition of MilliQ water acting as the aqueous phase. The samples were then subjected to vortex mixing for no less than 15 minutes. The homogeneous mixtures were stored in sealed glass vials and allowed to equilibrate in the dark for at least 48 hours.

Preparation of empty gels followed the same approach, without the addition of the respective APIs to the lipid/aqueous phase.

2.3.3 Preparation of cubic dispersions (cubosomes)

The method for the preparation of the cubosomes in this study followed that of Boge et al. with some minor modification [350]. MO LCP was formulated with the various antihistamines at a loading concentration of 1 wt% as described previously, before being subjected to fragmentation. The pre-loaded bulk gel (500 mg) was added to 20 ml of 1 wt% stabilizer Pluronic® F-127 solution prepared in PBS. Fragmentation was achieved by subjecting the LCP-stabilizer mixture to mixing using a magnetic stir bar followed by high shear homogenization at 14,000 rpm using a T25 digital ULTRA-TURRAX® disperser (IKA®-Werke GmbH & Co. KG, Germany) for 2 minutes. The samples were subjected to further fragmentation with an ATPIO ultrasonic microwave combined reaction system sonication probe operating at 40% of its maximum power on pulse mode (3 second pulses followed by a 7 second break) for an additional 5 minutes. The resultant opaline dispersions were stored in sealed glass vials. Antihistamine-loaded cubic phases were also dispersed in the absence of stabilizer to assess changes in physical properties of the systems.

2.3.4 Mesophase characterization

SAXS data collection

SAXS measurements were carried out after sample preparation (as described in sections 2.3.2 and 2.3.3) at the Solution State SAXS B21 beam line at Diamond Light Source on the Harwell Campus, Didcot, UK. The experiments used a beam of wavelength λ = 13.1 keV (~0.94644 Å) with a beam size at the sample of 1 mm x 1 mm. Data collection was performed at ambient temperature (20 °C). B21 utilizes a bending magnet source with a typical flux of approximately 4 x 10^{12} photons per second delivered directly to the sample. The photons were distributed over a large 0.8 x 2 mm cross-section which served to minimize radiation damage while also enhancing the signal of the particles. 2D diffraction images were recorded on an Eiger X 4M detector, with a detector face size of 155.2 mm x 162.5 mm and pixel size of 75 μm x 75 μm. The beam size at the detector was 50 μm x 50 μm. The detector was configured to measure a scattering vector (q) range from 0.0032 to 0.38 $Å^{-1}$. Samples were loaded into a custom 3-D printed sample holder designed

especially for viscous samples. The holder was 3-D printed from a mixture of methacrylic acid esters and photoinitiator comprising a window in which the sample was filled. The sample holder was made from stainless steel and had mica windows. Each sample was subjected to a 1 second X-ray exposure for 15 frames at one location and required manual loading.

SAXS data processing and analysis

Exposure of the lipid samples to the X-ray beam produced small angle diffraction images. The detector images were azimuthally reduced using DAWN, an eclipse-based workbench for carrying out scientific data analysis [351] and subsequently analysed using the lipidsaxs toolkit developed by Christopher Brasnett, University of Bristol, available at https://github.com//csbrasnett/lipidsaxs. The scattering intensity I (q) was represented as a function of the magnitude of the scattering vector according the equation:

$$\textbf{Equation 2.1: } q = \frac{4\pi \sin\theta}{\lambda}$$

where 2θ is the total scattering angle.

Lipid cubic phase structural dimensions calculations

Taking into account the space group, lattice parameter and water volume fraction of each of the different samples, the monolayer thickness and size of the water channels separating the lipid framework were determined as outlined by Szlezak, Nieciecka [212] and according to the following equations:

To compute the lipid volume fraction, first the water volume fraction was calculated according to:

$$\textbf{Equation 2.2: } \emptyset_{aq} = \frac{c_{aq}}{c_{aq} + (1 - c_{aq})(\frac{\rho_{aq}}{\rho_{MAG}})}$$

Where $\emptyset_{aq}$ is the volume fraction of the aqueous portion (0.386 and 0.496 for fully hydrated Q_{II}^{D} phase of MO and MPL respectively. and 0.416 and 0.584 when the dehydrated Q_{II}^{G} phase is seen for MO and MPL respectively [352, 353]), c_{aq} is the water weight fraction, ρ_{aq} denotes the

density of water (0.997 g cm^{-3}), and ρ_{MAG} represents the density of the MAG host lipid (0.942 g cm^{-3}[1, 2] for monoolein and 0.982 g cm^{-3} for monopalmitolein) [354].

By subtracting the water volume fraction from 1, the lipid volume fraction $\emptyset_{MAG}$ was determined [1]:

$$\textbf{Equation 2.3: } \emptyset_{MAG} = 1 - \emptyset_{aq}$$

From there the lipid monolayer thickness (l) could be extrapolated [354]:

$$\textbf{Equation 2.4: } \emptyset_{MAG} = 2A_o\left(\frac{l}{d}\right) + \frac{4}{3\pi\chi\left(\frac{l}{d}\right)^3}$$

Where A_o and the Euler characteristic χ are constants specific to the type of bicontinuous cubic phase related to the minimal surface area given in 2.2, d is the lattice parameter determined by SAXS for the phase in nm, and l is the lipid chain length or thickness of the assembled lipid monolayer.

Table 2.2. Surface area constants [151, 354]

	A_o	χ
Q_{II}^D	1.919	-2
Q_{II}^P	2.345	-4
Q_{II}^G	3.091	-8

Ultimately, the radius of the congruent aqueous channels (r_{aq}) within the network was calculated utilizing the calculated lipid chain length according to the following equation based on minimal surfaces [151, 212]:

$$\textbf{Equation 2.5: } r_{aq} = \left(\sqrt{\frac{-A_o}{2\pi\chi}}\right)d - l$$

Mucoadhesion studies

Mucoadhesion/bioadhesion of the cubosomes was evaluated using surface plasmon resonance (SPR; SPR Navi 200, BioNavis) in a similar manner to that described previously to investigate the mucoadhesive properties of block copolymer micelles [355]. Data was collected by instrument scientists at Bionavis, Tampere, Finland. Mucin-coated sensors were prepared using mucin from bovine submaxillary gland (M3895 SigmaAldrich). The coating was prepared according to the protocol proposed by Prosperi-Porta et al [355]. In brief, bare Au sensors for MP-SPR measurements were firstly cleaned using 1:1:5 (v/v) solution of $H_2O_2/NH_3/H_2O$ (10 min, 90°C). After thorough rinsing in MilliQ water and drying under nitrogen stream, the sensors were incubated in 100 µg/ml mucin solution for 24 h at room temperature in the dark. Mucin deposition was performed and measured in situ by MP-SPR (Appendix A). Based on the registered full SPR curves (not shown), the LayerSolver software by BioNavis enabled calculation of the optical thickness of the layers formed on the sensor surface. The calculated layer thickness was 3.88nm (± 0.11) resulting in surface coverage of 2.8 ng/mm^2 and refractive index of 1.41 (± 0.002) at 670 nm, which is typical for a glycoprotein layer. After mucin adsorption, the sensors were rinsed in water to remove any unbound residual mucin and sensors were stored dry until use.

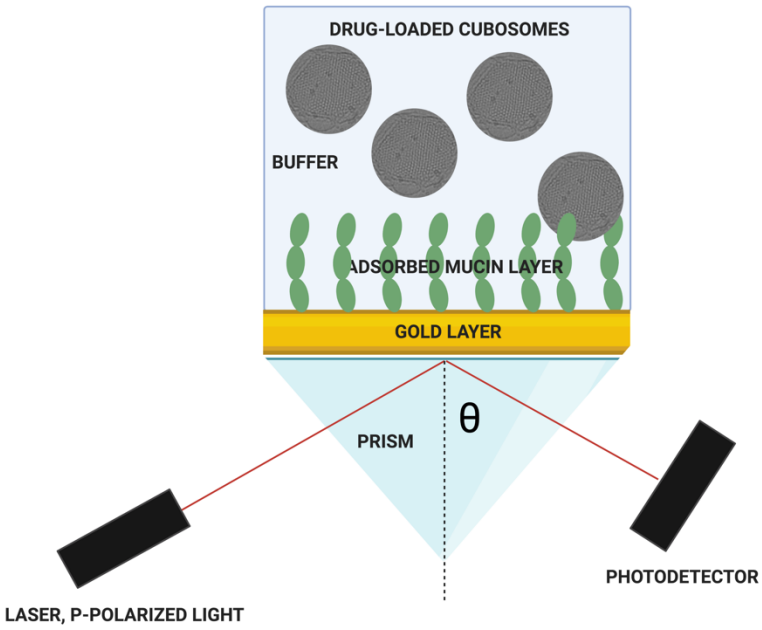

Figure 2.4. Schematic of SPR set-up for mucoadhesion studies showing the introduction of drug-loaded cubosomes onto the mucin-coated gold layer

Tests were performed using the MP-SPR 2-channel Navi 220A NAALI system equipped with two detection wavelengths (670 nm and 785 nm) with instrument injection loops set to 1000 µL volume. Samples were run at 37°C in PBS (pH 7.4) as running buffer. Empty cubosome test samples were added to PBS (pH 7.4) at a concentration of ~15 mg gel/mL. The flow rate was set to 20 µL/min for injection of cubosome samples and 50 µL/min for all washing steps. Before loading the samples, the sensor surface was pre-conditioned with short washing in CHAPS (3-[(3-cholamidopropyl)dimethylammonio]-1-propanesulfonate) detergent (20 mM, 1 min injection) followed by a 10 min baseline stabilization. Samples at a concentration of 1 mg/mL were subsequently loaded over a 40 min injection time to reach steady-state signal followed by 40 min PBS buffer flow to assess the dissociation phase. Samples were loaded in at least 3 repetitions, each injection separated by rejuvenation of the sensors by washing with CHAPS 20 mM solution (2 x 1 min injections at 50 µl/min). CHAPS provided sufficient surface regeneration and stable baselines between the samples.

2.3.5 Particle size estimation and zeta-potential studies [356]

Dynamic light scattering was utilized to estimate the particle size distribution (Z-average) and polydispersity (PDI) as well as the zeta potential (mV) of the cubic dispersions using PBS as the dispersant on a Zetasizer (Malvern Panalytical, United Kingdom) equipped with a 4 mW He–Ne laser (633 nm) which applies Brownian motion theories in its measurement. The viscosity of the dispersant was set at 0.8872 cP and the system was maintained at 25°C. Three measurements of 50 runs were taken for each sample and the mean value, along with the calculated standard deviation for particle size estimation (nm) were recorded using the Malvern Panalytical zetasizer software.

2.3.6 Drug release studies

PXRD

PXRD data were collected in reflection mode with an Empyrean diffractometer (PANalytical, Phillips) equipped with CuKα1,2 radiation (γ = 1.5406 Å) operating at 40 kV and 40 mA at room temperature. Samples were scanned between 2θ values of 5 and 40° at a step size of 0.01313° 2θ/s, 73 s per step.

Encapsulation efficacy

High performance liquid chromatography was used to quantify the encapsulation efficacy (EE%) of the antihistamine-loaded cubosomes. Freshly made cubosomes were removed from the dispersion media by centrifugation at 10 000g for 30 min. The concentration of free drug in the supernatant was then quantified by means of a chromatographic approach described below. The encapsulated drug could then be calculated as a % of the total added drug according to the following equation:

$$\textbf{Equation 2.6}: EE\ \% = \frac{Theoretical\ drug\ loading - free\ drug}{Theoretical\ drug\ loading} \times 100\ \%$$

Different buffers were investigated to study the release profiles of the four antihistamines from the LCP under different conditions of pH. Fasted-state simulated gastric fluid (FaSSGF) was prepared by dissolving pre-prepared simulated intestinal fluid (SIF) powder (Biorelevant.com) in acidic buffer (1.997 g NaCl in 1L water) adjusting the pH to 1.6 using 1M HCl with stirring according to the manufacturers guidelines. Simulated nasal fluid (SNF) was prepared as previously described by Farid et al. [357] (7.45 mg/mL NaCl; 1.29 mg/mL KCl; 0.32 mg/mL $CaCl_2.2H_2O$; made up to volume with deionised water) to give a solution pH of 6.4. The final buffer was phosphate buffered saline, prepared at pH 7.4.

The solubility of the four antihistamines were determined in the different release media studied. Excess amounts of each drug was added to 10 mL of media at 37 ºC with shaking at 150 rpm overnight. Undissolved drug was removed by filtration before the concentration of drug in each sample was determined after appropriate dilution by HPLC under the chromatographic separation conditions specified below.

The HPLC system used in this investigation was an Agilent 1200 Infinity Series (Agilent Technologies, Palo Alto, USA) comprising: G1311B 1260 quaternary pump, G1329B 1260 ALS autosampler, G1316A 1260 TCC (thermostated column compartment) and a G1365D 1260 MWD VL diode-array detector. The acquired data was processed with the Agilent OpenLAB CDS software. Chromatographic separations of antihistamine-containing samples were achieved using an Agilent Poroshell 120 PFP (3 x 100 mm, 2.7 µm) column fitted with a UHPLC Poroshell 120

guard module (3 x 5 mm, 2.7 µm). The system was maintained at 21°C with mobile phase delivered under isocratic conditions of 0.4 mL/min. The separation conditions for each antihistamine is described in 2.3. In all cases, mobile phase was delivered to the column at a flow rate of 0.5 mL/min. Samples were filtered through a 0.2 µm nylon filter (Fisherbrand®) and 8 µL injections were made.

Table 1.3. Chromatographic separation conditions for the various APIs

Antihistamine	Mobile phase (A:B)	Ratio (A:B)	Λ_{max} (nm)	Retention (min)
Diphenhydramine Hydrochloride (DPH)	Acetonitrile: 25 mM KH_2PO_4 (0.1 % Formic acid)	25:75	210	~ 4.8
Cetirizine Dihydrochloride (CZH)	Acetonitrile: 25 mM KH_2PO_4 (0.1 % Formic acid)	25:75	230	~ 14
Carbinoxamine maleate (CBX)	Acetonitrile: 25 mM KH_2PO_4 (0.1 % Formic acid)	20:80	260	~ 4.1
Azelastine Hydrochloride (AZL)	Acetonitrile: 50 mM KH_2PO_4	40:60	215	~ 4.9

All *in vitro* drug release testing of the antihistamines from the lipid formulations/dispersions was carried out in triplicate at 37 ± 0.1 ºC under shaking at 150 rpm. For bulk samples, over the course of the investigation at predetermined time-points the entire release media was withdrawn and the media was immediately replenished with freshly made stock. Release of the antihistamines from the cubosomal dispersions was tracked via dialysis. For this, the drug-loaded cubosomal dispersions were placed in Pur-A-Lyzer™ dialysis devices with a molecular weight cut-off of 6-8 kDa. Drug release was followed in 15 mL of each of the selected release media, where 1 mL of the sample media was removed at the predetermined time-points and immediately replenished with the same volume of fresh media. The dissolution samples were analyzed by means of a high

performance liquid chromatography (HPLC) method described previously to quantify the accumulated drug in solution.

Dissolution testing of the as-received free drug was carried out in parallel under the same conditions of temperature and agitation in Duran flasks containing 100 mL of the various biorelevant media under sink conditions. At pre-determined timepoints, 2 mL aliquots of the dissolution media were removed using preheated syringes (37 ºC) and immediately replaced with pre-warmed fresh media. Drug concentration was determined by means of HPLC after filtration through 0.2 µm filters and calculations took dilution factor into consideration.

2.3.7 Cell culture methods

NIH-3T3 cells were grown in Dulbecco's Modified Eagle's Medium (DMEM) (with sodium pyruvate) supplemented with 10% v/v fetal bovine serum (FBS), 1 % v/v L-glutamine, and 1 % penicillin-streptomycin at 37°C in humidified air containing 5 % CO_2. RBL-2H3 cells were cultured Eagle's Minimum Essential Medium (EMEM) (ATCC® 30-2003™) supplemented with 15 % v/v heat-inactivated fetal bovine serum (FBS) and 1% penicillin-streptomycin at 37°C in humidified air containing 5% CO_2.

2.3.8 Cell viability study: Cytotoxicity

The cytotoxic effect of the monoolein-based cubosomes formulated with and without the four antihistamine molecules was assessed by an MTT assay in NIH-3T3 and RBL-2H3 cells. Cells were plated in 96-well plates at a seeding density of 5 x 10^3 cells/well. Cells were allowed to reach confluence over 2 days before the experiments were carried out. The cells were then treated with cubosomes at a concentration of 100 µg/mL and incubated at 37°C for 24 h and 48 h. After the incubation period, the MTT reagent (3-(4,5-Dimethylthiazol-2-yl)-2,5-diphenyltetrazolium bromidefor) was added to samples for 2 h at 37°C. The MTT formazan crystals were then dissolved by solubilisation buffer (10% SDS in 0.01 M HCl) followed by further incubation for 4 h at 37 °C. The absorbance was read using a multi-well microplate spectrophotometric reader at 570 nm. Cell viability was determined as the percentage of absorbance values of treated cells to absorbance values of untreated control cells. A ratio of percentage reduction of cell viability relative to that of

control cells was used to express the obtained data. All measurements were carried out in at least triplicate.

2.3.9 Cellular uptake of cubosomal formulations

The difference in zeta potential between mammalian cells and the drug-loaded cubosomes was utilized to track the fusion and uptake of the lipid nanoparticles over time. Mammalian fibroblast cells (NIH-3T3) were selected as the model system. Cells were seeded in 6-well plates at a seeding density of 3 x 10^5 cells/well. Cells were allowed to reach confluence over 2 days before the experiments were carried out. The cells were then incubated in the presence of the various antihistamine-loaded MO cubosomes at a concentration of 100 µg/mL for different lengths of time (30 minutes, 2 hours, and 12 hours). The cells were harvested after this predetermined time by trypsinization, and the cell pellets were resuspended in 1mL of fresh DMEM media. The zeta potential of the treated cells was measured as previously described and compared against that of the untreated cells.

2.3.10 Anti immunoglobulin E- (IgE-) induced histamine release studies

RBL-2H3 cells were exposed to blank and antihistamine loaded cubosome formulations after IgE treatment and histamine release was tracked in a manner similar to that described previously [358]. Cells were seeded in 24-well plates at a seeding density of 1 × 10^6 cells/well. Cells were allowed to reach 90% confluence overnight before treatment. After this period, the media was aspirated away and replenished with fresh media containing 0.2 µg/mL IgE. Cells were incubated in the antibody media for 1 hour at 37°C. The media was once again aspirated away and cells were washed with release buffer (1 mM $CaCl_2$, 40 mM NaOH, 0.1% BSA, 119 mM NaCl, 5 mM KCl, 5.6 mM glucose, 25 mM piperazine-N, N-bis (2-ethanesulfonic acid) (PIPES), and 0.4 mM $MgCl_2$). The washed cells were subsequently treated with release buffer containing 1.25 µg/mL anti-IgE along with 100 µg/mL of the blank or antihistamine-loaded cubosome formulations . Cells were incubated for a further 10 minutes at which point the media was removed and the concentration of released histamine was determined by means of a competitive histamine enzyme-linked immunosorbent assay (ELISA) kit. Samples were diluted appropriately before analysis.

2.4 Results and Discussion

2.4.1 Mesophase characterization

There currently exists a wide range of host lipids capable of forming the cubic phase available commercially [161, 167, 172-175]. In this study two naturally occurring monoacylglycerol lipids, monoolein (MO) and monopalmitolein (MPL) have been selected to form cubic systems. Both host lipids are GRAS (Generally regarded as safe) listed digestive products of triglycerides present in the gastrointestinal tract, and were selected here on account of their biodegradable nature and inherent ability to maintain the cubic phase under physiological conditions [173, 352].

As described in chapter I, section 1.4, cubic phases are distinguishable by their discrete crystallographic space groups. Three inverse bicontinuous cubic phases exist; primitive (Q_{II}^{P}), gyroid (Q_{II}^{G}), and double-diamond (Q_{II}^{D}) with symmetry values of 229, 230, and 224 respectively. The MAG-water system typically accesses two types of cubic phase under equilibrium at room and body temperature depending on the level of hydration [177]. At lower water concentrations the gyroid or 'Q_{II}^{G} ' cubic phase is accessed and when hydration levels are increased the phase transitions to the more swelled and stable diamond cubic (Q_{II}^{D}) phase. The Q_{II}^{D} phase is stable against dilution and maintains its architecture when the water content is increased further to excess levels. The SAXS data collected at Diamond Light Source in the UK was analysed for mesophase characterization and dimensional analysis of the bulk and dispersed systems, with and without incorporated antihistamine molecules (at a loading concentration of 1 wt%) to investigate if the incorporation of the antihistamine molecules had altered the internal structure of the lipid systems. All samples, with and without the drug molecules, were found to exist in the cubic phase (Table 2.4 and Appendix A). Compatible reflections in the collected data were utilized and the absolute values were indexed to calculate the lattice parameter of bicontinuous cubic phase samples. As discussed in the introduction, CBX and DPH, being quite soluble in water, may preferentially reside in the water channels of the cubic phase, while the more lipophilic agents CZH and AZL may likely integrate into the lipid portion of the system.

Table 2.4. Phase identification and lattice parameters of assigned mesophases for bulk LCP loaded with different antihistamine APIs (1 wt%) from SAXS experiments with calculated dimensional values for lipid chain length (L) and water channel diameter (D_{H2O})

Host Lipid	API	Assigned mesophase	Lattice Parameter (nm)	L (nm)	D_{H2O} (nm)	Bonnet ratio (where applicable)
MO	-	Q_{II}^{D}	10.3	1.75	4.55	-
MO	DPH	Q_{II}^{D}	11.29	1.93	4.97	-
		Q_{II}^{D}	12.661	2.16	5.57	
MO	CBX	Q_{II}^{D}	11.818	2.01	5.22	-
MO	CZH	Q_{II}^{D}	10.467	1.78	4.61	-
MO	AZL	Q_{II}^{D}	10.797	1.84	4.75	-
		Q_{II}^{D}	12.047	2.05	5.31	
MPL	-	Q_{II}^{D}	11.41	1.56	5.8	-
MPL	DPH	Q_{II}^{D}	11.731	1.61	5.95	-
		Q_{II}^{D}	13.252	1.81	6.74	
MPL	CBX	Q_{II}^{D}	11.931	1.63	6.06	-
		Q_{II}^{D}	13.467	1.84	6.84	
MPL	CZH	Q_{II}^{D}	10.976	1.5	5.58	1.27
		Q_{II}^{G}	13.967	1.39	4.15	
MPL	AZL	Q_{II}^{D}	11.907	1.63	6.05	-
		Q_{II}^{D}	12.998	1.78	6.6	

Table 2.4 reports the assigned mesophases and their structural parameters for bulk antihistamine-loaded systems calculated from the collected 1 and 2D SAXS patterns, where sharp Bragg reflections indicative of long-range order were seen. For the majority, a cubic phase of crystallographic space group Q_{II}^{D} was accessed, with slightly larger lattice parameters (L) identified

than those previously reported [359, 360]. The more hydrophilic drugs, DPH and CBX, were expected to locate comfortably in the aqueous channels of the phases, defined as 4.55 nm and 5.8 nm for blank MO and MPL LCP respectively, both of which were prepared with water only. Hydrophobic molecules have the potential to disrupt the lipid bilayer network and induce phase transitions [361, 362] by integrating into the lipid bilayer and altering the liquid crystalline structure. The data collected for the MPL_CZH formulation highlighted coexisting inner cubic structures of $Q_{II}^{D} + Q_{II}^{G}$ spacegroup upon the incorporation of the hydrophobic molecule. However, when hydrophobic AZL was incorporated in the lipid cubic network Q_{II}^{D} symmetries prevailed. These bicontinuous cubic phases both conform to minimal periodic surfaces and their identification is achieved with the mid-plane of the membrane bilayers [146, 363, 364]. When equilibrium is reached, the average Gaussian curvatures of both phases should approach equal. A ratio known as Bonnet relation/ratio relates the unit cell parameters of the coexisting bicontinuous cubic phases with a theoretical value of 1.279 for Q_{II}^{G}/Q_{II}^{D} [363, 365-368]. In the case of the observed coexistence here where CZH is encapsulated in the lipid bilayer of the MPL system, the calculated Bonnet ratio of 1.27 is in excellent agreement with this proposed theoretical value.

Larger water channels were noted across all specimen relative to the blank systems, indicating swollen lipid systems. A more pronounced effect was noted when the highly water soluble DPH and CBX were incorporated into the aqueous conduits of the phase, with a lesser effect noted in the more hydrophobic molecules AZL and CZH. The presence of small and broad unassignable peaks in some samples could not be related to any cubic symmetry so it is unclear whether these relate to an intermediate/transitioning phase as has previously been described in a monoolein system [369]. Such intermediates exist at temperatures below 33ºC and are not accounted for in the lipidsaxs script .

The fully hydrated lipid cubic phase is resistant to dilution, maintaining its structural integrity even in excess water. However, when the bulk phase is fragmented, the resulting cubosomes are not stable long-term in aqueous solution because of the hydrophobic portions that are exposed at the particle surface as a minimal surface. Introducing amphiphilic copolymers that adsorb to the cubosome's surface reduces the interfacial free energy between the cubic phase and the water phase while maintaining the internal nanostructure of the phase [370]. Further, the weak electrostatic charge on the surface of the cubosomes (discussed later) lends a need for a suitable

stabilizer to reduce agglomeration of the dispersions. The accumulation of Pluronic F-127 on the external surface of the cubosomes has demonstrated enhanced steric stabilization of cubosomes in aqueous solution dispersions [146, 233, 234], and in particular those produced using monoolein, where a small amount of the stabilizer can also be incorporated into the internal labyrinth of the water channels [371].

In this investigation, pre-loaded sub-micron particles were produced through high energy homogenization and sonication of the bulk phase. As the differences in release properties between MPL and MO was minor, monoolein alone was selected to investigate the behaviour of antihistamine cubosomes, on account of its slightly more controlled release properties overall (section 2.4.6 below). In a similar way to that described for the bulk systems, SAXS was employed to reveal the architecture of theses MO lipid dispersions (Table 2.5) of predicted cubic symmetry. A similar trend in lattice parameter changes was seen across the cubosome samples compared to the corresponding bulk formulations, where calculated lattice parameter followed the trend CBX>DPH>AZL>CZH.

Table 2.5. Phase identification and lattice parameters of assigned mesophases for MO cubosomes loaded with different antihistamine APIs (1 wt%) from SAXS experiments

Host Lipid	API	Assigned mesophase	Lattice Parameter (nm)	L (nm)	D_{H2O} (nm)	Bonnet ratio (where applicable)
MO	CBX	Q_{II}^{D}	10.79	1.83	4.77	-
MO	DPH	Q_{II}^{D}	10.66	1.82	4.69	-
MO	CZH	Q_{II}^{D}	9.43	1.61	4.15	-
MO	AZL	Q_{II}^{D}	10.57	1.8	4.66	1.28
		Q_{II}^{G}	13.53	1.43	3.85	

A single Q_{II}^{D} symmetry was assigned for the DPH, CZH and CBX systems. The cubosomes maintained the cubic phase of the bulk systems from which they were conceived, with only minor reductions in unit cell parameter values calculated. An efficient concentration of the stabilizer can

halt transitions between the Q_{II}^{D} and Q_{II}^{G} structures [234, 372] while co-existence has been widely observed in cubosomal dispersions owed to the fluid and dynamic nature of their inner organization when fully hydrated [171, 372]. However, coexisting inner cubic structures of $Q_{II}^{D} + Q_{II}^{G}$ symmetries were identified upon indexing of the diffraction peaks for the MO_AZL cubosomes, with the calculated Bonnet ratio (1.28) in agreement with the theoretical values laid out. This coexistence may be influenced by the addition of the stabilizer which has been shown to stabilize the other cubic symmetries in some systems [192, 370, 373]. Pluronic F127 is a triblock copolymer consisting of two poly(ethyleneoxide) blocks as hydrophilic parts and a poly(propylene oxide) block as a hydrophobic part. It is possible that hydrophobic interactions between the F127 and the AZL destabilise portions of the Q_{II}^{D} leading to dehydration of the system and a transition to the $Q_{II}^{D} + Q_{II}^{G}$ symmetries. Several other suitable stabilizers have been reported in the literature and Pluronic 108 for example, was reported to coat only the surface of cubic nanoparticles without penetrating the internal structure of the system [374]. This may be a suitable alternative in this case to avoid potential interactions between the stabiliser and the drug that may induce unwanted phase transitions.

2.4.2 Properties of Cubic dispersions: Zetasizer Studies, encapsulation efficacies

The monoolein cubosomes were loaded with the antihistamines at a theoretical concentration of 1 wt%. HPLC was used to quantify the encapsulation efficacy (Table 2.6) by quantifying the amount of free drug in solution after the dispersion process. Encapsulated drug was then estimated according to equation 2.6. It is apparent that a better association between the lipid system and drug is seen in the cases of the hydrophobic agents, where loading efficacies of >93% were calculated for both AZL and CZH. Slightly lower encapsulation efficacies (87-90%) were calculated for the hydrophilic drugs which are mainly present in the water channels of the cubic network with little interaction at the lipid bilayer.

The particle size and zeta potential of the antihistamine-loaded cubosome formulations prepared with and without stabilizer Pluronic® F-127 are shown in table 2.6. Evaluation of the zeta potential of lipid nanoparticles aids in the prediction of their stability, tendency to aggregate (greater charge means stronger electrostatic repulsion between particles) [375, 376], performance, and cellular uptake *in vivo*. Modification of the cubosomes through incorporation of additives/APIs, or

alterations in surface chemistry, can alter the surface charge of the dispersions and, by default, their performance.

Samples prepared in the absence of Pluronic® F-127, demonstrated a large variation in nanoparticle size between the different samples encapsulating the four antihistamine molecules. The zeta potential results showed that both the blank and antihistamine-loaded cubosomes carried a negative charge. This has previously been associated with trace free fatty acids contaminating commercially available MAG lipids. These may carry a negative charge when ionized and alter the overall cubosome charge upon adsorbing onto its surface [377]. The lipids used here report purity >99%, but the potential of free oleic acid is still there. Zeta potential is taken as the overall charge the cubic nanoparticles acquire in a given dispersant and is a measure of the magnitude of repulsive/attractive forces between nanoparticles and serves as an efficient indicator of the storage stability of nanoparticles. The overall zeta potential of the samples was less than 30 mV in magnitude across the board and so the stability of the samples is likely reduced [378, 379].

Table 2.6. Properties of Antihistamine-loaded cubosomes measured within 1 hour of preparation

Pluronic® F-127 stabilizer	Drug	Theoretical drug loading (wt%)	EE (%)	Size ± SD (nm)	PDI	Zeta potential (mV)
0 wt%	-	-	-	182.7 ± 0.1	0.237	-6.86 ± 0.15
	DPH	1	87.48 ± 1.4	301 ± 23	0.38	-11.8 ± 0.96
	CBX	1	90.5 ± 1.2	289.3 ± 9.8	0.225	-2.94 ± 0.99
	AZL	1	93.12 ± 0.7	271.3 ± 19.6	0.199	-25.87 ± 0.54
	CZH	1	94.85 ± 0.7	152.8 ± 12	0.288	-15.47 ± 0.17
1 wt%	-	-	-	133.9 ± 0.1	0.247	0.969 ± 0.05
	DPH	1	87.48 ± 1.4	135.4 ± 1.2	0.193	7.54 ± 0.27
	CBX	1	90.5 ± 1.2	140.6 ± 4.5	0.165	4.6 ± 0.14
	AZL	1	93.12 ± 0.7	140.1 ± 2.3	0.169	17.4 ± 0.01
	CZH	1	94.85 ± 0.7	147.1 ± 4.9	0.225	2.08 ± 0.22

Particle size and ZP data was also collected for samples prepared with the commonly used stabilizing additive F127 (Table 2.6). The particle sizes of all cubosomes generated were in the nanosized range. The size varied slightly among the different encapsulated APIs compared with the blank system, with larger particle size ranging between ~ 135 and 147 nm. All samples displayed PDI values less than 0.23 and a size reduction of up to half with greatly reduced standard

deviation compared with the systems prepared without F-127. This result is in agreement with published data [234, 380, 381]. The surface charge also varied between the cubosomes loaded with different antihistamines, and in stark contrast to the negative charge recorded for the unstabilized samples, the study revealed positively charged cubosomes in all cases. This study identifies the positive impact of including the stabilizer on achieving cubic dispersions within the desired size range as nanoparticles of size <200 nm have shown improved cellular uptake over larger systems [245-247] and distribution displaying a reduced propensity to aggregate in solution. The stability of the cubosome-stabilizer systems was confirmed over a 5-day storage period, where no change is nanoparticle size was observed. Pluronic® F-127 has previously been shown in the literature to physically stabilize the colloidal cubic phase for months [382] so it is reasonable to predict a more lengthy stability period than shown here. The positive surface charge associated with the samples was predicted to further improve cellular uptake of the drug-loaded samples as cationic polymers form complexes and bind with the negatively charged plasma membrane of the cells to a higher degree than negatively charged or neutral molecules [383].

2.4.3 Cellular uptake of cubosomes [384]

As a means of studying the time-dependant interaction and possible uptake of the formulated cubosomes by cells, changes in the zeta potential of NIH-3T3 fibroblast cells incubated with the formulations were tracked over 12 hours. It has been described that positive or weakly negative charged nanoparticles should show enhanced cellular uptake [385, 386] on account of the negative zeta potential on the cell surface giving rise to strong electrostatic interactions with the with the negatively charged membrane. Previous reports showed that a 12 hour incubation with nanoparticles was sufficient for the cells to fully take up the dispersions; identified by an initial change and then stabilization of the of the cells back to that of the untreated cells after the nanoparticles were bound and subsequently internalized [384]. In this study, the cells were incubated with MO cubosomes for 30 minutes, 2 hours, and 12 hours before the zeta potential was measured and compared to that of the untreated cells.

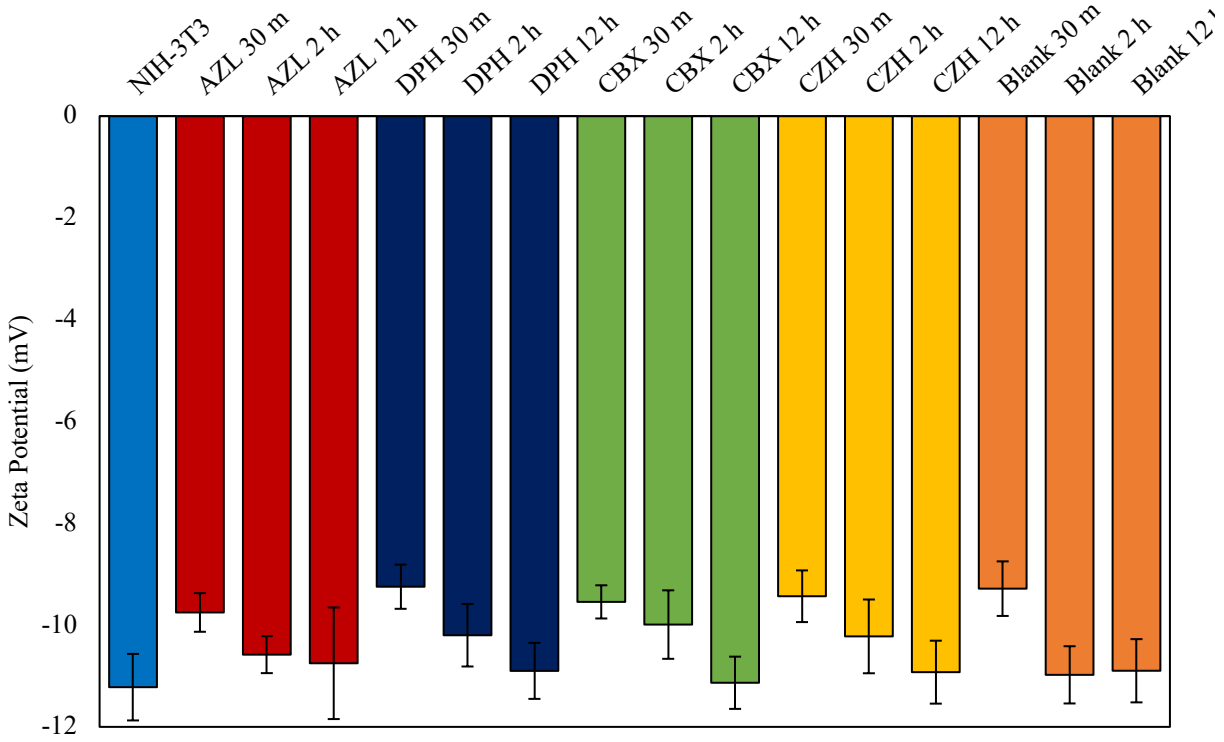

Figure 2.3. Zeta potential of NIH-3T3 cells treated with 10 µg/ml of MO cubosomes formulated with antihistamine molecules measured in DMEM media after 30 minutes, 2 hours, or 12 hours

Figure 2.3 shows the shifts in zeta potential of the NIH-3T3 cells incubated with the cubosomal formulations. After 30 minutes, a shift towards a less negative surface charge was noted across all samples compared to that of the untreated cells. This shift may signify the binding of the positively charged cubosomes at the cell surface, reducing the overall negative charge of cell membrane through electrostatic interactions [387]. When nanoparticles interact and adsorb onto the cell membrane, changes in zeta potential are seen as the adsorption of ions surrounding their surface and the surface of hydrodynamic shear and particle mobility are altered [384]. Uptake through the cell's plasma membrane after adsorption can occur by means of different mechanisms including phago- or endocytosis [384, 388]. Endocytosis is the process commonly observed in the internalization of nanoparticles, soluble molecules, proteins, and lipids [389-391] and is an energy dependent process [390, 392, 393]. The mechanism may be either non-specific or receptor mediated and has been widely described in the uptake of cubosomes [394-396]. After the 12 hour

exposure to the cubosomes, the zeta potential returned to a more negative value and approached that of the untreated cells, suggesting that the adsorbed cubosomes could have been taken up by the cells after this time. While these alterations in zeta potential suggest the uptake of the cubosomes by the cells, it is important to acknowledge that a volume of drug may be released prior to internalization, as described in the release profiles in section 2.4.6. In this case, the drugs would likely disperse in the surrounding tissue at the delivery site [390].

2.4.4 Cytotoxicity study

Monoolein-based cubosomes formulated with each of the four studied antihistamines were evaluated for cytotoxic effect in NIH-3T3 fibroblast cells and RBL-2H3 basophilic leukemia cells as a model by means of an MTT assay. While positively charged nanoparticles have been reported to improve drug delivery efficacy, an increase in the cytotoxic effect of these formulations has also been reported [397].

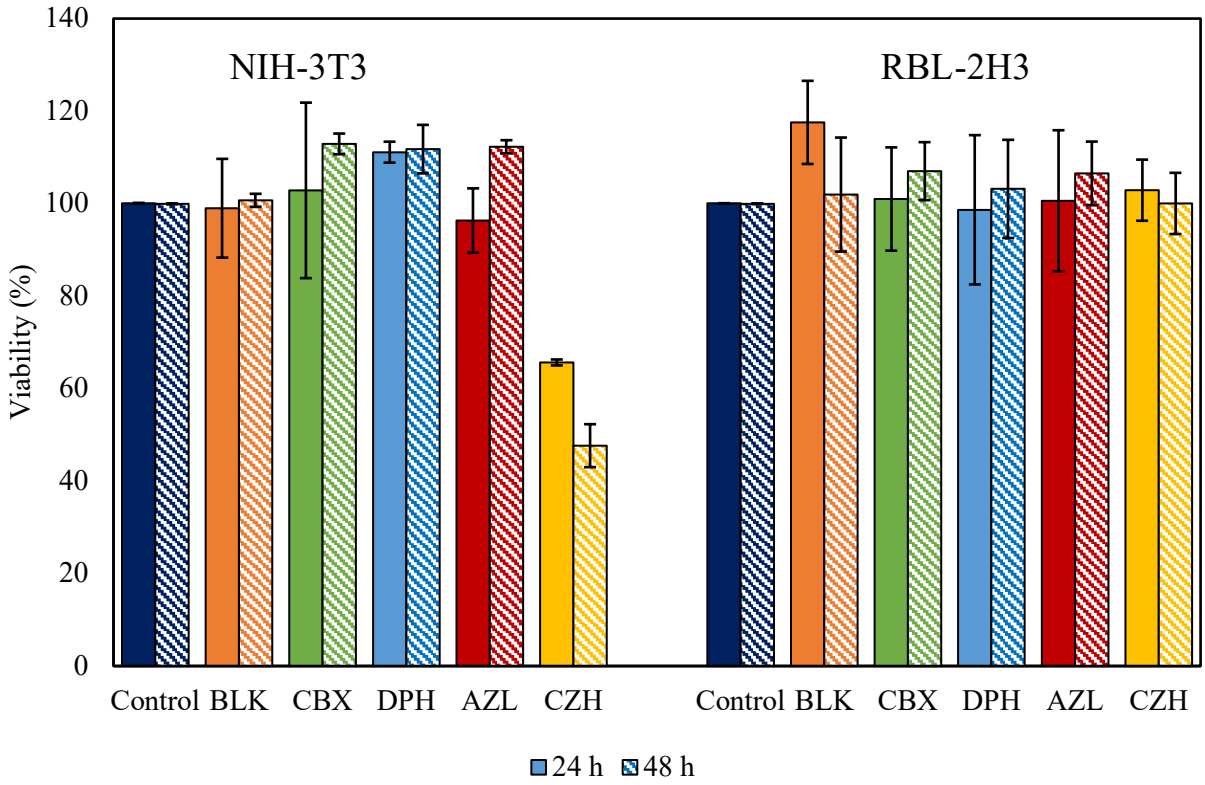

Figure 2.4. Cell viability, expressed as percentage of the control absorbance at 570 nm, induced in NIH-3T3 and RBL-2H3 cells after incubation for 24 h and 48 h in the presence of MO

cubosomes (delivered at ~100 µg/mL). formulated with and without antihistamine molecules. Data are expressed as a mean ± standard deviation (SD) of three independent experiment (minimum n=3).

Treatment with the lipid cubic dispersions containing antihistamine molecules did not appear to significantly negatively impact cell viability in the case of the RBL-2H3 samples, Figure 2.4 in agreement with published data [398, 399]. Similar results were observed in the case of the NIH-3T3 cells with the exception of those treated with CZH-loaded cubosomes when compared to the control system after 24 or 48 hours, at which point approximately 20 % of the loaded drug should have been released into solution (Figure 2.9 – drug release curve). Treatment with CZH at similar concentrations has previously been shown to be cytotoxic against epithelial cell lines [400]. However, a separate study by Salimi et al. studied the cytotoxic effect of a gradient of CZH concentrations on Chang cell lines and showed that concentrations of almost 200 times more than were studied here were required to induce cytotoxicity to the degree reported here [401]. That said, the Chang cells were only assessed over a 6 hour exposure period, where a reduction in viability over time was seen. These published studies further serve to highlight the variation in cell line sensitivity to the antihistamine, in agreement with the differences in tolerability shown here. Further, it is possible that the cubosomes have facilitated improved cellular uptake of the drug as reported in the literature [241, 396] and may also explain the increased toxic effect here. Regardless, the obtained results are in agreement with literature confirming the biocompatibility of monoolein-based cubosomes [396, 402] and the reduction in viability is likely owed to the encapsulated drugs.

2.4.5 Mucoadhesion studies

The high viscosity of the in situ formed cubic phase may facilitate its bioadhesive properties, which were demonstrated by Nielsen et al. [210] in proposing cubic phases of glyceryl monooleate (GMO) and monolinoleate as bioadhesive mucosal drug delivery systems. GMO itself is readily digested in the gastrointestinal tract presenting its bioadhesive properties [403]. In fact, the literature reports that GMO-based cubic phase gels have proven their ability to adhere to rabbit jejunum and have also been found to interact at a surface level in the vaginal cavity for a period of 6 h [210]. Targeting mucosal layers for targeted delivery has the advantage of overcoming the first

pass effect otherwise seen with enteral delivery routes to improve bioavailability and would provide a means for local delivery of antihistamine molecules to overcome the associated unwanted side effects of these molecules when systemically administered (especially 1st generation H_1 antihistamines) [404-408].

Here, MP-SPR was used to investigate the mucoadhesive nature of the antihistamine-cubosomes by studying their interaction with a mucin protein coated surface using unloaded monoolein cubosomes as a positive control for mucoadhesive comparison (Figure 2.2). Mucin is a highly glycosylated polymeric protein excreted [409] by goblet and submucosal glands and constitutes between 2-5% of the composition of the protective mucosal layer [410]. The highly entangled network of the mucin fibres are responsible for the sticky adhesive nature of the mucus [411] and provide a means for modelling the adhesive nature of our systems *in vitro*. The results obtained from this *in vitro* mucoadhesion investigation provide an estimate of cubosome residence time at a given mucosal site of administration [88].

The cubosomes formulated with or without antihistamine molecules exhibited relatively reproducible adsorption kinetics profile as observed from triplicate injections of the dispersed samples over mucin-coated sensors (Appendix A). Figure 2.5 represents an overlay of average sensograms registered for each sample. Equilibrium is reached within 40 minutes of injection. The data presented quite distinct behaviour between the different cubosomal formulations toward the mucin layer. The MO_AZL samples displayed the highest binding level at a constant concentration of 1 mg/mL even as compared to the reference MO_Blank (unloaded cubosomes) suggesting greater mucoadhesion. The MO samples loaded with DPH displayed a much lower binding capacity to mucin – displaying an equilibrium state signal 3-fold lower than the strongly bound MO_AZL sample. Compared to the MO_blank sample, the MO_CBX formulation also displayed reduced binding and, despite slower association, the MO_CZH could be considered to have similar binding efficiency to the reference. Differences in zeta potential were also thought to play a part in the variations in mucoadhesion, as the oligosaccharide chains of the mucin glycoprotein confer negative charge to the protein through carboxyl and sulfate groups [412]. The AZL system displayed the strongest positive charge, which also represented the strongest binding. Based on surface charge, the mucoadhesivity trend was expected to follow that DPH > CBX > CZH. However, it appears that DPH system displayed the lowest degree of binding and CZH cubosomes

were second in line to the AZL system. Based off these findings, the differences may be attributed to the nature and effect of the encapsulated antihistamine molecules themselves, with the hydrophilic molecules seemingly causing a greater reduction in binding when compared to the blank system. This may be due to the additional bonding and hydrophobic interactions between the lipophilic drugs and hydrophobic segments on the mucin glycoprotein.

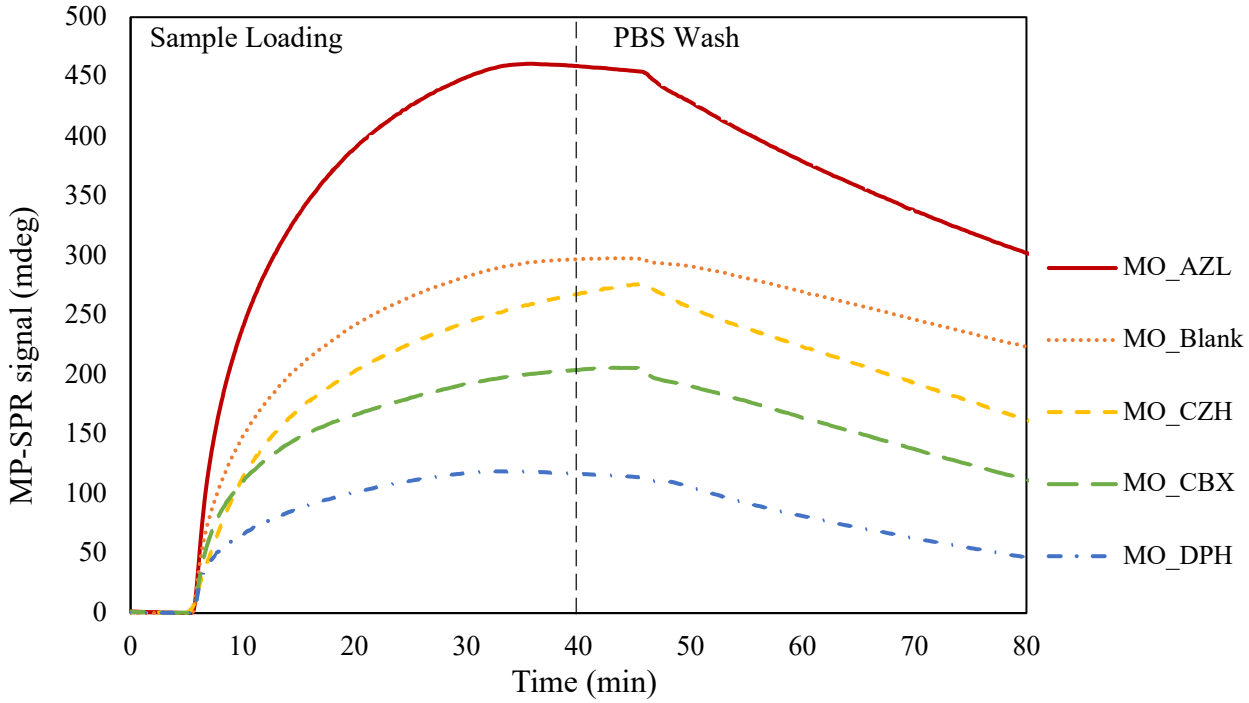

Figure 2.5. Kinetics of adsorption onto mucin-coated sensors measured for 5 tested cubosome formulations. Each sensogram is average MP-SPR signal from triplicate sample injections measures at 670 nm.

Despite a higher binding intensity observed in the case of the AZL loaded cubosomes, a faster rate of dissociation indicated by the slope of the reduction in relative intensity after the washing step was noted compared to the other formulations. This decline in intensity can be taken as representative of the stability of the adsorbed layer [413]. Regardless, the mucoadhesive nature demonstrated for these formulations support their potential to prolong the retention of an encapsulated drug molecule at the target site for improved bioavailability and is comparable to the mucoadhesion of other DDS including pectins [414] and hyaluronic acid-coated niosomes [415].

The kinetic profiles showed various binding level at equilibrium but also different behaviour in association/dissociation phases. Although the cubosome injection concentration was not varied, an attempt was made by the team at Bionavis at calculating local kinetic parameters (K_D, k_a and k_d) using the TraceDrawer™ software for BioNavis. The obtained values (Table 2.7) confirm differences in maximum binding levels (R_{max}) and distinct association/dissociation constants between the various monoolein samples. It is noted that in common practice, kinetic parameters should ideally be calculated against multiple concentration responses which will be the object of further studies.

Table 2.7. Calculated kinetic values obtained from TraceDrawer™ for MP-SPR instruments*. Fitting was performed according to One-to-Two interaction model on the measured sensogram for 1mg/mL concentration i.e., 2.8mM (monoacylglycerol lipid content)

	MO_Blank	MO_DPH	MO_CZH	MO_AZL	MO_CBX
Rmax [mdeg]	**330**	**173**	**433**	**525**	**247**
ka1 (1/(M*s))	1,27E+00	4,46E-01	1,10E-01	4,07E-01	3,19E+07
kd1 (1/s)	**4,65E-05**	**4,04E-04**	**1,31E-04**	**2,17E-05**	**9,15E-05**
KD1 (M)	4,70E-05	9,06E-04	1,19E-03	5,34E-05	2,86E-12
ka2 (1/(M*s))	1,02E+00	4,09E-01	6,64E-01	1,06E+00	4,97E-01
kd2 (1/s)	2,08E-04	5,40E-04	2,91E-04	3,78E-04	3,01E-04
KD2 (M)	2,29E-04	1,32E-03	4,38E-04	3,57E-04	6,05E-04
Chi2 (mdeg^2)	8,71	24,16	15,26	27,85	29,29

*The best fitting was obtained for One-to-Two binding model which might be the closest theoretical model considering mucin layer with virtually different binding sites to the injected analyte. In this context a model where one ligand would bind at least two different binding sites on the surface is considered.

SPR studies were performed initially at 37°C but to investigate the impact of temperature on the mucoadhesion of samples, two samples (MO-CZH and MO-DHP) were run under conditions closer to room temperature (22°C). The resultant sensogram (Appendix A) highlights the direct effect of experimental temperature on cubosome binding to the mucin layer. Both tested samples exhibited reduced binding as a result of the decrease in temperature that may be explained by changes in the mucin-layer structure and properties. Through hydrogen bonding, electrostatic and hydrophobic interactions, and weak Van der Waal forces, mucin molecules cross-link in solution

to form aggregates. As the number of these cross-links increase, the protein aggregates form viscous adhesive gels, an effect that is greatly influenced by temperature [416, 417].

Adhesion of the systems to the mucosal layer increases drug residence time for absorption that might otherwise be cleared through mucociliary clearance [19, 405, 418, 419].

2.4.6 Drug release studies

The solubility of the antihistamine molecules at 37°C was studied in the different biorelevant media, and the variations in solubility at different pH are shown in table 2.8. There is an obvious increase in solubility of the drugs as the pH becomes more acidic from the PBS at 7.4, to the SNF at pH 6 and further to FaSSGF at pH 1.6. This trend is seen across all of the antihistamine molecules as determined by HPLC. This may be related to their associated pKa values (Table 2.8). AZL [420], DPH [421], and CBX [422] are weak bases and under acidic conditions are protonated and in turn are more polar thus increasing their solubility. This trend is shown in Table 2.8, where decreasing the pH towards a more acidic environment increases the saturated solubilities of the drugs. CZH is considered a weak acid [423] but under acidic conditions is considered to be zwitterionic.

Table 2.8. Saturated solubility of the model antihistamine drugs

Antihistamine	**pKa value**	**Solubility in PBS Buffer pH ~7.4 (mg/mL)**	**Solubility in SNF Buffer pH ~6.4 (mg/mL)**	**Solubility in FaSSGF Buffer pH ~1.6 (mg/mL)**
Diphenhydramine Hydrochloride (DPH)	8.76 (weak base [421])	888 ± 1.1	980 ± 0.1	1200 ± 0.1
Carbinoxamine maleate (CBX)	8.88 (weak base [422])	320 ± 0.63	510 ± 0.04	760 ± 0.02
Cetirizine Dihydrochloride (CZH)	2.19, 2.93 and 8.00 (weak acid [423])	4.6 ± 0.02	6.93 ± 0.49	11 ± 0.06
Azelastine hydrochloride (AZL)	8.87(weak base [420])	1.33 ± 0.01	1.4 ± 0.02	6.3 ± 0.04

Based on these marked variations in solubility, it was hypothesized that the pH of the dissolution medium would likely influence the release rates of the antihistamines into the dissolution medium. *In vitro* release data of the H_1 receptor antagonists into biorelevant media was obtained over a two week period and quantified using HPLC.

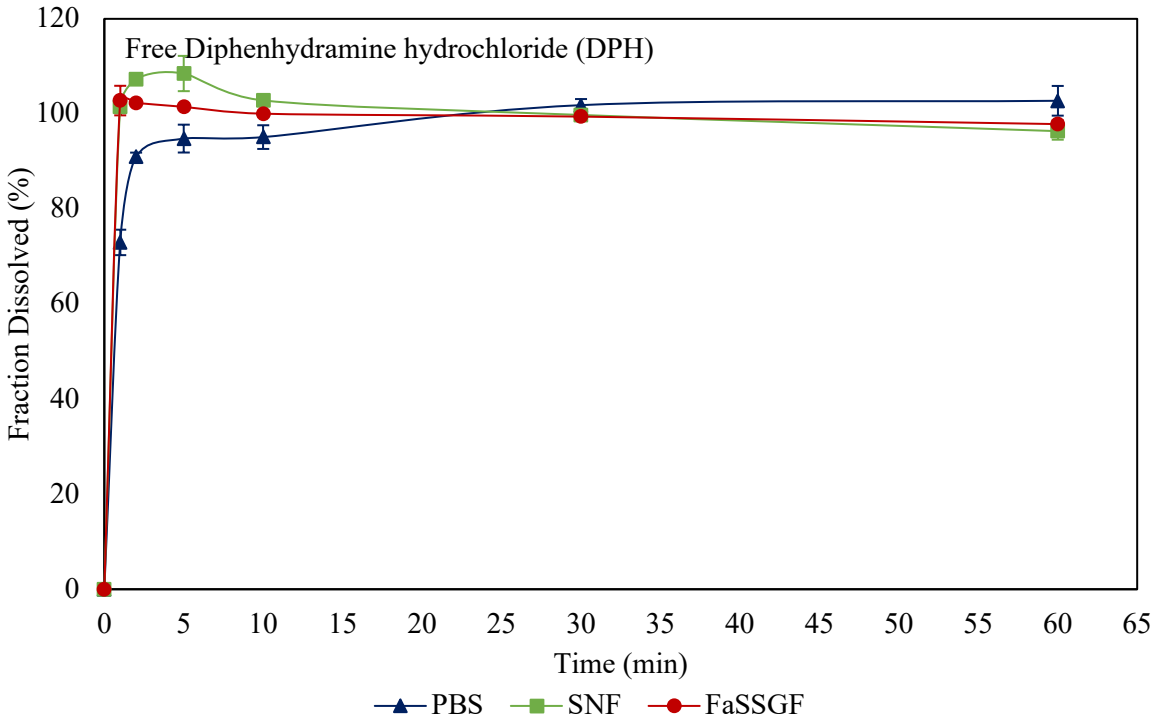
Free Diphenhydramine hydrochloride (DPH)
Fraction Dissolved (%)
120
100
80
60
40
20
0
0 5 10 15 20 25 30 35 40 45 50 55 60 65
Time (min)
PBS
SNF
FaSSGF

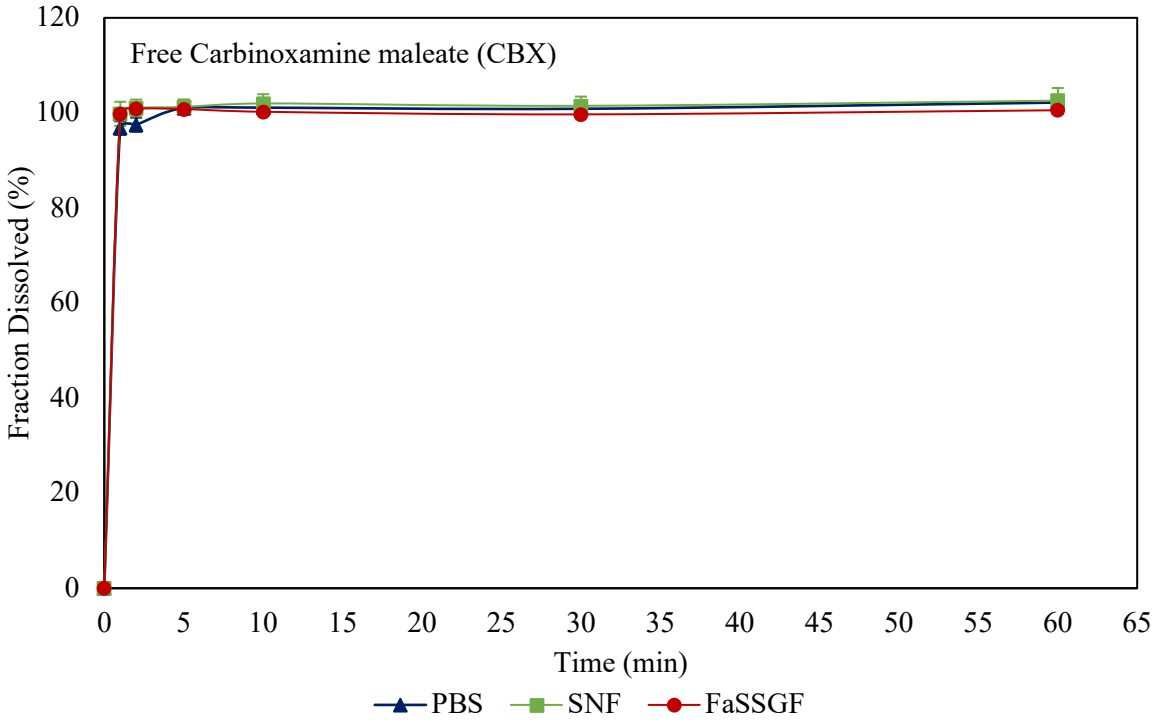
Free Carbinoxamine maleate (CBX)
Fraction Dissolved (%)
120
100
80
60
40
20
0
0 5 10 15 20 25 30 35 40 45 50 55 60 65
Time (min)
PBS
SNF
FaSSGF

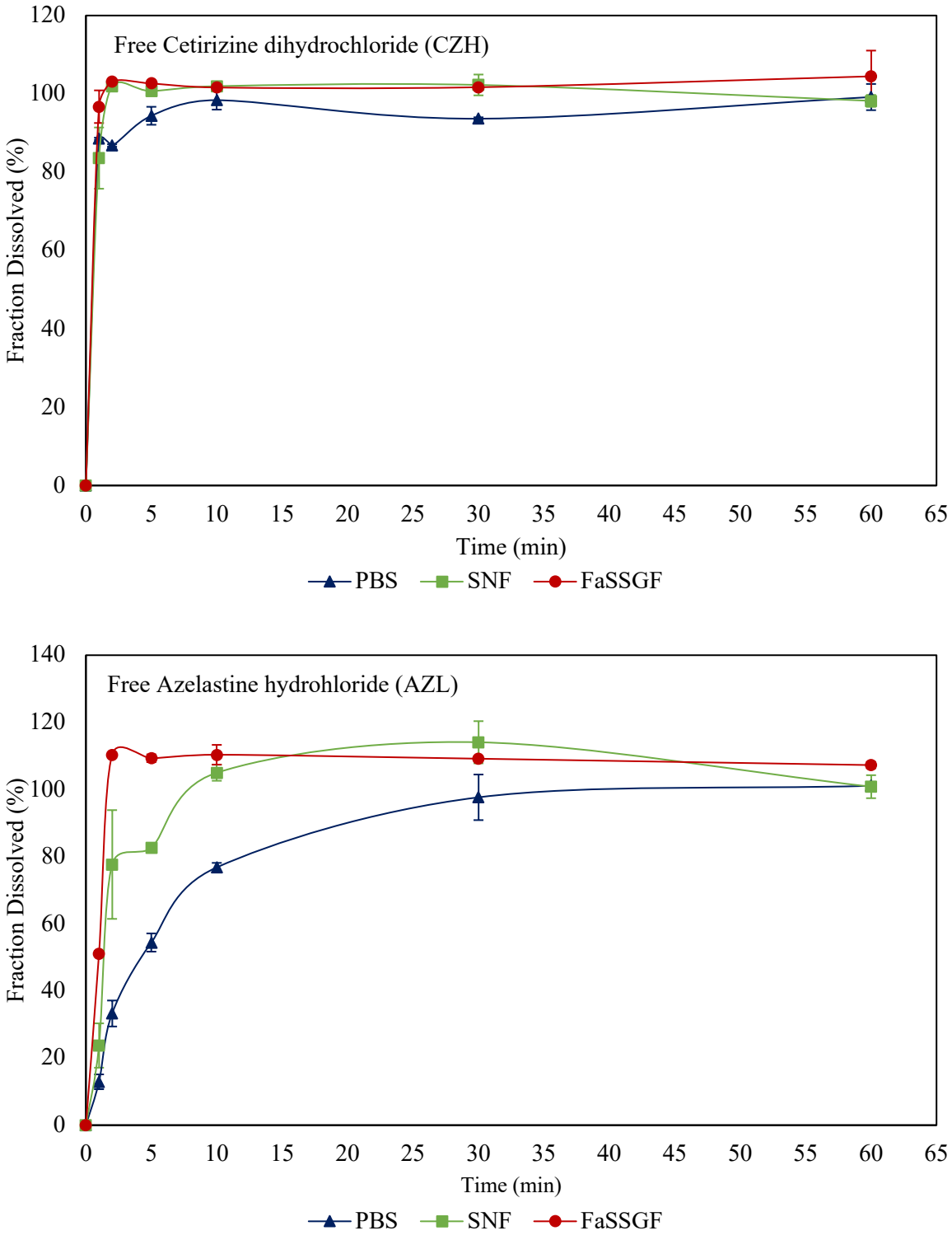

Figure 2.6. In-vitro dissolution profiles of as-received (free) antihistamine drug at 37°C in phosphate buffered saline media at pH ~ 7.4, SNF at pH 6.4 or FaSSGF at pH ~ 1.6. Each point represents the mean (±SD) of two determinations.

The as-received drugs were all crystalline (PXRD diffractogram, appendix A) and in agreement with structures reported in the literature [424-427]. They all rapidly dissolved, under sink conditions, in all three aqueous media, Figure 2.6. In most cases complete solubilization was recorded within the first 10 minutes (Figure 2.6) with only AZL showing a more prolonged release as the pH increased due to its hydrophobic nature and lower solubility. Even so, almost 80% of AZL was in solution after the first 10 minutes and 100% within the first hour.

The dissolution profiles of the antihistamines from the bulk MAG systems at 37°C into the dissolution media are depicted in Figure 2.7. The dissolution profiles of the selected antihistamines demonstrated extended release profiles into the dissolution media maintained at 37°C over a 216 hour investigation when compared to the free as-received drugs (Figure 2.6). The release followed a biphasic pattern for most of the loaded systems, with an initial burst release in the first 8 hours (with the exception of CBX in FaSSGF that was rapidly released). Although the release in this initial period was rapid, a slower release of the drug remaining in the system was observed thereafter.

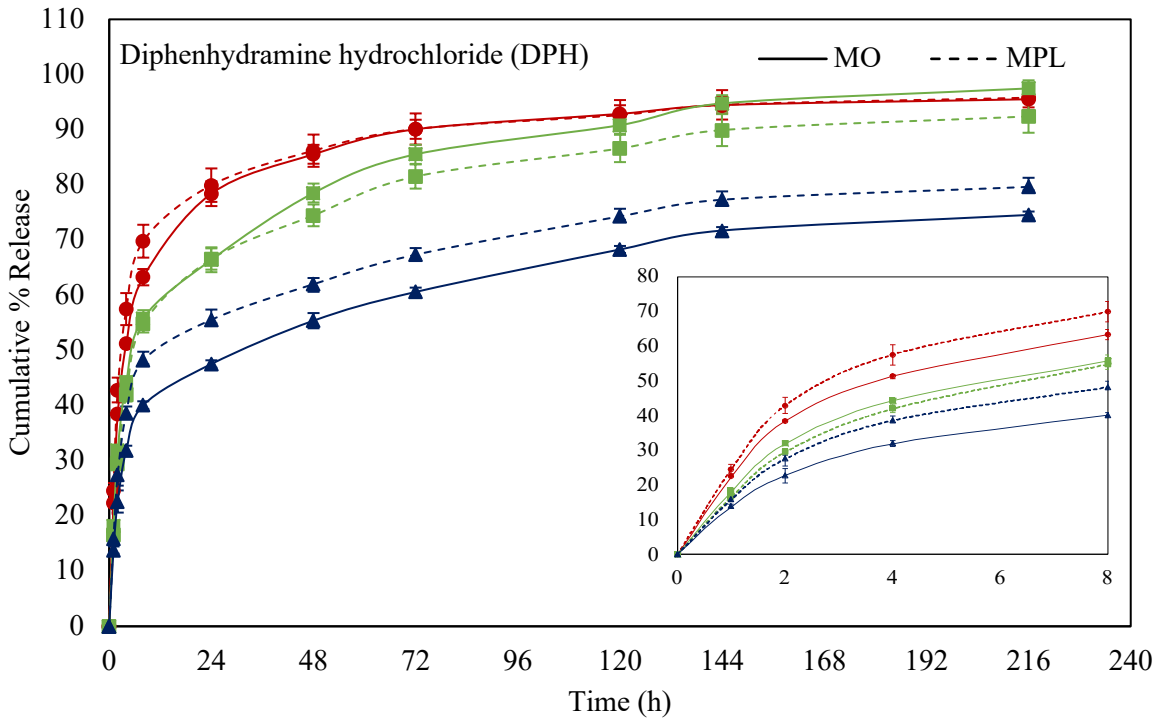

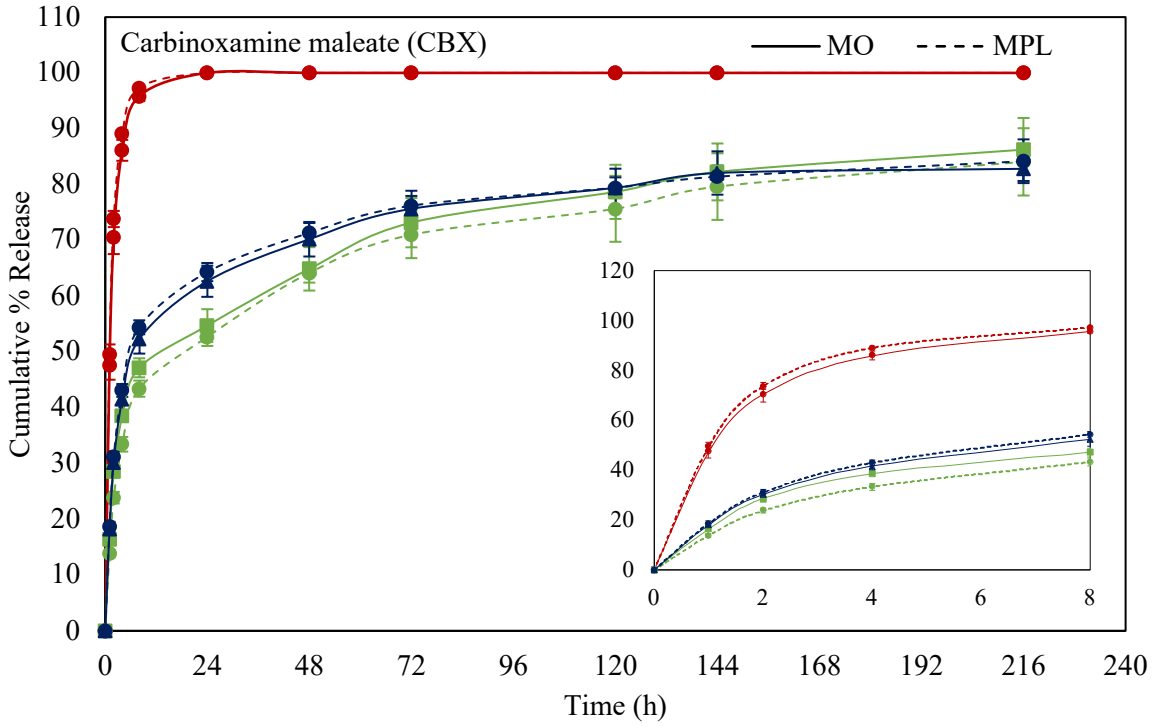
Carbinoxamine maleate (CBX)
MO
MPL
Cumulative % Release
Time (h)
0
10
20
30
40
50
60
70
80
90
100
110
0
24
48
72
96
120
144
168
192
216
240
0
20
40
60
80
100
120
0
2
4
6
8

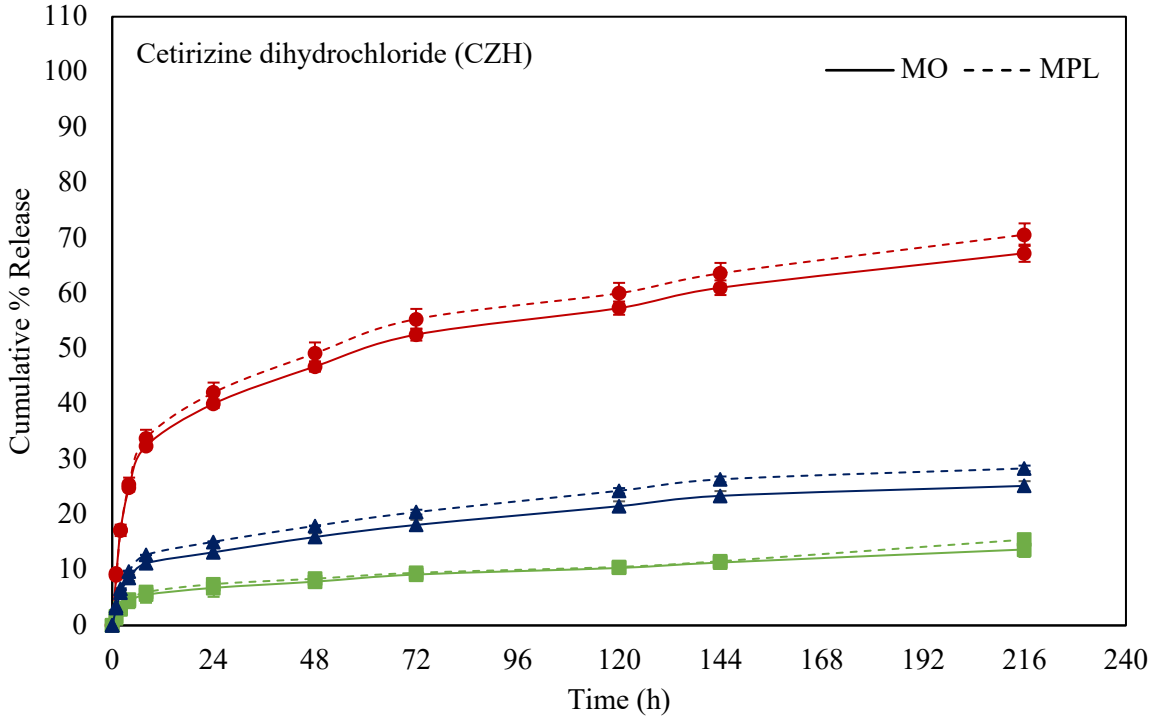
Cetirizine dihydrochloride (CZH)
MO
MPL
Cumulative % Release
Time (h)
0
10
20
30
40
50
60
70
80
90
100
110
0
24
48
72
96
120
144
168
192
216
240

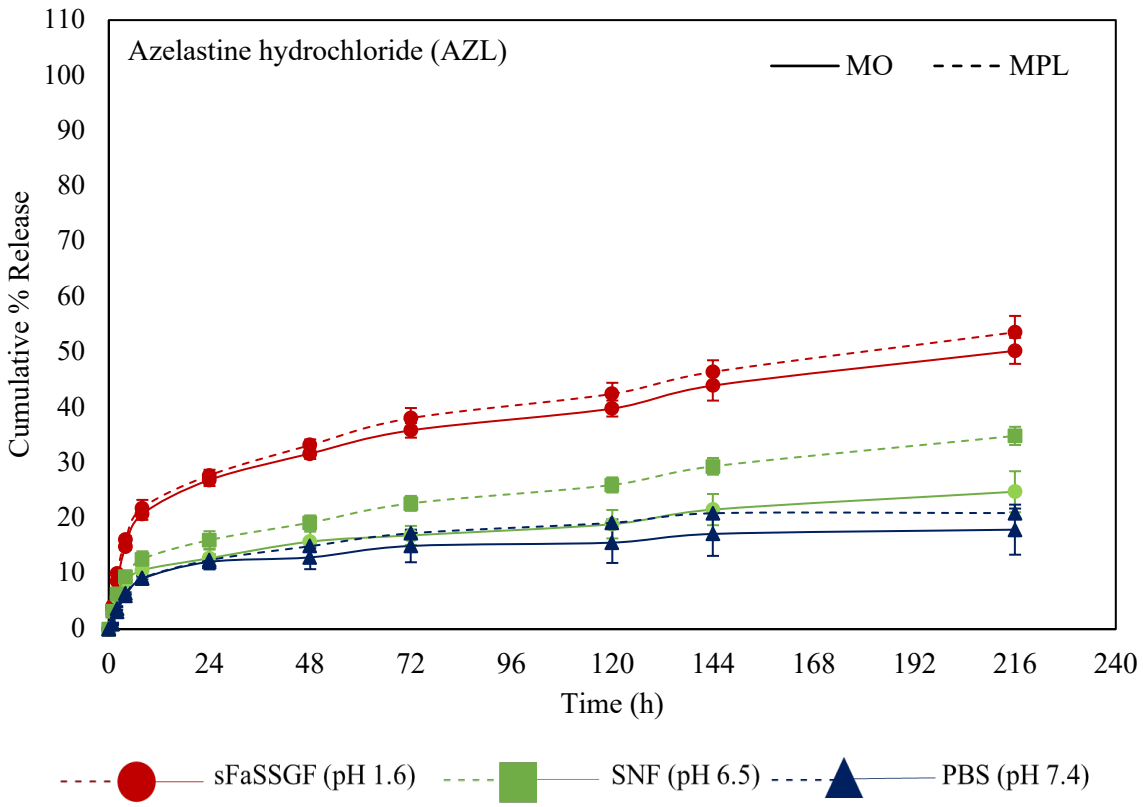

Figure 2.7. In-vitro antihistamine release profiles from bulk lipid cubic formulations prepared with monoolein or monopalmitolein incubated at 37°C in phosphate buffered saline media at pH ~ 7.4, SNF at pH 6.4 or FaSSGF at pH ~ 1.6. Each point represents the mean (±SD) of three determinations.

The dissolution profiles from MO and MPL LCP systems exhibited comparable controlled release properties, with a slightly prolonged API release profile seen with the MO LCP systems compared to the MPL lipid system. The variations in release, although relatively small, may be considered to be related to observed differences in the structural dimensions of the cubic phases of both systems, where differences in water channel diameter were calculated (Table 2.4). This results in variations in water uptake capacity where the osmotic effect is pertinent to the ratio of the size of the incorporated molecule to the water channel diameter [170]. It is clear from the assembled release profiles that pH was highly influential in the rate of release into the various media.

At physiological pH (7.4), the cumulative release of the two hydrophilic molecules within the first 24 hour testing period was 47.5 ± 0.7 and 55.6 ± 1.8 % for the DPH and, 62.7 ± 2.3 and 64.3 ± 1.6 % for the CBX from MO and MPL respectively within the first 24 hours. The more hydrophobic agents (CZH and AZL) displayed much more prolonged accumulation profiles from both systems, which was to be expected as the release of such lipophilic molecules from the lipid cubic phase has been shown to be degradation controlled [428]; and in the absence of lipolytic enzymes [257, 428], the breakdown of the cubic phases is retarded. At the end of the testing period, no significant degradation of the LCP in PBS was observed, suggesting that the release of the drug from its network was limited by the breakdown of the lipid cubic network and not driven solely by simplistic diffusive mechanisms. This supports the theory that the release of the hydrophobic compounds from LCP is substantially degradation-driven.

Based on available literature and the solubility studies conducted here, an increase in release rate was expected across the samples when a more acidic environment was created. SNF was chosen to represent the conditions of the nasal passage of relevance for topical application of the antihistamine-LCP formulation. The pH of the simulated nasal fluid was slightly lower than that of the PBS buffer at pH 6.4 and followed the same pattern in the cases of the AZL and DPH, while the dissolution rate is relatively constant in this pH range for CBX.

A medium representing the fasted conditions in a human stomach, so-called FaSSGF, was selected to study the release behaviour of the antihistamines from the lipid formulations into media at low pH for potential oral delivery applications. For both hydrophilic antihistamines, DPH and CBX , between 70 and 97% of the encapsulated drug had gone into solution within the first 8 hours of testing, as shown in the magnified portions displayed on the dissolution curves, with the difference in profiles between the two different host lipid systems of different water channel diameter noted once again. Similarly in the case of the hydrophobic drugs, the release was greatly accelerated in the acidic medium where twice the concentration of AZL was released into FaSSGF compared to PBS, and almost 3-fold more in the case of CZH over the testing period. The stability of lipid cubic gels was monitored in FaSSGF over the testing period and a loss of 21.6 ± 5.7 % of its original mass was recorded after 10 days. This loss in mass shown in figure 2.8 likely contributed to the drug release rate. Although this increase in release rate was observed for CZH at the most acidic pH (although it has been described as a weak acid [423]), where the COOH

functional group potentially remained un-ionized while both tertiary amines (Figure 2.1) were likely protonated and positively charged owing to the jump in solution concentration, the trend deviated from that of the other molecules when considering the rate of release into SNF and PBS. Variations in ionic strength of the buffers may explain this deviation, where the salinity effect of the various ions in terms of their kosmotropic/chaotropic [429-431] properties as defined by the Hofmeister series may serve to stabilize/destabilize the system (see also chapter V), in turn affecting its controlled release properties [432].

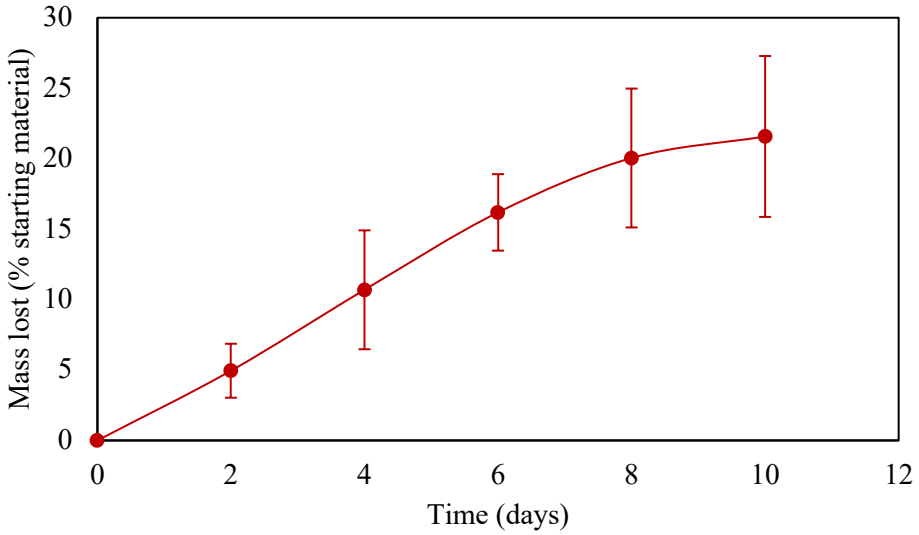

Figure 2.8. Degradation behaviour (mass lost) of MO lipid cubic formulations in simulated FaSSGF solution at 37°C and 150 rpm

The duration of release from antihistamine-loaded cubosomes of MO were significantly shorter than its bulk predecessor, where complete release was noted within the first 48 hours across all samples likely owed to an increased surface area or the dissolution of drug on or near the surface of the cubosomes. Similar trends to those of the bulk systems were noted in the dissolution curves across all four cubosomes formulations (Figure 2.9), with further accelerated release observed in the case of the samples immersed in FaSSGF compared to PBS. Although release from the cubosomes was notably faster than that observed from the bulk gel systems, the dissolution rates are obviously slower than the free drug in solution, figure 2.6. The more lipid soluble drugs (AZL, CZH) displayed a more prolonged release pattern compared to the other antihistamines, with

curves comparable with those described in the literature for more poorly soluble pharmaceuticals [344, 433].

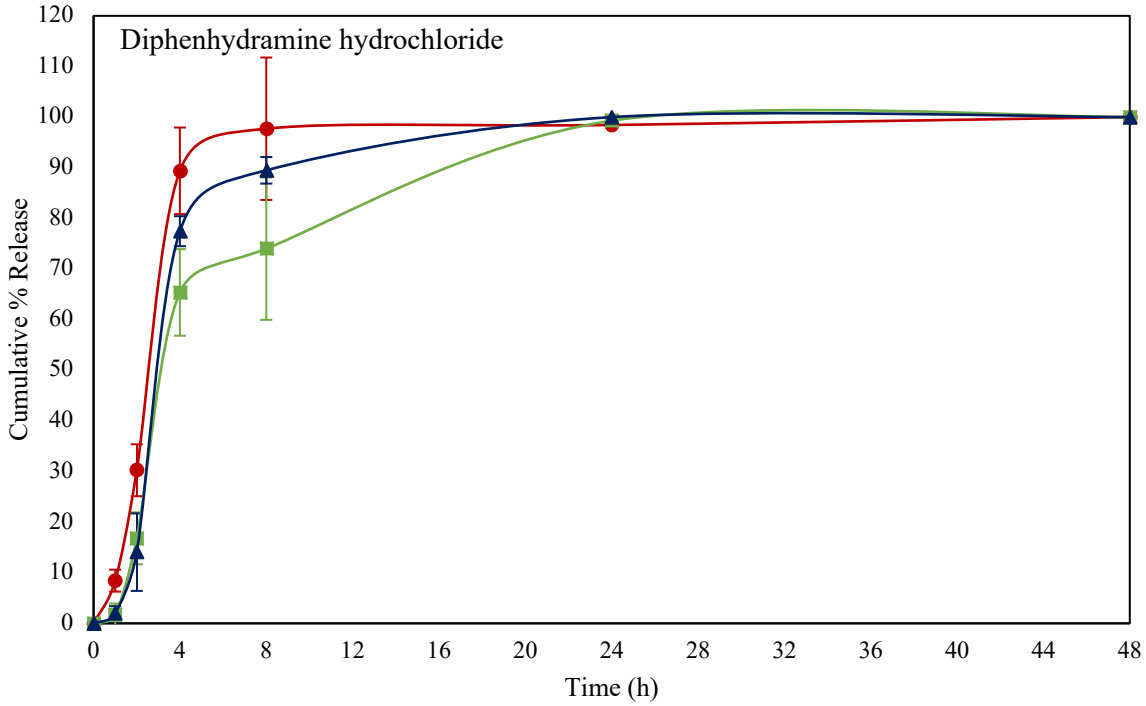

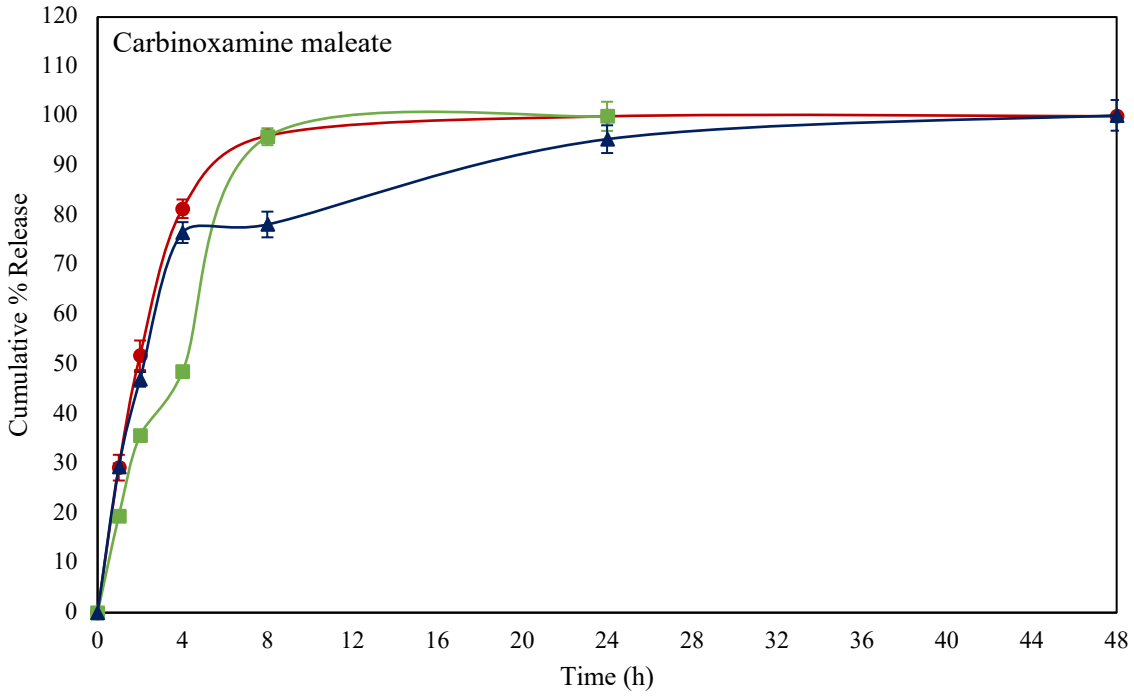

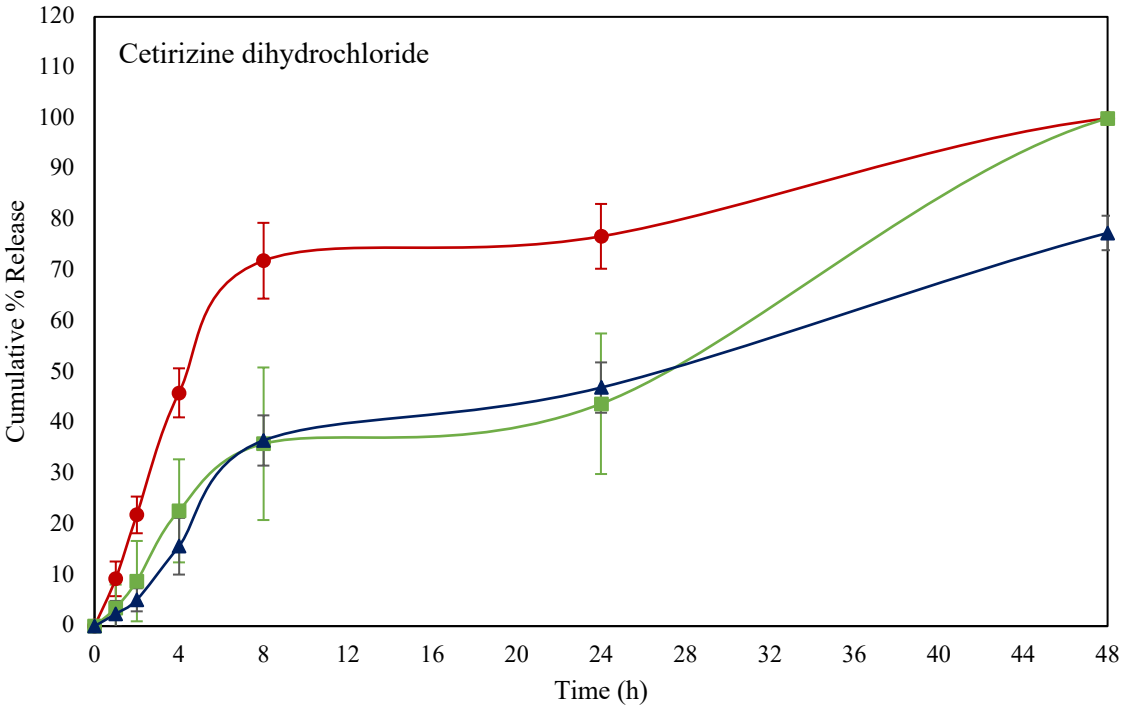
Cetirizine dihydrochloride
Cumulative % Release
Time (h)
0
10
20
30
40
50
60
70
80
90
100
110
120
0
4
8
12
16
20
24
28
32
36
40
44
48

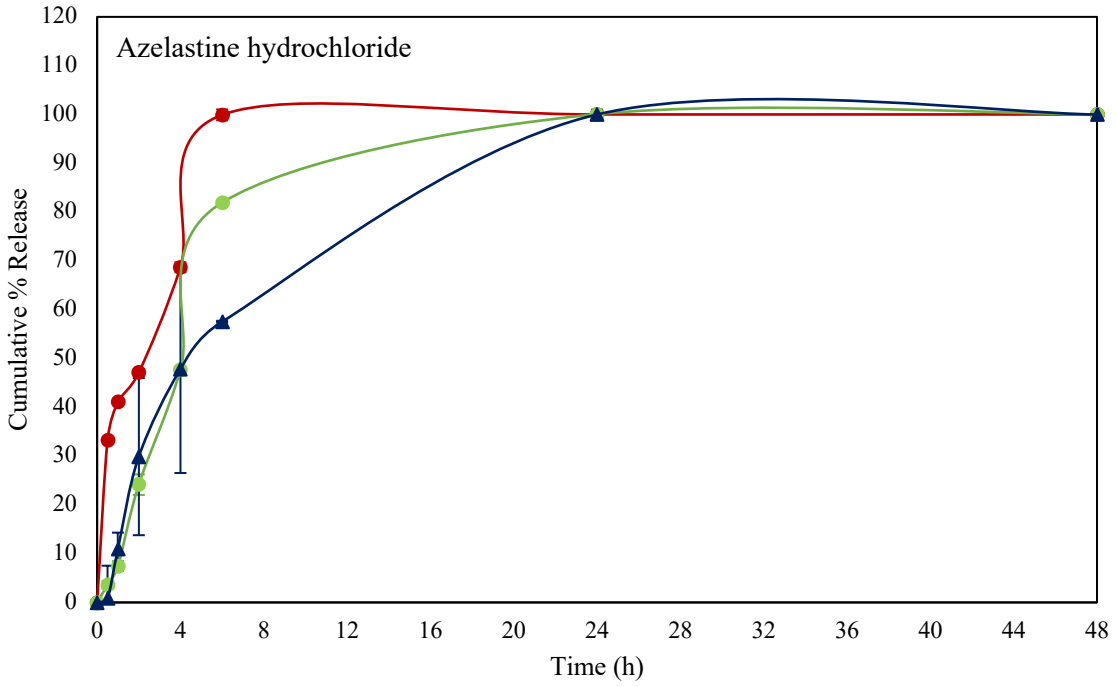
Azelastine hydrochloride
Cumulative % Release
Time (h)
0
10
20
30
40
50
60
70
80
90
100
110
120
0
4
8
12
16
20
24
28
32
36
40
44
48


sFaSSGF (pH 1.6)
SNF (pH 6.5)
PBS (pH 7.4)

Figure 2.9. In-vitro antihistamine release profiles from dispersed lipid cubic formulations (cubosomes) prepared with monoolein incubated at 37°C in phosphate buffered saline media at pH ~ 7.4, SNF at pH 6.4 or FaSSGF at pH ~ 1.6. Each point represents the mean (±SD) of three determinations.

Variations in the pH or ionic strength of a dissolution medium have been shown in the literature to greatly influence the release behaviour of active ingredients from the lipid cubic phase causing significant changes in their profiles [56, 58, 215]. For some drugs, the release was accelerated under acidic conditions when compared to its behaviour at neutral pH [58, 215]. This has been attributed not only to differences in the solubility of the encapsulated drug within certain pH ranges as seen previously, but also to changes in the lipid matrix itself. It has been suggested that the ionization of the fatty acid chain under neutral conditions may be responsible for the slowed-down release of the encapsulated drugs, whereas the acid chains are unionized in acidic environments [215, 434]. "Relocation" of encapsulated drugs when different pH stresses are applied have be described where the formation of less soluble ion pairs between positively charged drugs and the negatively charged fatty acid chains of the lipids may impede their dissolution. This has been demonstrated for drugs including doxorubicin [359] where at neutral pH the drugs may reside in the lipid portion owed to hydrophobic tendencies, but once the pH is altered, and subsequently the solubility and ionization state of the molecule, the drug may partition into the aqueous channels or *vice versa*. This will directly impact the rate of drug release which is directly correlated with its location in the matrix [435]. It is acknowledged that the recommended dosage requirements vary for the individual drugs tested (Table 2.1) but the lipid cubic formulations were prepared at the same loading concentration (1 wt%) to minimize the number of variables potentially affecting drug release [216].

2.4.7 RBL-2H3 inhibitory effect study

Antihistamine molecules delivered in high concentrations have demonstrated the ability to impede IgE-mediated histamine release from basophilic and mast cells *in vitro* [436, 437]. The RBL-2H3 cell-line can be activated to secrete histamine by aggregation of their high affinity IgE receptors or with calcium ionophores [438, 439]. In this study, the ability of the encapsulated antihistamines (delivered at a cubosome concentration of ~100 µg/mL corresponding to ~1 µg/mL

of drug) to inhibit histamine release from a basophilic leukemia cell line (RBL-2H3) with known IgE-induced histamine degranulation properties was investigated. The inhibitory effect of the antihistamine formulations was quantified using a histamine ELISA kit and the resultant profiles are displayed in figure 2.10. The antihistamine molecules CZH and AZL belonging to this group have previously shown selective H_1-receptor antagonism and the ability to inhibit mediator release and inhibition of eosinophil migration or degranulation [440]. Similarly, free CZH has been shown to inhibit histamine release in RBL-2H3 cells at concentrations as low as 15 ng/mL [358].

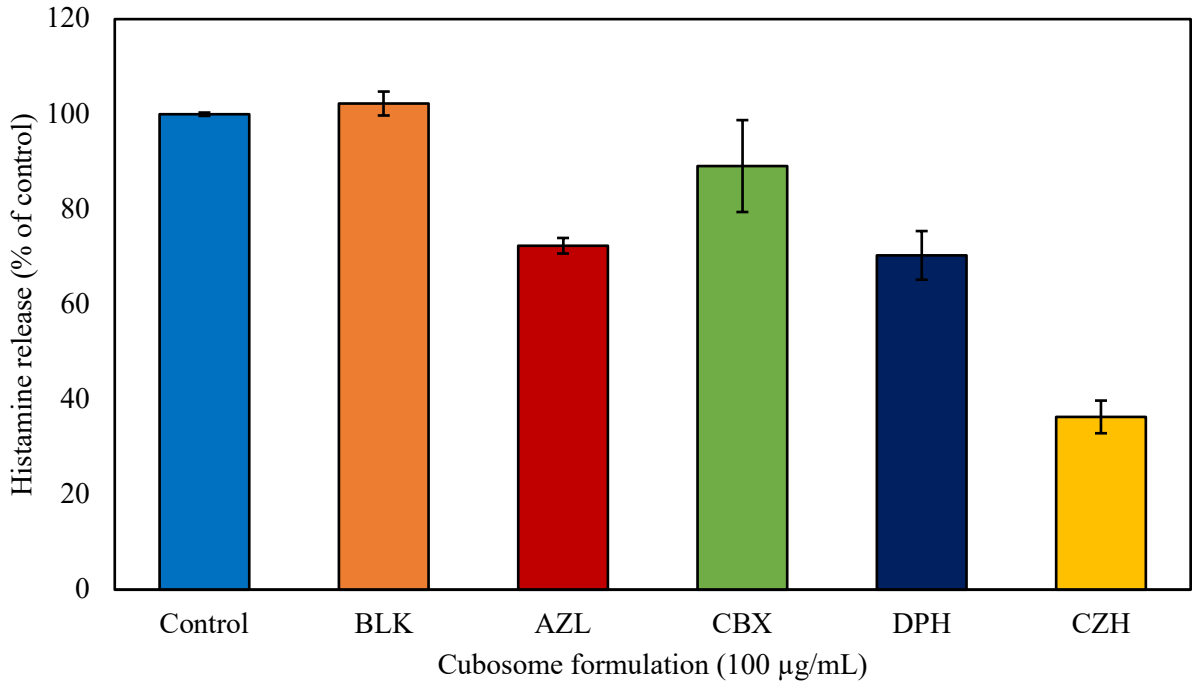

Figure 2.10. Histamine release induced in RBL-2H3 cells after incubation for 10 minutes in the presence of MO cubosomes (100 µg/mL) formulated with and without antihistamine molecules. Samples were read at 450 nm and are expressed as percentage of the control. Data are expressed as a mean ± standard deviation (SD) of duplicated experiments.

The cells were most sensitive to cetirizine dihydrochloride (CZH), showing that incubation with the cubosomal formulation for as little as 10 minutes was sufficient in reducing histamine release by over 60% compared to the control. The ability of CZH to inhibit mediator release upon pre-treatment has been reported in the literature, with studies claiming that at high dosage concentrations the drug halted histamine release in clinical trials in humans [441-444]. Similar

results to those seen here have been reported for free CZH treatment at the same concentration, where a reduction in histamine release of almost 80% from the RBL-2H3 cell model was reported [358]. AZL and DPH loaded in cubosomes exerted a similar inhibitory effect on the histamine release, with a reduction of approximately 30% observed in each case. The inhibitory effect of first-generation antihistamine DPH against antigen-induced IgE mediated histamine release has previously been shown, where the released histamine was halved when the drug was present in concentrations up to 0.5 mM [437]. Similarly, AZL has been found to significantly inhibit anti-IgE-stimulated basophil histamine release [445], specifically in animal models [446-448]. The smallest effect was observed in the case of the hydrophilic CBX formulation, with just over 10% less histamine quantified in those samples, an effect that was found not significant (at $p<0.05$). To our knowledge, CBX has not been reported in similar studies monitoring IgE-stimulated histamine release. This insignificant reduction in mediator release may be explained by differences in *in vivo* mediator release suppression between certain models where the role of histamine in inflammatory response is dependent on the organ and complemented by the effects of other mediators such as leukotrienes and prostaglandins - which are reported to be site-specific [313, 348].

These results serve to highlight the non-interfering effect of the cubosomal carrier on the effect of these molecules and, given the muco-adhesiveness and the prolonged release profiles discussed above, Figure 2.10 also highlights the long acting potential of these antihistamine cubosome formulations. Efficient accumulation of drug carriers smaller than 200 nm has previously been demonstrated in cells of certain pathologies [245-247]. It is possible that the response seen in this study is a cumulative result from the effect of antihistamine drug that has been released from the cubosomal dispersions before cellular uptake as well as unreleased encapsulated drug where cells may retain or internalize the lipid nanoparticles. Importantly, the lipid cubic system and its associated nanodispersions, cubosomes [380], have been classified as a potential intermediates in membrane fusion [146, 449]; where after adsorption of the material on the cell membrane, the two lipid bilayers fuse thus mitigating toxicity and enhancing the cellular delivery of the targets (A process also described in the internalization of viruses [450]). These fusogenic drug carriers are capable of evading endocytic internalization to effectively deliver targets. An important consideration in the study of drug release and uptake, is the rate at which fusion occurs versus drug release. Whether or not release after adsorption of the system to the cell surface outpaces fusion is

an important consideration. In this context both must be fully understood and would require further studies in this case. It has been demonstrated here that the rate of release is highly dependent on the physicochemical properties and location of the drug molecule within the lipid system (Figures 2.7 and 2.9 dissolution profiles). It is therefore reasonable to assume that both factors may contribute to drug delivery, with one factor or the other dominating in specific circumstances and for specific lipid formulations.

2.5 Conclusion and leading research questions

In this study MAG lipid cubic phases and their dispersions have shown potential as mucoadhesive controlled release systems for the delivery of four commercially available antihistamine molecules. Through high resolution SAXS and dynamic light scattering the impact of incorporating these molecules on the lipid cubic structure, its toxicity, bioactivity and mucoadhesivity has been studied. Lipid cubic systems have been hailed for its mucoadhesive nature [403]. The impact on the degree of mucoadhesion of encapsulating the antihistamine molecules in the lipid cubic dispersions was tracked on mucin-coated MP-SPR sensors. Here, this approach has proven to be an efficient tool to investigate the adhesion of lipid-based nanoparticles to mucin layers and have confirmed the mucoadhesive nature of the systems. The results presented distinct binding profiles depending on the properties of the drug incorporated into the cubic network, with the most favourable adhesion seen with AZL, an effect that may be attributed to surface charge and hydrophobic interactions. The bioadhesive nature of these systems presents an opportunity for tapping into improved retention, absorption, and subsequently bioavailability of the molecules through local delivery of antihistamines to mucosal membranes facilitating retention of the active ingredients within the nasal mucosal cavity or at gastrointestinal sites for the treatment of allergic reactions (this could be extended to other mucosa including buccal, vaginal [123], pulmonary, and those of the renal system). Likely owing to their increased surface area, cubosomes are said to be more bioadhesive in nature than bulk gels so that they can be conveniently used in topical and mucosal delivery of different drugs. A major challenge in the area of bioadhesive drug delivery systems is uncontrollable hydration of bioadhesive formulations at the delivery site [403]. The system's resistance to dilution beyond a maximum hydration level eliminate the need for overcoming this obstacle as far as the cubosomal formulations are concerned.

Changes in zeta potential were used to track the efficient cellular uptake of positively charged cubosomes stabilized with commonly used surfactant Pluronic® F-127. By studying the changes in zeta potential, cubosomes were found to interact at the surface of the cell surface and suspected internalization of the dispersions was observed after a 12 hour incubation of a model fibroblast cell line where the zeta potential returned to that of untreated cells. In this time, no cytotoxic effect was observed in two model cell lines, with the exception of CZH that appeared to reduce cell viability by half after a 48 hour incubation in fibroblast cells. With the ultimate application in therapies for the treatment of allergic reactions, the formulations were shown to inhibit mediator release from basophilic mast cells by more than half in some cases compared to the untreated control. Furthermore, prolonged release of both sets of first and second generation antihistamine molecules from the bulk and dispersed systems compared to the free drugs were shown, highlighting the prolonged release capabilities of the lipid matrix. The impact of drug solubility and environmental pH on the dissolution properties were studied. The changes in the release pattern of the antihistamines at lower pH may be relevant in the treatment of gastric-related allergic reactions including acid-reflux, which occurs as a result of histamine release and interaction from parietal cells which stimulate acid production in the lining of the stomach. It is important to note however that it is primarily H2 receptor antagonists that are indicated for this type of application, but regardless the system described here may be of potential use in this area.

From this work, it is apparent that the physicochemical properties of a given molecule govern its location within the cubic network, with hydrophobic molecules residing in the lipid bilayer while water soluble molecules inhabit the congruent water channels of the mesophase. Chapter III will explore a novel approach to garnering further control of the liberation of different active pharmaceutical ingredients from the matrix.

Chapter III: Modulating the Release of Pharmaceuticals from Lipid Cubic Phases using a Lipase Inhibitor

3.1 Introduction

This chapter has been modified from a published manuscript titled "*Modulating the release of pharmaceuticals from lipid cubic phases using a lipase inhibitor*" published in The Journal of Colloid and Interface Science, Vol. 573 in 2020. In this chapter, a novel approach to controlling the lipolytic degradation of the lipid system to garner further control of the release of a hydrophobic model drug, a clofazimine salt, is introduced.

3.2 Background

The monoacylglycerol lipid family has been widely studied for their ability to form the lipid cubic phase (Chapter I, section 1.4). These formulations are susceptible to lipolysis by a variety of enzymes, including lipases and esterases, which attack the ester bond present on the lipid chain bridging the oleic acid component to the glycerol backbone (Chapter I, section 1.6). The release of poorly soluble molecules residing in the lipid membrane portions of the phase is limited by the breakdown of the matrix, thus presenting a potential means for further controlling and sustaining the release of therapeutic agents by targeting the matrix stability and its rate of degradation. The aims of the present study were twofold: to evaluate an approach to regulate the rate of degradation of lipid cubic phase drug delivery systems by targeting the enzyme interactions responsible for their demise; and to study the subsequent drug release profiles from bulk lipid cubic gels using model drugs of contrasting hydrophobicity. Here, hybrid materials consisting of cubic phases with monoacylglycerol lipids of different chain lengths formulated with a potent lipase inhibitor tetrahydrolipstatin were designed. Modulation of the release of a hydrophobic model pharmaceutical, a clofazimine salt, was obtained by exploiting the matrices' enzyme-driven digestion. A stable cubic phase is described, displaying controlled degradation with at least a 4-fold improvement compared to the blank systems shown in inhibitor-containing cubic systems. Sustained release of a model hydrophobic pharmaceutical was studied over 30 days to highlight the advantage of incorporating an inhibitor into the cubic network to achieve tunable lipid release systems. This is done without negatively affecting the structure of the matrix itself, as shown by comprehensive small-angle x-ray scattering experiments.

The challenges in the delivery of therapeutic agents *in vivo* include controlling and maintaining their release at therapeutically effective doses over a sustained period of time, long enough for them to exhibit their desired effect. Smart design of delivery systems can help overcome these challenges. This is particularly applicable in the design of delivery matrices for pharmaceuticals of poor water solubility, which is believed to account for between 70 and 90% of new drugs in development [106, 107]. Lipid carrier systems have proven their potential in controlled delivery applications on account of their unique microstructure [161, 162, 165, 231] and amphiphilic character, as well as the biodegradable and biocompatible nature of the lipids used [167, 168].

The lipid cubic matrix's application in sustained release, while proven to be very promising, is somewhat limited as a consequence of its shorter release profile which is often less than 24 hours for hydrophilic agents [123, 174] (as shown in Chapter II, section 2.4.6) and its highly viscous consistency which has been likened to toothpaste [145]. Additionally, the integrity of monoacylglycerol derived cubic phase (MAG LCPs) gels in particular are greatly compromised by the presence of lipolytic enzymes [174, 257, 258] capable of hydrolysing the ester linkage connecting the acyl chain (oleic acid) to the glycerol backbone [257-259]. This likely influences the release kinetics of any membrane-embedded hydrophobic drugs with which it is formulated as has been described for numerous hydrogel systems [271]. The main perpetrators are a family of enzymes, lipases, that are found in the body, often accompanied by other offending abettors such as esterases. Lipases are water-soluble and act at an oil-water interface during lipolysis of triglycerides in any aqueous system through a series of intricate steps [257], with the surface area being the rate limiting factor [258, 260].

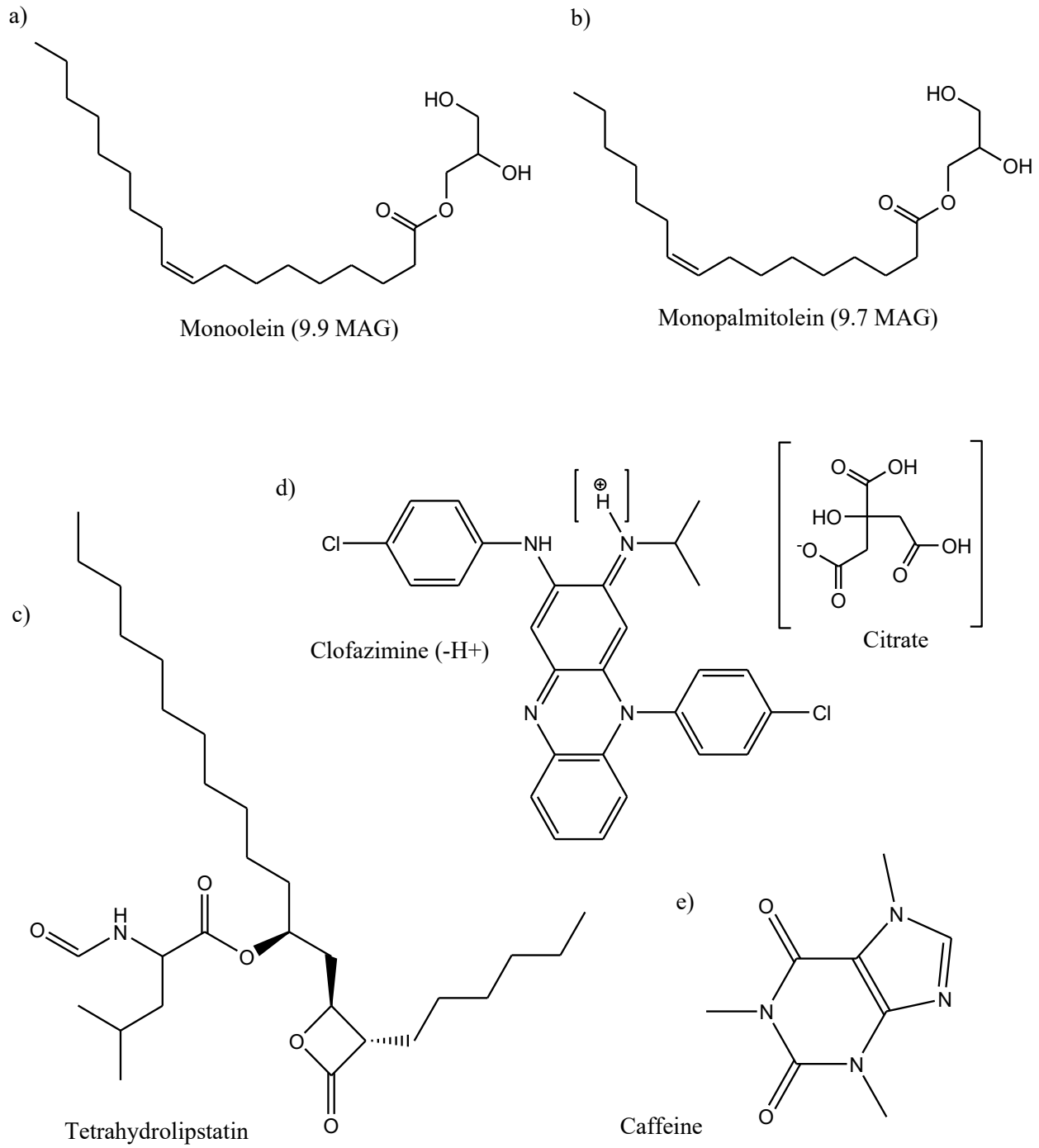

Figure 3.1. Chemical structures of: a) monoolein (9.9 MAG) and b) monopalmitolein (9.7 MAG) both possessing an ester linkage linking the oleic acid chain to the glycerol backbone; c) lipase inhibitor tetrahydrolipstatin (THL); d) hydrophobic model active pharmaceutical ingredient (API) clofazimine-citrate; e) hydrophilic model API caffeine

The inhibition of lipase interactions through steric approaches has previously been described as a means to impede the digestion of lipid-based formulations for drug delivery [451-455]. Additionally, a class of lipids exist that have been synthesized such that their structure greatly resembles that of monoolein, except that the glyceryl ester group is replaced by a glycerate [252]. As an alternative approach here, a novel chemical approach to achieve regulated degradation and subsequent controlled drug release from bulk lipid cubic systems is presented by targeting these lipase enzyme interactions through the incorporation of a known inhibitor into the lipid network. The stability of two bulk LCP matrices is examined over time in the presence of a hydrophilic or a hydrophobic active pharmaceutical ingredient (API) and in the presence of tetrahydrolipstatin (THL), a potent active site-directed lipase inhibitor [456-460]. THL is FDA approved and indicated for the treatment of obesity at concentrations that well exceed those used in this study [461]. A surface loop system employed by pancreatic lipases controls access to their active site. In the presence of lipid substrates and other amphiphiles, the surface loop, or 'lid', undergoes a conformational change thus exposing the enzyme's catalytic site [262]. Upon exposure, tetrahydrolipstatin exerts its inhibitory effect upon binding the pancreatic lipase at its catalytic serine residue as it forms a stable monolayer at the oil-water interface [453, 462, 463]. Following a nucleophilic attack of the serine active site on the b-lactone group [464, 465], the THL forms a stoichiometric acyl-enzyme complex with the various lipases [456, 457, 466] to impede the catalytic degradation of the lipid formulation (Schematic displayed in appendix B).

Lipolysis and its inhibition are considered to be a set of competitive processes, often occurring simultaneously both *in vitro* and in biological systems when an inhibitor and a lipid substrate co-exist [467]. The efficacy and rate of the individual processes are dependent on factors including concentration and surface area and are related to the ratio of lipid substrate to enzyme inhibitor. The inhibitor selected in this investigation was incorporated into the lipid cubic gels at different concentrations in a bid to stabilize and control their digestion by pancreatic lipase. A range of THL loadings from 0.35 to 2.5 wt% were selected to demonstrate the relationship between inhibitor concentration and the rate of competitive lipolysis, subsequently allowing for the tunable degradation-driven release of hydrophobic pharmaceuticals from their network. Within this range of inhibitor concentrations, the cubic phase is accessed and maintained under the experimental conditions described in this investigation, without any observed phase transition.

THL is practically insoluble in water [468] and so was expected to reside mainly in the lipidic domain of the cubic phase, while its hydrophilic portions may partition into the aqueous channel compartment. In a similar way that a lipid/water interface is necessary for lipase catalysis, inhibition of the enzyme by THL is possible at this boundary [260, 462]. This means that most likely only the THL available at the surface of the lipid network in the LCP can carry out its inhibitory function while the THL integrated in the inner bilayers would serve as a reservoir, reaching the lipid/water interface upon the degradation of the gel [451, 469, 470]. This repository provides fresh inhibitor to the system for the entirety of its life, where continuous, controlled degradation at the surface of the gel exposes encapsulated THL to the lipolytic enzyme. A clofazimine citrate salt and caffeine were selected as model APIs for release studies based on their different propensities to dissolve in water (~40 mg/L [471] and ~51 g/L [472] at 37°C for the CFZ-citrate and caffeine respectively). Their structures are shown in Figure 3.1. .

3.4 Materials and Methods

3.4.1 Materials

All solvents were analytical grade and purchased from FisherScientific; Monoolein 9.9 MAG (1-(9Z-octadecenoyl)-rac-glycerol) and monopalmitolein 9.7 MAG (1-(9Z-hexadecenoyl)-rac-glycerol) were acquired from JenaBioscience, Germany at >99% purity; Phosphate buffered saline (PBS) tablets were purchased from Merk (Saint Louis, MO); Water was purified in the lab using a Milli-Q Water System (Millipore Corporation, Bedford, MA); Clofazimine (CAS registry number 2030-63-9) was purchased from Beijing Mesochem Technology Co., Ltd. The clofazimine-citrate salt form was produced previously by our group [471]; Lipase isolated from porcine pancreas was purchased from Merck, Germany (Type II, 100-500 units/mg protein (using olive oil (30 min incubation)), 30-90 units/mg protein (using triacetin), L3126 SIGMA); Pancreatin isolated from porcine pancreas was purchased from Merck, Germany (4x USP Specifications L1750 SIGMA), 30-90 units/mg protein (using triacetin), L3126 SIGMA); Caffeine (99% purity, Sigma-Aldrich); Tetrahydrolipstatin (Orlistat) (99% purity, Sigma-Aldrich).

3.4.2 Preparation of MAG LCP matrix formulations

Viscous lipid cubic phase formulations were obtained by dispensing appropriate volumes of molten monoacylglycerol (MAG) (Monoolein (MO) ≥60 mg/sample or monopalmitolein (MPL) ≥50 mg/sample) in glass vials. Fusion of dry MAG crystals to the melt was achieved at 40 °C. This was followed by the addition of the aqueous solution in excess volumes (≥45 wt% and ≥55 wt% for MO and MPL LCP respectively) according to their respective phase diagrams [173, 177, 352]. The samples were then subjected to vortex mixing for at least 15 minutes and equilibrated and stored in sealed glass vials out of direct light at room temperature until an optically clear and visually homogenous sample was achieved and for no longer than three weeks.

A range of MAG lipidic mixtures with 0.35, 0.7, 1.5 and 2.5 wt% THL were prepared by first dissolving the inhibitor in the appropriate weighed amounts of molten lipids. Homogeneous blends were achieved by subjecting the molten solution to brief vortex mixing with gentle heating. Mesophase samples were then generated by mixing weighed quantities of MAG lipid-THL formulations with Milli-Q water corresponding to ratios at excess hydration according to the MAG lipid-water phase diagrams (≥ 40% - 50% w/w).

The same approach was taken for the incorporation of the hydrophobic API (CFZ-citrate salt) into the LCP whereby the API crystals were dispersed in the molten MAG at the desired percentage weight before the introduction of water to the system to form the cubic phase. For the hydrophilic API, caffeine, the caffeine was dissolved in the water used to prepare the cubic phase and this was added to the blank molten lipid. Both the caffeine and the CFZ-citrate salt samples were prepared at concentrations of 1 and 3 wt% API.

3.4.3 Mesophase characterization

Polarizing Light Microscopy

Polarized light was utilized to assign the predicted liquid crystalline mesophase accessed. A spatula tip of the generated mesophase was transferred to a glass microscope slide and immediately covered with a glass coverslip. The sample was examined under normal and cross polarized light at room temperature on a Zeiss AxioScope Optical microscope equipped with polarized light filter

and a cross-polarizer. Image acquisition was carried out using an AxioVision 4.8 imaging system by Carl Zeiss Ltd. Non-birefringence in refraction was identified by the appearance of a black image or zone on the camera.

SAXS

Small angle X-ray scattering was performed to confirm mesophase assignments for the formulations and to assign lattice parameters.

Mesophase Characterisation

Mesophase samples with discrete composition were prepared as previously described for various concentrations of tetrahydrolipstatin within the range of 0 to 2.5 wt%. To study the metastability of the phases over a prolonged period of time, samples were prepared 3 weeks, 4 days, 2 days and 1 hour prior to SAXS data collection. Samples were stored in sealed vials until just before data acquisition to avoid any sample dehydration through atmospheric exposure. Another set of samples were tested to determine the loading capabilities of the phase with the model APIs, prepared as previously described at concentrations of 1 and 3 wt%.

SAXS measurements were carried out after sample preparation at the Solution State SAXS B21 beam line at Diamond Light Source on the Harwell Campus, Didcot, UK as previously described [428]. The relative positions of the distinct Bragg peaks were indexed and served in distinguishing the space groups and lattice parameters, correlating with Miller indices [473] of the bulk cubic phases and their dispersions. The water channel diameter and lipid chain length were calculated as previously described [428], where surface area constants Å and Euler Poincare constant (χ) were utilised [151, 354] according to equations 2.2 through 2.5.

A further calculation was applied in this study where the area at the interface per lipid molecule in the unit cell of the cubic phase (a_i) was calculated directly according the following [354]:

First, the lipid molecular volume (v_{MAG}) was determined according to [1]:

$$\textbf{Equation 3.1: } v_{MAG} = \frac{\left(\frac{MW_{MAG}}{Avogadro's\ number}\right)}{\rho_{MAG}}$$

Where MW_{MAG} is the molecular weight ($g.mol^{-1}$) for the host lipid, taken as 356.6 and 328.5 $g.mol^{-1}$ for MO and MPL respectively.

From there, the area at the interface per lipid molecule was calculated according to the following equation:

$$\textbf{Equation 3.2: } a_i = 2v_{MAG}\frac{(A_o d^2 + 2\pi\chi l^2)}{\emptyset_{MAG} d^3}$$

Where $A_o d^2 + 2\pi\chi l^2$ is equal to the area at the head group at the interface integrated over a single monolayer

3.4.4 Enzyme stock preparation

A 5 mg/mL solution was prepared by dissolving the lipase in 0.1 M phosphate buffered saline (PBS), pH 7.4 ± 0.2. The preparation was carried out on ice to avoid denaturation or premature activation of the enzyme. Enzyme solutions were stored on ice or in the fridge and only used for up to one hour after preparation. New solutions were prepared for experiments thereafter. It is acknowledged that at this concentration, proteins displaying interfacial activity are prone to aggregation, however all samples were treated identically in this investigation under the same experimental conditions of enzyme exposure.

For the clofazimine salt, ultrapure water was substituted for the PBS in the preparation of the enzyme solution to prevent ion displacement from the citrate salt form of the API leading to reduced aqueous solubility [471].

3.4.5 Swelling and degradation Behaviour

To investigate the time-dependent swelling and degradation behaviour of the lipid cubic phase gels prepared with different commercial lipids, pharmaceuticals and THL, dynamic swelling

studies were performed. After sufficient equilibration the gels were weighed before submersion in 1ml of phosphate buffered saline solution (pH 7.4 ± 0.2), both in the presence and absence of enzyme. The sample vials were tightly capped and maintained at 37°C. The samples were shaken at 200 rpm throughout the investigation to ensure homogenous exposure of the sample to the enzyme. Porcine pancreatic lipase was selected for the study. For the clofazimine salt, ultrapure water was again substituted for the PBS to prevent ion displacement from the citrate salt form of the API leading to reduced aqueous solubility [471].

The swelling and degradation ratios of the gels were studied by means of a standard gravimetric method. The gels were removed from the media at regular intervals and their liquid uptake and mass loss was characterized by measuring the change in their mass. The gels were rinsed with purified MilliQ water to remove any residual salts potentially deposited on the surface of the gel from the swelling media and lipase solution debris. The excess surface water was then removed from samples by gentle blotting with lint-free Kimwipes™ before the samples were weighed on an analytical balance.

The swelling ratio and rate of degradation in terms of relative weight % were calculated against the initial sample mass as per the following equation:

Equation 3.3: $$Swelling\ Ratio\ or\ Residual\ Weight\ \% = \frac{W_1 - W_0}{W_0} \times 100\%$$

Where W_0 is the initial gel weight before submersion in the media and W_1 is the weight of the gel at a measured time point after immersion in the media.

3.4.6 Drug release studies

The release of the model pharmaceuticals CFZ-citrate and caffeine from the LCP was tracked at timed intervals for up to 31 days in PBS or water for caffeine and CFZ-citrate respectively. Drug release measurements consisted of removing the entire solution from the sink and immediately replenishing it with fresh release media. Throughout the measurement, the samples were shaken at 200 rpm in an incubator at 37°C. The concentration of CFZ-citrate and caffeine in the sink were measured by UV-vis spectrometry for CFZ-citrate and high performance liquid chromatography (HPLC) for caffeine, due to interference from the lipids in solution.

3.4.7 High Performance Liquid Chromatography

The HPLC system used in this investigation was an Agilent 1200 Infinity Series (Agilent Technologies, Palo Alto, USA) comprising: G1311B 1260 quaternary pump, G1329B 1260 ALS autosampler, G1316A 1260 TCC (thermostated column compartment) and a G1365D 1260 MWD VL diode-array detector. The acquired data was processed with the Agilent OpenLAB CDS software.

Chromatographic separations of caffeine-containing samples were achieved using an Agilent Poroshell 120 PFP (3 x 100 mm, 2.7 µm) column fitted with a UHPLC Poroshell 120 guard module (3 x 5 mm, 2.7 µm). The system was maintained at 20°C with a run time of 10 minutes. The mobile phase which comprised A: HPLC Analytical grade Acetonitrile (Fisher Scientific) and B: deionized water (A:B 15:85, v/v) was delivered to the column at a flow rate of 0.64 mL/min which yielded a column back pressure of ~290 bar. Samples were filtered through a 0.2 µm nylon filter (Fisherbrand®) and 8 µl injections were made. UV detection was conducted at a wavelength of 274 nm.

3.4.8 UV-visible Spectroscopy

The concentration of CFZ citrate was determined by means of UV-vis spectrophotometry. A full spectrum was obtained on a double beam UV-1800 Shimadzu UV-Visible spectrophotometer to ascertain λ_{max} for the drug, which was determined as 488 nm. Absorbance values of release samples were then obtained with appropriate dilution at this wavelength and Beer-Lambert's Law was then utilized to calculate the concentration of the API in the sample.

3.4.9 Drug release kinetics

The release data obtained for the release of caffeine and clofazimine citrate in the presence or absence of the THL inhibitor from the two MAG LCP formulations were treated according to a number of release models: zero-order (cumulative % drug released v time (min)); first order (Log cumulative % drug released v time (min)); Higuchi (cumulative % drug released v square root of time); Hixson-Crowell (cube root % total drug - cube root of % unreleased drug v time (min)); and Korsmeyer-Peppas (log cumulative % drug released v log time) to obtain the correlation

coefficient. The diffusion coefficient (n) was estimated from the linear regression line of the Korsmeyer-Peppas model for each sample.

3.5 Results and Discussion

3.5.1 Mesophase characterization

In this study, lipid cubic phases were successfully formed using monoolein and monopalmitolein in the presence of hydrophobic and hydrophilic pharmaceutical compounds as well as a lipase inhibitor, the chemical structures of which are shown in Figure 3.1. A range of characterization techniques can be applied in the distinction of these phases. This investigation utilized simple polarizing light microscopy and more thorough small-angle X-ray scattering approaches to assign mesophase properties to the test formulations. One can determine whether a test material is anisotropic or isotropic in nature and measure its birefringence simply by using cross-polarized microscopy (CPLM) [474]. As the highly ordered cubic phase exhibits optical isotropy and its refraction is non-birefringent in nature, it gives rise to a dark background between crossed polars as the phase is essentially 'invisible' against the dark stage [475]. The lamellar and hexagonal liquid crystalline phases on the other hand, are anisotropic and optically birefringent thus split the plane of the incident light appearing as textured multi-coloured patterns. This distinction allowed for the identification of the phases of our formulations. Indeed, when the fresh formulations under investigation in this study were exposed to cross-polarized light, a dark image was observed with no obvious signs of birefringence suggesting a structure of cubic architecture.

While CPLM allows for differentiation between mesophases, its usefulness is limited by an inability to distinguish between the various types of discrete cubic phases and it provides no means for dimensional analysis. Small angle X-ray scattering investigations enabled the lattice dimensions and unambiguous space group symmetry to be assigned to each sample. They also allowed for the effect of THL and API loading on the phase properties, and its impact on the stability of the phase to be tracked. With a favourable effect in terms of stability against lipolytic enzymes anticipated, phase identification was required to confirm the loading capabilities of the MAG LCP systems. Lipid cubic phases typically give rise to diffraction patterns similar to those of powder X-ray diffraction; characterized by a series of sharp, clearly defined concentric rings owing to their randomly orientated domains of cubic symmetry [170]. Figure 3.2 shows the 1D

azimuthally integrated SAXS patterns of freshly made MAG LCP systems of MO and MPL. Bragg peaks have been indexed according to the Miller indices of the reflection plane to assign the mesophase. The relative positions of the reflection lines indicated the presence of highly ordered bicontinuous cubic phases in our samples. As expected, in all of the systems for both host lipids, the phase in equilibrium with excess water was of the cubic-Q_{II}^{D} type with lattice parameters (Table 3.1) slightly higher than those referenced in the literature [359, 360]. The calculated water channel diameter dimensions however (Table 3.1) were in agreement with published values [123, 169] with larger values for channel diameter calculated for the MPL system as expected [353].

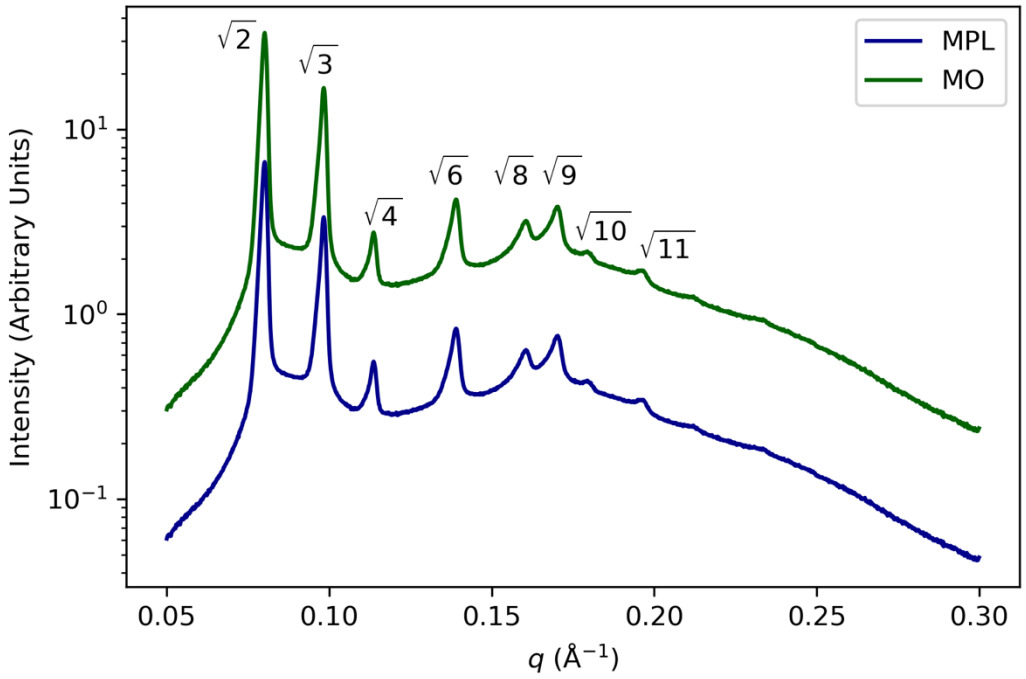

Figure 3.2 1D azimuthally integrated SAXS patterns of fresh monoolein (MO) and Monopalmitolein (MPL) of blank cubic mesophases. The peaks of both patterns have been indexed according to the Q_{II}^{D} mesophase. Repetitions (see appendix B) demonstrated no impact on the mesophase from radiation damage.

Samples prepared below excess hydration levels saw a transition from the Q_{II}^{D} to Q_{II}^{D} + Q_{II}^{G} that occurred across all specimen, even in those prepared fresh on the day of testing (data not shown). In these dual-phase regions, the individual lattice parameter of the respective phases should remain constant with little influence from the sample make-up as a whole. In Table 3.1, the transition from

a single phase to the co-existence of two bicontinuous cubic phases in the monoolein/water system is seen as dehydration of the sample occurs [177, 352], likely occurring during transferal to the sample stage and also during storage [476]. It is also possible that the fresh formulations had not yet fully equilibrated to a homogeneous hydration state at the time of testing, which could explain the coexistence of two cubic phases. The coexistence between the Q_{II}^{D} and Q_{II}^{G} is supported by the Bonnet ratio between the lattice parameters: the ratio of unit cell dimensions of coexisting cubic phases related through Bonnet transformations [368]. In the case of coexistence between Q_{II}^{D} and Q_{II}^{G} mesophases, the Bonnet ratio should be 1.57. It should also be noted at this point, that in utilizing X-rays for sample research, the impact of radiation damage on any given specimen, especially those soft biomaterials such as lipid mesophases, is a justified concern. However, the work of Cherezov and colleagues attests that the radiation dosage and exposure time used in this investigation is not likely to have a significant impact on the MAG mesophases under examination [477]. Here, 15 frames per sample recorded sequentially in one single location were analyzed and no significant difference was observed in the series plots (appendix B).

Table 3.1. Phase identification and lattice parameters of assigned mesophases at varied THL loadings from SAXS experiments with calculated dimensional values for lipid chain length (L) and water channel diameter (DH2O). Samples assigned F were made fresh on the day of SAXS experiments.

Host Lipid	THL (wt%)	Storage (days)	Phase	Lattice Parameter (nm)	L (nm)	D_{H2O} (nm)	Bonnet ratio (where applicable)
MO	0	F	Q_{II}^{D}	10.17	1.74	4.475	-
MO	0	21	n/a*	-	-	-	-
MO	0.7	F	Q_{II}^{D}	9.92	1.69	4.369	-
MO	1.5	F	Q_{II}^{D}	9.6	1.64	4.227	-
MO[CE]	1.5	21	Q_{II}^{D}	9.63	1.65	4.228	1.49
		21	Q_{II}^{G}	14.34	1.43	4.25	
MO	2.5	F	Q_{II}^{D}	9.24	1.58	4.064	-
MPL	0	F	Q_{II}^{D}	10.8	1.48	5.482	-
MPL	0	21	n/a*	-	-	-	-
MPL	0.7	F	Q_{II}^{D}	10.47	1.43	5.320	-
MPL	1.5	F	Q_{II}^{D}	9.96	1.36	5.059	-
MPL[CE]	1.5	21	Q_{II}^{D}	10.38	1.42	5.276	1.56
		21	Q_{II}^{G}	16.20	1.62	4.794	
MPL	2.5	F	Q_{II}^{D}	9.88	1.35	5.025	-

[CE] samples that presented the coexistence of two mesophases; [a] *one single peak detected i.e. no mesophase; storage time of sample in sealed vial prior to SAXS

Table 3.1 reports the mesophases assigned for samples doped with varying concentrations of THL, the lipase inhibitor, up to 2.5 wt% obtained from SAXS experiments. The formulations of both MO and MPL at increasing concentrations of THL present cubic structures almost identical to those of the blank matrices. Figure 3.3 shows the effect of incorporating increasing concentrations of the hydrophobic THL in MAG LCP systems of MO and MPL on the SAXS patterns. The addition of the lipase inhibitor appeared to bear no major effect on the peak positioning with only minor shifts in scattering vector q observed. The integrated SAXS patterns demonstrated how increasing the concentration of the THL lipstatin saw a shift towards higher q for the LCP systems. This is directly related to the swelling of the phase; with higher q indicating a smaller lattice parameter of the mesophase. The lattice spacing and space group assignment provide a metric for the estimation of cubic phase structural dimensions, which can aid in host lipid selection and loading capacity determination. The volume fraction of the lipid component along with d-spacing values were essential parameters in estimating the internal dimensions of the mesophases [354]. Values pertaining to the structural dimensions of the cubic formulations were calculated utilizing these parameters as well as the phase identity obtained from the SAXS experiments according to equations 2.2 through 2.5. In bicontinuous cubic phases, under conditions of equilibrium, the characteristic lattice spacing is directly related to the diameter of its penetrating water channels; and an increase in parameters is observed with increasing hydration. This increase is seen only within certain limits [352].

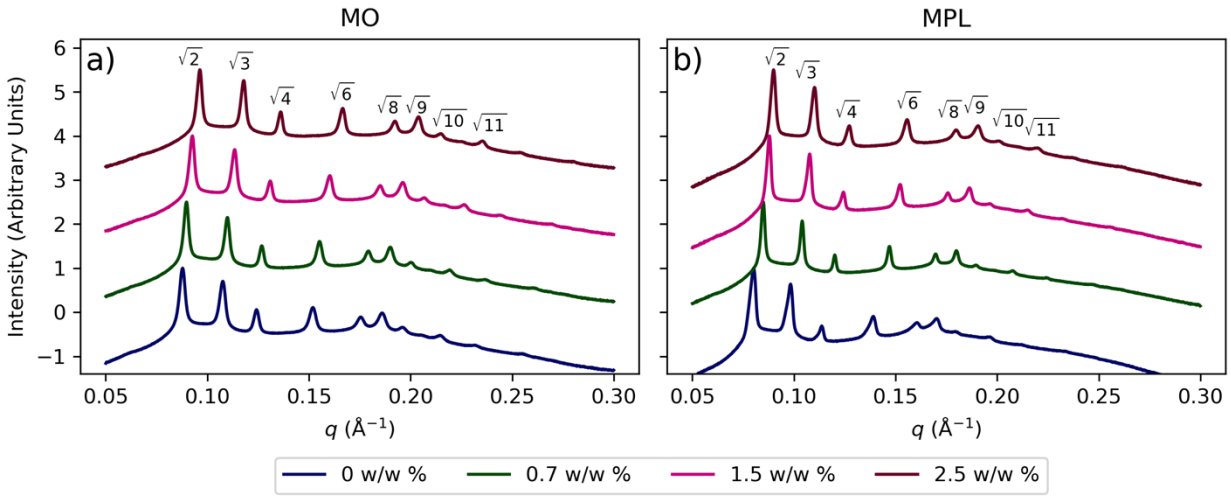

Figure 2.3. Azimuthally integrated SAXS patterns of monoolein (MO, a) and monopalmitolein (MPL, b) mesophases doped with increasing concentrations of THL from 0 (fresh) – 2.5 w/w %. The patterns have been indexed according to the Q_{II}^{D} mesophase.

In the case of the monoolein LCP system, the amount of the hydrophobic THL added appeared to be inversely related to the aqueous channel diameter; reducing by a little over 0.4 nm as the weight percent of THL increased from 0 to 2.5 % w/w, Table 3.1. A decrease in water channel diameter is also evidenced by higher q values as shown in Figure 3.3 This coincided with a slight reduction in lattice parameter for these samples. A similar relationship was seen in the LCP systems prepared with the shorter chain monopalmitolein host lipid whereby an increase in THL loading saw a reduction in both the water channel diameter and lipid layer depth. Indeed, the reduction in this case was slightly higher than that in the MO 9.9 MAG monoolein system, with a reduction of almost 0.5 nm observed.

The impact of THL on the stability of the LCP systems over time was also investigated where the metastability of the phase structure over 3 weeks was studied. Diffraction patterns were examined in relation to those samples freshly prepared on the day of testing. A phase transition, similar to that observed in the samples prepared below excess hydration, was seen in those samples stored over a 3 week period when prepared with the inhibitor, where peak broadening and the co-existence of two cubic systems ($Q_{II}^{D} + Q_{II}^{G}$) was presented (Figure 3.4 (a) and (b)). However, in samples prepared without the THL, the initial phase transitioned even further beyond the liquid crystalline region entirely, highlighting the stabilizing effect of the THL inhibitor on the LCP

mesophase. Smooth, sharp diffraction rings corresponding to discrete cubic phase symmetry are highlighted in the 1D azimuthally integrated SAXS patterns for the fresh samples in Figure 3.4 (a) and (b).

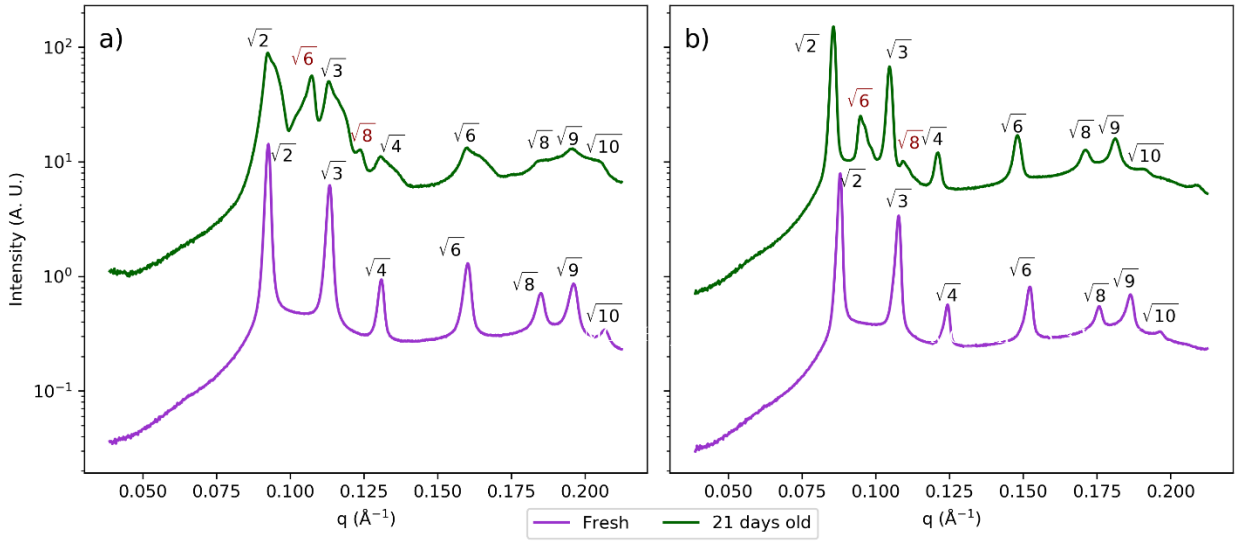

Figure 3.3. The effect of incorporating the hydrophobic THL lipstatin on the stability of monoolein (a) and monopalmitolein (b) lipid systems over 3 weeks at 37° C. Bragg peaks have been indexed according to the Miller indices of the reflection plane to assign mesophase. 1D azimuthally integrated SAXS patterns of blank mesophases and those doped with 1.5 w/w % THL in order of decreasing storage time prior to analysis. The patterns have been indexed to either the Q_{II}^{D} (black text) or Q_{II}^{G} (red text) mesophase.

The observed increase in stability of the MAG LCP systems over time owed to the presence of the inhibitor may be related to changes in the packing frustration of the phases. When considering the phase behaviour of pure monoacylglycerols such as MO and MPL, there are really only two major influential parameters at play – temperature and water content. However, when you venture outside of pure lipid systems and begin to consider how their behaviour is affected or driven by other compositional factors such as the inclusion of additive molecules, one might find that the phase behaviour changes, potentially deviating from their classical binary behaviour. The impact of introducing a third contributing factor stretches the system beyond this simplistic model to a much more complex ternary system [478]. The introduction of hydrophobic molecules in particular has been shown to induce changes on the molecular level, subsequently altering the morphology of the phase. These studies described the effect on packing frustration (the energy cost associated

with deviation from the favoured shape in a particular phase) of MO cubic phases induced by the addition of a hydrophobic long chain alkane tricosane [153]. They have demonstrated the relationship between the packing frustration and cubic phase stability, whereby the introduction of the hydrophobic molecules reduced the frustration by partitioning into the hydrocarbon chain domains [152, 479], subsequently stabilizing the mesophase [480]. The stabilizing effect may also be explained by an interaction between the hydrophilic moieties of the tetrahydrolipstatin molecule and the water present in the penetrating channels. It is possible that hydrogen bonding between water and the carbonyl or amide groups of THL, Figure 3.1, could retain water molecules in the matrix, thus maintaining the cubic phase over the three week storage period investigated, where dehydration of the blank systems resulted in the disassembly of the mesophase. More thorough SAXS investigations into the exact location of the inhibitor in the phase would be required to corroborate this theory.

Ultimately, the objective of this study was to control the rate of release of hydrophobic drugs from LCP systems. To assess the suitability of the THL-containing LCP systems as controlled drug delivery matrices, two model pharmaceutical agents (caffeine and CFZ-citrate salt) were selected based on their propensity to dissolve in water. Samples were prepared with increasing amounts of both APIs (1 and 3 wt%) in a bid to establish the carrying capacity of the cubic phase for APIs located in different regions of its network. The resulting mesophases and their corresponding dimensional estimations are shown in Table 2.2. As with samples without added API, coexistence between Q_{II}^{D} and Q_{II}^{G} mesophases is supported by the Bonnet ratio.

Table 2.2. Phase identification and lattice parameters of assigned mesophases for varied THL and model API loading from SAXS experiments with calculated dimensional values for lipid chain length (L) and water channel diameter (D_{H2O})

Host Lipid	THL (wt%)	API	Storage (days)	Phase	Lattice Parameter (nm)	L (nm)	D_{H2O} (nm)	Bonnet ratio (where applicable)
MO^{CE}	0	CFZ 3%	2	Q_{II}^{D}	10.74	1.83	4.732	-
			2	Q_{II}^{D}	9.55	1.63	4.207	
MO^{CE}	1.5	CFZ 1%	2	Q_{II}^{D}	8.89	1.52	3.904	1.58
			2	Q_{II}^{G}	14.01	1.85	3.246	
MPL^{CE}	0	CFZ 1%	2	Q_{II}^{D}	11.12	1.52	5.654	-
			2	Q_{II}^{D}	12.44	1.71	6.305	
MPL^{CE}	0	CFZ 3%	2	Q_{II}^{D}	9.65	1.32	4.904	-
			2	Q_{II}^{D}	10.56	1.44	5.370	
MPL^{CE}	1.5	CFZ 1%	2	Q_{II}^{D}	10.62	1.46	5.380	-
			2	Q_{II}^{D}	11.84	1.62	6.012	
MO	0	Caff 1%	2	Q_{II}^{D}	10.07	1.72	4.432	-
MO	0	Caff 3%	2	Q_{II}^{G}	15.09	1.99	3.502	-
MO	1.5	Caff 1%	2	Q_{II}^{D}	9.71	1.66	4.271	-

MPL^{CE}	0	Caff 1%	2	Q_{II}^{D}	11.75	1.61	5.964	1.54
			2	Q_{II}^{G}	18.11	1.81	5.36	
MPL^{CE}	0	Caff 3%	2	Q_{II}^{D}	11.82	1.62	5.997	1.53
			2	Q_{II}^{G}	18.11	1.81	5.36	
MPL	1.5	Caff 1%	2	Q_{II}^{D}	10.46	1.43	5.316	-

^{CE} samples that presented the coexistence of two mesophases *one single peak detected i.e. no mesophase; storage time of sample in sealed vial prior to SAXS

The incorporation of the hydrophobic CFZ citrate salt into the lipid matrices lead to an increase in the lattice parameter, and the width of the water channels. This effect was more pronounced in the case of the upper loading of 3 wt% API. In the MPL system, the coexistence of a second double diamond cubic phase structure is observed with larger structure parameter values at both API loadings (+ 0.91 to 1.32 Å). In the MO LCP-THL system, a phase coexistence was observed, with reduced water channel diameter and shift to higher q (Å) noted. The incorporation of hydrophilic caffeine at 1 wt% loading into the MO LCP formulations did not significantly affect the lattice parameter and size of water channels. The relatively small size of the molecule (0.243 nm^3) [481] meant that it could be easily accommodated in the aqueous channels (4.48 ± 0.03 and 5.48 ± 0.13 nm in MO and MPL LCP respectively, shown as the mean value of 3 samples ± standard deviation) of the matrix and therefore the Q_{II}^{D} structure was preserved. The presence of the caffeine (1 wt%) in the 1.5 wt% THL LCP system left the phase seemingly unaffected, with a single Q_{II}^{D} space group maintained for both MO and MPL host lipid LCPs that were comparable to the blank systems. It is clear that the structural parameters of the Q_{II}^{D} regions are greater than those of the Q_{II}^{G} . This is expected as the Q_{II}^{D} phase is accessed at a higher hydration point than the Q_{II}^{G} region, which in turn influences the physical dimension of the unit cell [177, 352]. The presence of an unassignable peak between 0.134 and 0.136 $Å^{-1}$ in the MO samples containing the caffeine API may be owed to API precipitation or formation of a caffeine hydrate in the system as the sharp Bragg peak was not

observed in the blank system and could not be assigned to any mesophase. Its presence does however allude to the existence of a crystal of some sort.

The release kinetics of the cubic phase are governed by the phase identity and the capacity of its aqueous channels. In addition to the effect the physio-chemical properties of the matrix itself have on the diffusion of the API, the properties of the API being incorporated also influence the transport properties of the matrix and have been reported to induce phase transformations upon formulation [123, 168, 212]. It is therefore imperative to ensure that the incorporated API does not disrupt the assembly of the cubic phase lattice structure which may in turn affect its function. In some cases, this may limit the use of the cubic phase as a drug delivery matrix. While some dimensional changes in the crystallographic unit cell were observed upon the incorporation of both model drugs, the conclusion was drawn that the molecular distribution of the lipid cubic phases was not significantly altered by their presence at concentrations below 3 wt%. Additionally, the incorporation of the lipase inhibitor THL did not induce a phase transition and both systems have shown the ability to preserve the cubic structures at room temperature, showing only a small increase of the crystallographic unit cell parameter. This is important as major changes in the phase properties or transitions out of the cubic region caused by the incorporation of an API, may render the system unsuitable for certain applications as their release kinetics are governed by the mesophase of the lipid delivery system.

3.5.2 Swelling and degradation

As previously discussed, the integrity of lipid cubic systems, especially those generated from MAG host lipids, is vulnerable in the presence of a family of enzymes referred to as lipases [482]. This in turn may directly impact the release of the APIs that it encapsulates. In humans three major lipases exist, where their role is in the digestion and catabolism of dietary fatty intake [463, 483, 484]. The lipase family of enzymes display significant sequence homology between species and this investigation utilized a model lipase from porcine pancreas to which tetrahydrolipstatin has the ability to bind and inhibit through irreversible interactions [485]. The lipolysis of the cubic phase in solution was followed both visually and gravimetrically. At predetermined time points, the mass of the gel was measured and the residual weight % was calculated (equation 3.3). The degradation could also be tracked visually, and its initiation was indicated by the formation of an

off-yellow oil layer on the outer surface of the gel. The digestion eventually resulted in an entirely cloudy solution with the oily layer sitting on top.

For both MAG LCP systems, those exposed to lipolytic enzyme in the incubation medium saw a rapid decline in original mass for the blank MAG lipid cubic systems compared to those incubated in enzyme-free PBS buffer. The integrity of the MO LCP was compromised, and the enzyme action broke down the entire gel after a 7 day exposure. The gel that was spared lipase exposure maintained almost half of its original mass over the testing period of 12 days. Similarly, in the MPL LCP system, the gel maintained 94 ± 0.53 % of its original mass after 17 days in the enzyme free buffer, while the cubic gel exposed to lipase was digested to its oleic acid and glycerol components over the course of 10 days. In fact, the gel incubated in lipase-free buffer was subject to a loss of only 13 ± 2.5 % over a testing period of 36 days.

Tetrahydrolipstatin is a potent lipase inhibitor and the lipophilic molecule exerts its inhibitory effect upon binding the pancreatic lipase at its serine active site as previously mentioned in the introduction to this study. THL was incorporated into cubic formulations generated from both host lipids at increasing concentrations to study its effectiveness in impeding their lipolysis. Concentrations of 0.35, 0.7, 1.5 and 2.5 wt% were chosen to study the potential tunability of the systems in terms of the LCP lifespan compared to the blank systems as a means of further controlling the rate of release of hydrophobic APIs in particular, which is concomitant with hydrolytic digestion.

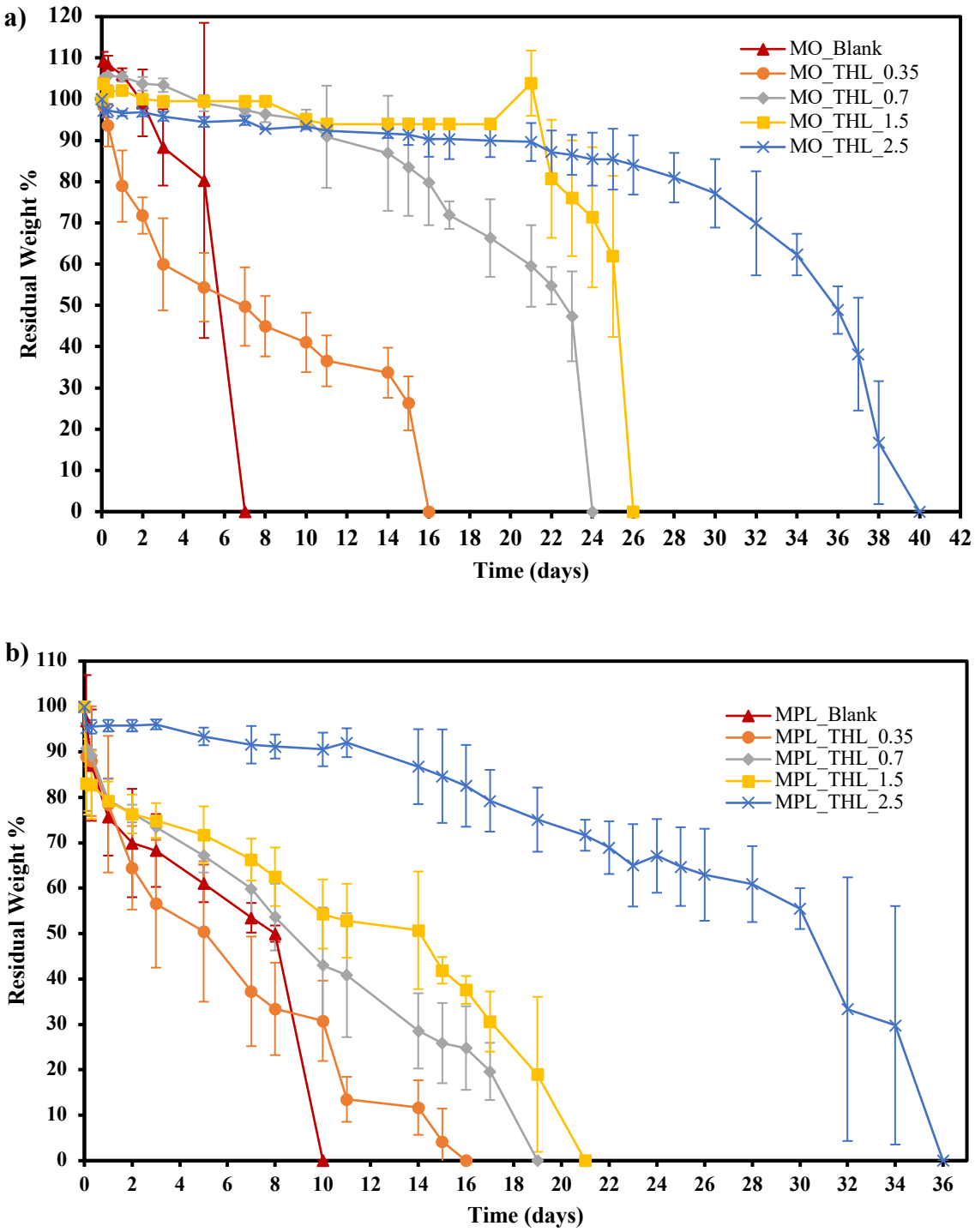

Figure 3.5. Swelling and degradation profile of: a) Monoolein and b) Monopalmitolein LCP formulations (Blank or formulated with THL) in Physiological Buffer (1X PBS) incubated at 37°C in the presence of lipase enzyme. Each point represents a mean value ± standard deviation of three determinations.

Figure 3.5 (a) shows the enzyme-driven hydrolysis of the monoolein LCP gels, both with and without THL up to 2.5 wt% embedded in its network. Increasing the concentration of the THL in the lipid network incrementally decreased the degradation rate of the gels by almost 6 fold at the highest loading compared to the LCP without inhibitor. Even at the lowest inhibitor concentration (0.35 wt%), the loss in original mass was slowed down and the systems maintained 49.7 ± 9.5 % of their original mass after 7 days when the blank LCP had been fully digested into their soluble oleic acid and glycerol components.

A control group was also studied, where MO LCP was incubated with lipase and free THL in solution at a concentration of 1.5 mg/mL. Here, an increase in stability was observed as the samples were fully degraded after 15 days compared to the degradation rate of the MO LCP with lipase, where they had fully degraded by day 7. The rapid loss in mass may have occurred as a result of a combination of phase change and mass depletion rather than solely the lipolysis of the lipid component itself. In this control group, the THL in solution was replenished with each change of media at least every 24 hours, and yet the MO LCP with the THL incorporated into its network displayed greater stability and did not fully degrade until day 24. These latter samples only had the initial 1.5 mg/ml of THL added for the duration the experiment and the depletion in mass occurred with little initial swelling observed, possibly on account of the hydrophobic effect of the membrane bound inhibitor pointing towards a predominantly surface-driven digestion pattern.

The same experimental conditions were tested on the MAG LCP of shorter chain length, monopalmitolein, Figure 3.5 (b). Once again, an increase in stability was noted in the presence of the THL, even at the lowest loading of 0.35 wt% where the LCP samples maintained between ~31 - 33 % of their original mass at 10 days by when the blank gels were completely broken down. There was no observed swelling between tested time-points indicating that the diffusion of enzyme solution into the phase did not outpace the degradation. The 0.35 wt% samples were not fully digested until after 15 days in incubation.

Both systems were considered to be comparable in terms of tunable stability, and for the majority the error, while still relatively small, between samples may be generally explained by the variation in distribution of the lipstatin between gel formulations. Although all samples were prepared following identical protocols of manual and vortex mixing, the hydrophobic inhibitor is suspended

rather than dissolved within the formulation and is likely not completely homogeneous. While the two LCP systems appear to follow similar digestive trends, the incorporation of the THL showed a more prolonged stability period in the MO LCP versus the MPL system compared to the samples prepared without the inhibitor in their respective profiles. This difference may be attributed to the difference in water channel diameters and lipid packing described already in the SAXS section of this investigation, where the wider diameter of aqueous channels in the MPL system allowed for a higher penetration of the external lipase solution into the phase's aqueous network, in turn speeding up the degradation process. The SAXS data clearly showed a lower degree of swelling of MO LCP in the presence of THL under conditions of excess water (shown by higher q values) suggesting that lower volumes of lipase solution could penetrate and diffuse into the phase.

The faster degradation of the MPL LCP system may therefore be attributed to the higher surface area associated with the lipid portion of the phase. The interfacial area per lipid molecule of both MAG LCP systems was calculated using equation 3.2 which utilized the lattice parameter and calculated lipid chain length obtained from the SAXS data. The calculated surface area was shown to be larger in the shorter chain MPL system (Table 3.3). This provides the lipase with a larger access area at the interface required for it to carry out its lipolysis. On the contrary, the surface area is seen to increase as the water channel diameter decreases with higher THL loadings. Despite this, the degradation is clearly slowed down by the THL's presence which may seem counter-intuitive. It is however hypothesized that with the larger associated surface area of the lipid portion, comes greater inhibitor exposure at the interface where lipase acts.

Table 3.3. Calculated interfacial area per lipid molecule (a_i) of MAG LCP generated at different THL loadings

Host Lipid	THL %	Storage (days)	mesophase	a_i (nm^2)
MO	0	F	Q_{II}^{D}	3.13 x 10^{-22}
MO	0.7	F	Q_{II}^{D}	3.22 x 10^{-22}
MO	1.5	F	Q_{II}^{D}	3.32 x 10^{-22}
MO	2.5	F	Q_{II}^{D}	3.45 x 10^{-22}
MPL	0	F	Q_{II}^{D}	3.43 x 10^{-22}
MPL	0.7	F	Q_{II}^{D}	3.54 x 10^{-22}
MPL	1.5	F	Q_{II}^{D}	3.73 x 10^{-22}
MPL	2.5	F	Q_{II}^{D}	3.75 x 10^{-22}

Once again, the digestion of the LCP samples was easily trackable upon visual inspection. After prolonged lipase exposure, the sample appearances became cloudier in colour, with a brittle core covered in a more viscous outer layer. The samples prepared with the inhibitor maintained the characteristically clear colour of the lipid cubic phase for longer than those blank samples; with the change in appearance noted after only 3 days in incubation for the blank gels compared to 7 days in the doped gels.

To confirm that the THL-containing samples maintained the cubic phase as well as the system mass in the presence of the lipase solution, LCP samples were prepared for both host lipid systems with and without THL at 1.5 wt% incorporated into the membrane and were exposed to lipase solution for 3 days before SAXS analysis was conducted. In both cases, the Q_{II}^{D} structure was preserved despite a reduction in mass noted for the samples prepared in the absence of THL (Table 3.4).

Table 3.4. Phase identification and lattice parameters of assigned mesophases for varied THL loading exposed to lipase from SAXS experiments

Host Lipid	THL (wt%)	Storage (days)	Mesophase	Lattice Parameter	L (nm)	D_{H2O} (nm)
MO[CE]	0	3	Q_{II}^{D}	10.64	1.81	4.693
			Q_{II}^{D}	9.66	1.65	4.248
MO	1.5	3	Q_{II}^{D}	9.68	1.65	4.265
MPL[CE]	0	3	Q_{II}^{D}	10.56	1.45	5.355
			H_{II}	9.35	-	-
MPL[CE]	1.5	3	Q_{II}^{D}	10.31	1.41	5.238
			Q_{II}^{D}	9.35	1.28	4.749

L is the lipid chain length/monolayer thickness (nm); D_{H20} is the diameter of the water channels (nm);[CE] samples that presented the coexistence of two mesophases; storage time of sample in sealed vial prior to SAXS

In the more readily digested MPL system in the absence of THL, the SAXS data demonstrated a transition of the LCP to what appears to be a hexagonal phase (H_{II}) within the network after exposure to the lipase. It is described in the literature that both the instinctive formation of the phase and the thermodynamic stability of the LCP are driven by an opposition between a pair of free energy terms. When this competition between the curvature energy of the individual monolayers and stretching energy of the lipid chains exists in its least frustrated state, it is suggested to be responsible for the nature of the solid state phase and its position on the phase diagram [151]. The hexagonal phase comprises an arrangement of limitless water rods divided by lipid bilayers in a two dimensional lattice and the transition to the phase upon lipase interaction has previously been reported where the presence of the lipase in solution served to increase the curvature of the system, subsequently altering the molecular structure inducing a phase transition

[146, 257]. This was not seen in the MO system although the presence of a second Q_{II}^{D} lattice was noted where only one existed in the sample containing the inhibitor. The same phenomenon was seen in the MPL system even in the sample formulated with the inhibitor.

Additionally, the immediate impact of lipolytic enzymes on the structure of the phase was also studied by swelling the lipids in an enzyme solution at a concentration of 5 mg/mL (Table 3.5, appendix B).

Table 3.5. Phase identification and lattice parameters of assigned mesophases for LCP formulated with various biologically enzymes from SAXS experiments. Enzyme stock solutions were prepared at 5 mg/mL concentration

Host Lipid	**Buffer**	**Assigned mesophase**	**Lattice Parameter (nm)**	**L (nm)**	**D_{H2O} (nm)**
MO	Lipase	Q_{II}^{D}	10.37	1.77	4.56
MO	Pancreatin	Q_{II}^{D}	10.29	1.76	4.53
MPL	Lipase	Q_{II}^{D}	11.34	1.55	5.76
MPL	Pancreatin	Q_{II}^{D}	11.23	1.54	5.7

While changes in internal dimensions were noted (reduced water channel diameter) compared to those systems swelled in water, both MO and MPL systems formed the Q_{II}^{D} phase in the presence of the enzymes. This was unsurprising as the lipid cubic phase is commonly used in protein crystallization techniques [145] and readily incorporates proteins of different sizes and charge. These results prove that the phase changes and break down of the system over time in the enzyme media are not caused by disruption caused by the size or shape of the proteins when taken up by the mesophase, but solely the hydrolysis of the individual lipid molecules by the enzymes.

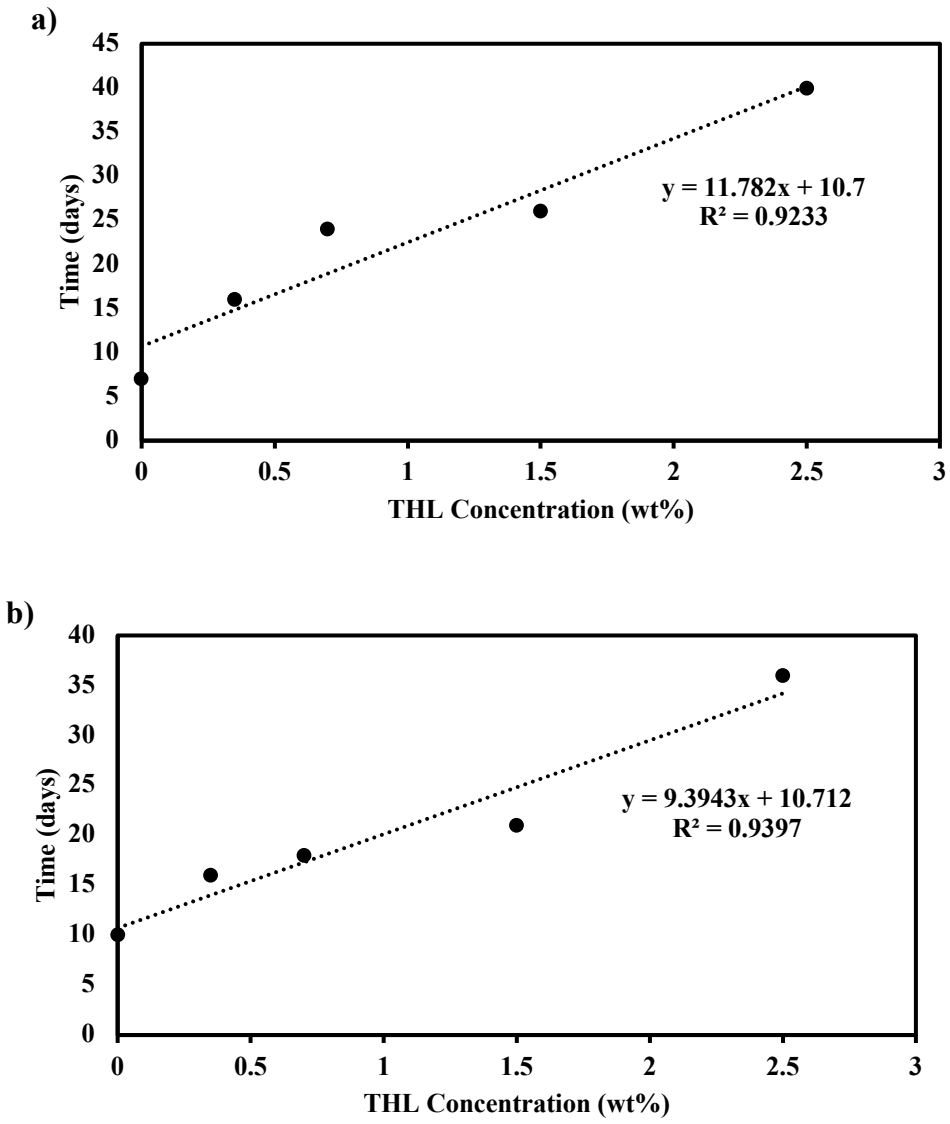

Figure 3.6. Stability plots for a) MO-THL and b) MPL-THL LCP-inhibitor systems showing increasing THL concentration plotted against the stability (days) of the cubic phase in lipase solution.

From the stability tests conducted in the presence of lipase, it may be possible to control the duration of the prolonged release of hydrophobic molecules from LCP matrix networks using lipase inhibitors, allowing for the selection of the most suitable system for a given clinical drug delivery application. Figure 3.6 shows stability plots for both of the LCP-inhibitor formulations; where increasing THL concentration was plotted against the stability of the phase in lipase

solution. These models may provide researchers with a mode of predicting the phase stability against lipase digestion up to 40 or 36 days for the MO- and the MPL- THL LCP systems respectively across a range of inhibitor concentrations from 0 to 2.5 wt%.

3.5.3 Drug release studies

Numerous approaches have been described to modulate the kinetics of drug release to systematically control or prolong the drug delivery period of hydrophilic agents [168, 170, 435, 486, 487]. This study sought to investigate the impact of addressing the rate of degradation of the phase as a means to control the release of model APIs. A particular interest lay with understanding in its impact on hydrophobic pharmaceuticals. It was hypothesized that the incorporation of the inhibitor would have greater influence on the predicted degradation-driven release of hydrophobic agents and little to no effect on more water-soluble molecules.

Clofazimine (CFZ), an antimycobacterial agent indicated for the treatment of leprosy, was selected as a model drug on account of its Biopharmaceuticals Classification System (BCS) class II properties of low aqueous solubility. Our group has previously developed a number of novel salt forms of clofazimine in a bid to improve the uptake of the drug *in vivo* [471]. One of these salts, co-formed with a citrate ion, was selected for this study on account of its enhanced aqueous solubility (~40 mg/L) which made studying its release possible. Not only that, but the API itself has shown high uptake in micelles and liposomes [488] and so its highly lipophilic nature [489] render CFZ a perfect subject to profile the release of membrane anchored molecules from our LCP-inhibitor systems.

The release of CFZ-citrate from the MAG systems, with and without THL and in the presence of lipase at 37°C, is displayed in Figure 3.7. Upon initiation of significant digestion of the LCP matrices after approximately 24 hours in both systems in the absence of the inhibitor, CFZ-citrate release appears to be inversely proportional to the residual mass of the matrix. In the case of lipophilic APIs such as CFZ citrate which are thought to be predominantly located in the lipid bilayer, the rate of their diffusion is believed to be limited by their partitioning into the bilayers and is controlled by the erosion and breakdown of the carrier [174]. The release of the CFZ salt was found to be slower in the MO-based LCP compared to the MPL system under identical conditions. This result was expected from the faster degradation observed for MPL (Figure 3.5) in

the absence of THL and presence of lipase, where the gel was entirely digested into its core constituents. The oil layer maintained the characteristic red colour of the CFZ indicating that some of the API remained bound to the lipid digestion products at the end of the LCP gel degradation.

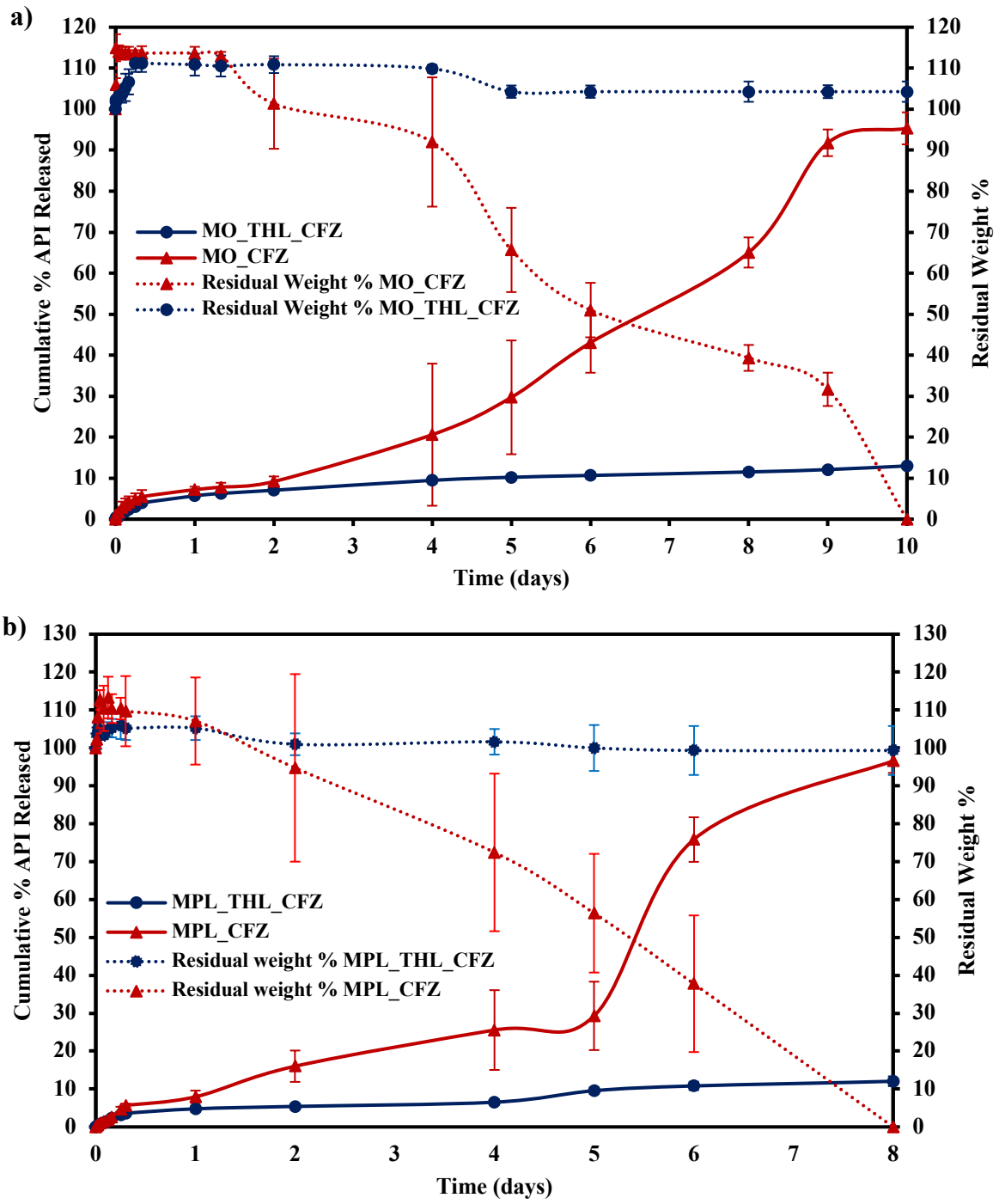

Figure 3.7. Dissolution profiles of the hydrophobic model drug Clofazimine-citrate salt (1 wt%) from a) MO and b) MPL LCP formulations (Blank or formulated with 1.5 % w/w THL) into water incubated at 37°C in the presence of lipase enzyme showing the corresponding swelling and degradation behaviour of the gels. (Water replaced PBS for the release study with CFZ-citrate.) Each point represents a mean value ± standard deviation of three determinations.

The influence of THL on the dissolution profiles is also clearly represented in Figure 3.7 compared to the samples without the inhibitor; showing the prolonged release of the hydrophobic model drug upon its addition to the mesophases. The release rates were significantly slower in the systems that had the THL in their network with less than 20% cumulative release in both host lipid formulations after the testing period, indicating that its incorporation can control the rate at which the drug is eliminated from the gels. As discussed, this control is believed to be owed to the interaction of the THL with the lipase, thus inhibiting the degradation of the cubic mesophase. In the absence of the inhibitor, the lipase acts at the lipid/water interface to breakdown the matrix into an oily emulsion enabling the CFZ-citrate to partition into the media while this effect is delayed by the presence of the THL.

In the MO system formulated with 1.5 wt% THL, the CFZ salt continued to be released into solution at a steady rate over a 3 week testing period. After a 21 day incubation at 37°C and 200 rpm approximately 25% of the drug was released. 40% of the original CFZ salt loading in the MPL-THL system was released from the bulk phase after this period. The MO-based gel mass had not reduced beyond 20% of its original weight and the MPL system maintained almost 60% of its original mass after this time. These results highlight the influence of tunable degradation of the cubic phase on controlled release of hydrophobic agents.

The release data for these hydrophobic API systems was fitted to a number of theoretical and empirical drug release models to study the effect the incorporation of the inhibitor had on controlling the release of CFZ-citrate (appendix B). The literature indicates the Korsmeyers-Peppas, first-order kinetics and Higuchi models as the most representative of release from cubic phases [359]. These mathematical models, among others, were applied. However, in this case, the release data did not appear to fit well with these fundamental models described, although the best fit was indeed seen with zero-order and Korsemeyer-Peppas release kinetics indicating an anomalous non-Fickian diffusion transport that is both diffusion and swelling/erosion controlled. In examining the coefficient values (n) obtained for the CFZ salt from the Korsemeyer-Peppas model, values pointing towards non-Fickian case 2 relaxation or super-case transport-2 mechanism were calculated ($n > 0.45$) on account of the hydrophobic salt's location in the lipid membrane. This supported the theory that erosion was a driving force in its release [359]. In both cases, higher coefficient values were observed in the gels without the inhibitor, where significant degradation

was observed over the testing period directly related to the release of the drug into solution. These values allude to deviation from straight-forward diffusive transport and the results reiterate the influence the swelling and erosion of the matrix has on release of CFZ and serves to further affirm the concept of targeting degradation as a reasonable approach to extend the control inherently offered by the cubic phase itself without altering its phase structure.

While it is generally accepted that release of APIs from bioerodible polymers, such as lipid-based systems, is biphasic, driven by both diffusion and matrix effect [271], it is clear from the model plots and the respective r^2 values obtained (appendix B) that the release from these LCP-inhibitor formulations is not simplistic, nor two-dimensional. While these mathematical models provided us with an indication of the release kinetics at play, there are several influential factors in this ternary system that drive the liberation of the hydrophobic API from its network. This makes it difficult to apply the existing simplistic mathematical models to its release, most of which assume a spherical-shaped system, which of course is not this case here. The release profile is, without dispute, complex with a combination/opposing effect of the variables on water uptake and digestion responsible.

As the release kinetics of APIs from LCP depend on their location within the matrix [271], it was expected that the dissolution of the two model agents would follow different kinetics. To highlight the influence of the APIs location within the matrix on its release profile, caffeine was reconstituted in MAG LCP formulations to act as a model hydrophilic agent and the effect of encapsulation with lipase inhibitor THL on its release was studied. Release data was obtained and quantified using HPLC. The dissolution profiles of the hydrophilic model drug from these systems are shown in Figure 3.8, plotted with the degradation profiles of the matrices.

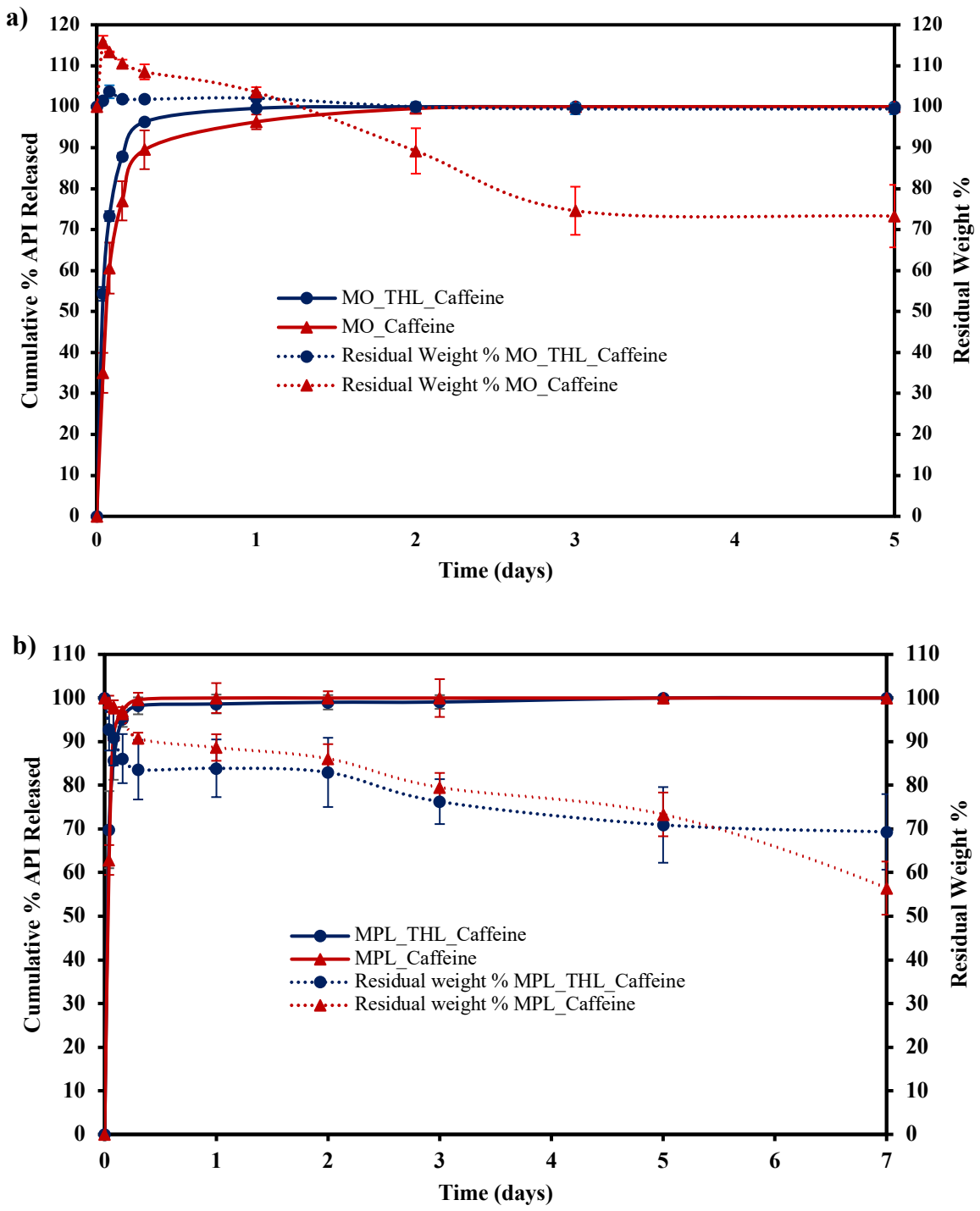

Figure 3.8. Dissolution profiles of the hydrophilic model drug Caffeine (1 wt. %) from a) MO and b) MPL LCP formulations (Blank or formulated with 1.5 % w/w THL) into Physiological Buffer (1X PBS pH 7.4) incubated at 37°C in the presence of Lipase enzyme showing the

corresponding swelling and degradation behaviour of the gels. Each point represents a mean value ± standard deviation of three determinations.

It was seen that the MO and MPL LCP systems were comparable as far as the release of the caffeine is concerned, although a slightly slower release was observed from the MO LCP system. The variations in release may once again be attributed to differences in the water channel diameter of the two systems owing to an osmotic effect; whereby different volumes of water can enter the respective network of channels, and is related to the ratio of the molecule size to water channel diameter [170]. It is obvious from the dissolution profiles of these formulations that the release of caffeine was not greatly influenced by the introduction of THL into MAG systems, as simple diffusive mechanisms were driving its release and were largely independent of matrix effect. A decrease in water channel diameter of almost 0.65 nm calculated in the MPL-inhibitor system upon the addition of caffeine may account for the slighter slower elution observed in the inhibitor system [170]. The theories put forward by Clogston and Caffrey suggested that as the size of the water channel approaches the size of the molecule that it encapsulates, the diffusion of said molecule is slowed or prevented. However, the narrower water channel diameter in our systems still well exceeded that of the caffeine molecule, even if it were to exist as a dimer or trimer and so explains the relatively analogous release profiles with and without the THL inhibitor. The SAXS data showed only minor reductions in water channel diameter upon the addition of 1 wt% caffeine to the monoolein LCP-inhibitor system evidenced in the largely comparable release profiles with and without THL. However, the MO-THL samples did display slightly faster diffusive transport compared to the blank MO-caffeine system despite a decrease in water channel diameter of ~0.6 nm, which contradicts the aforementioned theory. It is most likely explained by the fluid nature of the phase as it has been suggested that the inherent flexibility of the liquid crystalline phase may provide evolving fluid channels that facilitate the movement of molecules through the network [170].

The release data collected from the caffeine system was also treated against a number of mathematical models to obtain a correlation coefficient (r^2), which allowed for evaluation of the kinetics of release of the hydrophilic model API from LCP. The more simplistic release profile was seen to fit better with the linear models compared to the vastly complex elution behaviour

seen in the CFZ salt model. The results (appendix B) indicate that the caffeine does indeed predominantly partition into the aqueous channel network from which it diffuses into the media with little influence from the digestion of the matrix itself. In contrast to the kinetics of CFZ release, when the release data from the various caffeine systems were fitted to the zero-order kinetic equation, the relatively small regression values suggested that the system did not obey the model. However, the dissolution results were found to have a better fit with first order kinetics. The correlation coefficient in this case was closest to unity suggesting that the release of caffeine from LCP most likely follows first order kinetics. This data strongly confirms the expected diffusion-controlled kinetics. In first-order release, the rate of drug diffusion is dependent on the concentration of the API incorporated in the formulation.

Ultimately, this confirms the hypothesis that the incorporation of THL would likely not affect the release kinetics of the hydrophilic agent as its release is, for the most part, independent of the breakdown of the matrix. For this reason, the system would be suitable for a combined therapy application, whereby two or more active agents with opposite solubility properties could be incorporated into the lipid system with the hydrophilic agent being released within the first few days and more controlled, sustained release of a hydrophobic agent could be achieved.

While this investigation focused primarily on an application with bulk lipid cubic gels, there is recognizable scope to extend this approach further to its cubic nanodispersions. In this case, the inhibitor may be encapsulated within the cubosomal network, either pre- or post-fragmentation. The technique of controlling release using inhibitors may be particularly appropriate for these formulations, as cubic nanosystems are more readily degraded by enzymes owing to their increased lipid-media interfacial area. In this instance, the rate of enzymatic digestion versus the length of time required for these nanoparticles to bind with, and be taken up through the cell membrane will determine the release kinetics of an encapsulated drug in a given environment. Here, factors such as pH and enzyme concentration will contribute to these interactions governing the rate at which both occur. Depending on proposed application, one may be interested in tailoring a system that favours one or the other. For example, a cubosomal-inhibitor hybrid system may be attractive where overcoming the blood-brain barrier is desired, as cubosomes have readily demonstrated their ability to do so [473, 490]. Here the inhibitor may serve to maintain the nanoparticle architecture for sufficient time to allow successful transition across the barrier to

deliver the desired drug at the target site. Future work will focus on defining these interactions to distinguish the dominating action, if any.

3.6 Conclusions and Leading Research Questions

Lipid cubic systems derived from biodegradable MAG lipids are highly susceptible to lipolytic degradation by lipase enzymes *in vivo*, potentially limiting their application in drug delivery. In this study, it has been demonstrated that controlled release of hydrophobic APIs can be achieved with a novel formulation approach through the incorporation of small doses of lipase inhibitors, using tetrahydralipstatin as a model. Comprehensive SAXS experiments have shown, notwithstanding some minor alterations in structural parameters, that the incorporation of the inhibitor bore no negative impact on the phase behaviour of our lipid cubic formulations below loading concentrations of ≤ 2.5 wt%.

The influence of hydrolytic enzymes on the stability of the cubic phase has been widely demonstrated [257-259]. The true effect of these enzymes responsible for catalyzing the hydrolysis of lipid membranes was studied here to better predict the degradation rate of the formulated LCP in vivo. Phase stability in the presence of these enzymes was found to control the degradation-driven drug elution. Through the incorporation of THL, the lipid vehicles have demonstrated finely tunable rates of degradation that can be optimally coordinated to release hydrophobic pharmaceutical, and biological molecules over a desired period of time before the gel succumbs to complete digestion. Using CFZ citrate as a model drug, the LCP-inhibitor systems could extend its release profile beyond the one week duration in the blank LCP systems to weeks, and potentially even months through interactions with the lipases responsible for matrix digestion. These hybrid lipid cubic systems may also provide means of delivering inhibitors to control the action of these enzymes. Tetrahydralipstatin is a potent inhibitor of many other lipolytic enzymes additional to the pancreatic lipase studied here. These include gastric lipase, and carboxyl ester lipases. Thus, the approach described here may have a more far-reaching relevance. Should dosage requirements be defined and applied in the formulation, our LCP-inhibitor system could potentially be applied in a variety of drug administration routes with numerous possible target delivery sites where different lipolytic enzymes may be at play. Leading on from the promising results shown here, Chapter IV delves further into the interactions at play between the enzyme inhibitor and the lipid

ligand with the hydrolytic enzyme assisted by *in silico* techniques, with an aim of understanding, what is perceived to be, the competitive process.

Chapter IV: Probing the mechanism behind the inhibitor-controlled degradation of lipid cubic formulations

4.1 Introduction

In this chapter the interactions and cofactors that influence the digestion of MAG derived lipid cubic phases are investigated and within this framework the inhibitory and stabilizing action of the encapsulated THL inhibitor is explored. Unlike regular enzymes that transform soluble substrates, lipolytic enzymes act at the interface between their aqueous medium and the insoluble lipid substrate. Compounds that bind or interact at this interface, including endogenous factors and ions, have the ability to enhance or inhibit the activity of these enzymes to varying extents. This study deals with the interplay between the lipolysis rate and the interfacial interaction of porcine pancreatic lipase with lipid cubic substrates encapsulating a known lipase inhibitor tetrahydrolipstatin (THL) that also acts at this interfacial region. In the present work, inhibitor-modified monoolein lipid cubic formulations designed to encapsulate and control the release of a BCS class IV drug paclitaxel (PTX) were examined under simulated lipolysis in the presence of lipase and its effectors colipase and calcium. Here, thermodynamic measurements and molecular dynamics simulations of the competitive inhibition of pancreatic lipase by THL have been combined with experimental dynamic digestion studies to reveal the role and mode of action of the studied lipase effectors in designing a degradation-controlled release system for the poorly soluble drug PTX.

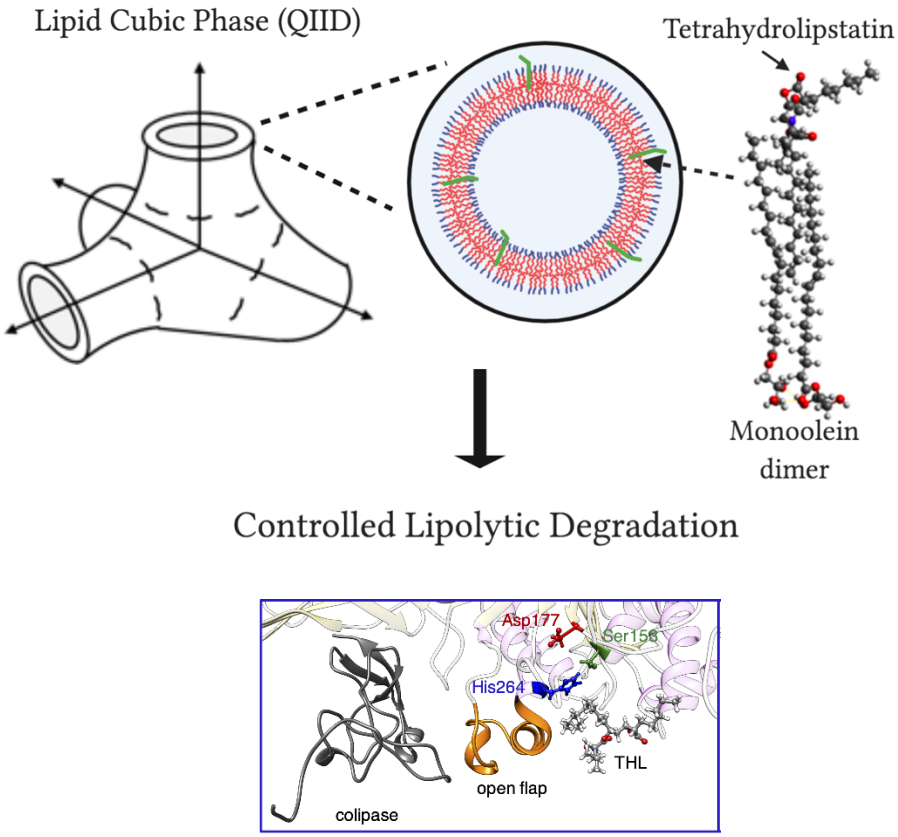

Figure 4.1. Graphical depiction of the incorporation of THL into the lipid bilayer of the lipid cubic phase and its subsequent controlled lipolytic degradation through interaction at the lipase serine active site.

In the interest of transparency, the author wished to credit Dr Shayon Bhattacharya and Dr Damien Thompson at the University of Limerick for their contribution to this chapter in carrying out molecular dynamics simulations and Dr Vivek Verma for carrying out DFT calculations. Cryo-TEM data was collected by Pasi Laurinmaki at the University of Helsinki, Finland.

4.2 Background

Recent advances in drug discovery by automated synthesis, combinatorial chemistry and high throughput screening have identified a large number of poorly soluble, high molecular weight drug candidates with presumed poor ability to permeate biological membranes [491]. Their physicochemical properties place them in the most difficult class IV category of the Biopharmaceutical Classification system (BCS) (Figure 1.1) [4]. Efforts to improve their

bioavailability may require reverting back to the lead optimisation phase to alter the chemical structure in an attempt to improve the physicochemical properties of the Active Pharmaceutical Ingredient (API) [492]. Currently, almost half of marketed drugs can be characterized as poorly soluble [493, 494] and it is reported that the proportion of new chemical entities (NCEs) in drug development displaying poor solubility may be upwards of 75% [106, 495, 496], highlighting issues with solubility as a major obstacle in drug development [497]. Resorting to changing the chemical structure is costly and may not resolve issues with poor membrane permeability. Thus, significant effort has been expended towards developing carrier systems to deliver poorly soluble drugs [215, 252, 435, 486, 487], which can be engineered to also achieve a targeted release in response to environmental stimuli and changes [58, 498-501].

In this work, paclitaxel has been selected as the model hydrophobic BCS IV drug [502] to investigate its release *via* a novel carrier system. Paclitaxel (PTX) is a widely used and effective anti-tumour agent that carries out its function by binding tubulin and impeding DNA duplication [503] but displays very low solubility in aqueous phases [504] and poor permeability across biological barriers [505]. Further, PTX is a known substrate of P-glycoprotein (P-gp) [506], which actively transports PTX back into the extracellular space, reducing effective absorption, permeability, and retention of the drug within the cell [507]. Currently, PTX is reconstituted in mixed solvents composed of polyethoxylated castor oil and dehydrated alcohol for intravenous administration. The known side effects of this formulation, including allergic reaction, neurotoxicity, and nephrotoxicity [508], have motivated development of nanostructured alternatives for PTX delivery [509-512] including lipid-based carrier systems [513-516].

The incorporation of lipophilic drug molecules into lipid-based delivery formulations has been shown to improve the bioavailability of otherwise problematic drugs [120, 297-301]. They do so in a number of ways: increasing drug solubilization by stimulating the secretion of bile into the small intestine, facilitating the solubilization capacity in the intestines through the assembly of micellar structures, and by improving enterocyte-based transport including inhibition of the P-gp efflux system [109, 110]. Among the plethora of lipid-based formulations, it has been discussed earlier in Chapter I section 1.5 why the lyotropic liquid crystalline phases stand out due to their non-toxic, biocompatible and biodegradable nature as well as their bioadhesive properties [1] and thermostability [167, 177, 371, 517]. For this particular application, their autonomous assembly

that is independent of organic solvent is attractive as it eradicates the need for harmful carriers such as polyethoxylated castor oil.

As previously demonstrated in chapter III, an important consideration in the design of these carrier-based drug delivery systems is the degradation behaviour of the host system. In this context, the digestion of the lipid component can significantly impact the performance of lipid-based drug delivery systems. Hence, *in vitro* tests are an important first step in gaining predictive information about the physicochemical changes to the host that will occur *in vivo*. Dietary lipids such as monoolein (MO) shown in figure 4.2 and other MAGs are rapidly digested *in vivo* by the lipase family of enzymes [257], disassembling the liquid crystalline matrix, as described in chapter II. This process has been shown to be accelerated by the presence of a number of cofactor molecules including calcium [518-520] and colipase, an important polypeptide cofactor of the pancreatic lipase (Figure 4.2) [521]. The colipase functions by anchoring the lipase at the lipid-water interface [522, 523], a prerequisite for the digestion of any lipid substrate by lipolytic enzymes. While this rapid enzymatic digestion limits the ability of current MAG LCP to provide sustained release over very long periods [123], particularly following oral administration, it provides a novel means of controlling drug release by targeting and modulating the biological lipolytic degradation process. It has been shown that lipolytic enzyme interactions can be modulated through the incorporation of known lipase inhibitor tetrahydrolipstatin (THL) into the lipid cubic phase to modulate the release of the model small hydrophobic drug clofazimine (CFZ) from LCP (Chapter II).

In this study, monoolein-based lipid cubic formulations designed to encapsulate and control the release of the notorious BCS class IV drug PTX were examined under simulated lipolysis with the aim of better understanding the mechanisms of lipid digestion *in vivo.* A combination of experiments probing the effect of PTX on the lipid cubic structure and examining the degradation profiles of PTX monoolein based lipid formulations with molecular dynamic simulations are conducted to elucidate the role of the lipase cofactor colipase in the competitive inhibition of pancreatic lipase by THL and in the degradation of the lipid cubic system and subsequent release kinetics of PTX. Here this hybrid system is presented as an approach to resolve the issues of low bioavailability of poorly water-soluble drugs by encapsulating the lipophilic drug in the lipid-based matrix. This deeper understanding of the mechanisms at play may guide us towards the design of a broadly applicable, tunable carrier for a wide range of poorly soluble APIs, while overcoming

the issues of instability associated with the lipid mesophase through the inclusion of THL in the formulation.

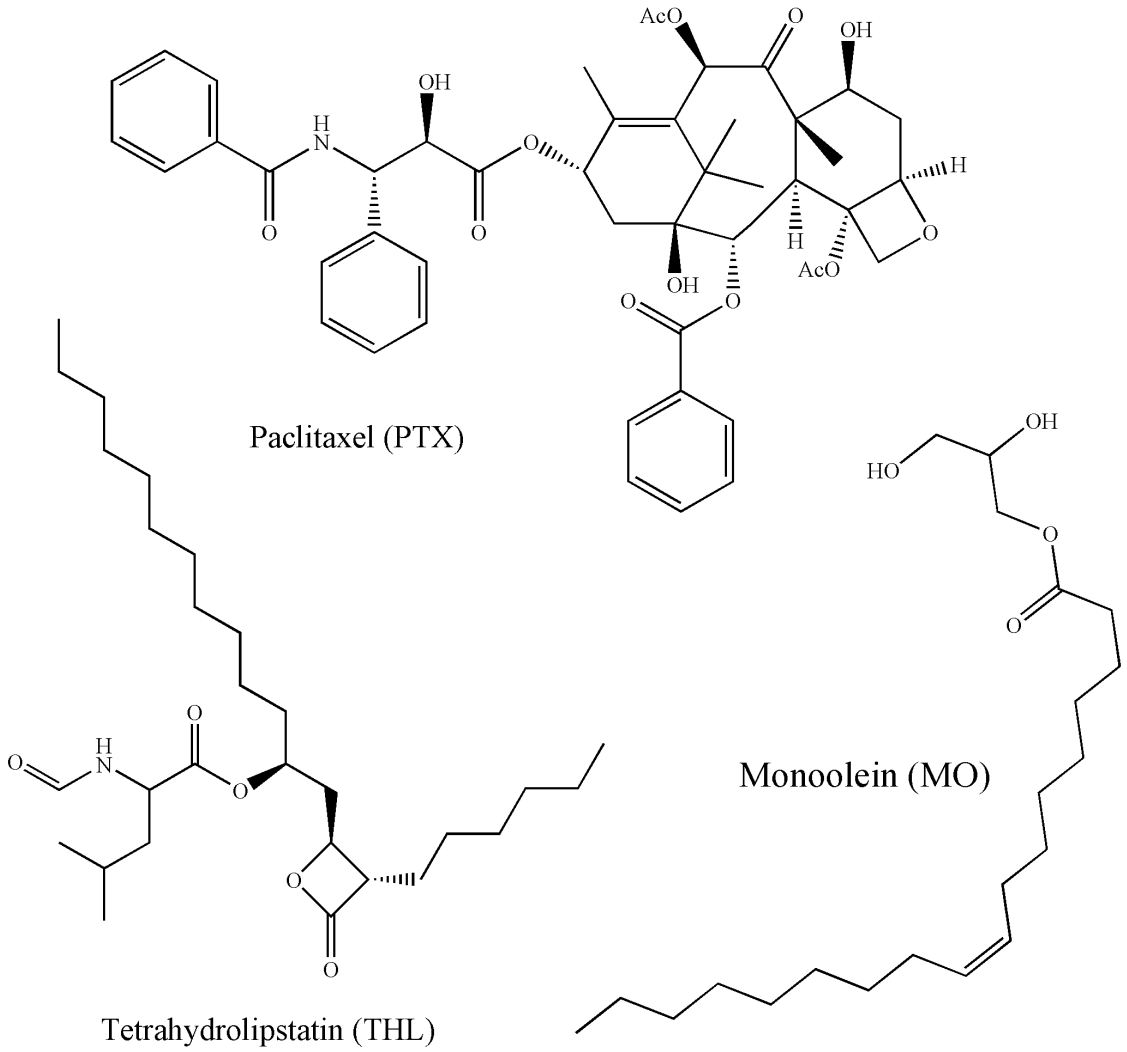

Figure 4.2. Chemical structures of tetrahydrolipstatin (THL), monoolein (MO), and paclitaxel (PTX)

4.3 Materials and Methods

4.3.1 Materials

All solvents were analytical grade and purchased from Fisher Scientific. Monoolein 9.9 MAG (1-(9Z-octadecenoyl)-rac-glycerol) was acquired from JenaBioscience, Germany at >99% purity. Phosphate buffered saline (PBS) tablets and heptakis(2,6-di-*O*-methyl)-β-cyclodextrin (HCD) were purchased from Merk (Saint Louis, MO). Water was purified in the lab using a Milli-Q Water System (Millipore Corporation, Bedford, MA). Lipase isolated from porcine pancreas was purchased from Merck, Germany (Type II, 100-500 units/mg protein (using olive oil (30 min incubation)). Anhydrous Paclitaxel was provided by Yunnan Hande Bio-Tech Co. Ltd., China (Lot: CP-160301) and Tetrahydrolipstatin (Orlistat/THL) (99% purity) was purchased from Sigma-Aldrich.

4.3.2 PTX characterization

PXRD was used to confirm the crystallinity of the as-received PTX prior to reconstitution within the lipid cubic phase. Data was collected in reflection mode with an Empyrean diffractometer (PANalytical, Phillips) equipped with CuKα1,2 radiation (γ = 1.5406 Å) operating at 40 kV and 40 mA at room temperature. Samples were scanned between 2θ values of 5 and 40° at a step size of 0.01313° 2θ/s, 73 s per step.

4.3.3 Preparation of PTX-LCP matrix formulations

Anhydrous paclitaxel was first dissolved in ethanol at a concentration of 40 mg/mL. Fusion of dry lipid crystals to the melt was achieved in an oven at 40–45°C. Appropriate volumes of molten monoolein (MO) (~60 mg/sample) were added to glass vials and calculated volumes of the PTX solution were added to the lipid to deliver various concentrations of PTX up to a maximum of 6 mg. The mixture was once again heated above 40°C and gently vortexed for 5 minutes to ensure a homogenous blend. The ethanol was evaporated in a vacuum oven before the addition of the aqueous solution (MilliQ water) to initiate the formation of the lipid cubic phase. Water was added in excess to alleviate dehydration of the samples during storage (~45 wt%) according to its phase diagram [173, 177, 352]. The samples were then subjected to further vortex mixing for no less than 15 minutes. The homogeneous mixtures were stored in sealed glass vials and left to equilibrate in

the dark for at least 48 hours. Final PTX concentrations of between 1 to 6 mg/100 mg gel were achieved.

For the preparation of inhibitor-containing LCP formulations, the THL was first physically mixed in the appropriate volume of molten lipid before PTX was added followed by the mixing, evaporation, water addition, and equilibration steps outlined above. The THL-lipidic formulations were prepared at a concentration of 1.5 wt%. Preparation of empty gels followed the same approach, without addition of either drug or inhibitor to provide a control dataset.

The method for the preparation of the cubosomes for cryo-TEM analysis of the effect of encapsulating PTX followed that of Boge et al. with some minor modification [350]. LCP was formulated with PTX and/or THL as already described, before being subjected to fragmentation. The pre-loaded bulk gel (500 mg) was added to 20 ml of 1 wt% stabilizer Pluronic® F-127 solution prepared in water. Fragmentation was achieved by subjecting the LCP-stabilizer mixture to mixing using a magnetic stir bar followed by high shear homogenization at 14,000 rpm using a T25 digital ULTRA-TURRAX® disperser (IKA®-Werke GmbH & Co. KG, Germany) for 2 minutes. The samples were subjected to further fragmentation with an ATPIO ultrasonic microwave combined reaction system sonication probe operating at 40% of its maximum power on pulse mode (3 second pulses followed by a 7 second break) for an additional 5 minutes. The resultant opaline dispersions were stored in sealed glass vials.

4.3.4 Mesophase characterization

SAXS

Small angle X-ray scattering was performed to confirm the mesophase nature of the bulk formulations. SAXS measurements were carried out after sample preparation at the Solution State SAXS B21 beam line at Diamond Light Source on the Harwell Campus, Didcot, UK [428]. Small angle diffraction images were processed and the relative positions of the distinct Bragg peaks were indexed and used to deduce the space groups and lattice parameters by correlating with Miller indices [473] as already described. Similarly, the water channel diameter and lipid chain length were calculated as previously described [428], with surface area and Euler Poincare constant (χ) used [151, 354] to track any changes induced upon drug loading.

Differential scanning calorimetry (DSC)

The thermal behaviour of mixtures of monoolein and PTX was examined on a Netzsch Polyma 214 calorimeter (Netzsch, Germany). DSC analysis was performed by heating the sample from 25°C to 280°C at a rate of 10°C/min to determine the sample melting point (endothermic peak), melting range and onset temperature. Samples tested included (i) 6 wt% PTX-LCP, (ii) PTX-pure monoolein blend (1:2), (iii) blank monoolein LCP and (iv) free PTX to identify changes in the crystalline structure of the PTX upon formulation with the host lipid carrier system. Where PTX was formulated with lipid, samples (i) and (ii), the PTX was first dissolved in ethanol and the solvent was evaporated before thermal analysis was conducted.

Particle size estimation and zeta-potential studies

Dynamic light scattering (DLS) was utilized to estimate the particle size distribution (Z-average) and polydispersity (PDI) as well as the zeta potential (mV) of the cubic dispersions for cryo-TEM using PBS as the dispersant on a Zetasizer (Malvern Panalytical, United Kingdom) equipped with a 4 mW He–Ne laser (633 nm) which applies Brownian motion theories in its measurement. The viscosity of the dispersant was set at 0.8872 cP and the system was maintained at 25°C. Three measurements of 50 runs were taken for each sample and the mean value, along with the calculated standard deviation for particle size estimation (nm) were recorded using the Malvern Panalytical zetasizer software.

Cryo-TEM

For the cryo-TEM analysis, vitrified cubosome samples formulated with PTX or THL were prepared in a similar manner to those methods described by Nilsson et al. [524]. For comparative purposes blank monoolein cubosomes were also studied. 3 microliter aliquots of the investigated sample were applied with a pipette onto Quantifoil R 1.2/1.3 holey carbon grids (Quantifoil Micro Tools GmbH, Großlöbichau, Germany) maintained at 22°C and 80 % relative humidity in a sample chamber of a Leica EMGP vitrification device (Leica Microsystems, Wetzlar, Germany). The grids were then vitrified by rapid plunging into liquid-nitrogen cooled ethane. The samples were observed in a Talos Arctica transmission electron microscope (Thermo Fisher Scientific) at 200 kV under low-dose conditions (~15 e/A2) at a constant temperature of ~-190 °C. The images were recorded at a nominal magnification of 120 000x resulting in a final image sampling of 1.24 Å/px.

4.3.5 PTX binding energy with lipid and lipase inhibitor using DFT calculations

The binding energy of PTX-lipid and PTX-lipase inhibitor dimer was calculated using the method that has been successfully applied for small and medium sized API molecules such as risperidone [525], tolbutamide [526], and carbamazepine [527]. The equilibrium geometries of the 1:1 PTX-PTX, PTX-lipid, and PTX-lipase inhibitor dimer in isolation (gas phase) were calculated with Density Functional Theory (DFT) using a B97-D3 Grimme's functional [528], and a Gaussian-type 6-31G(d, p) basis set [529]. Single point energies for the fully optimised structures were calculated using a double hybrid B2PLYP-D3 [530] functional combined with an exact Hartree Fock exchange with an MP2-like correlation and long-range dispersion corrections with a basis set of quadruple-ζ valence quality (def2-QZVPP) [531]. Single point energy calculations for PTX-PTX dimer was calculated using B97-D3 Grimme's functional due to large heavy atoms along with number of atoms exceeding 200, which was possible with B2PLYP-D3 functional. The binding energy was calculated as follows:

Equation 4.1: $$\Delta E_{\text{bind}} = E_{\text{A-B}} - \left(E_{\text{A}} + E_{\text{B}}\right)$$

where, $E_{A\text{-}B}$ is the single point energy of the given PTX-lipid and PTX-lipase inhibitor dimer, while E_A and E_B are the respective single point energies of the isolated monomers, A and B, in the gas phase.

4.3.6 In silico predictive modelling of enzyme, lipid substrate, and inhibitor interactions

Structure of pancreatic lipase and its catalytic pocket

The starting conformation of the full-length lipase enzyme was obtained from the 2.8 Å resolution crystal structure of the porcine pancreatic triacylglycerol lipase/colipase complex (PDB code 1ETH [532]). The lipase structure has two identical subunits. One subunit was used for this study. A mobile domain flap (or lid or loop; Cys238-Cys262) controls enzyme activity [533] by regulating entry of substrates/inhibitors (see Fig. C1A), . The cofactor colipase (shown as licorice) opens the flap by binding to the smaller C-terminal α-sheet-rich domain which activates the catalytic site on the larger N-terminal β-helix-rich domain [534]. The active site at the N-terminal

domain houses the catalytic triad Ser153 (green)-His264 (blue)-Asp177 (red) responsible for the LCP MAG lipid digestion and hydrolysis to triacylglycerol [535].

Molecular docking

In order to generate physically realistic potential starting structures of complexes for molecular dynamics (MD) simulations, molecular docking of lipase with inhibitor THL and with native ligand MO was performed. The crystal structure of pancreatic lipase (PDB code 1ETH) was used as a template for the generation of pancreatic ligand/inhibitor complex models using AutoDock 4.2 [536]. Fig. C1B shows the 3D structures of THL and MO that were obtained from ChemSpider [537]. As static docking incorporates torsional degrees of freedom only in the ligand molecule, structures of complexes using flexible docking with AutoDock were generated, where the lipase Ser153 side chain was allowed to reorient in response to the THL or MO binding. A 50 X 50 X 50 $Å^3$ grid was used to accommodate all possible THL or MO poses and centered on the Ser153 catalytic site of the lipase (Fig C1C). 26 torsions in the THL structure and 21 torsions in the MO structure were rendered flexible, and four side chain torsions in the Ser153 of the lipase were rotatable. A Lamarckian genetic algorithm [538] was used as a search algorithm to explore the docking space. Four best docked complexes ranked according to their binding energies are provided in Tables C1 and C2, and their corresponding poses are shown in Figs. C1D and C1E for THL and MO as ligands, respectively. The most favourable complex from each of the THL-lipase and MO-lipase docked poses was selected as the starting structure for the MD simulations. The same docked poses of substrate and inhibitor with lipase were further used to perform MD simulations with the inclusion of colipase in the systems.

Atomistic molecular dynamics simulations

For simulations with inclusion of the enzyme cofactor colipase (THL-lipase/colipase and MO-lipase/colipase), the same THL and MO poses were used in the starting structures. In order to compare the affinity of inhibitor to lipase in presence of Ca^{2+} and in the presence of colipase/Ca^{2+}, we considered the native PDB structure (PDB 1ETH) with the Ca^{2+} intact and incorporated the same docked THL poses in each complex to produce the initial structures for MD. The lipase, colipase and Ca^{2+} were represented by CHARMM36m forcefield parameters [539] and the CHARMM General Force Field (CGenFF) [540, 541] was used to represent the topology and

parameters for THL and MO. The six systems THL-lipase, THL-lipase/colipase, THL-lipase/Ca^{2+}, THL-lipase/colipase/Ca^{2+}, MO-lipase and MO-lipase/colipase, were solvated in cubic simulation cells with water molecules represented by the CHARMM-modified TIP3P [542] water model and a minimum distance of 20 Å between any protein atom and any box edge. MD simulations were carried out using the Gromacs 2018.4 [543, 544] package with an integration time step of 2 fs implemented in the leapfrog integrator [545] with bond lengths to hydrogen constrained using the LINCS [546] (protein) and the SETTLE [547] (water) algorithms. Snapshots were saved every 2 ps. Background ions were added to neutralize protein formal charges and to mimic physiological ionic strengths (0.15 M NaCl). Long-range electrostatics were treated by the Particle mesh Ewald (PME) method [548]. Protein and non-protein molecules (water and ions) were coupled separately to an external heat bath (310 K) with a coupling time constant of 1 ps using the velocity rescaling method [549]. All systems were minimized for 100 ps, and equilibrated for 1 ns in constant volume NVT ensemble followed by another 1 ns of NPT equilibration with the reference pressure at 1 bar and a time constant of 4 ps using the Berendsen barostat [550]. The production runs were carried out in constant pressure NPT ensemble using the Parrinello-Rahman barostat [551]. All simulations were run for 500 ns (in all, two microsecond dataset of equilibrated molecular dynamics), and all reported values were generated using structures sampled during the last 200 ns (based on the convergence of the time evolution of cumulative average secondary structure of lipase; Figs. C1F-I). All analyses of interaction energies, interaction distances, and secondary structures were performed with Gromacs tools and trajectories were visualised using VMD [552] and UCSF Chimera [553].

Computation of binding energy by MM/PBSA

The binding energies ($\Delta E_{binding}$) between the ligand (native MO or inhibitor THL), and lipase or lipase/colipase, written lipase(colipase) for short below, were calculated using the molecular mechanics energies combined with Poisson–Boltzmann continuum solvation (MM/PBSA) [554] method implemented in Gromacs (*g_mmpbsa*) [555]. The binding energies include the solvation effect of interfacial water in addition to the non-covalent van der Waals (vdW) and electrostatic interaction energies as shown below:

$$\textbf{\textit{Equation}}\ \mathbf{4.2}:$$

$$\Delta E_{binding} = \Delta E_{binding,vacuum} + \Delta G_{solv,complex} - \left(\Delta G_{solv,ligand} + \Delta G_{solv,protein}\right)$$

$$\textbf{\textit{Equation}}\ \mathbf{4.3}: \Delta G_{solv} = \Delta G_{polar} + \Delta G_{nonpolar}$$

where $\Delta E_{binding,\ vacuum} = \Delta E_{MM}$ (molecular mechanics energy = electrostatic energy + vdW energy in vacuum), $\Delta G_{solv,\ complex}$ = free energy of solvation of the ligand-lipase(colipase) complex, $\Delta G_{solv,\ ligand}$ = solvation energy of the THL or MO, $\Delta G_{solv,\ protein}$ = solvation free energy of lipase(colipase), ΔG_{polar} = polar solvation free energy or electrostatic component of solvation free energy, and $\Delta G_{nonpolar}$ = nonpolar solvation free energy approximated by the solvent accessible surface area (SASA) times a constant factor. It should be noted that although the ΔG_{solv} is a free energy term, the $\Delta E_{binding,\ vacuum}$ does not consider the change in entropy due to binding, and hence is not a free energy term. Therefore, the total binding energy ($\Delta E_{binding}$) only approximates the free energy, with entropy contributions considered minimal in the present case as the THL and MO ligands both bind to the same site and are similar in size (typical of competitive native *vs.* inhibitor ligand binding) [556].

4.3.7 Digestion Studies

Dynamic degradation studies were carried out on the lipid cubic preparations formulated with a monoacylglycerol lipid, the antineoplastic agent paclitaxel, and lipase inhibitor THL using previously described methods (Chapter II, section 2.3.4) Equilibrated samples were submersed in 1 mL of digestion media and the sample was maintained at 37°C with continuous mixing at 150 rpm.

The influence of lipase cofactor colipase on the reaction was investigated using digestion media at pH 7.4. For samples studied in the presence of colipase, enzymes were first dissolved in distilled water at a lipase concentration of 8 mg/mL (100-500 units/mg protein (using olive oil (30 min incubation)) and 50 mg/mL of colipase separately. The digestion media was prepared by mixing the enzyme and cofactor in PBS buffer at pH 7.4 at a volume ratio of 1:0.6:0.4 lipase:colipase:buffer. One sample group was also exposed to $CaCl_2$ present in the buffer at 5 mM

concentration. The media was allowed to equilibrate for 10 minutes at 37°C before being added to the LCP sample vial and media was replenished with freshly prepared media throughout the duration of the experiment.

The swelling ratio and rate of degradation in terms of relative weight % were calculated against the initial sample mass as per the following equation:

Equation 4.4: $Swelling\ Ratio\ or\ Residual\ Weight\ \% = \frac{W_1 - W_0}{W_0} \times 100\%$

where W_0 is the initial gel weight before immersion in the media and W_1 is the weight of the submerged gel at a measured time point.

As a control experiment, free PTX was incubated in the digestion media and subsequently analyzed through HPLC for any degradation or changes in structure indicated by split peaks and additional or reduced peaks. The test demonstrated that the enzymes did not interfere with detection of the drug peak.

4.3.8 Solubility study of PTX to facilitate in vitro drug release studies

Excess amounts of anhydrous PTX were added to glass vials containing 10 mL of a range of dissolution media; phosphate buffered saline (PBS), water, acetonitrile, ethanol, methanol, or 2% heptakis(2,6-di-*O*-methyl)-β-cyclodextrin (HCD, previously used as dissolution media to enhance PTX solubility [557]). Upon addition of PTX to the dissolution medium, sample vials were inverted several times to ensure all of the poorly wettable drug particles were suspended. The samples were stirred using PTFE magnetic stirrers at 150 rpm on a submersible stirrer plate in a water bath maintained at 37°C overnight. After the 16 hour incubation period, 5 mL of sample was withdrawn and centrifuged for 10 minutes at 13,000 rpm. The supernatant was then passed through a pre-heated nylon filter (0.22 µm). The first 2 mL was discarded and HPLC analysis was carried out on the remaining filtrate under the previously described separation conditions.

4.3.9 Degradation controlled in vitro drug release studies

The *in vitro* dissolution profiles of paclitaxel from LCP matrices were tracked by quantifying the drug remaining in the matrix after incubation in PBS containing lipolytic enzyme. The gels

were solubilized in acetonitrile at time intervals up to 30 days, and the concentration of unreleased drug was subsequently quantified using high performance liquid chromatography (HPLC). Dissolution samples were maintained at 37°C under shaking at 150 rpm for the duration of the investigation.

The HPLC system used in this investigation was an Agilent 1200 Infinity Series (Agilent Technologies, Palo Alto, USA) comprising: G1311B 1260 quaternary pump, G1329B 1260 ALS autosampler, G1316A 1260 TCC (thermostated column compartment) and a G1365D 1260 MWD VL diode-array detector. The acquired data was processed with the Agilent OpenLAB CDS software.

Chromatographic separation of paclitaxel-containing samples was achieved using an Agilent Poroshell 120 PFP (3 x 100 mm, 2.7 µm) column fitted with a UHPLC Poroshell 120 guard module (3 x 5 mm, 2.7 µm). The system was maintained at 25°C with a run time of 18 minutes. The mobile phase which contained HPLC Analytical grade Acetonitrile (Fisher Scientific) and deionized water (A:B 13:87, v/v) was delivered to the column at a flow rate of 1 mL/min which yielded a column back pressure of ~260 bar. Samples were filtered through a 0.2 µm Nylon filter (Fisherbrand®). The volume of analyte injected was within the range of 0.5 to 10 µl. Column effluent was detected at a UV detector wavelength of 228 nm.

4.4 Results and Discussion

4.4.1 PTX-LCP matrix formulation and characterization

The highly hydrophobic nature and aggregation propensity of paclitaxel made it necessary to first dissolve it in organic solvent prior to incorporation in the lipid to ensure its homogeneous distribution in an aqueous based system. Within this system, there was the potential for the formulation approach and physicochemical properties of PTX to affect the behaviour of the matrix due to PTX's large size (853.9 g/mol) and highly hydrophobic nature. For this reason, small-angle X-ray scattering (SAXS) was employed to study the effect, if any, of PTX encapsulation on the cubic internal structure to decipher the loading capacity of the system.

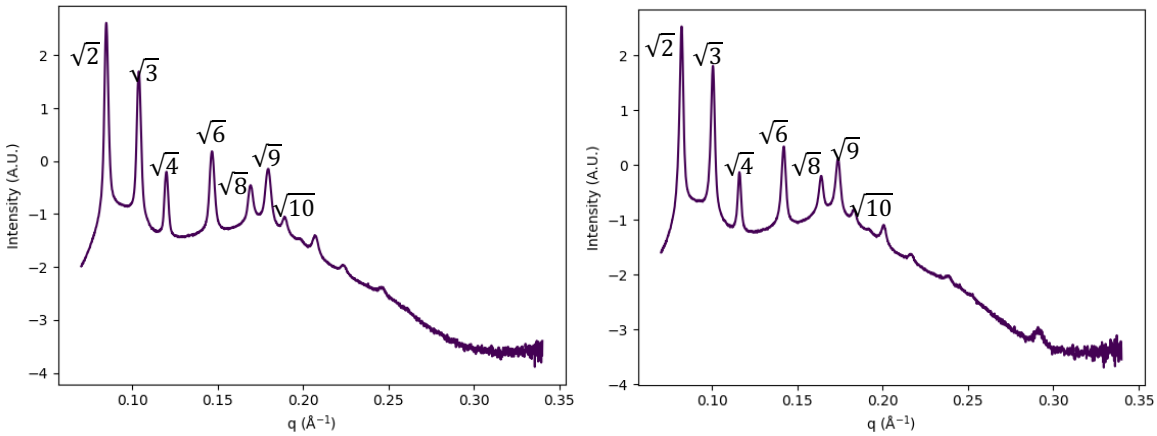

Figure 4.3. Representative azimuthally integrated SAXS intensity versus scattering vector, *q plot* of blank monoolein system (left) and paclitaxel-loaded monoolein at 4 wt% loading (right). The peaks of the pattern has been indexed according to the Q_{II}^{D} mesophase and highlight the stability of the phase against the introduction of PTX into its lipid network.

Three bicontinuous cubic phases exist; primitive (Q_{II}^{P}), gyroid (Q_{II}^{G}), and double-diamond (Q_{II}^{D}) varying in internal organization and distinguishable by their discrete crystallographic space groups. However, only two of these cubic phase (Q_{II}^{D} and Q_{II}^{G}) are typically accessed in the monoolein-water system under equilibrium [177]. The more stable and swelled Q_{II}^{D} phase is accessed when hydration levels are increased by a transition through the Q_{II}^{G} phase. These lipid cubic mesophases give rise to diffraction patterns reminiscent of powder X-ray diffraction; characterized by a series of sharp and clearly defined concentric rings [170]. Here, Bragg peaks have been indexed according to the Miller indices of the reflection plane to assign the mesophase. The relative positions of these reflection lines from our samples confirms highly ordered bicontinuous cubic phases. Table 4.1 displays the assigned mesophases and calculated lattice parameters of the formulations encapsulating PTX up to a concentration of 6 wt%. The dominating phase in equilibrium across our samples was of the cubic-Q_{II}^{D} type to an upper limit of 5 wt%. At the highest loading concentration (6 wt%) however, the onset of a phase transition is observed, where a coexistence of both the Q_{II}^{D} and Q_{II}^{G} type symmetries is noted. Lipophilic molecules have previously been shown to induce such phase transitions in lipid cubic samples [361, 362] by integrating into the lipid bilayer and altering the liquid crystalline structure. Complexation of the drug and the fatty acid of the lipid can alter the symmetry and physical structure of the mesophase.

This effect is dependent on the ratio of the solubilized guest component to lipid and is controlled also by the water content. The PTX loading capacity of the Q_{II}^{D} cubic phase described here is similar or slightly higher compared to those described in the literature for other highly hydrophobic agents such as vitamin K [360] and tea tree oil [558].

Table 4.1. Phase identification and lattice parameters of assigned mesophases from SAXS experiments with calculated dimensional values for lipid chain length (L) and water channel diameter (D_{H2O}).

Host Lipid	THL (wt%)	PTX (wt%)	Assigned mesophase	lattice parameter (nm)	L (nm)	D_{H2O} (nm)	Bonnet Ratio (Where applicable)
MO	-	-	Q_{II}^{D}	10.31	1.75	4.55	-
MO	-	1	Q_{II}^{D}	10.91	1.86	4.81	-
MO	-	2	Q_{II}^{D}	10.9	1.86	4.8	-
MO	-	3	Q_{II}^{D}	10.83	1.84	4.78	-
MO	-	4	Q_{II}^{D}	10.72	1.83	4.72	-
MO	-	5	Q_{II}^{D}	10.72	1.83	4.72	-
MO[CE]	-	6	Q_{II}^{D}	10.74	1.83	4.73	1.29
			Q_{II}^{G}	13.82	1.82	3.21	
MO	1	-	Q_{II}^{D}	9.5	1.62	4.18	-
MO	1	1	Q_{II}^{D}	10.7	1.82	4.72	-

[CE] samples that presented the coexistence of two mesophases

Dimensional analysis was conducted to calculate the water channel diameter and the monolayer thicknesses were determined using the method of Szlezak, Nieciecka [212]. It is clear that the incorporation of PTX into the lipid system has an effect on the internal dimensions of the cubic formulations. The calculated dimensions for the lipid chain length at all PTX loadings are almost 0.1 nm larger than those calculated for the blank system, and an increase of up to 0.24 nm is seen for the PTX-LCP formulations compared to the THL-containing system without PTX. As the %

loading of PTX is increased, a slight reduction in both the water channel diameter and monolayer thickness is observed. This change, may be caused by the portioning of the drug between individual lipid molecules, “closing the gap” between the lipid chains in the cubic framework.

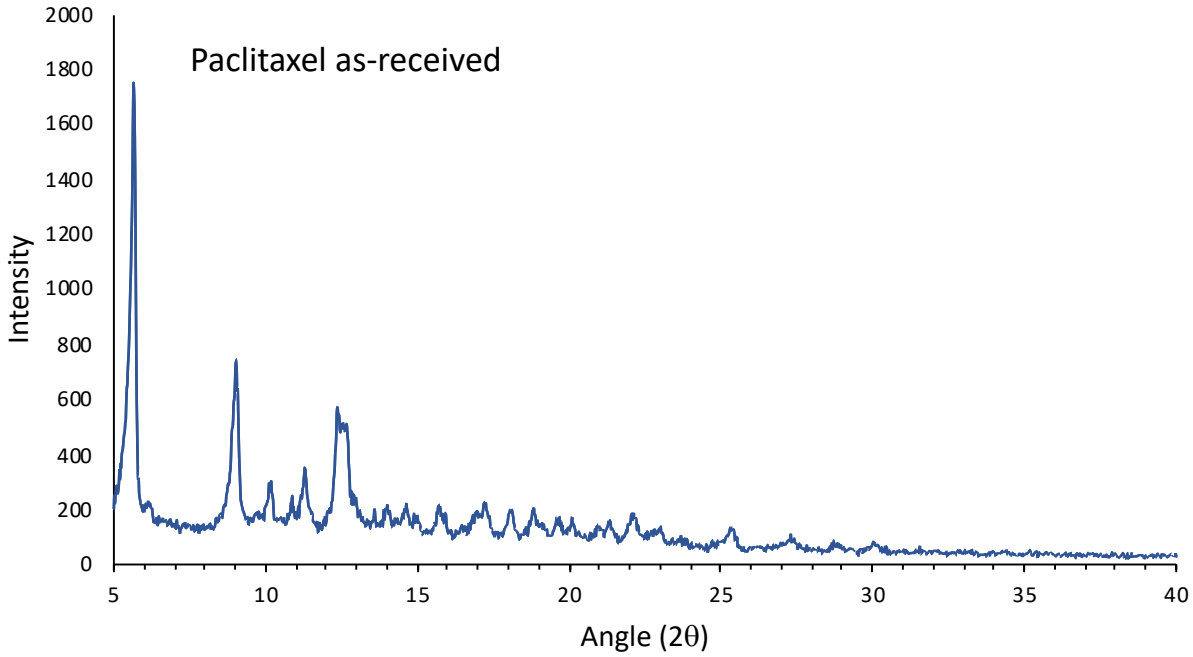

Figure 4.4. Diffractogram of the as-received PTX

PXRD of the as-received PTX was carried out to determine the crystallinity of the drug prior to encapsulation in the lipid cubic phase. Figure 4.4 shows the collected diffractogram that presents sharp diffraction peaks indicating crystallinity in the as-received drug. The solid-state behaviour and extent of hydrogen bonding exhibited within a crystal structure has a direct impact on the physical properties of the material [559]. This is of particular relevance in the drug delivery, as it influences the dosing, solubility, and bioavailability of the drug [560]. For this reason, a DSC study was carried out to study the blending behaviour and degree crystallinity of PTX throughout the formulation of the PTX LCP systems, Figure 4.5.

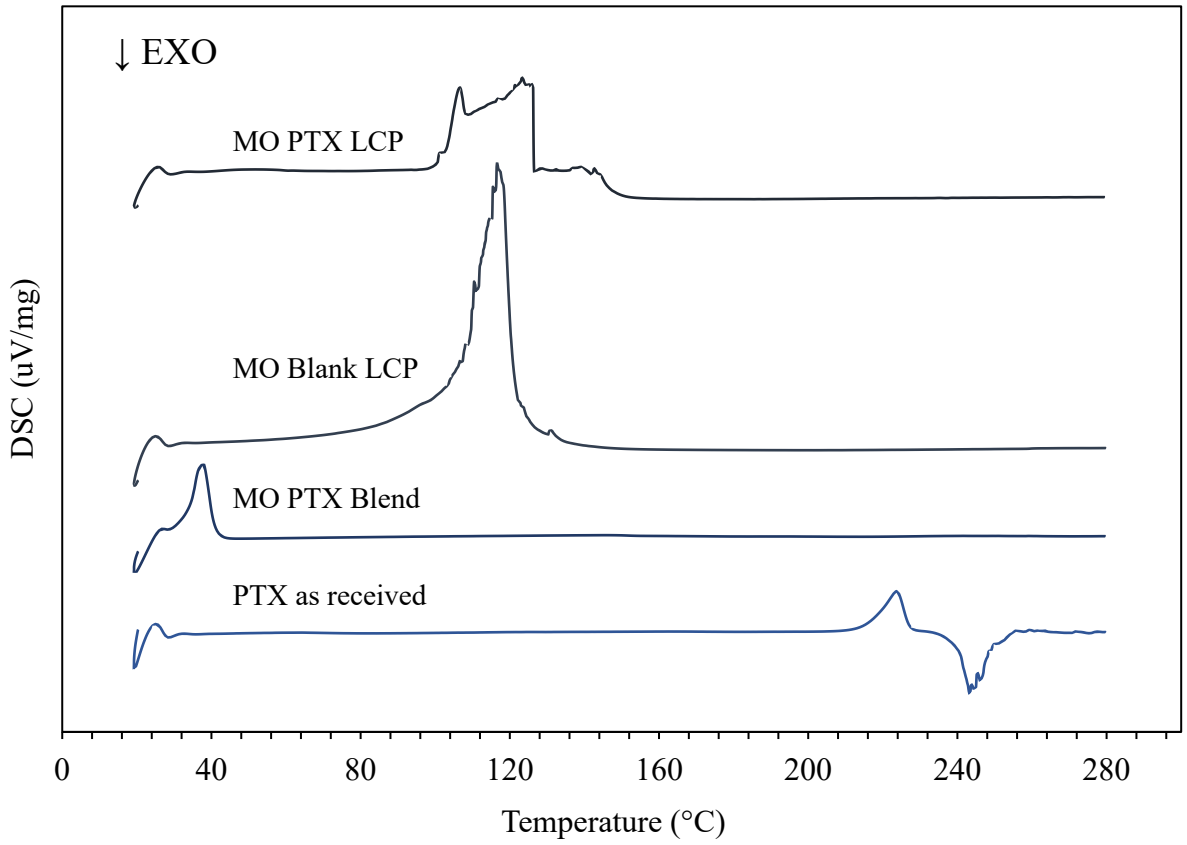

Figure 4.5. Thermograms of paclitaxel and lipid bulk formulations: MO PTX-LCP is loaded at a PTX concentration of 6 wt%; MO PTX blend is 50 wt% PTX dissolved in pure monoolein; blank monoolein LCP contains no PTX; and as received PTX.

The as-received free PTX produced a sharp endothermic peak at approximately 225°C, confirming it exists in its crystalline form (that is likely the anhydrate form [504, 561, 562]), supported by the PXRD diffractogram (Figure 4.4). At approximately 35°C, a single endotherm indicates the melting peak of the MO [174].When the molten lipid is blended with PTX in the absence of water and after ethanol removal, the endothermic peak corresponding to the crystalline form of PTX is still absent, likely indicating the presence of an amorphous form of the drug [561]. Upon addition of water to form the LCP the absence of this characteristic peak was also noted. Similar behaviour has been reported in the literature for a variety of drugs including diclofenac sodium, penciclovir, and poorly soluble clozapine when incorporated into lipid matrices [345, 563-565]. Generally, amorphous materials possess higher saturation solubility than crystalline materials, resulting in their better behaviour in terms of drug delivery and bioavailability. The

same can be said for paclitaxel which has been reported to demonstrate an increased dissolution rate in its non-crystalline form when compared to its crystalline counterparts [562, 566]. The indication of an amorphous form of PTX in the lipid formulation may therefore be advantageous in terms of its *in vivo* performance. It is noted however, that the risk of spontaneous recrystallization and subsequent reduction in bioavailability is always a concern for amorphous formulations upon delivery.

Lipid cubic dispersions (cubosomes) were prepared and the effect of incorporating the drug into the particles was investigated by cryo-TEM. The internal structure of the lipid cubic phase is said to be resistant to dilution [230], and so lends itself to dispersion into nanoparticles that maintain the structural integrity of the lipid cubic phase as shown with the monoolein system in chapter II. This allows us to visually track the effect of introducing these highly hydrophobic drugs into the lipid matrix. The particle size and zeta potential of these paclitaxel and inhibitor-loaded cubosome formulations are shown in Table 4.2. The particle size of the different formulations demonstrated a successful fragmentation approach for producing nanosystems in solution, with the blank cubosomes being larger than those described in the literature at 188.2 ± 4.1 nm compared to reported sizes of 131.5 ± 10 nm [567] and 133.9 ± 0.1 (Chapter II, Table 3.1). This may be attributed to the formulation approach, where the bulk LCP was formulated in stabilizer solution prepared in water here versus PBS for the antihistamine-loaded cubosomes. The size increased slightly with the addition of THL and PTX compared with the blank system, with PTX responsible for a larger increase in particle size, attributed to the relatively large size of the molecule. All samples displayed PDI values less than 0.23.

Table 4.2. Properties of paclitaxel and/or tetrahydrolipstatin loaded cubic dispersions for cryo-TEM

Paclitaxel (wt%)	Tetrahydrolipstatin (wt%)	Size ± SD (nm)	PDI	Zeta potential ± SD (mV)
-	-	188.2 ± 4.1	0.141	- 1.6 ± 0.18
-	1.5	202.2 ± 3.9	0.181	- 1.54 ± 0.2
1	-	211.8 ± 3.9	0.188	- 0.99 ± 0.16
1	1.5	210.1 ± 6	0.187	-1.14 ± 0.2

In addition to the dimensional and zeta analysis, the submicron dispersed cubic particles were investigated by cryo-TEM. The obtained images (Figure 4.6) reveal the internal structure of blank

and loaded cubic dispersions that have been stabilised with Pluronic® F-127. The nanoscale structures displayed the expected onion-like geometry and organization for particles of cubic structure [244, 568] with lattice periodicity and densely packed nanochannels.

The majority of the particles visible in the cryo-TEM images are highly ordered of size 100-200 nm in agreement with the DLS size analysis.

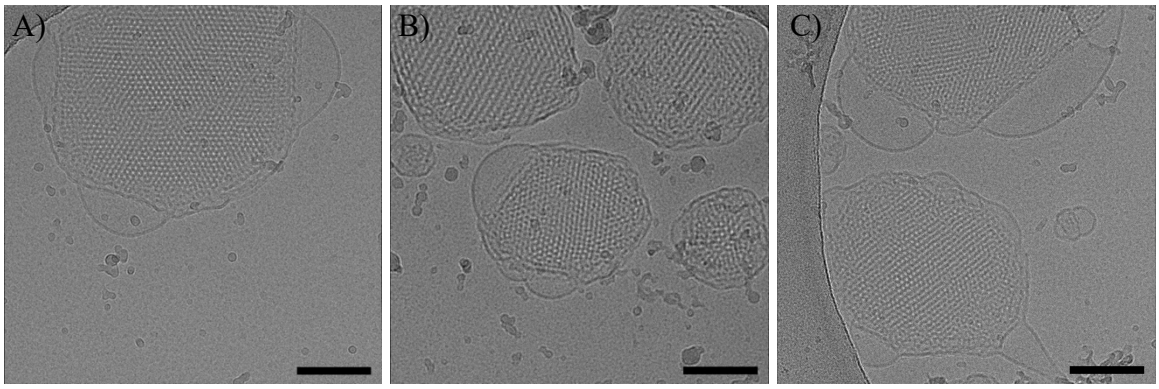

Figure 4.6. Cryo-TEM images of selected samples after vitrification from 37°C. A) Blank monoolein cubosomes (MO_Blank); B) monoolein cubosomes formulated with 2 wt% PTX (MO_PTX); and C) monoolein cubosomes formulated with 1.5 wt% THL (MO_THL). All cubosomes were stabilised with Pluronic F-127. Scale bars represent 100 nm.

While structures indicating the formation of highly ordered nanoparticles were confirmed by cryo-TEM, the images obtained also showed the presence of surface-attached vesicles that appeared lamellar in structure. Although the high shear techniques used here to disperse the cubic phase results in the desired size reduction of the cubic dispersion, the approaches have the downfall of concurrently producing lipid vesicles. In particular, these large surface vesicles have previously been reported in monoglyceride cubosomes for which Pluronic® F-127 was employed in the stabilization approach [234, 235]. The number of these non-cubic vesicles is likely related to stabiliser concentration [234]. Heat-treatment has been reported to reduce the number of vesicles present in a sample [569], however for the purpose of this study the presence of these vesicles was not of great concern.

As established by SAXS, the low concentration of PTX added to the lipid formulations for cryo-TEM analysis does not induce major changes in the Pn3m internal structure. Such is the case at

concentrations at or below 5 wt%. Similarly, the incorporation of the THL inhibitor at the studied concentration (1.5 % w/w) did not induce an unwanted phase transition. The cryo-TEM results obtained here further demonstrate no clear obstruction in the repetitious texture of the internal network that might otherwise be induced by the formation of large PTX crystals within the membrane. That said, further analysis of these nanoparticles would be required to categorise the periodicity to either cubic or hexagonal space groups as previously described by Sagalowicz et al. [570]. In their study Sagalowicz et al. employed a controlled tilting of the specimen to observe different orientations of the same particle providing a 3D representation of the particles. This coupled with fast Fourier transform (FFT) analysis [524] would provide a clearer picture of the nature of the nanoparticles formed from cubic bulk systems.

4.4.2 PTX binding energy with lipid and lipase inhibitor using DFT calculations

The absence of thermal peaks from DSC analysis, combined with the changes in dimensional parameters observed in the SAXS investigation of the PTX formulated with monoolein point toward an interaction between the lipophilic PTX and the lipid excipient of the cubic system inhibiting the recrystallisation of the PTX once encapsulated. To corroborate this, binding energies of the formulation constituents were calculated with Density Functional Theory (DFT). Figure 4.7 presents the DFT-calculated (1:1) MO-MO, PTX-MO, PTX-PTX, and PTX-THL interaction energies for the most favourable interaction sites. The PTX-PTX dimer binding appears to be stronger (-145.3 kJ/mol) compared to that of the PTX-MO binding (-42 kJ/mol). In theory, this would suggest that the PTX would preferentially bind a second PTX molecule to recrystallise in the formulation approach. However, assuming that after solvent evaporation the PTX is soluble at the molecular level in MO, where it is bound through multiple hydrogen bonding of PTX with the hydroxyl (-OH) group on MO, the inherent insolubility of PTX in aqueous media may prevent dissolution of the molecules into water inhibiting the recrystallization event from happening. Given the similarities in the MO-MO and the PTX-MO binding energies, it is reasonable to assume that the PTX is energetically able to disrupt the MO-MO interaction and insert itself into the MO membrane, potentially in a MO-PTX-MO system. This result is in agreement with the thermal analysis data which demonstrates the absence of any ordered arrangements of the drug when formulated with monoolein, even in the presence of water – an advantageous feature in terms of drug dissolution and bioavailability [562, 566].

Additionally, although less favourable in terms of relative binding energy, hydrogen bonding exists between the hydroxyl (-OH) group of PTX with the aldehyde oxygen of THL. While the concentration of THL in the formulation is relatively low, there is the potential for further inhibition of PTX re-crystallization through these interactions.

Further, the DFT data supports the theory that the lipophilic PTX interacts with the lipid membrane of the cubic network, potentially sandwiching between the individual lipid molecules to evade the water present in the swollen channels. This may explain why at the higher loading concentrations studied here phase transitions in the system were induced as the lipid bilayer may be “pushed apart” by the incorporation of high concentrations of the large hydrophobic drug interrupting the ordered bilayer.

A B C. D.

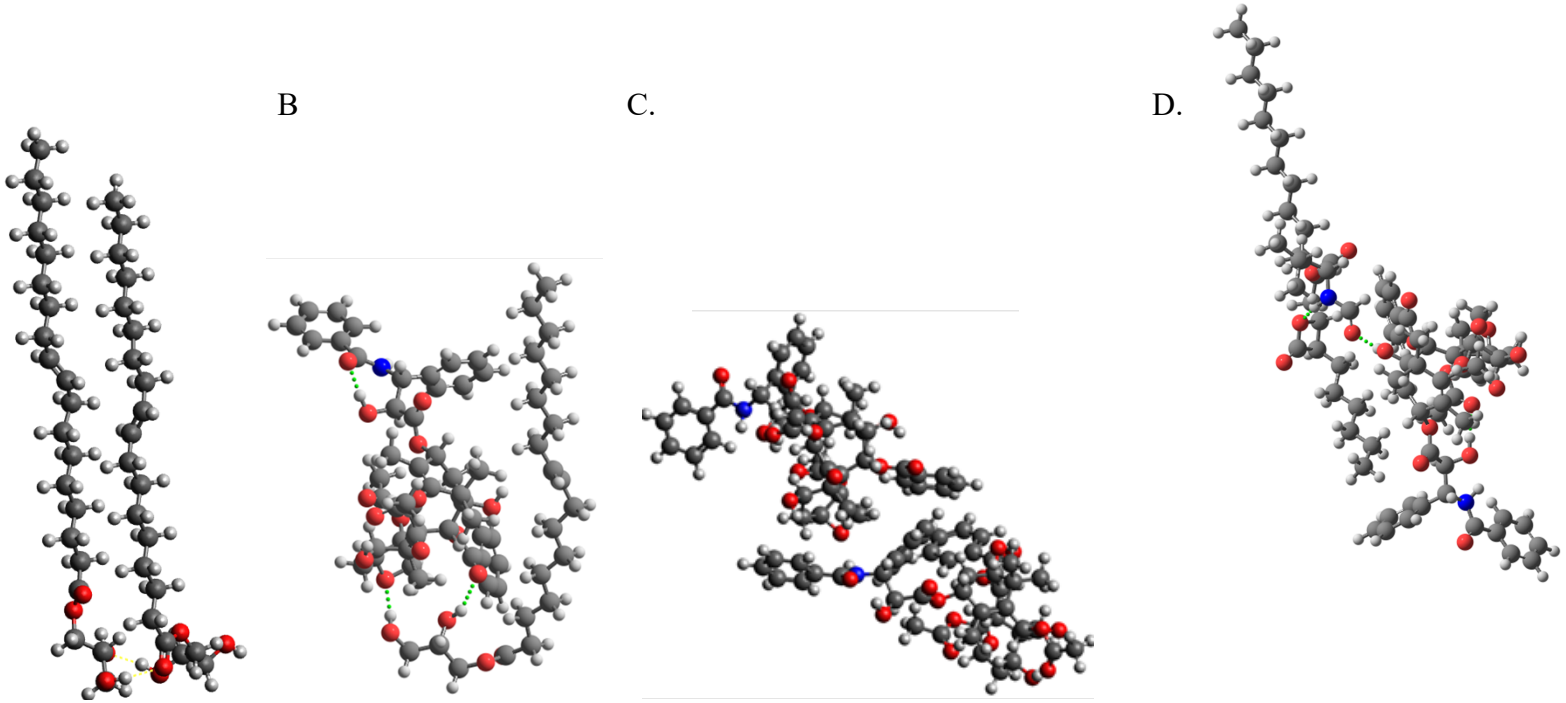

System	MO-MO dimer	PTX-MO	PTX-PTX dimer	PTX-THL
Binding energy (kJ/mol)	-56	-42	-145.3	-13.7

Figure 4.7. Optimized geometry of A) MO dimer; B) MO-PTX; C) PTX dimer; and D) PTX-THL at B97-D3/6-31G(d,p) level. Binding energy in kJ mol^{-1}, calculated at B2PLYP-D3/def2-QZVP level for A, B, and D, and with B97-D3 Grimme's functional for C. Hydrogen – white, carbon – grey, oxygen – red, nitrogen – blue; intra and inter molecular hydrogen bonds are shown with dotted green lines.

4.4.3 Modelling of interactions and binding affinities between the components of lipid cubic formulation *via* atomistic molecular dynamics simulations

For sustained delivery of PTX from LCP matrices, control over the enzymatic degradation rates by pancreatic lipase, can potentially be achieved by a lipase inhibitor, tetrahydrolipstatin (THL), as indicated in chapter III. However, this relies on the preferential binding of THL to the lipase active site over the lipid components of the monoolein (MO)-based LCP matrix. In order to gain a deeper understanding of the atomic-level interactions and relative binding affinities of the lipid substrate MO and inhibitor THL with the enzyme lipase, fully atomistic molecular dynamics (MD) simulations of MO-lipase and THL-lipase complexes (with/without colipase) were designed from a preliminary screening of the most plausible binding poses of these complexes *via* macromolecular docking.

MD simulations (Aappendix C) show that the active site of the lipase (involving the catalytic triad Ser153-Asp177-His264) is more accessible to the natural substrate MO than the inhibitor THL. A hinge-like motion of the mobile flap domain (Cys238-Cys262) closing access of THL to the catalytic pocket of lipase (Figure 4.8, A, left panel) is observed, whereas the flap presents an open configuration in the presence of MO (Figure 4.8, A, right panel). The more favourable interactions of MO over THL (by ~6.5 kJ/mol averaged over the last 200 ns) are predominantly vdW in nature (Figure 4.8, B, left panel; see also Appendix C for running averages), highlighting the dominant lipophilic nature of both THL and MO. However, minor improvement in electrostatic charged interactions also boosts MO recognition, as the negatively charged acidic group in MO is stabilized by the positively charged imidazole group of His264 in the catalytic pocket of lipase (Appendix C).

A

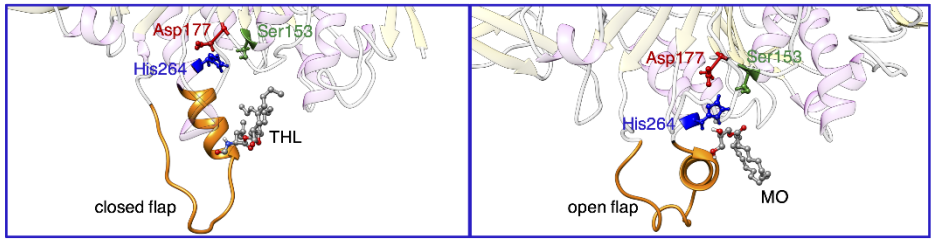
Asp177
Ser153
His264
THL
closed flap
Asp177
Ser153
His264
MO
open flap

B

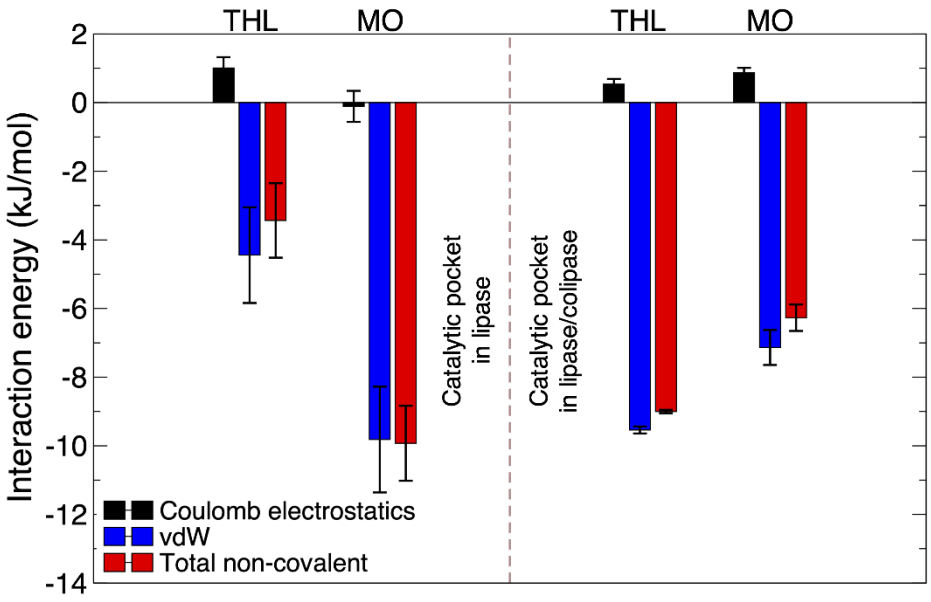
THL
MO
THL
MO
Interaction energy (kJ/mol)
2
0
-2
-4
-6
-8
-10
-12
-14
Catalytic pocket in lipase
Catalytic pocket in lipase/colipase
Coulomb electrostatics
vdW
Total non-covalent

C

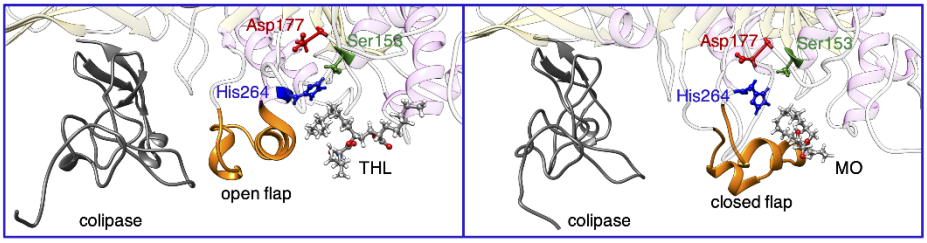
Asp177
Ser156
His264
THL
open flap
colipase
Asp177
Ser153
His264
MO
closed flap
colipase

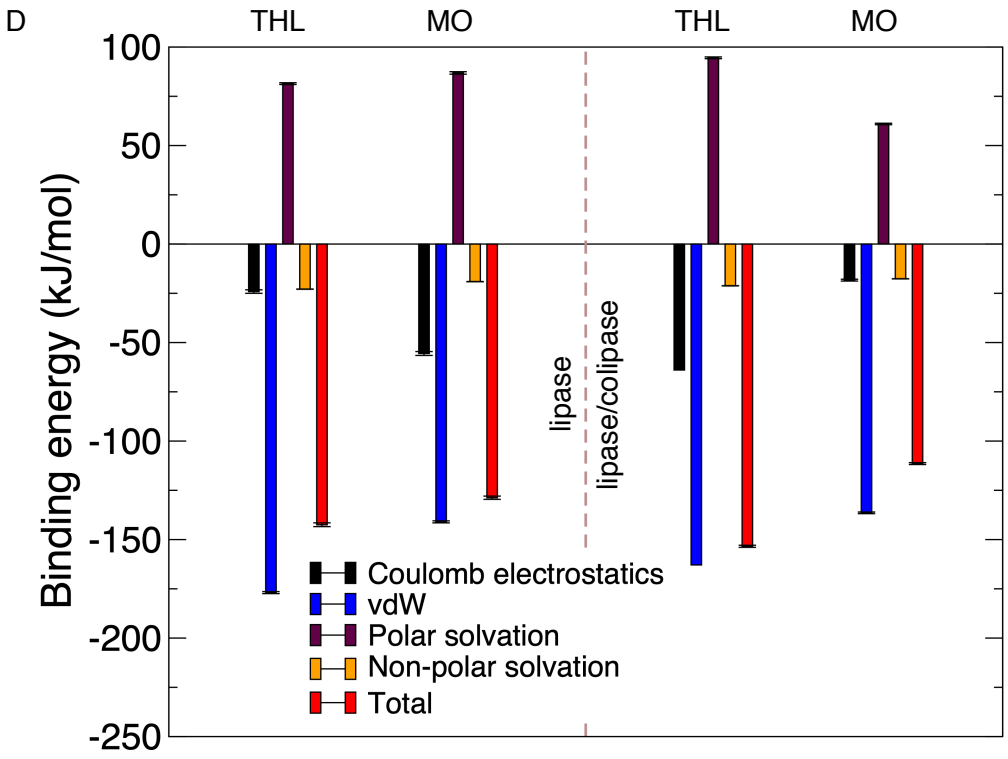

Figure 4.8. (A) Representative snapshots from MD simulations of the inhibitor Tetrahydrolipstatin (THL) with pancreatic lipase (left panel) and substrate lipid Monoolein (MO) with lipase (right panel) in the absence of cofactor colipase. The catalytic triad Ser153, Asp177 and His264 are coloured in green, red and blue, respectively with the mobile flap domain shown in orange. **(B)** Interaction energies between THL/MO and the catalytic pocket in lipase without (left panel) and with (right panel) colipase. **(C)** Representative snapshots of THL-lipase (left panel) and MO-lipase (right panel) complexes in the presence of colipase. **(D)** Binding energies between THL/MO and lipase in the absence of colipase (left) and in the presence of colipase (right).

The influence of the cofactor colipase [534, 571] on binding specificity is revealed in a 500 ns MD simulation in the presence of colipase (Appendix C) which reveal that THL is now able to access the lipase catalytic pocket while keeping the mobile flap open throughout (Figure 4.8, C, left panel). This cofactor induced loop dynamics which promote favourable THL interactions with the catalytic pocket (Appendix C). By contrast, access of the MO substrate to lipase is slightly more restricted as the flap closes the catalytic pocket during binding in the presence of the colipase (Figure 4.8, C, right panel and Appendix C). The average interaction energies (Figure 4.8, B, right panel) indicate that THL interacts more favourably with the catalytic pocket than MO (by ~2.5

kJ/mol dominated again by vdW interactions) when colipase is present. In order to substantiate the involvement of colipase in facilitating the movement (opening or closing) of the mobile flap domain in lipase, which in turn might modulate the molecular recognition of THL over MO, the interaction energies of the mobile flap domain with colipase were computed for the first 300 ns and the last 200 ns of simulations (Appendix C). The flap-colipase interactions are clearly more favourable for the last 200 ns with THL binding than with MO binding, confirming the participation of colipase in stabilising the open configuration.

To further probe the contribution of water in binding of both THL and MO to lipase, the binding energies were computed using the MM/PBSA [554] method (refer to section 4.3.6) in the absence and presence of colipase. It should be noted that the binding energies here were calculated with the full-length lipase enzyme and not just the residues in the catalytic triad, as was done previously in the calculation of the interaction energies. Therefore, the involvement of other residues in lipase (apart from the catalytic pocket) are taken into account when considering binding energies. In the absence of colipase, it was observed that the overall predicted binding of THL to lipase (Figure 4.8, D) is favoured over MO-lipase binding energy (by ~13 kJ/mol, averaged over the last 200 ns). The vdW component is the major contributor of binding energy in line with the observation from interaction energies with the catalytic pocket (Figure 4.8, B, left panel), although diametrically opposing the favourability of THL over MO, which identifies the involvement of residues in vdW interactions other than those belonging to the catalytic pocket. The overall improvement in binding of THL over MO with lipase thus originates from a concerted contribution from direct vdW and non-polar solvation energies. The binding energies are more favourable for THL-lipase in the presence of colipase too, with contributions majorly from vdW component (Figure 4.8, D), also in agreement with the catalytic pocket interactions (Figure 4.8, right panel). However, the Coulomb electrostatics contribute more for THL-binding than MO-binding in this case, coupled with an equally proportional penalty from polar solvation energy. The binding of THL to lipase is improved in the presence of colipase (by ~11 kJ/mol), while MO bound to lipase less favourably when colipase is present (Figure 4.8 D), which may point towards time-dependent modulation by loop dynamics.

Additionally, the residue-wise energy decomposition contributing towards the overall binding energy was accounted for (Appendix C S2E-H). Without colipase, the more favourable THL

binding over MO binding is primarily facilitated by Ile79 and Ile252 in the flap domain of lipase (Figure 4.8, D), while Thr256 in the flap penalises binding of THL. With regards to the residues in the catalytic pocket, Gly151 (in the vicinity of Ser153), Leu176 (close to Asp177) and His264 also penalise binding of THL. In the presence of colipase, Ile79 penalises binding of THL with negligible contribution from Ile252, and stabilising contribution from Thr256 along with Gly114 (Figure 4.8). Leu176, Pro178 (close to Asp177) and His264 in the catalytic pocket also contribute favourably towards THL binding. Although the contributions from colipase indirectly binding to THL/MO is negligible as expected given the X nm separation, the altered loop dynamics with colipase co-bound (Appendix C S2D, S2F) influences MO *vs.* THL binding specificity.

Calcium has been shown to significantly increase the activity of lipase against lipid substrates [518-520], although the exact role of calcium in the activation of pancreatic lipase is still not fully elucidated. Given the reported influence of calcium ions on the lipolytic activity of the enzyme, preliminary studies have been carried out to probe the influence, if any, of Ca^{2+} on the inhibitory propensity of THL by computing interaction energies of the inhibitor-enzyme complex in its presence.

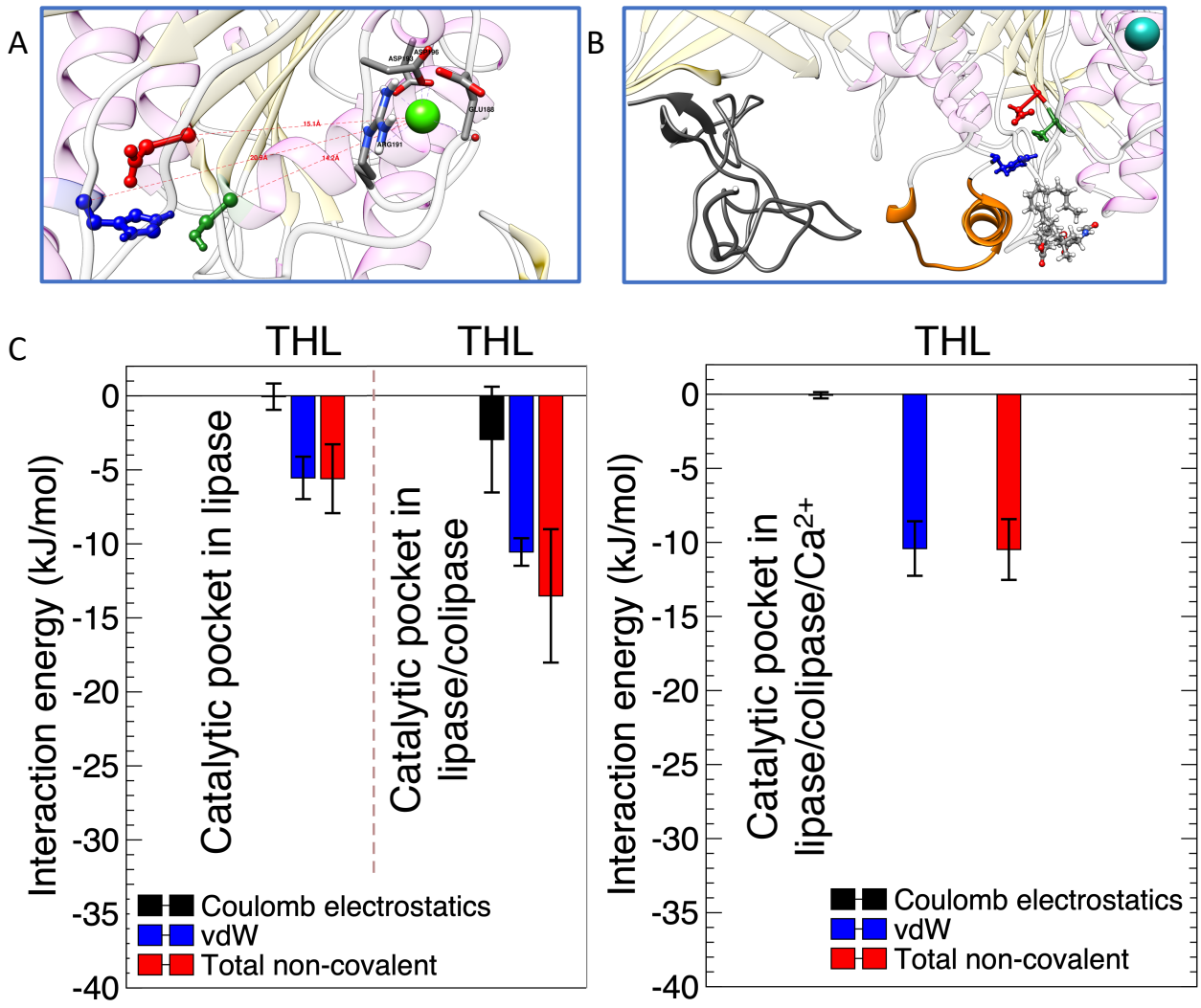

Figure 4.9. (A) Representative snapshot of PDB structure 1ETH, showing the Ca^{2+} coordinated to residues Glu188, Arg191, Asp193 and Asp196 with the measured distances from the catalytic triad Ser153, Asp177 and His264 shown **(B)** Representative snapshot from MD simulations of the inhibitor tetrahydrolipstatin (THL) with pancreatic lipase in the presence of cofactors colipase and calcium (Ca^{2+}). In both (A) and (B) the catalytic triad Ser153, Asp177 and His264 are coloured in green, red and blue, respectively with the mobile flap domain shown in orange. **(C)** Interaction energies between THL and the catalytic pocket in lipase without (left panel) and with colipase (middle panel), and interaction energies between THL and the catalytic pocket in lipase with colipase and Ca^{2+} (right panel).

In the PDB structure 1ETH, the Ca^{2+} is coordinated to residues Glu188, Arg191, Asp193 and Asp196 (Figure 4.9 A) forming a distorted square pyramid geometry. Here, the Ca^{2+} site is located

far away from the catalytic triad in the initial PDB structure (14.2 Å from Ser153, 15.1Å from Asp177 and 20.9 Å from His264). Although the Ca^{2+} site is not likely to be directly involved in catalysis, it appears to play a structural role in maintaining the conformation of the loop connected between Ca^{2+} site and Asp177. The simulations for 500 ns revealed that the Ca^{2+} remains intact in position and bound to its coordinated residues in lipase both in presence and absence of colipase. The flap (Cys238-Cys262) enclosing the active catalytic triad (Ser153, Asp177 and His264) remains in an open conformation throughout the course of simulation facilitating favourable access of the THL to the catalytic pocket. The THL in the Ca^{2+}-colipase-lipase system presents a less favourable interaction with the enzyme compared to the THL in the colipase-lipase system. From the interaction data, the THL may inhibit lipase less efficiently in presence of Ca^{2+} and colipase than in their absence, but the most profound inhibition would be expected where calcium is excluded from the lipase-colipase system. The predicted rank order for inhibiting propensity of THL may then be summarized as: lipase & colipase > lipase & colipase & Ca^{2+} > lipase. However, more comprehensive binding energy studies with the inclusion of the effect and contribution of solvation are required to give a clearer representation of the true effect of calcium on the system using the MM/PBSA [554] method (refer to section 4.3.6). There, the binding energies would be calculated for the full length enzyme, including all residues and not solely the catalytic triad. Changes in the relationships of calculated interaction energies between the various systems without the inclusion of calcium have already been noted, so it is expected that is will influence the conclusions drawn here. These calculations, as well as interaction energy calculations for the MO-lipase-colipase system in the presence of calcium, are required to predict the effect of calcium on the degradation kinetics of the cubic phase containing the inhibitor. The presence of calcium may influence the competitive nature of the binding of the lipase for its natural MO substrate and the THL inhibitor, impacting the degradation kinetics.

In summary, the predicted interactions and binding profiles from MD simulations suggest that the significant inhibition of pancreatic lipase by THL can impede the catalytic degradation of MO in lipid formulations by lipase. Altered loop dynamics in the presence of the cofactor colipase raises the predicted inhibitory activity of THL but further modelling is required to predict the impact of calcium on this inhibitory activity.

4.4.4 Enzyme-driven degradation behaviour

To support the *in silico* predictions of the binding energies between the lipase (w and w/o colipase) and the lipid or inhibitor molecules, the enzyme-driven degradation behaviour of the LCP matrix *in vitro* was examined experimentally. Based on the simulations of MO-lipase and THL-lipase complexes it was predicted that the THL should inhibit the lipolytic activity on the MO, an effect that would be enhanced in the presence of the enzyme's cofactor colipase. In line with the predicted altered loop dynamics in the presence of colipase, the binding of the inhibitor at the active site would be enhanced and subsequently would hinder the binding of the lipolytic enzyme to the lipid substrate. Based on these predictions, a controlled and prolonged digestion of the cubic lipid phase containing THL was anticipated under simulated lipolysis.

The concentration of lipase taken in these studies was in excess of those described in normal human serum in order to predict its behaviour at the upper limit of enzyme exposure [572]. Here, a gravimetric approach was taken to track the digestion of the formulated phases. The depletion in mass was followed and quantified using equation 4.4 until the samples were completely broken down to their oleic acid and glycerol constituents. The constructed stability profile is displayed in figure 4.10.

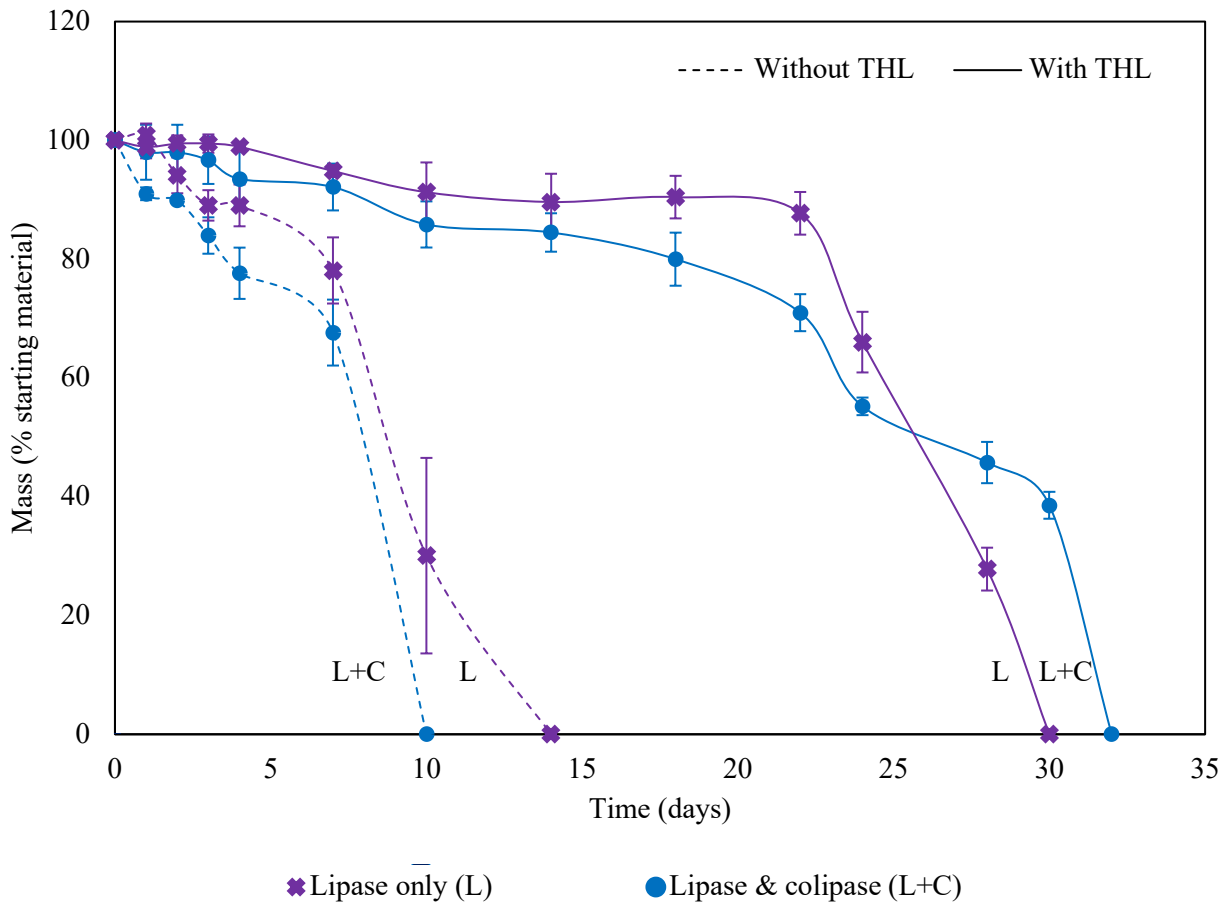

Figure 4.10. Degradation behaviour of paclitaxel-lipid controlled-release formulation in lipase-containing PBS or lipase and co lipase containing PBS with and without THL at 37°C and 200 rpm.

The PTX loaded cubic phases formulated without the inhibitor saw a relatively rapid chemical degradation over a 14 day period for both systems with and without colipase. At that timepoint, the lipid systems were completely digested to leave behind only an oily layer. For future studies it is important to note that reduction in the chain length of the lipid substrate to medium and short chain lipids (from the C18 MO used in these studies) could increase the rate of degradation [573, 574]. At 14 days, where the samples in the absence of the inhibitor were fully digested, the gels incorporating THL maintained upwards of 84% of their original mass. This improvement in stability can be ascribed to the presence of the THL, which is a potent inhibitor of a number of lipolytic enzymes [453, 462, 463]. These results support the explanation that the anchoring of the enzyme to the lipid cubic phase is sterically/chemically hindered by the incorporation of the lipase

inhibitor [575-577]. THL is hydrophobic in nature [468] and as a consequence resides mainly in the lipidic domain of the cubic phase. THL acts at the oil/water interface during lipolysis [260, 462] and so it is reasonable to assume that the THL integrated in the inner bilayers likely serves as a reservoir, carrying out its inhibitory function upon reaching the lipid/water interface throughout the progressive degradation of the lipid matrix [451, 469, 470].

Inclusion of the cofactor in digestion media has previously been reported to improve the activity of lipase on glyceride substrates several fold [521]. As clearly demonstrated in figure 4.10, the digestion process was, as expected, accelerated by the inclusion of the enzyme cofactor colipase (L+C). With THL incorporated, the lipase and colipase (L+C) samples were found to degrade faster over the first 24 days, compared to those in the presence of lipase alone. However, after the 24 day period, the inhibitor containing samples exposed to the colipase (L+C) showed a more sustained stability. The systems exposed to lipase alone displayed an initial extended lag phase where limited hydrolysis was seen finally followed by an accelerated digestion where the remaining lipid substrate was consumed rapidly. Despite displaying a faster digestion rate in the early stages of the study, the digestion curve demonstrates a more controlled lipolysis over the testing period when THL is present, especially upon exposure to the enzyme-cofactor mix – an important feature of a controlled drug delivery system which serves to reduce the risk of burst release and minimise possible toxicities associated with same.

Based on the MD simulations (section 4.4.3), the inclusion of calcium in the digestion media was expected to influence the stabilising effect of the inhibitor on the MO system. For this reason, the digestion medium was supplemented with calcium as a further lipase activation approach (Figure 4.11).

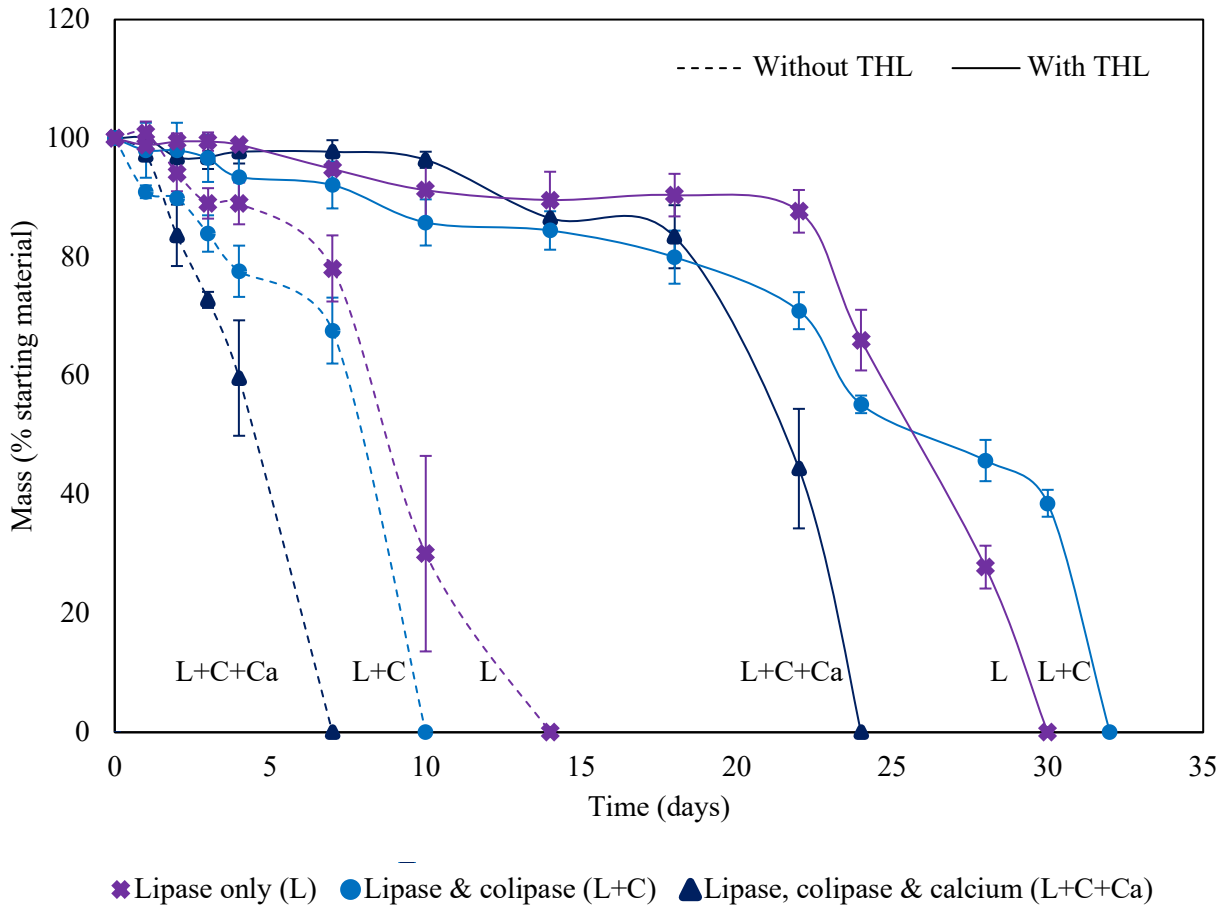

Figure 4.11. Degradation behaviour of paclitaxel-lipid controlled-release formulation in lipase digestive media showing the impact of including calcium in the media with and without THL and colipase at 37°C and 200 rpm.

The predicted rank order for inhibiting propensity of THL was estimated from MD simulations to be lipase & colipase > lipase & colipase & Ca^{2+} > lipase. Although the stability of the system was indeed prolonged compared to the lipase & colipase sample, the addition of the calcium was shown to further accelerate the digestion of the lipid cubic samples in the presence of THL (within 24 days (Figure 4.11) compared to 30 when exposed to lipase alone). When THL was excluded from the MO LCP, the inclusion of calcium in the lipase-colipase media resulted in the fastest matrix digestion after only 7 days, compared to 10 and 14 days for the lipase & colipase, and lipase only systems respectively. This indicates that the presence of calcium may increase the binding affinity of lipase to MO and may reduce the ability of THL to competitively bind with the lipase. This needs to be confirmed by a comparison of the interaction energy calculations for the MO-

lipase-colipase and the THL-lipase-colipase systems in the presence of calcium . Calcium has been shown to significantly increase the activity of lipase against lipid substrates [518-520], potentially be impeding its inhibition by the digestive products of the reaction (fatty acids) which block access of the lipase at the activity interface [575, 578]. It is predicted, at this stage, that a more favourable competitive interaction of the lipase with MO over THL in the presence of calcium will be observed from the *in silico* modelling studies.

Paclitaxel has previously been shown to interact with lipid membranes in small unilamellar lipid vesicles composed of 1-palmitoyl-2-oleoyl-sn-glycero-3-phosphocholine (POPC) [579]. Here DFT and thermal analysis have been utilised to demonstrate that the PTX interacts with the hydrophobic region of the lipid. The highly lipophilic BCS IV drug resides within the lipid portion of the cubic network where it loosely interacts with bicontinuous lipid layer away from water. The inclusion of PTX in the formulation approach directly impacts the internal dimensions of the system such that larger water channel dimensions (D_{H2O}) of up to 0.26 nm wider than the blank were observed in the SAXS analysis. This increase in water channel diameter could in theory serve as an accelerating effector of digestion, whereby the wider diameter of aqueous channels in the MO_PTX system might allow for a higher penetration of the external lipase solution into the phase's aqueous network compared to a blank system. However, previous studies by our group have shown that in the presence of lipase, blank monoolein cubic mesophase systems are rapidly digested by the enzyme within 7 days (Figure 3.5) [428]. This suggests that the PTX itself exhibits an inhibitory effect on digestion when incorporated into the system, possibly owing to a hydrophobic effect of the membrane bound drug. Additionally, the positioning of the drug within the membrane may shield or block access of the lipase hindering the surface-driven digestion.

4.4.5 *In vitro* drug release studies

Solubility studies were carried out on PTX to assess the most appropriate dissolution media to determine its release kinetics from the lipid cubic phases. The calculated saturated solubility of the drug in the various dissolution media (appendix C), highlighted the practically insoluble and undetectable nature of PTX in aqueous-based media compared to organic solvents. While information reported in previous studies on the dissolution behaviour of hydrophobic drugs such as paclitaxel in organic solvents is useful [580], these studies may not be representative of the true

dissolution behaviour of the drug under physiological conditions [494] and would not be useful for predicting the release behaviour from a lipid matrix, due to the rapid dissolution of the lipid matrix in organic solvents. For these reasons, the decision was made to focus solely on aqueous-based physiologically relevant media.

Due to the apparent inherent insolubility of paclitaxel, and its propensity to precipitate upon contact with aqueous media, an accurate quantification of its slow degradation-controlled release into biorelevant media was not directly measurable. Solubility limits of highly hydrophobic drugs must be taken into account as an underestimation of drug release can occur, where liberated drug may precipitate and go undetected, resulting in false sustained drug release behaviour being reported [581]. For this reason, an alternative approach was taken to study the dissolution of paclitaxel from the lipid cubic phase. Samples of PTX loaded lipid cubic phases, formulated with or without THL, were exposed to lipase enzyme over 30 days. Over the course of the study, at pre-determined time-points the reaction was stopped, the cubic phase was removed from the release media, dissolved in acetonitrile and the % of PTX remaining in individual samples was quantified using HPLC. The compiled release profiles are represented in figure 4.12, where the calculated % of drug release is plotted along with the % of mass loss according to the mass of the starting material against time.

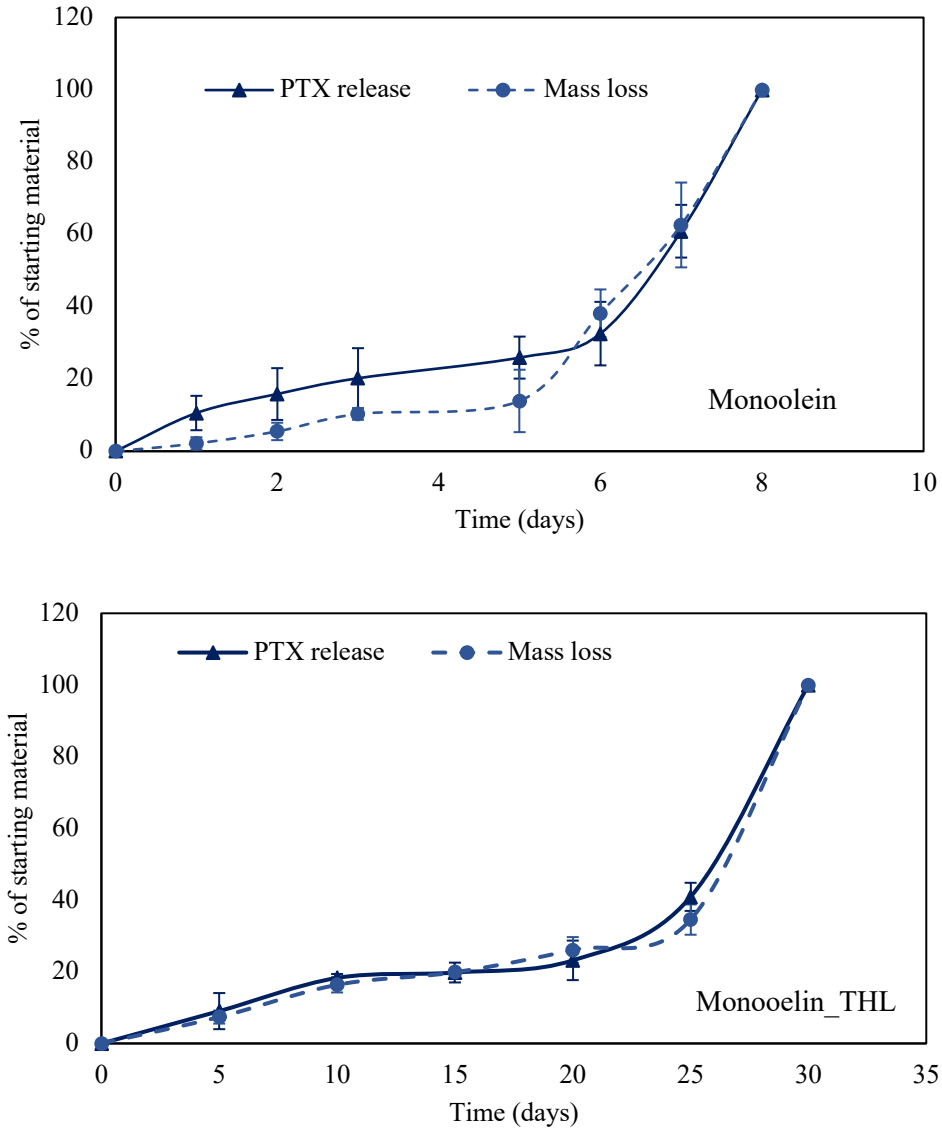

Figure 4.12. In vitro dissolution profile of paclitaxel from LCP (formulated at a concentration of 2 wt%) with/without THL (loaded at a concentration of 1.5 wt%) into PBS in the presence of lipase measured by quantifying unreleased drug using HPLC. Samples were shaken at 150 rpm at 37°C

These profiles demonstrate the direct correlation between the release of a hydrophobic agent and the stability/digestion of the lipid cubic phase. As shown in the degradation studies, the presence of the inhibitor in the system has the ability to greatly extend the stability of the LCP-PTX system exposed to high concentrations of the hydrolytic enzyme. It may therefore be reasonable to claim

the ability to predict and tune the duration of release of a hydrophobic molecule from a lipid cubic systems with any given inhibitor concentration [428].

4.5 Conclusions

Lipid cubic delivery systems provide a route for improving the *in vivo* behaviour of hydrophobic drugs by tapping into the intestinal absorption pathways of dietary glycerides. The complex cubic lattice network of the systems provide a versatile means to control and sustain the release of the encapsulated payload. Water-immiscible drugs such as paclitaxel studied in this investigation will reside in the lipid portion of the cubic network, meaning that their liberation from the mesophase is governed by the hydrolysis rate of the surrounding lipid matrix.

This study sought to characterise the modulation of the lipolysis of a lipid cubic phase by unravelling the impact and mode of action of lipase inhibitors, colipase, calcium ions and hydrophobic therapeutic agents on the enzymatic activity of lipases. In doing so, it was possible to decipher the impact on the digestion rate of the matrix and subsequent release of the encapsulated drug. In this context, it has been demonstrated that controlled release of the highly hydrophobic drug PTX through the concurrent incorporation of small doses of lipase inhibitor tetrahydralipstatin in the lipid cubic matrix without significantly impacting the internal structure of the lipid cubic matrices as shown by high resolution techniques such as SAXS and cryo-TEM. Through a combination of experimental and *in silico* approaches the significant inhibition of pancreatic lipase by THL has been demonstrated, whereby it can impede the catalytic degradation of monoolein and in turn garner further control of the release of PTX without significantly disrupting the internal structure of these systems. MD simulations confirmed that the catalytic triad of the pancreatic lipase is more accessible to the natural substrate MO than the inhibitor THL, where a surface loop exposes the active site to its lipid substrate while the mobile flap domain closes to hinder access of THL to the catalytic pocket of the enzyme. In contrast, the presence of the lipase cofactor colipase presents the inhibitor with a more favourable binding at this catalytic site compared to that of its lipid substrate. When the full length of the lipase enzyme is taken into account, beyond the isolation of the catalytic triad, our simulations identified a more favourable predicted binding of the inhibitor compared to its lipid counterpart. In this context, the stability of the PTX-containing lipid cubic samples under simulated lipolysis were extended at least two-fold

when THL was included in the formulation. Preliminary *in silico* studies have presented calcium as a further influential factor in the interactions between THL and the lipase enzyme, where the potential degree of the THL's inhibitory action is reduced its presence. More comprehensive calculations are required along with further simulations to establish the influence of calcium on the binding of lipase with its natural substrate MO to draw comparisons between both systems in establishing the nature of the perceived competitive process. The results discussed here evidence the capabilities of the inhibitor system to modulate and extend the degradation-controlled release properties of the PTX from lipid cubic mesophases, which have the potential to overcome issues of bioavailability associated with the notorious BCS IV drug along with others that present similar challenges in drug delivery applications.

Chapter V: Formulation strategies for the lipid cubic phase

5.1 Introduction

The high viscosity and stiffness of the fully swollen lipid cubic phase may limit its potential for drug delivery applications. In this work, a double-barrelled syringe apparatus is explored for generation of the lipid cubic phase for surgical and controlled drug-delivery applications. Additionally, as an alternative formulation approach, the impact of in situ formation in a range of physiological media on the internal structure of the cubic-Q_{II}^{D} type mesophase *in vitro* is investigated. Lipid cubic phases were formed directly in phosphate buffered saline, simulated gastric fluid and simulated nasal fluid with the aim of predicting in situ gelling behaviours of the system for site-directed drug delivery applications to overcome delivery issues and systemic toxicity.

5.2 Background

Within this thesis, a commonly used [582, 583] and straight forward melt-hydration approach for generating the lipid cubic has been employed. The approach simply involves introducing water to molten lipid containing the bio-/pharmaceutical of interest in glass vials or ampules with agitation to ensure formation of a homogeneous mixture followed by incubation in sealed vials to allow complete equilibration of the system. Although the stiffness and viscosity of the fully assembled cubic phase prove beneficial in slowing down the diffusion of drugs through its network for controlled delivery, the highly viscous consistency of the lipid cubic phase makes handling the gel post-formation a challenge. It is therefore desirable to improve the ease of handling and to define the stability of the phase in the approach. In many cases, dispersion of the phase into lipid cubic nano-suspensions (cubosomes) may overcome the challenge of viscosity for oral or spray delivery routes and also for topical applications. However, the bulk cubic phase should not be overlooked for its potential in prolonged and controlled topical drug delivery to enhance permeation of a range of drugs [209, 584, 585]. Further, the cubic phase is a self-gelling system, which eliminates the need for additional gelling agents (eg. tragacanth, carbomer, sodium alginate, gelatin, polyvinyl alcohol clays, etc. [586]) in the formulation approach. However, the fully swollen system is easily dehydrated during storage (Chapter IV, figure 3.4) inducing unwanted phase transitioning over time, so due consideration should be given to designing tools for real-time

formation of the cubic phase in a clinical setting. For this reason, alternative strategies for formulating the lipid cubic phase have been explored to facilitate its applicability in a clinical setting. In this context, the aims of the present study were twofold: (i) to demonstrate a double barrel syringe assembly with water in one syringe, and lipid in the other to rapidly form the cubic phase through a mixer unit attachment, and (ii) to demonstrate the in situ forming properties of the system through injection of molten lipid from a single barrel syringe into simulated body fluid.

Custom tools and procedures have previously been developed to formulate and handle the lipid cubic phase. The coupled syringe mixer is a well-known mixing assembly which was designed for viscous lipid mesophase samples, such as the cubic phase for protein crystallization applications [587].

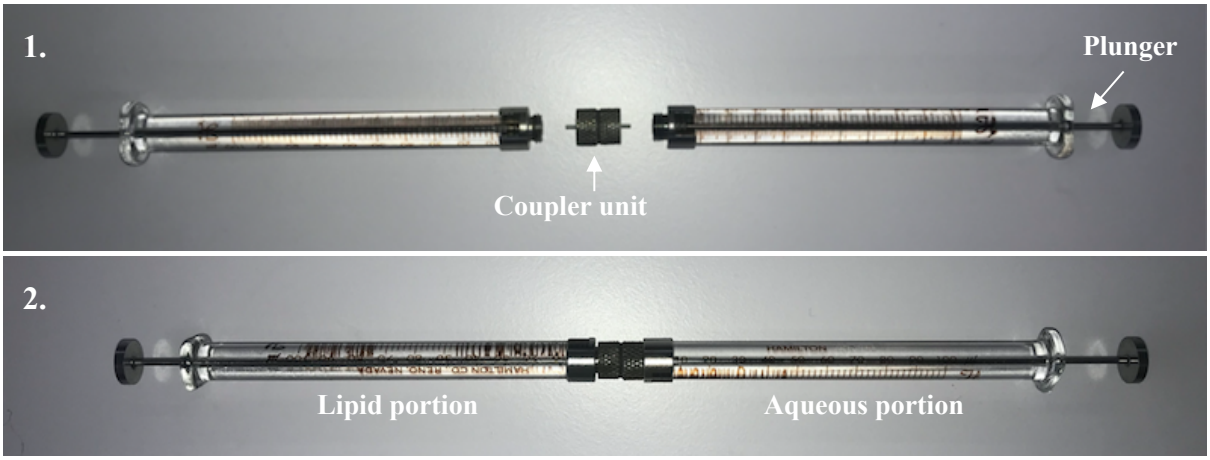

Figure 5.1. Homogenization and spontaneous self-assembly of the lipid cubic phase using the coupled syringe mixing aparatus. Image 1 shows the apparatus before assembly and image 2 shows the assembled system where the compound-containing lipid component would be present in one of the syringes and the aqueous phase in the other in appropriate ratios.

The mixer apparatus itself comprises a set of glass positive displacement Hamilton® syringes (Figure 5.1). The micro-syringes are linked by a narrow-bore coupler unit. Molten lipid is loaded within one of the syringes and the water component in the other at a known ratio (w/w). The cubic phase is achieved by repeatedly passing the contents of the syringes back and forth, blending the mixture until homogenous and until the desired phase is observed [588]. The micro-syringes are ideal for mixing the microliter volumes used in the preparation of lab scale lipid cubic phase but

achieving a homogenous mixture of gel volumes required for drug delivery applications through the narrow coupler unit would require a significant amount of mixing. In this study, commercially available syringe-mixer units already used to accurately mix and dispense viscous biomaterials in surgical procedures were investigated.

Further, the potential for in situ forming lipid cubic systems are discussed here as an alternative approach to overcoming issues with handling. As already discussed, the location of the cubic phase on the MAG-water phase diagram, where it lies sandwiched between the lamellar and reversed hexagonal phases respectively (Chapter I, section 1.4), facilitate its in situ formation. By raising the temperature or hydration of a lamellar system, geometrical reorganization ensues inducing a transition from the inherently fluid and injectable lamellar phase to the stiff three dimensional cubic phase. This presents an alternative approach to delivery of the viscous cubic phase where it may be possible to deliver a lipid-drug mixture in the absence of water or a less viscous lamellar formulation containing the desired pharmaceutical ingredient to subsequently form the viscous cubic phase upon contact with excess water in biological fluid.

Previous work has demonstrated the feasibility of the MAG-water systems as excellent in situ forming biodegradable matrix type drug delivery systems [589-592]. However, these studies fell short in detailed studies of the impact of biological fluids on in the internal structure of the phase upon contact. Esposito et al. investigated a glycerol monooleate-poloxamer system for delivery of tetracycline for a periodontal application, where the lipid mixture was delivered directly to the periodontal pocket. The in situ forming system demonstrated prolonged release *in vivo* and clinical efficacy [591]. The results presented by Esposito et al. were important in understanding the capacity of the cubic phase for such applications but no details of the structural properties and state of the lipid formulation upon contact with biological fluids were described. Similarly, a study carried out on the in situ formation of the cubic phase are oral administration of cubic precursor molecules neglected these structural studies [590]. Geraghty et al. reported a lamellar system formed upon the incorporation of muscarinic drugs that could be delivered to a vaginal delivery site where upon imbibing water would transition to the viscous cubic phase [592]. However, this study did not provide *in vivo* data, and the media used to swell the system was water which is not entirely representative of biological conditions. As has been shown in chapters II and IV, as well as from the literature [191, 192], the release rate of drugs from mesophase systems is highly

dependent on both the phase present and the capacity of the aqueous channels. Additionally, variations in ionic strength where the salinity effect explained by the kosmotropic/chaotropic properties of the ions present in the swelling media [429-431] have been shown to stabilize or destabilize the system, in turn affecting its controlled release properties [432]. In this framework, understanding the swelling and mesophase properties of MAG systems formed in situ is important to understand the controlled release capabilities of the system. For this reason, three biologically relevant buffers have been selected as the swelling media for the formulations. The buffer effect on the internal structure of MAG mesophases compared to the systems swelled in water was established by means of SAXS. In this sense, understanding these structural changes is important in the design of these systems, as changes in their phase structure/symmetry directly influences the release kinetics [191, 192].

5.3 Materials & Methods

5.3.1 Materials

Monoolein 9.9 MAG (1-(9Z-octadecenoyl)-rac-glycerol) and monopalmitolein 9.7 MAG (1-(9Z-hexadecenoyl)-rac-glycerol) were acquired from JenaBioscience, Germany at >99% purity; Phosphate buffered saline (PBS) tablets were purchased from Merk (Saint Louis, MO); FaSSGF (Fasted state simulated gastric fluid) powder was purchased from Biorelevant.com Ltd; Water was purified in the lab using a Milli-Q Water System (Millipore Corporation, Bedford, MA).

5.3.2 Double-barrelled syringe method

A FibriJet® double-barrelled syringe (3 mL, 1:1 ratio) coupled with a mixer unit (3 cm, stream output with 2.03 mm inner diameter) suitable for high viscosity samples (Figure 5.2) was studied as a tool for rapid generation and dispensing of the cubic phase. Lipid (monoolein or monopalmitolein) was added to one side of the applicator assembly and the aqueous phase was contained within the other in a similar manner to the Hamilton® syringe set up [587]. The two components were simultaneously and slowly dispensed at equal volumes through the mixer unit into a collection vial and analysed by SAXS within 10 minutes to define the mesophase accessed.

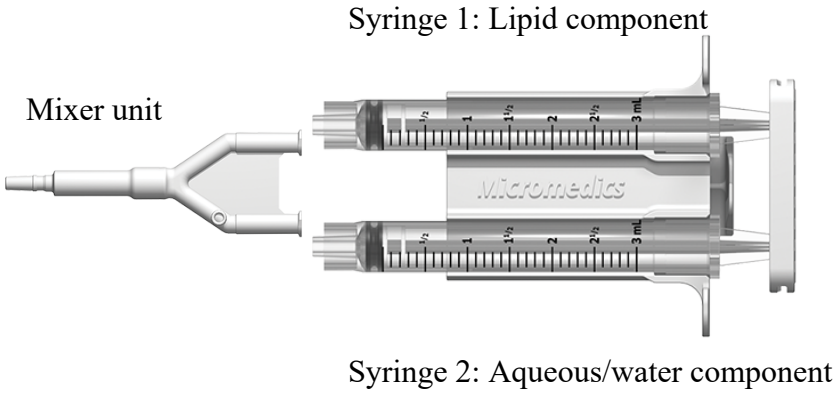

Figure 5.2. FibriJet® double-barrelled syringe (DBS) coupled with 3 cm mixer unit for fast cubic phase formulation

Monopalmitolein is liquid at room temperature and so required no pre-heating to achieve fluid molten lipid. Monoolein was heated in an oven at 35ºC to facilitate its transferal to the syringe unit as it is waxy at room temperature. Prior to mixing with the aqueous phase, the loaded syringe unit was once again heated to 35ºC to allow the lipid to easily travel through the syringe into the mixer unit.

5.3.3 'In situ' forming cubic phases: studying the effect of swelling buffer

Different buffers were investigated to study their effect on the formation of the lipid cubic phase in situ. Fasted-State Simulated Gastric Fluid (FaSSGF) was prepared by dissolving pre-prepared FaSSGF powder (Biorelevant.com) in acidic buffer (1.997 g NaCl in 1L water) with an adjusted pH of 1.6 reached using 1M HCl with stirring according to the manufacturers guidelines. Simulated nasal fluid (SNF) was prepared as previously described by Farid et al. [357] (7.45 mg/mL NaCl; 1.29 mg/mL KCl; 0.32 mg/mL $CaCl_2.2H_2O$; made up to volume with deionised water) to give a solution pH of 6.4. The final buffer was phosphate buffered saline, prepared at pH 7.4 (137 mM NaCl, 2.7 mM KCl and 10 mM phosphate buffer solution (Na_2HPO_4 & KH_2PO_4)). To simulate the formation of the cubic phase 'in situ', the molten lipid was delivered to 1 mL of the three simulated body buffers and left to equilibrate for 48 hours in sealed glass vials.

5.3.4 SAXS for mesophase assignment

Small angle X-ray scattering was performed to confirm the mesophase nature of the lipid cubic samples prepared by means of (i) the double-barrelled syringe method, and (ii) when molten lipid was injected directly into the various biorelevant media. SAXS measurements were carried out within 10 minutes after sample preparation at the Solution State SAXS B21 beam line at Diamond Light Source on the Harwell Campus, Didcot, UK [428]. Small angle diffraction images were processed and the relative positions of the distinct Bragg peaks were indexed and used to deduce the space groups and lattice parameters by correlating with Miller indices [473] as already described. Similarly, the water channel diameter and lipid chain length were calculated as previously described [428], with surface area and Euler Poincare constant (χ) used [151, 354] to track any changes induced upon drug loading.

5.4 Results & Discussion

5.4.1 Double-barrelled syringe method

A dehydration effect in the stored lipid cubic phase over time has been demonstrated (Chapter IV, figure 3.4), which induces a phase transition. For topical drug delivery applications, it may be more effective to prepare the cubic phase at the time of administration. Samples were prepared here using a double-barrelled syringe unit to investigate the suitability of existing biomaterial applicators. A mixer unit specified for viscous samples was chosen and SAXS was employed as before to assign mesophase(s) accessed and to calculate the corresponding internal dimensions.

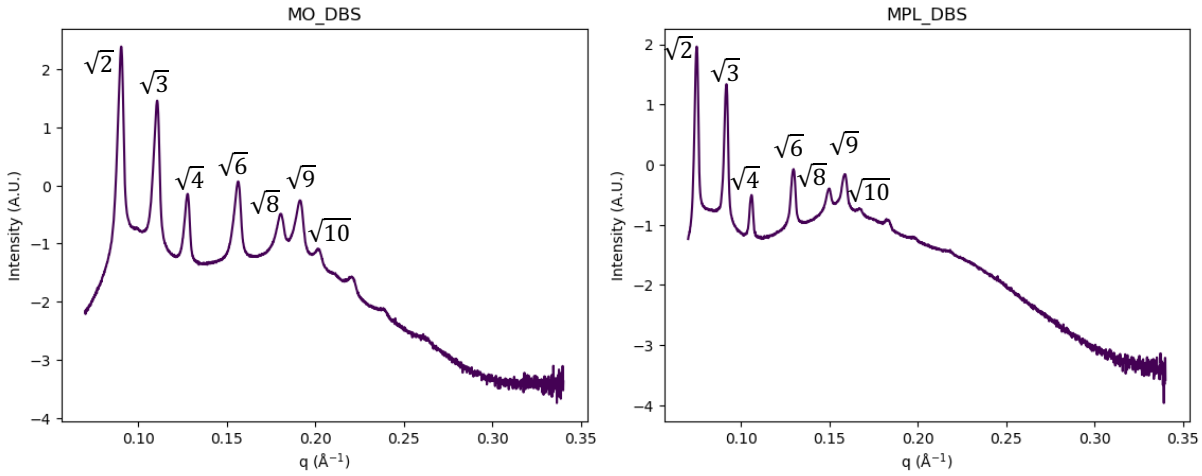

Figure 5.3. 1D azimuthally integrated SAXS patterns of monoolein (MO) and monopalmitolein (MPL) cubic mesophases prepared by means of the double-barrelled syringe fitted with mixer-unit. Samples were analysed within 10 minutes after dispensing through the mixer unit. The peaks of the patterns have been indexed according to the Q_{II}^{D} mesophase

Here, the distinct Bragg peaks have been indexed according to the Miller indices of the reflection plane to assign the mesophase (Figure 5.3). The relative positions of these reflection lines from our samples confirm highly ordered bicontinuous cubic phases of the cubic-Q_{II}^{D} type formed through hydration in the mixer unit. Table 5.2 displays the assigned mesophases and calculated lattice parameters of these formulations.

Table 5.2. Phase identification and lattice parameters of assigned mesophases for LCP formulated by double-barrelled syringe approach and analysed within 10 minutes post-dispensing

Host Lipid	**Assigned mesophase**	**Lattice Parameter (nm)**	**L (nm)**	**D_{H2O} (nm)**
MO	Q_{II}^{D}	9.82	1.67	4.33
MPL	Q_{II}^{D}	11.85	1.32	6.62

The cubic formulations shown here are comparable to the cubic systems formulated by the simple melt-hydration approach used throughout this thesis and those reported in the literature

[123, 169, 353, 359, 360]. This highlights the potential of real-time generation of the cubic phase for clinical application without the need for pre-formulation and lengthy equilibration times. Although pharmaceuticals were not included in the studied formulations here, it would be possible to introduce hydrophilic agents in the aqueous phase and lipophilic molecules within the lipid either dissolved or in suspension. Further, this approach would allow for personal and tailored dosing, where unique drug loading concentration could be made for a given patient by simply varying the amount of drug added to either the lipid or aqueous components.

Monopalmitolein is particularly attractive for this approach, as the lipid is fluid at room temperature facilitating easy delivery through the syringe to the mixer unit. Other lipids such as monoolein that are solid or waxy at room temperature require pre-heating to facilitate transferal to the syringe and for ease during mixing. This can be done in an oven, water-bath or simply using the warmth of the palm of your hand. Further, monoopalmitolein forms Q_{II}^{D} phase at 50 wt% hydration, and the Q_{II}^{D} phase is accessed at 40 wt% hydration in the monoolein system, beyond which it exists in excess water. Therefore, the DBS assembly that dispenses equal volumes of lipid and aqueous media are ideal for these lipids and any of those that form the cubic phase at hydration levels at or below 50 wt%. Lipids that require a higher degree of hydration to assemble the fully swollen cubic phase may not be suitable, unless they were to be delivered to an internal delivery site where the system would further swell in biological fluid.

5.4.2 'In situ' forming cubic phases: studying the effect of swelling buffer

In order to assess the impact of salts and other components present in biologically relevant media on the lipid mesophase formed, the swelling capacity and internal dimensions of the molten lipid swelled in excess media of varying pH and composition were monitored by means of SAXS analysis. The resultant 1D azimuthally integrated SAXS patterns of MO cubic mesophases swelled in PBS buffer at pH ~ 7.4, SNF at pH 6.4, or FaSSGF at pH ~ 1.6 are shown in figure 5.3 and 5.4 where the distinct Bragg peaks have been indexed according to the Q_{II}^{D} mesophase. The collected data identified the fully swollen cubic phase in all swelling media samples, and therefore the media can be said not affect the ability of the MAG lipid to access the desired mesophase.

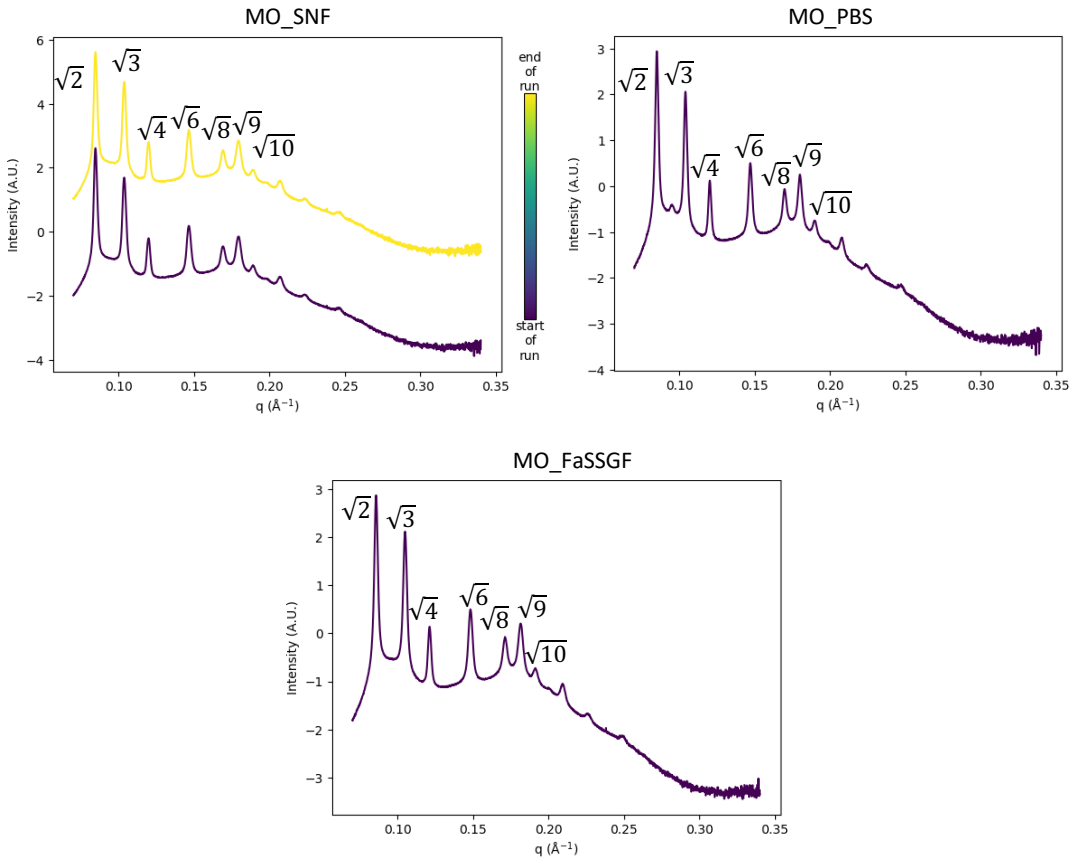

Figure 5.3. 1D azimuthally integrated SAXS patterns of monoolein (MO) cubic mesophases swelled in a variety of bio-relevant media of varied pH (PBS buffer at pH ~ 7.4, SNF at pH 6.4 or FaSSGF at pH ~ 1.6). The peaks of the patterns have been indexed according to the Q_{II}^{D} mesophase and the MO_SNF figure highlights the stability of the system against the X-ray exposure over 15 frames.

Once the resistance of the Q_{II}^{D} mesophase to environmental pH was shown, it was important to study the ionic effect on the systems as it has been reported that ions in solution have the ability to expand or reduce the lattice constant of the phase [593]. Subsequently, the internal dimensions of the phase, including water channel diameter, are altered which can directly impact the controlled release properties of the system [191, 192]. This is an important consideration where local delivery or in situ forming gels are concerned, as behavioural predictions made in the design of these systems using water alone are likely not representative of the true biological effect. For this reason, the internal dimensions of the phase were calculated and the results are reported in table 5.3.

Table 5.3. Comparison of phase identity and lattice parameters of assigned mesophases for LCP formulated in water and with various biologically relevant buffers of different pH (PBS buffer at pH ~ 7.4, SNF at pH 6.4 or FaSSGF at pH ~ 1.6) from SAXS experiments

Host Lipid	Buffer	Assigned mesophase	Lattice Parameter (nm)	L (nm)	D_{H2O} (nm)
MO	Water	Q_{II}^{D}	10.3	1.75	4.55
MO	PBS	Q_{II}^{D}	10.45	1.78	4.61
MO	SNF	Q_{II}^{D}	10.49	1.78	4.64
MO	FaSSGF	Q_{II}^{D}	10.26	1.75	4.49

The results show that the cubic phases formed from the various buffers differ in their internal diameter although MO in SNF and PBS are seen to be comparable. The composition of SNF and PBS buffers does not differ drastically, although PBS does include phosphate salts which may affect the stabilization of the system [593]. A reduction in lattice parameter and therefore internal dimensions is seen when the sample is prepared in FaSSGF. This may be influenced by the presence of components other than salts in the simulated gastric fluid, such as the glycerophospholipid mixture lecithin which is lipid soluble and pepsin which is a water soluble protein. Previous studies carried out by Chang et al. identified a decrease of over 10% in swelling capacity in the cubic phase of a Myverol^{TM} derived system at media with lower pH (0.1M HCl) compared to PBS at pH 7.4 [215]. Myverol is a monoglyceride mixture, made up predominantly of monoolein (>86%) while the remainder is composed of other monoglycerides such as monostearin, monopalmitin and monoarachidin [594]. The group related this effect to the presence of free fatty acids in the lipid mixture with the hypothesis being that at normal biological pH, these fatty acids are ionized and thus interacting and absorbing more water. In acidic pH however, these fatty acids are thought to be non-ionized and are therefore more readily solubilized in the lipid membrane of the mesophase ultimately decreasing the capacity for water uptake [215]. While the study carried out by Chang et al. did not calculate the internal dimensions of the systems studied, it is reasonable to assume that changes in water channel diameter seen across the samples prepared

in the three buffers here would contribute to differences in the swelling capacity of the system in the same way.

It would be remiss to overlook the potential impact of the ionic composition of the media used here [432]. Across the samples, an increase in lattice parameter of the PBS and SNF samples compared to the control sample is seen. X-ray diffraction data suggests that kosmotropic solutes reduce the interfacial area of the Q_{II}^{D} cubic phase of MAGs by stabilizing the structure of bulk water, thus reducing the amount of water molecules present at the lipid/water interface [595]. Chaotropic solutes however, present the opposite effect, where chaotropes expand the interfacial area [593, 596, 597]. Given what is known about the geometrical relation of the lipid cubic structure [598], the relationship between an increase or decrease of the area at the water/lipid interface of Q_{II}^{D} cubic phases with an observed increase and decrease of the lattice constants respectively has been reported in a similar manner to that observed for lamellar and inverted hexagonal phases [596, 599]. Specifically, these reports suggest that kosmotropes reduce the interfacial area at this boundary and thus reduce the lattice parameter for cubic phases [593] while chaotropes have the opposite effect (assuming negligible effect on lipid molecular length caused by solute composition). FaSSGF contains NaCl, a known kosmotropic solute with strong hydration behaviour [600, 601], however, it also contains sodium taurocholate, which along with other sterols has been shown to directly affect the Q_{II}^{D} cubic reducing the lattice parameter when present in a salt solution [478]. The sterols, also including cholesterol, possess a large headgroup and reduce the negative curvature of the system altering the rigidity of the bilayer of the cubic phase through hydrogen bonding [602] and have been shown to induce a phase transition from the Q_{II}^{D} to the L_{α} through an intermediate Q_{II}^{G} region [478].

5.5 Conclusions

Although pre-formed bulk lipid cubic phase may have limited applicability in parenteral drug delivery due to its viscous and stiff nature, alternative delivery strategies exist where the cubic phase can be delivered to the body more efficiently. Taking advantage of the location of the lipid cubic phase on its phase diagram and the ability of the MAG-water system to transition between the various liquid crystalline mesophases, in situ formation of the cubic phase upon contact of the molten lipid with aqueous biological fluids presents an attractive route for localized or enteral drug

delivery. Although not relevant for MO (which form the Q_{II}^{D} cubic phase between room temperature (RT) and body temperature), other cubic phases (for example phytantriol [167]) are sensitive to changes in temperature between RT and body temperature, further facilitating this putative in situ gelling system. In this study the impact of ions, small molecules and proteins present within biological fluids on the lipid phase behaviour swelled in various biologically relevant media in place of water have been investigated. By means of SAXS the collective impact of ionic effect and composition on the lattice parameter and subsequent water uptake of the Q_{II}^{D} cubic phase has been calculated. Changes in internal dimensions not only impact the drug release kinetics but also the stability of the phase in enzymatic environments, where systems with larger water channels may imbibe more enzymatic media, potentially accelerating the digestive process due to a larger interfacial surface area for lipolysis. Understanding these effects of biologically relevant ions and small molecules on the phase behaviour of this complex system is of great importance from a biological and medical viewpoint in order to make predictions on the performance of the system *in vivo*.

Here also, the feasibility of a single-use double-barrelled syringe equipped with a mixer unit has been explored as a suitable set up for rapidly forming the viscous cubic phase of MO and MPL in potential medical applications. This approach overcomes the need for storage of the easily dehydrated lipid cubic phase system and would facilitate personal and tailored dosing, where variations in drug loading concentration could be made for a given patient by simply concentrating or diluting the amount of drug added to either the lipid or aqueous components.

Chapter VI Conclusions & Future directions

This PhD thesis focused on the study of lipid cubic phases and their dispersions as encapsulating matrices for the controlled delivery of active pharmaceutical ingredients. This chapter summarises the key conclusions that may be drawn from the research carried out within this extensive and comprehensive study.

6.1 Conclusions

The development of effective carrier systems that are capable of delivering sustained and therapeutically relevant doses of drugs has earned its place at the forefront of research over the last decade. The introduction to this thesis has provided an extensive discussion on the numerous and expansive challenges these systems are tasked with overcoming to effectively improve the therapeutic index of existing and new drug entities. The amphiphilic, biocompatible, and biodegradable nature of the lipid cubic phase has merited the system as a worthy and versatile candidate for controlled drug delivery.

The first aspect of this thesis investigated the capabilities of two MAG derived (MO and MPL) lipid cubic phases and its dispersions in a controlled release capacity using a selection of four antihistamine molecules of varied physicochemical properties, specifically varying degrees of aqueous solubility. Through high resolution analytical techniques including SAXS, coupled with dynamic light scattering the impact of incorporating these molecules into the cubic network has been studied. Decelerated and biphasic release of both sets of first and second generation antihistamine molecules was observed from the bulk and dispersed systems compared to the free drugs, highlighting the prolonged release capabilities of the lipid matrix. A clear focus was given the impact of drug solubility and environmental pH on the dissolution properties and have presented a greatly reduced release rate for the hydrophobic AZL and CZH compared to the freely water soluble DPH and CBX. The pH of the selected biorelevant dissolution media was shown to impact the release rates of these drugs from the system, with the acidic environment created by the FaSSGF media greatly accelerated the release of the molecules from the lipid matrix, an effect that has been widely reported in the literature [58, 215]. This change in dissolution rate may be attributed to a matrix effect where the fatty acid chain may be ionized or unionized under certain

conditions dictating the release of the encapsulated drugs [215, 434] which is directly correlated with its location in the matrix [170, 435].

In this thesis the lipid cubic phase and its dispersions have also been highlighted as potential mucoadhesive controlled release systems, an area that to our knowledge has not been extensively explored to date. MP-SPR has been shown to be an efficient tool to investigate adhesion of lipid cubic systems to mucin layers as an alternative approach to studying the mucoadhesive nature of the systems without the need for tissue samples. A potential real-world application in the mucosal delivery of antihistamine molecules through the mucosa of the nasal cavity was discussed and the impact of four commercially available molecules on the mucoadhesive nature of the system has been explored. The need for these *in vitro* tests in matrix design and in predicting their behaviour *in vivo* was highlighted by the distinct binding profiles of the systems, directly affected by the passenger molecule and its properties. The bioadhesive nature of these systems should prove an important tool in improving retention time and absorption of passenger drugs at a target delivery site, reducing systemic toxicity, increasing bioavailability of the drug and enabling long-acting therapeutic effects. While hydrophilic compounds and large polar molecules follow paracellular diffusion, lipophilic molecules rely on transcellular transport across lipid bilayers in cell membranes [603]. As a consequence, the bioadhesive nature of the lipid cubic phase is particularly influential in improving the bioavailability of poorly soluble and lipophilic drugs, that can be rapidly absorbed when delivered and retained at the mucosal membrane due to its high surface area and contact with the heavily vascularised anatomy. Where antihistamine molecules are concerned, in particular the first-generation molecules having the ability to cross the blood brain barrier and elicit unwanted side effects, mucosal delivery has the added bonus of containing the molecules at a target site while efficiently delivering effective concentrations to the affected organ. Efficient cellular uptake of the drugs reconstituted in cubosomes has been demonstrated by monitoring changes in zeta potential at the surface of fibroblast model cells over 12 hours. With the aid of competitive ELISA, the ability of the drug formulations to inhibit mediator release has been illustrated, by more than half in some cases, from basophilic mast cells (RBL2H3 cells) with the propensity to release histamine upon IgE induction [358, 604]. In this time, metabolic assays identified no cytotoxic effect caused by the systems in the two studied cell lines, with the exception

of one of the hydrophobic drugs CZH, that appeared to reduce cell viability by half after a 48 hour incubation in fibroblast cell line.

While this initial investigation answered a number of questions, the results also brought forward several additional research objectives towards the design of effective drug carrier systems. For one, additional studies were required to clarify the relationship between the location of the drug molecule in the system leads and the varied release kinetics. Further, there was a keen interest in identifying and optimising formulation approaches to further control the release through targeting lipolysis of the system. It is understood that the solubility properties of a given molecule govern its location within the cubic network, with hydrophobic molecules residing in the lipid bilayer while water soluble molecules inhabit the congruent water channels of the mesophase. As a result, the release kinetics of water-soluble molecules is limited by their diffusion through the water channels of the system, with little effect from the lipid bilayer itself. Hydrophobic drugs on the other hand, rely on the depletion of the lipid bilayer surround them to be liberated into solution. Lipid cubic systems such as those studied in this thesis that are derived from biodegradable MAG lipids are highly susceptible to lipolytic degradation by lipase enzymes *in vivo*. While this is important in achieving total release of the encapsulated drugs, the rate at which this digestion occurs may limit their application in drug delivery. In the second research study reported in this thesis, the controlled release of hydrophobic APIs was achieved by means of a novel formulation approach through the incorporation of small doses of lipase inhibitors, using tetrahydralipstatin as a model. Exploiting the biodegradable nature of MAG lipids in lyotropic liquid crystalline mesophases in this way, presents a means of establishing further control of the release kinetics of poorly soluble molecules reconstituted within the lipid envelope. However, the interactions between the lipid excipient and the molecules that it encapsulates with endogenous enzymes (lipases and esterases), as well as the physicochemical transitions that arise, are multifaceted and difficult to predict. *In vitro* tests that mimic the fate of a lipid formulation upon exposure to the gastrointestinal and enzymatic environment of the body are therefore heavily relied upon to rationalise formulation development of biodegradable drug delivery systems.

Under simulated lipolysis *in vitro*, two stable cubic phases incorporating tetrahydrolipstatin formulated from monoolein or monopalmitolein have been designed and investigated. Both systems displayed controlled degradation with at least a 4-fold improvement compared to the blank

systems; a stability that can be tuned by varying the concentration of the incorporated inhibitor, thereby presenting a framework from which formulators can select the most promising formulation approach for a specific drug to be delivered over a desired duration. In these systems, sustained release is achieved by interrupting the interactions of lipolytic enzymes at the lipid/water interface through the introduction of a molecule that competes for their active site at this boundary impeding the hydrolysis. A hydrophobic, and industrially relevant small molecule drug, a clofazimine citrate salt, was selected to demonstrate the feasibility of this approach by means of gravimetric and dissolution studies under simulated lipolysis. Both lipid systems demonstrated extended stability, and subsequently coordinated prolonged release over 30 days with a direct relationship between the rate of lipid digestion and molecule release observed. This novel formulation is achieved without negatively affecting the structure of the matrix itself, as shown by comprehensive small-angle X-ray scattering experiments. By adjusting the concentration of the lipase inhibitor, one could potentially tailor a system with desired stability for any given drug delivery applications where hydrophobic drugs are required. Tetrahydralipstatin is a potent inhibitor of many other lipolytic enzymes additional to the pancreatic lipase studied here. These include gastric lipase, and carboxyl ester lipases. Thus, the concept studied described here may have a more far-reaching relevance, especially for the rapidly degraded dispersions of the cubic phase that may be suitable for oral delivery.

The number of new chemical entities identified annually is rising with thanks to progress in automated synthesis, combinatorial chemistry, and high throughput screening. However, a disproportionate number of these molecules in drug development display poor solubility [106, 495, 496] and significant efforts are required to improve their bioavailability [492] if they are to progress to commercialization. The BCS class IV drugs [4] includes a large number of poorly soluble, high molecular weight drug candidates with presumed poor ability to permeate biological membranes [491]. The promise of biodegradable lipid-based drug delivery systems such as LCP in improving the solubilization and bioavailability of these difficult lipophilic drugs has been discussed at length [120, 297-301]. They have the potential to do so by stimulating the secretion of endogenous lipids (bile salts and phospholipids), by assembling micellar structures, and by improving enterocyte-based transport including inhibition of the P-gp efflux system [109, 110]. In the third chapter of this thesis a BCS class IV drug paclitaxel, a clinically relevant antineoplastic

agent, has been selected as a model drug to asses lipid cubic systems with the ultimate aim of designing a system for improving the *in vivo* behaviour of hydrophobic drugs by exploiting the intestinal absorption pathways of dietary glycerides. For this particular application, the mesophase's autonomous assembly is independent of organic solvent and so is an additional attractive feature for the delivery of PTX as it eradicates the need for harmful carriers such as polyethoxylated castor oil commonly used in their formulation. SAXS and cryo-TEM confirmed that the incorporation of THL and PTX in the cubic phase and its dispersions did not negatively influence the formation of the Q_{II}^{D} mesophase.

Paclitaxel, like most water-immiscible drugs, inhabits the lipid bilayer of the cubic network. The liberation of the molecule from the mesophase has been studied and the hydrolysis rate of the surrounding lipid matrix has been proven as the rate limiting step, in a similar way to that observed for CFZ. In the initial lipolysis studies the action of lipases on the lipid mesophase and how this could be controlled by THL to regulate the release of the drug payload has been clearly demonstrated. Further to this investigation, the third body of work within this thesis sought to clarify this modulation by unravelling the impact and mode of action of lipase inhibitors, relevant lipase cofactors (colipase and calcium ions) and the hydrophobic therapeutic agent itself on the enzymatic activity of lipases. In doing so, it was possible to decipher the impact on the digestion rate of the matrix and subsequent release of the encapsulated PTX model drug that was extended almost 4-fold to 30 days.

Through a combination of gravimetric mass monitoring, high-resolution characterisation techniques and *in silico* approaches, the significant inhibition of pancreatic lipase by THL has been explained at a molecular level. The PTX-loaded LCP samples were exposed to lipase alone, and a mixture of lipase and its co-factor colipase to monitor their lipolysis in the presence and absence of THL by a simple gravimetric approach. The inhibitor-containing samples exposed only to lipase demonstrated a biphasic digestion, with a delayed start followed by a rapid loss in mass. Although an accelerated mass loss was observed in the samples exposed to the enzyme-cofactor mix in the initial stages of the study, the THL appeared to coordinate a more controlled lipolysis when colipase was present. This pattern of digestion is more attractive in controlled drug delivery where the risk of burst release and possible toxicities associated with same are minimised by delivering consistent concentrations of drug as the lipid vehicle is digested. As expected [518-520], improved

lipase activation was illustrated through supplementation of the digestion media with calcium in the form of $CaCl_2$ across both THL and inhibitor free samples. To compliment experimental data, MD simulations were utilized and confirmed that the catalytic triad of the pancreatic lipase is more accessible to the natural substrate MO than the inhibitor THL, where a surface loop exposes the active site to its lipid substrate while the mobile flap domain closes to hinder access of THL to the catalytic pocket of the enzyme. Interestingly however, a more favourable binding at this Ser153-Asp177-His264 catalytic triad is presented to the inhibitor compared to that of its lipid substrate. Additionally, when overall binding is taken into account, beyond the isolation of the catalytic triad, our simulations identified a more favourable predicted binding of the inhibitor compared to its lipid counterpart. These findings agreed nicely with those of our digestion studies. The data reported within this study highlights the capabilities of the inhibitor system to modulate and extend the degradation-controlled release properties of the PTX from lipid cubic mesophases. This approach has far-reaching relevance, where our novel systems have the potential control and sustain the release of these molecules to overcome issues of bioavailability associated with the notorious BCS IV drug along with others that present similar challenges in drug delivery applications.

The final consideration of this thesis was in bridging the gap between fundamental science and applying the concepts in a clinical setting. The highly viscous and stiff nature of the fully swollen bulk lipid cubic phase may waive, or at least hamper, its application in parenteral drug delivery. Notwithstanding these limitations, alternative delivery strategies have been presented for these fascinating systems. For one, the transitional nature of liquid crystalline phases presents an opportunity for capitalizing on the fluid-like consistency of the lamellar phase to easily deliver the reconstituted drug to target delivery sites where they can self-assemble into the cubic symmetries upon hydration by biological fluids. The MAG cubic phase's sensitivity to temperature between RT and body temperature, further facilitates this putative in situ gelling system. An important consideration where in situ gelling is desired, is the impact of biologically relevant ions, endogenous proteins, and sterols on the structure of the desired phase. Here, by means of SAXS the collective impact of ionic effect and media composition on the lattice parameter and subsequent water uptake of the Q_{II}^{D} cubic phase using three biologically relevant media (PBS buffer at pH ~ 7.4, SNF at pH 6.4 or FaSSGF at pH ~ 1.6) has been demonstrated. In good agreement with the

literature, the pH and ionic composition of the swelling media was shown to alter the lattice parameters and internal dimensions of the phase, potentially owing to ionization of fatty acids. By clarifying these effects on the phase behaviour of this complex system, our data may facilitate predictions on the *in vivo* stability and performance of these systems from a biological and medical viewpoint.

With the aim of presenting a suitable set up for rapidly forming the cubic phase of MO and MPL in potential medical applications, the feasibility of a single-use double-barrelled syringe equipped with a mixer unit has also been demonstrated. This straight-forward approach overcomes the need for storage of the easily dehydrated lipid cubic phase system while effectively and efficiently assembling a Q_{II}^{D} cubic phase with the versatility of encapsulating hydrophobic or hydrophilic drugs or proteins.

6.2 Final words and future directions

The lipid cubic phase has yet to reach the market in a drug delivery application. However, the results and data presented in this work enriches the existing knowledge of drug reconstitution in lipid cubic mesophases, confirming the potential of bicontinuous cubic phase as a versatile and useful biological membrane mimic for safe and effective controlled drug delivery. Furthermore, our novel approach to exploit and control the biodegradation of the mucoadhesive matrix in lipolytic environments presents a general strategy for the design of tailorable release systems for troublesome lipophilic molecules. Nevertheless, further investigations should seek to study the success of this approach for extending the stability of rapidly digested cubosomes. This may include a combination of pH-stat or HPLC experiments to extract and quantify liberated fatty acids, with high resolution techniques like SAXS and cryo-TEM to track changes in size and internal structure of the systems. Elucidating this response, and coupled with the data already presented in this thesis, may guide us towards the design of a broadly applicable, tunable carrier systems for countless drug payloads, while overcoming the issues of instability and administration associated with the lipid mesophase. Providing these predictions serves to rationalise formulation development to improve bioavailability and reduce attrition rates of otherwise shelved NCEs. Further, as the majority of stabilizers are believed to predominantly coat the outer surface of cubosomes, they present a means for targeting cells of interest. For example, biotin- [567] and

folate- [605] modified F108 stabilizer has been shown to increase the uptake of cubosomes in HeLa cancer cell lines that overexpress biotin and folate receptors to improve the chemotherapeutic activity of anticancer agents. In this context, the influence of different stabilizers on MAG cubosomal systems should be explored.

References

1. Kulkarni, C.V., et al., *Monoolein: a magic lipid?* Physical Chemistry Chemical Physics, 2011. **13**(8): p. 3004-3021.
2. Wade, A. and P. Weller, *Lactose*. 2 ed. Handbook of Pharmaceutical Excipients, 2nd edn. Pharmaceutical Press, London. 1994. 252-261.
3. Kola, I. and J. Landis, *Can the pharmaceutical industry reduce attrition rates?* Nature reviews Drug discovery, 2004. **3**(8): p. 711-716.
4. Amidon, G.L., et al., *A theoretical basis for a biopharmaceutic drug classification: the correlation of in vitro drug product dissolution and in vivo bioavailability.* Pharmaceutical research, 1995. **12**(3): p. 413-420.
5. Laxminarayan, R., et al., *Drug resistance*, in *Disease Control Priorities in Developing Countries. 2nd edition*. 2006, The International Bank for Reconstruction and Development/The World Bank.
6. Naik, A., Y.N. Kalia, and R.H. Guy, *Transdermal drug delivery: overcoming the skin's barrier function.* Pharmaceutical science & technology today, 2000. **3**(9): p. 318-326.
7. Yang, R., et al., *Getting drugs across biological barriers.* Advanced Materials, 2017. **29**(37): p. 1606596.
8. Patel, M.M., et al., *Getting into the brain.* CNS drugs, 2009. **23**(1): p. 35-58.
9. Prausnitz, M.R., S. Mitragotri, and R. Langer, *Current status and future potential of transdermal drug delivery.* Nature reviews Drug discovery, 2004. **3**(2): p. 115-124.
10. Hadgraft, J. and R.H. Guy, *Transdermal drug delivery: Developmental issues and research initiatives.* Drugs and the pharmaceutical sciences, 1989. **35**.
11. Bronaugh, R.L. and H.I. Maibach, *Percutaneous absorption: drugs--cosmetics--mechanisms--methodology: drugs--cosmetics--mechanisms--methodology*. 1999: CRC Press.
12. Viswanathan, P., Y. Muralidaran, and G. Ragavan, *Challenges in oral drug delivery: a nano-based strategy to overcome*, in *Nanostructures for oral medicine*. 2017, Elsevier. p. 173-201.
13. Radomsky, M.L., et al., *Controlled vaginal delivery of antibodies in the mouse.* Biology of reproduction, 1992. **47**(1): p. 133-140.
14. Greenblatt, D.J., *Intramuscular injection of drugs.* New England Journal of Medicine, 1976. **295**(10): p. 542-546.
15. ZELMAN, S., *Notes on techniques of intramuscular injection. The avoidance of needless pain and morbidity.* The American journal of the medical sciences, 1961. **241**: p. 563-574.
16. Xiao, L., et al., *Subcutaneous injection of botulinum toxin a is beneficial in postherpetic neuralgia.* Pain Medicine, 2010. **11**(12): p. 1827-1833.
17. Mathaes, R., et al., *Subcutaneous injection volume of biopharmaceuticals—pushing the boundaries.* Journal of pharmaceutical sciences, 2016. **105**(8): p. 2255-2259.
18. Türker, S., E. Onur, and Y. Ózer, *Nasal route and drug delivery systems.* Pharmacy world and Science, 2004. **26**(3): p. 137-142.
19. Marttin, E., et al., *Nasal mucociliary clearance as a factor in nasal drug delivery.* Advanced drug delivery reviews, 1998. **29**(1-2): p. 13-38.
20. Sarkar, M.A., *Drug metabolism in the nasal mucosa.* Pharmaceutical research, 1992. **9**(1): p. 1-9.
21. Arora, P., S. Sharma, and S. Garg, *Permeability issues in nasal drug delivery.* Drug discovery today, 2002. **7**(18): p. 967-975.
22. Patton, J.S., *Mechanisms of macromolecule absorption by the lungs.* Advanced drug delivery reviews, 1996. **19**(1): p. 3-36.
23. Sung, J.C., B.L. Pulliam, and D.A. Edwards, *Nanoparticles for drug delivery to the lungs.* Trends in biotechnology, 2007. **25**(12): p. 563-570.

24. Yang, W., J.I. Peters, and R.O. Williams III, *Inhaled nanoparticles—a current review.* International journal of pharmaceutics, 2008. **356**(1-2): p. 239-247.
25. Athamneh, T., et al., *Alginate and hybrid alginate-hyaluronic acid aerogel microspheres as potential carrier for pulmonary drug delivery.* The journal of supercritical fluids, 2019. **150**: p. 49-55.
26. Emami, F., S.J.M. Yazdi, and D.H. Na, *Poly (lactic acid)/poly (lactic-co-glycolic acid) particulate carriers for pulmonary drug delivery.* Journal of Pharmaceutical Investigation, 2019: p. 1-16.
27. Courrier, H., N. Butz, and T.F. Vandamme, *Pulmonary drug delivery systems: recent developments and prospects.* Critical Reviews™ in Therapeutic Drug Carrier Systems, 2002. **19**(4-5).
28. Chen, Q.Z., I.D. Thompson, and A.R. Boccaccini, *45S5 Bioglass®-derived glass–ceramic scaffolds for bone tissue engineering.* Biomaterials, 2006. **27**(11): p. 2414-2425.
29. Maquet, V. and R. Jerome. *Design of macroporous biodegradable polymer scaffolds for cell transplantation*. in *Materials Science Forum*. 1997. Trans Tech Publ.
30. Hutmacher, D.W., *Scaffolds in tissue engineering bone and cartilage.* Biomaterials, 2000. **21**(24): p. 2529-2543.
31. Hirabayashi, H. and J. Fujisaki, *Bone-specific drug delivery systems.* Clinical pharmacokinetics, 2003. **42**(15): p. 1319-1330.
32. Torchilin, V.P., *Drug targeting.* European Journal of Pharmaceutical Sciences, 2000. **11**: p. S81-S91.
33. Langer, R., *Where a pill won't reach.* Scientific American, 2003. **288**(4): p. 50-57.
34. Kostarelos, K., *Rational design and engineering of delivery systems for therapeutics: biomedical exercises in colloid and surface science.* Advances in colloid and interface science, 2003. **106**(1-3): p. 147-168.
35. Langer, R., *Drugs on target.* Science, 2001. **293**(5527): p. 58-59.
36. LaVan, D.A., D.M. Lynn, and R. Langer, *Moving smaller in drug discovery and delivery.* Nature Reviews Drug Discovery, 2002. **1**(1): p. 77-84.
37. Langer, R., *Drug delivery and targeting.* NATURE-LONDON-, 1998: p. 5-10.
38. Langer, R., *New methods of drug delivery.* Science, 1990. **249**(4976): p. 1527-1533.
39. Yang, W.-W. and E. Pierstorff, *Reservoir-based polymer drug delivery systems.* Journal of laboratory automation, 2012. **17**(1): p. 50-58.
40. Van Duong, T. and G. Van den Mooter, *The role of the carrier in the formulation of pharmaceutical solid dispersions. Part I: crystalline and semi-crystalline carriers.* Expert opinion on drug delivery, 2016. **13**(11): p. 1583-1594.
41. Van Duong, T. and G. Van den Mooter, *The role of the carrier in the formulation of pharmaceutical solid dispersions. Part II: amorphous carriers.* Expert opinion on drug delivery, 2016. **13**(12): p. 1681-1694.
42. Chasin, M., *Biodegradable polymers as drug delivery systems*. Vol. 45. 1990: Informa Health Care.
43. Adeoye, O. and H. Cabral-Marques, *Cyclodextrin nanosystems in oral drug delivery: a mini review.* International journal of pharmaceutics, 2017. **531**(2): p. 521-531.
44. Devi, K. and U. Bhosale, *Formulation and optimization of polymeric nano drug delivery system of acyclovir using 3^2 full factorial design.* Int. J. PharmTech Res, 2009. **1**(3): p. 644-653.
45. Singh, S., *Nanomedicine–nanoscale drugs and delivery systems.* Journal of nanoscience and nanotechnology, 2010. **10**(12): p. 7906-7918.
46. Crommelin, D.J. and A.T. Florence, *Towards more effective advanced drug delivery systems.* International journal of pharmaceutics, 2013. **454**(1): p. 496-511.
47. Yan Lee, P. and K. KY Wong, *Nanomedicine: a new frontier in cancer therapeutics.* Current drug delivery, 2011. **8**(3): p. 245-253.
48. Heidel, J.D. and M.E. Davis, *Clinical developments in nanotechnology for cancer therapy.* Pharmaceutical research, 2011. **28**(2): p. 187-199.

49. Ansari, S., F. Islam, and M. Sameem, *Influence of nanotechnology on herbal drugs: A Review.* Journal of advanced pharmaceutical technology & research, 2012. **3**(3): p. 142.
50. Mukerjee, A. and J.K. Vishwanatha, *Formulation, characterization and evaluation of curcumin-loaded PLGA nanospheres for cancer therapy.* Anticancer research, 2009. **29**(10): p. 3867-3875.
51. Taylor, M., et al., *Six bioabsorbable polymers: in vitro acute toxicity of accumulated degradation products.* Journal of applied biomaterials, 1994. **5**(2): p. 151-157.
52. Hasırcı, V., et al., *Versatility of biodegradable biopolymers: degradability and an in vivo application.* Journal of biotechnology, 2001. **86**(2): p. 135-150.
53. Mura, S., J. Nicolas, and P. Couvreur, *Stimuli-responsive nanocarriers for drug delivery.* Nature materials, 2013. **12**(11): p. 991-1003.
54. Gulzar, A., et al., *Stimuli responsive drug delivery application of polymer and silica in biomedicine.* Journal of Materials Chemistry B, 2015. **3**(44): p. 8599-8622.
55. Chilkoti, A., M.R. Dreher, and D.E. Meyer, *Design of thermally responsive, recombinant polypeptide carriers for targeted drug delivery.* Advanced drug delivery reviews, 2002. **54**(8): p. 1093-1111.
56. Rahanyan‐Kägi, N., et al., *Stimuli‐Responsive Lipidic Cubic Phase: Triggered Release and Sequestration of Guest Molecules.* Chemistry–A European Journal, 2015. **21**(5): p. 1873-1877.
57. Fong, W.-K., et al., *Alkylation of spiropyran moiety provides reversible photo-control over nanostructured soft materials.* Biointerphases, 2012. **7**(1-4): p. 3.
58. Negrini, R. and R. Mezzenga, *pH-responsive lyotropic liquid crystals for controlled drug delivery.* Langmuir, 2011. **27**(9): p. 5296-5303.
59. Gupta, P., K. Vermani, and S. Garg, *Hydrogels: from controlled release to pH-responsive drug delivery.* Drug discovery today, 2002. **7**(10): p. 569-579.
60. Bolla, P.K., et al., *A review on pH and temperature responsive gels and other less explored drug delivery systems.* Journal of Drug Delivery Science and Technology, 2018. **46**: p. 416-435.
61. Alvarez‐Lorenzo, C., L. Bromberg, and A. Concheiro, *Light‐sensitive intelligent drug delivery systems.* Photochemistry and photobiology, 2009. **85**(4): p. 848-860.
62. Linsley, C.S. and B.M. Wu, *Recent advances in light-responsive on-demand drug-delivery systems.* Therapeutic delivery, 2017. **8**(2): p. 89-107.
63. Madan, M., et al., *In situ forming polymeric drug delivery systems.* Indian journal of pharmaceutical sciences, 2009. **71**(3): p. 242.
64. Li, J. and D.J. Mooney, *Designing hydrogels for controlled drug delivery.* Nature Reviews Materials, 2016. **1**(12): p. 1-17.
65. Ganji, F. and F.E. VASHEGHANI, *Hydrogels in controlled drug delivery systems.* 2009.
66. Hoare, T.R. and D.S. Kohane, *Hydrogels in drug delivery: Progress and challenges.* Polymer, 2008. **49**(8): p. 1993-2007.
67. Ishii, S., J. Kaneko, and Y. Nagasaki, *Development of a long-acting, protein-loaded, redox-active, injectable gel formed by a polyion complex for local protein therapeutics.* Biomaterials, 2016. **84**: p. 210-218.
68. Miyazaki, S., et al., *In situ gelling xyloglucan formulations for sustained release ocular delivery of pilocarpine hydrochloride.* International journal of pharmaceutics, 2001. **229**(1-2): p. 29-36.
69. Smart, J., I. Kellaway, and H. Worthington, *An in‐vitro investigation of mucosa‐adhesive materials for use in controlled drug delivery.* Journal of Pharmacy and Pharmacology, 1984. **36**(5): p. 295-299.
70. Ruel-Gariepy, E. and J.-C. Leroux, *In situ-forming hydrogels—review of temperature-sensitive systems.* European Journal of Pharmaceutics and Biopharmaceutics, 2004. **58**(2): p. 409-426.

71. Thilek Kumar, M., et al., *Ph-Induced in situ gelling systems of indomethacin for sustained ocular delivery.* Indian journal of pharmaceutical sciences, 2005. **67**(3): p. 327-333.
72. Gao, W., et al., *Nanoparticle-hydrogel: a hybrid biomaterial system for localized drug delivery.* Annals of biomedical engineering, 2016. **44**(6): p. 2049-2061.
73. Eckmann, D., et al., *Nanogel carrier design for targeted drug delivery.* Journal of Materials Chemistry B, 2014. **2**(46): p. 8085-8097.
74. Basso, J., et al., *Hydrogel-based drug delivery nanosystems for the treatment of brain tumors.* Gels, 2018. **4**(3): p. 62.
75. Shah, S., P.K. Sasmal, and K.-B. Lee, *Photo-triggerable hydrogel–nanoparticle hybrid scaffolds for remotely controlled drug delivery.* Journal of Materials Chemistry B, 2014. **2**(44): p. 7685-7693.
76. Shin, S. and L.D. Shea, *Lentivirus immobilization to nanoparticles for enhanced and localized delivery from hydrogels.* Molecular Therapy, 2010. **18**(4): p. 700-706.
77. Oh, J.K., et al., *The development of microgels/nanogels for drug delivery applications.* Progress in Polymer Science, 2008. **33**(4): p. 448-477.
78. Chacko, R.T., et al., *Polymer nanogels: a versatile nanoscopic drug delivery platform.* Advanced drug delivery reviews, 2012. **64**(9): p. 836-851.
79. Gothwal, A., I. Khan, and U. Gupta, *Polymeric micelles: recent advancements in the delivery of anticancer drugs.* Pharmaceutical research, 2016. **33**(1): p. 18-39.
80. Lu, Y. and K. Park, *Polymeric micelles and alternative nanonized delivery vehicles for poorly soluble drugs.* International journal of pharmaceutics, 2013. **453**(1): p. 198-214.
81. Behl, C., et al., *Optimization of systemic nasal drug delivery with pharmaceutical excipients.* Advanced drug delivery reviews, 1998. **29**(1-2): p. 117-133.
82. Patil, S.B. and K.K. Sawant, *Development, optimization and in vitro evaluation of alginate mucoadhesive microspheres of carvedilol for nasal delivery.* Journal of microencapsulation, 2009. **26**(5): p. 432-443.
83. Illum, L., et al., *Bioadhesive microspheres as a potential nasal drug delivery system.* International journal of pharmaceutics, 1987. **39**(3): p. 189-199.
84. Björk, E. and P. Edman, *Characterization of degradable starch microspheres as a nasal delivery system for drugs.* International journal of pharmaceutics, 1990. **62**(2-3): p. 187-192.
85. Salem, H.F., et al., *Nanosized nasal emulgel of resveratrol: preparation, optimization, in vitro evaluation and in vivo pharmacokinetic study.* Drug development and industrial pharmacy, 2019. **45**(10): p. 1624-1634.
86. Mahajan, H.S., S.K. Shah, and S.J. Surana, *Nasal in situ gel containing hydroxy propyl β-cyclodextrin inclusion complex of artemether: development and in vitro evaluation.* Journal of Inclusion Phenomena and Macrocyclic Chemistry, 2011. **70**(1-2): p. 49-58.
87. Aspden, T.J., et al., *Chitosan as a nasal delivery system: the effect of chitosan solutions on in vitro and in vivo mucociliary transport rates in human turbinates and volunteers.* Journal of pharmaceutical sciences, 1997. **86**(4): p. 509-513.
88. Carvalho, F.C., et al., *Mucoadhesive drug delivery systems.* Brazilian Journal of Pharmaceutical Sciences, 2010. **46**(1): p. 1-17.
89. Khutoryanskiy, V.V., *Advances in mucoadhesion and mucoadhesive polymers.* Macromolecular bioscience, 2011. **11**(6): p. 748-764.
90. Li, H., R.J. Hardy, and X. Gu, *Effect of drug solubility on polymer hydration and drug dissolution from polyethylene oxide (PEO) matrix tablets.* AAPS PharmSciTech, 2008. **9**(2): p. 437-443.
91. Elgadir, M., et al., *Impact of chitosan composites and chitosan nanoparticle composites on various drug delivery systems: A review.* Journal of food and drug analysis, 2015. **23**(4): p. 619.
92. Mufamadi, M.S., et al., *A review on composite liposomal technologies for specialized drug delivery.* Journal of drug delivery, 2011. **2011**.

93. Hadjiargyrou, M. and J.B. Chiu, *Enhanced composite electrospun nanofiber scaffolds for use in drug delivery.* Expert opinion on drug delivery, 2008. **5**(10): p. 1093-1106.
94. Lasserre, A. and P.K. Bajpai, *Ceramic drug-delivery devices.* Critical Reviews™ in Therapeutic Drug Carrier Systems, 1998. **15**(1).
95. Bajpai, P.K. and G.A. Graves, *Porous ceramic carriers for controlled release of proteins, polypeptide hormones, and other substances within human and/or other mamillian species and method*. 1980, Google Patents.
96. Yi, Z., et al., *Hierarchical porous hydroxyapatite fibers with a hollow structure as drug delivery carriers.* Ceramics International, 2016. **42**(16): p. 19079-19085.
97. Parent, M., et al., *Design of calcium phosphate ceramics for drug delivery applications in bone diseases: A review of the parameters affecting the loading and release of the therapeutic substance.* Journal of Controlled Release, 2017. **252**: p. 1-17.
98. Morris, L.M. and P.K. Bajpai, *Development of a resorbable tricalcium phosphate (TCP) amine antibiotic composite.* MRS Online Proceedings Library Archive, 1987. **110**.
99. Mouriño, V. and A.R. Boccaccini, *Bone tissue engineering therapeutics: controlled drug delivery in three-dimensional scaffolds.* Journal of the Royal Society Interface, 2010. **7**(43): p. 209-227.
100. Meenach, S.A., J.Z. Hilt, and K.W. Anderson, *Poly (ethylene glycol)-based magnetic hydrogel nanocomposites for hyperthermia cancer therapy.* Acta Biomaterialia, 2010. **6**(3): p. 1039-1046.
101. Gobbo, O.L., et al., *Magnetic nanoparticles in cancer theranostics.* Theranostics, 2015. **5**(11): p. 1249.
102. Wu, M. and S. Huang, *Magnetic nanoparticles in cancer diagnosis, drug delivery and treatment.* Molecular and clinical oncology, 2017. **7**(5): p. 738-746.
103. Williams, H.M., *The application of magnetic nanoparticles in the treatment and monitoring of cancer and infectious diseases.* Bioscience Horizons: The International Journal of Student Research, 2017. **10**.
104. Shin, J., et al., *Hollow manganese oxide nanoparticles as multifunctional agents for magnetic resonance imaging and drug delivery.* Angewandte Chemie International Edition, 2009. **48**(2): p. 321-324.
105. Strickley, R.G., *Currently marketed oral lipid-based dosage forms: drug products and excipients.* Drugs and the Pharmaceutical sciences, 2007. **170**: p. 1.
106. Vithani, K., et al., *Colloidal aspects of dispersion and digestion of self-dispersing lipid-based formulations for poorly water-soluble drugs.* Advanced drug delivery reviews, 2019. **142**: p. 16-34.
107. Gigliobianco, M., et al., *Nanocrystals of poorly soluble drugs: Drug bioavailability and physicochemical stability.* Pharmaceutics, 2018. **10**(3): p. 134.
108. Ghadi, R. and N. Dand, *BCS class IV drugs: Highly notorious candidates for formulation development.* Journal of Controlled Release, 2017. **248**: p. 71-95.
109. Porter, C.J., N.L. Trevaskis, and W.N. Charman, *Lipids and lipid-based formulations: optimizing the oral delivery of lipophilic drugs.* Nature reviews Drug discovery, 2007. **6**(3): p. 231-248.
110. O'Driscoll, C.M., *Lipid-based formulations for intestinal lymphatic delivery.* European Journal of Pharmaceutical Sciences, 2002. **15**(5): p. 405-415.
111. Rane, S.S. and B.D. Anderson, *What determines drug solubility in lipid vehicles: is it predictable?* Advanced drug delivery reviews, 2008. **60**(6): p. 638-656.
112. Chakraborty, S., et al., *Lipid–an emerging platform for oral delivery of drugs with poor bioavailability.* European Journal of Pharmaceutics and Biopharmaceutics, 2009. **73**(1): p. 1-15.
113. Kalepu, S., M. Manthina, and V. Padavala, *Oral lipid-based drug delivery systems–an overview.* Acta Pharmaceutica Sinica B, 2013. **3**(6): p. 361-372.

114. Pouton, C.W., *Lipid formulations for oral administration of drugs: non-emulsifying, self-emulsifying and 'self-microemulsifying'drug delivery systems.* European journal of pharmaceutical sciences, 2000. **11**: p. S93-S98.
115. Pouton, C.W., *Formulation of poorly water-soluble drugs for oral administration: physicochemical and physiological issues and the lipid formulation classification system.* European journal of pharmaceutical sciences, 2006. **29**(3-4): p. 278-287.
116. Anton, N. and T.F. Vandamme, *Nano-emulsions and micro-emulsions: clarifications of the critical differences.* Pharmaceutical research, 2011. **28**(5): p. 978-985.
117. Nigade, P.M., S.L. Patil, and S.S. Tiwari, *Self emulsifying drug delivery system (SEDDS): A review.* International Journal of Pharmacy and Biological Sciences, 2012. **2**(2): p. 42-52.
118. Beloqui, A., et al., *Mechanism of transport of saquinavir-loaded nanostructured lipid carriers across the intestinal barrier.* Journal of Controlled Release, 2013. **166**(2): p. 115-123.
119. Nazaruk, E., E. Górecka, and R. Bilewicz, *Enzymes and mediators hosted together in lipidic mesophases for the construction of biodevices.* Journal of colloid and interface science, 2012. **385**(1): p. 130-136.
120. Peltier, S., et al., *Enhanced oral paclitaxel bioavailability after administration of paclitaxel-loaded lipid nanocapsules.* Pharmaceutical Research, 2006. **23**(6): p. 1243-1250.
121. Jain, S., et al., *Ethosomes: a novel vesicular carrier for enhanced transdermal delivery of an antiHIV agent.* Indian journal of pharmaceutical sciences, 2004. **66**(1): p. 72.
122. Lasic, D.D. and D. Papahadjopoulos, *Medical applications of liposomes*. 1998: Elsevier.
123. Shah, J.C., Y. Sadhale, and D.M. Chilukuri, *Cubic phase gels as drug delivery systems.* Advanced Drug Delivery Reviews, 2001. **47**(2-3): p. 229-250.
124. Tardieu, A. and V. Luzzati, *A novel cubic phase—a cage-like network of rods with enclosed spherical micelles.* Biochimica et Biophysica Acta (BBA)-Biomembranes, 1970. **219**(1): p. 11-17.
125. Larsson, K., K. Fontell, and N. Krog, *Structural relationships between lamellar, cubic and hexagonal phases in monoglyceride-water systems. Possibility of cubic structures in biological systems.* Chemistry and Physics of Lipids, 1980. **27**(4): p. 321-328.
126. Ericsson, B., et al., *Cubic phases as delivery systems for peptide drugs*. 1991, ACS Publications.
127. Rizwan, S., et al., *Characterisation of bicontinuous cubic liquid crystalline systems of phytantriol and water using cryo field emission scanning electron microscopy (cryo FESEM).* Micron, 2007. **38**(5): p. 478-485.
128. Kumar, R. and A. Philip, *Modified transdermal technologies: Breaking the barriers of drug permeation via the skin.* Tropical Journal of Pharmaceutical Research, 2007. **6**(1): p. 633-644.
129. Chien, Y.W., *Logics of transdermal controlled drug administration.* Drug Development and Industrial Pharmacy, 1983. **9**(4): p. 497-520.
130. Cevc, G., *Drug delivery across the skin.* Expert opinion on investigational drugs, 1997. **6**(12): p. 1887-1937.
131. Woo, J.S., et al., *Enhanced oral bioavailability of paclitaxel by coadministration of the P-glycoprotein inhibitor KR30031.* Pharmaceutical research, 2003. **20**(1): p. 24-30.
132. Butani, D., C. Yewale, and A. Misra, *Amphotericin B topical microemulsion: formulation, characterization and evaluation.* Colloids and Surfaces B: Biointerfaces, 2014. **116**: p. 351-358.
133. Yan, Y.-D., et al., *Effect of dose and dosage interval on the oral bioavailability of docetaxel in combination with a curcumin self-emulsifying drug delivery system (SEDDS).* European journal of drug metabolism and pharmacokinetics, 2012. **37**(3): p. 217-224.
134. Garg, B., et al., *Systematic development of solid self-nanoemulsifying oily formulations (S-SNEOFs) for enhancing the oral bioavailability and intestinal lymphatic uptake of lopinavir.* Colloids and Surfaces B: Biointerfaces, 2016. **141**: p. 611-622.

135. Jaafar-Maalej, C., et al., *Ethanol injection method for hydrophilic and lipophilic drug-loaded liposome preparation.* Journal of liposome research, 2010. **20**(3): p. 228-243.
136. Nii, T. and F. Ishii, *Encapsulation efficiency of water-soluble and insoluble drugs in liposomes prepared by the microencapsulation vesicle method.* International journal of pharmaceutics, 2005. **298**(1): p. 198-205.
137. Rathore, A., et al., *Mannosylated liposomes bearing Amphotericin B for effective management of visceral Leishmaniasis.* Journal of liposome research, 2011. **21**(4): p. 333-340.
138. Vural, I., C. Sarisozen, and S.S. Olmez, *Chitosan coated furosemide liposomes for improved bioavailability.* Journal of biomedical nanotechnology, 2011. **7**(3): p. 426-430.
139. Das, B., et al., *Transferosomal gel for transdermal delivery of risperidone: Formulation optimization and ex vivo permeation.* Journal of Drug Delivery Science and Technology, 2017. **38**: p. 59-71.
140. Mehnert, W. and K. Mäder, *Solid lipid nanoparticles: production, characterization and applications.* Advanced drug delivery reviews, 2012. **64**: p. 83-101.
141. Negi, J.S., et al., *Development and evaluation of glyceryl behenate based solid lipid nanoparticles (SLNs) using hot self-nanoemulsification (SNE) technique.* Archives of pharmacal research, 2014. **37**(3): p. 361-370.
142. Ravi, P.R., et al., *A hybrid design to optimize preparation of lopinavir loaded solid lipid nanoparticles and comparative pharmacokinetic evaluation with marketed lopinavir/ritonavir coformulation.* Journal of Pharmacy and Pharmacology, 2014. **66**(7): p. 912-926.
143. Arai, T., et al., *Novel local drug delivery system using thermoreversible gel in combination with polymeric microspheres or liposomes.* Anticancer research, 2010. **30**(4): p. 1057-1064.
144. Bastiancich, C., Vanvarenberg, K., Ucakar, B., Pitorre, M., Bastiat, G., Lagarce, F., Préat, V. and Danhier, F.,, *Lauroyl-gemcitabine-loaded lipid nanocapsule hydrogel for the treatment of glioblastoma.* Journal of Controlled Release, 2016. **225**: p. 283-293.
145. Caffrey, M., *A comprehensive review of the lipid cubic phase or in meso method for crystallizing membrane and soluble proteins and complexes.* Acta Crystallographica Section F: Structural Biology Communications, 2015. **71**(1): p. 3-18.
146. Larsson, K., *Cubic lipid-water phases: structures and biomembrane aspects.* The Journal of Physical Chemistry, 1989. **93**(21): p. 7304-7314.
147. Gruner, S.M., et al., *Lipid polymorphism: the molecular basis of nonbilayer phases.* Annual review of biophysics and biophysical chemistry, 1985. **14**(1): p. 211-238.
148. Luzzati, V., T. Gulik-Krzywicki, and A. Tardieu, *Polymorphism of lecithins.* Nature, 1968. **218**(5146): p. 1031-1034.
149. Cherezov, V., H. Fersi, and M. Caffrey, *Crystallization screens: compatibility with the lipidic cubic phase for in meso crystallization of membrane proteins.* Biophysical journal, 2001. **81**(1): p. 225-242.
150. Chung, H. and M. Caffrey, *The curvature elastic-energy function of the lipid-water cubic mesophase.* Nature, 1994. **368**(6468): p. 224.
151. Anderson, D.M., S.M. Gruner, and S. Leibler, *Geometrical aspects of the frustration in the cubic phases of lyotropic liquid crystals.* Proceedings of the National Academy of Sciences, 1988. **85**(15): p. 5364-5368.
152. Duesing, P., R. Templer, and J. Seddon, *Quantifying packing frustration energy in inverse lyotropic mesophases.* Langmuir, 1997. **13**(2): p. 351-359.
153. Shearman, G.C., et al., *Calculations of and evidence for chain packing stress in inverse lyotropic bicontinuous cubic phases.* Langmuir, 2007. **23**(13): p. 7276-7285.
154. Salim, M., et al., *Amphiphilic designer nano-carriers for controlled release: from drug delivery to diagnostics.* MedChemComm, 2014. **5**(11): p. 1602-1618.

155. Israelachvili, J.N., *Intermolecular and surface forces*. 2015: Academic press.
156. Mouritsen, O.G., *Lipidology and lipidomics—quo vadis? A new era for the physical chemistry of lipids.* Physical Chemistry Chemical Physics, 2011. **13**(43): p. 19195-19205.
157. Seddon, J.M. and R.H. Templer, *Cubic phases of self-assembled amphiphilic aggregates.* Philosophical Transactions of the Royal Society of London. Series A: Physical and Engineering Sciences, 1993. **344**(1672): p. 377-401.
158. Zabara, A., et al., *The nanoscience behind the art of in-meso crystallization of membrane proteins.* Nanoscale, 2017. **9**(2): p. 754-763.
159. Delacroix, H., *Crystallographic analysis of freeze-fracture electron micrographs: application to the structure determination of cubic lipid-water phases.* Journal of microscopy, 1998. **192**: p. 280-292.
160. Razumas, V., et al., *Effects of distearoylphosphatidylglycerol and lysozyme on the structure of the monoolein-water cubic phase: X-ray diffraction and Raman scattering studies.* Chemistry and physics of lipids, 1996. **84**(2): p. 123-138.
161. Eriksson, P.-O. and G. Lindblom, *Lipid and water diffusion in bicontinuous cubic phases measured by NMR.* Biophysical journal, 1993. **64**(1): p. 129-136.
162. Lindblom, G. and L. Rilfors, *Cubic phases and isotropic structures formed by membrane lipids—possible biological relevance.* Biochimica et Biophysica Acta (BBA)-Reviews on Biomembranes, 1989. **988**(2): p. 221-256.
163. Cribier, S., et al., *Cubic Phase of Lipid-containing Systems: A Translational Diffusion Study by Fluorescence Recovery After Photobleaching.* Journal of molecular biology, 1993. **229**(2): p. 517-525.
164. Small, D.M., *Physical chemistry of lipids*. 1986: Plenum Press.
165. Landau, E.M. and J.P. Rosenbusch, *Lipidic cubic phases: a novel concept for the crystallization of membrane proteins.* Proceedings of the National Academy of Sciences, 1996. **93**(25): p. 14532-14535.
166. Demurtas, D., et al., *Direct visualization of dispersed lipid bicontinuous cubic phases by cryo-electron tomography.* Nature communications, 2015. **6**(1): p. 1-8.
167. Barauskas, J. and T. Landh, *Phase behavior of the phytantriol/water system.* Langmuir, 2003. **19**(23): p. 9562-9565.
168. Clogston, J., *Applications of the lepidic cubic phase: from controlled release and uptake to in meso crystallization of membrane proteins*. 2005, The Ohio State University.
169. Wyatt, D. and D. Dorschel, *A cubic-phase delivery system composed of glyceryl monooleate and water for sustained release of water-soluble drugs.* Pharmaceutical technology, 1992. **16**(10): p. 116-116.
170. Clogston, J. and M. Caffrey, *Controlling release from the lipidic cubic phase. Amino acids, peptides, proteins and nucleic acids.* Journal of controlled release, 2005. **107**(1): p. 97-111.
171. Angelov, B., et al., *Identification of large channels in cationic PEGylated cubosome nanoparticles by synchrotron radiation SAXS and Cryo-TEM imaging.* Soft Matter, 2015. **11**(18): p. 3686-3692.
172. Chung, H. and M. Caffrey, *Polymorphism, mesomorphism, and metastability of monoelaidin in excess water.* Biophysical journal, 1995. **69**(5): p. 1951-1963.
173. Briggs, J., *The phase behavior of hydrated monoacylglycerols and the design of an X-ray compatible scanning calorimeter*. 1994, The Ohio State University.
174. Norling, T., et al., *Formulation of a drug delivery system based on a mixture of monoglycerides and triglycerides for use in the treatment of periodontal disease.* Journal of clinical periodontology, 1992. **19**(9): p. 687-692.
175. Hato, M., et al., *Phase behavior of phytanyl-chained akylglycoside/water systems.* Trends in Colloid and Interface Science XVI, 2004: p. 56-60.

176. Hasenhuettl, G.L., *Food emulsifiers and their applications*, G.L. Hasenhuettl and R.W. Hartel, Editors. 2008, Springer Science and Business Media.
177. Qiu, H. and M. Caffrey, *The phase diagram of the monoolein/water system: metastability and equilibrium aspects.* Biomaterials, 2000. **21**(3): p. 223-234.
178. Takahashi, H., I. Hatta, and P.J. Quinn, *Cubic phases in hydrated 1: 1 and 1: 2 dipalmitoylphosphatidylcholine-dipalmitoylglycerol mixtures.* Biophysical journal, 1996. **70**(3): p. 1407-1411.
179. Aleandri, S., et al., *Design of light-triggered lyotropic liquid crystal mesophases and their application as molecular switches in "on demand" release.* Langmuir, 2015. **31**(25): p. 6981-6987.
180. Ganem-Quintanar, A., D. Quintanar-Guerrero, and P. Buri, *Monoolein: A review of the pharmaceutical applications.* Drug Development and Industrial Pharmacy, 2000. **26**(8): p. 809-820.
181. Fong, W.-K., et al., *Responsive self-assembled nanostructured lipid systems for drug delivery and diagnostics.* Journal of colloid and interface science, 2016. **484**: p. 320-339.
182. Caffrey, M. and V. Cherezov, *Crystallizing membrane proteins using lipidic mesophases.* Nature protocols, 2009. **4**(5): p. 706-731.
183. Burdock, G.A., *Fenaroli's handbook of flavor ingredients*. 2016: CRC press.
184. Seddon, J.M., *Structure of the inverted hexagonal (HII) phase, and non-lamellar phase transitions of lipids.* Biochimica et Biophysica Acta (BBA)-Reviews on Biomembranes, 1990. **1031**(1): p. 1-69.
185. Qiu, H. and M. Caffrey, *Lyotropic and thermotropic phase behavior of hydrated monoacylglycerols: structure characterization of monovaccenin.* The Journal of Physical Chemistry B, 1998. **102**(24): p. 4819-4829.
186. Wagner, E., *Panthenol und Phytantriol in der Kosmetik.* Parfümerie und Kosmetik, 1994. **75**(4).
187. Ribier, A. and B. Biatry, *Cosmetic or dermatological composition in the form of an aqueous and stable dispersion of cubic gel particles based on phytanetriol and containing a surface-active agent which has a fatty chain, as dispersing and stabilizing agent*. 1998, Google Patents.
188. Shi, X., et al., *Comparative studies on glycerol monooleate-and phytantriol-based cubosomes containing oridonin in vitro and in vivo.* Pharmaceutical development and technology, 2017. **22**(3): p. 322-329.
189. Wadsten-Hindrichsen, P., et al., *Aqueous self-assembly of phytantriol in ternary systems: effect of monoolein, distearoylphosphatidylglycerol and three water-miscible solvents.* Journal of colloid and interface science, 2007. **315**(2): p. 701-713.
190. Lagerwall, J.P. and G. Scalia, *A new era for liquid crystal research: Applications of liquid crystals in soft matter nano-, bio-and microtechnology.* Current Applied Physics, 2012. **12**(6): p. 1387-1412.
191. Antognini, L.M., et al., *Quantifying the transport properties of lipid mesophases by theoretical modelling of diffusion experiments.* The Journal of chemical physics, 2016. **145**(8): p. 084903.
192. Guillot, S., et al., *Direct and indirect thermal transitions from hexosomes to emulsified micro-emulsions in oil-loaded monoglyceride-based particles.* Colloids and Surfaces A: Physicochemical and Engineering Aspects, 2006. **291**(1-3): p. 78-84.
193. Siekmann, B., et al., *Preparation and structural investigations of colloidal dispersions prepared from cubic monoglyceride–water phases.* International journal of pharmaceutics, 2002. **244**(1-2): p. 33-43.
194. Attama, A.A. and C.C. Müller-Goymann, *Effect of beeswax modification on the lipid matrix and solid lipid nanoparticle crystallinity.* Colloids and Surfaces A: Physicochemical and Engineering Aspects, 2008. **315**(1-3): p. 189-195.
195. Forbes, R., A. Cooper, and H. Mitchell, *The composition of the adult human body as determined by chemical analysis.* J Biol Chem, 1953. **203**(1): p. 359-366.
196. Engström, S., et al., *A study of polar lipid drug systems undergoing a thermoreversible lamellar-to-cubic phase transition.* International journal of pharmaceutics, 1992. **86**(2-3): p. 137-145.

197. Caboi, F., et al., *Addition of hydrophilic and lipophilic compounds of biological relevance to the monoolein/water system. I. Phase behavior.* Chemistry and physics of lipids, 2001. **109**(1): p. 47-62.
198. Costa, P. and J.M.S. Lobo, *Modeling and comparison of dissolution profiles.* European journal of pharmaceutical sciences, 2001. **13**(2): p. 123-133.
199. Gouda, R., H. Baishya, and Z. Qing, *Application of mathematical models in drug release kinetics of carbidopa and levodopa ER tablets.* J. Dev. Drugs, 2017. **6**(02): p. 1-8.
200. Wagner, J.G., *Interpretation of percent dissolved-time plots derived from in vitro testing of conventional tablets and capsules.* Journal of pharmaceutical sciences, 1969. **58**(10): p. 1253-1257.
201. Hixson, A. and J. Crowell, *Dependence of reaction velocity upon surface and agitation.* Industrial & Engineering Chemistry, 1931. **23**(8): p. 923-931.
202. Siepmann, J. and N.A. Peppas, *Higuchi equation: derivation, applications, use and misuse.* International journal of pharmaceutics, 2011. **418**(1): p. 6-12.
203. Korsmeyer, R.W., et al., *Mechanisms of solute release from porous hydrophilic polymers.* International journal of pharmaceutics, 1983. **15**(1): p. 25-35.
204. Ritger, P.L. and N.A. Peppas, *A simple equation for description of solute release II. Fickian and anomalous release from swellable devices.* Journal of controlled release, 1987. **5**(1): p. 37-42.
205. Peppas, N.A. and J.J. Sahlin, *A simple equation for the description of solute release. III. Coupling of diffusion and relaxation.* International journal of pharmaceutics, 1989. **57**(2): p. 169-172.
206. Mikac, U., et al., *Dynamics of water and xanthan chains in hydrogels studied by NMR relaxometry and their influence on drug release.* International journal of pharmaceutics, 2019. **563**: p. 373-383.
207. Sheikh, F.A., et al., *Linseed hydrogel based floating drug delivery system for fluoroquinolone antibiotics: Design, in vitro drug release and in vivo real-time floating detection.* Saudi Pharmaceutical Journal, 2020. **28**(5): p. 538-549.
208. Caccavo, D., *An overview on the mathematical modeling of hydrogels' behavior for drug delivery systems.* International journal of pharmaceutics, 2019. **560**: p. 175-190.
209. Bender, J., et al., *Lipid cubic phases for improved topical drug delivery in photodynamic therapy.* Journal of Controlled Release, 2005. **106**(3): p. 350-360.
210. Nielsen, L.S., L. Schubert, and J. Hansen, *Bioadhesive drug delivery systems: I. Characterisation of mucoadhesive properties of systems based on glyceryl mono-oleate and glyceryl monolinoleate.* European journal of pharmaceutical sciences, 1998. **6**(3): p. 231-239.
211. Kossena, G.A., et al., *A novel cubic phase of medium chain lipid origin for the delivery of poorly water soluble drugs.* Journal of controlled release, 2004. **99**(2): p. 217-229.
212. Szlezak, M., et al., *Monoolein cubic phase gels and cubosomes doped with magnetic nanoparticles–hybrid materials for controlled drug release.* ACS applied materials & interfaces, 2017. **9**(3): p. 2796-2805.
213. Gan, L., et al., *Recent advances in topical ophthalmic drug delivery with lipid-based nanocarriers.* Drug discovery today, 2013. **18**(5-6): p. 290-297.
214. Boyd, B.J., et al., *A lipid-based liquid crystalline matrix that provides sustained release and enhanced oral bioavailability for a model poorly water soluble drug in rats.* International journal of pharmaceutics, 2007. **340**(1-2): p. 52-60.
215. Chang, C.-M. and R. Bodmeier, *Effect of dissolution media and additives on the drug release from cubic phase delivery systems.* Journal of Controlled Release, 1997 **46**(3): p. 215-222.
216. Burrows, R., J. Collett, and D. Attwood, *The release of drugs from monoglyceride-water liquid crystalline phases.* International journal of pharmaceutics, 1994. **111**(3): p. 283-293.
217. Chang, C.M. and R. Bodmeier, *Swelling of and drug release from monoglyceride‐based drug delivery systems.* Journal of pharmaceutical sciences, 1997 **86**(6): p. 747-752.

218. Sadhale, Y. and J.C. Shah, *Stabilization of insulin against agitation-induced aggregation by the GMO cubic phase gel.* International journal of pharmaceutics, 1999. **191**(1): p. 51-64.
219. Lee, K.W., et al., *Nanostructure of liquid crystalline matrix determines in vitro sustained release and in vivo oral absorption kinetics for hydrophilic model drugs.* International journal of pharmaceutics, 2009. **365**(1-2): p. 190-199.
220. Almsherqi, Z.A., S.D. Kohlwein, and Y. Deng, *Cubic membranes: a legend beyond the Flatland* of cell membrane organization.* The Journal of cell biology, 2006. **173**(6): p. 839-844.
221. Drummond, C.J. and C. Fong, *Surfactant self-assembly objects as novel drug delivery vehicles.* Current opinion in colloid & interface science, 1999. **4**(6): p. 449-456.
222. Sadhale, Y. and J.C. Shah, *Glyceryl monooleate cubic phase gel as chemical stability enhancer of cefazolin and cefuroxime.* Pharmaceutical development and technology, 1998. **3**(4): p. 549-556.
223. Engstrom, S., B. Lindman, and K. Larsson, *Method of preparing controlled-release preparations for biologically active materials and resulting compositions*. 1992, Google Patents.
224. van Dalsen, L., et al., *9.8 MAG: A New Host Lipid for In Meso (Lipid Cubic Phase) Crystallization of Integral Membrane Proteins.* Crystal Growth & Design, 2020. **21**(1): p. 490-500.
225. Osornio, Y.M., et al., *Design and synthesis of lipids for the fabrication of functional lipidic cubic-phase biomaterials.* The Journal of organic chemistry, 2012. **77**(23): p. 10583-10595.
226. Nazaruk, E., et al., *Charged additives modify drug release rates from lipidic cubic phase carriers by modulating electrostatic interactions.* Journal of Electroanalytical Chemistry, 2018. **819**: p. 269-274.
227. Andersson, S.J., M.; Lidin, S.; Larsson, K., *Structure of the cubosome - a closed lipid bilayer aggregate.* Zeitschrift für Kristallographie-Crystalline Materials, 1995. **210**(5): p. 315-318.
228. Yaghmur, A. and O. Glatter, *Characterization and potential applications of nanostructured aqueous dispersions.* Advances in colloid and interface science, 2009. **147**: p. 333-342.
229. Karami, Z. and M. Hamidi, *Cubosomes: remarkable drug delivery potential.* Drug discovery today, 2016. **21**(5): p. 789-801.
230. Garg, G., S. Saraf, and S. Saraf, *Cubosomes: an overview.* Biological and Pharmaceutical Bulletin, 2007. **30**(2): p. 350-353.
231. Luzzati, V. and F. Husson, *The structure of the liquid-crystalline phases of lipid-water systems.* The Journal of cell biology, 1962. **12**(2): p. 207-219.
232. Peng, X., et al., *Characterization of cubosomes as a targeted and sustained transdermal delivery system for capsaicin.* Drug design, development and therapy, 2015. **9**: p. 4209.
233. Gustafsson, J., et al., *Cubic lipid− water phase dispersed into submicron particles.* Langmuir, 1996. **12**(20): p. 4611-4613.
234. Gustafsson, J., et al., *Submicron particles of reversed lipid phases in water stabilized by a nonionic amphiphilic polymer.* Langmuir, 1997. **13**(26): p. 6964-6971.
235. Spicer, P.T., et al., *Novel process for producing cubic liquid crystalline nanoparticles (cubosomes).* Langmuir, 2001. **17**(19): p. 5748-5756.
236. Rizwan, S., et al., *Preparation of phytantriol cubosomes by solvent precursor dilution for the delivery of protein vaccines.* European Journal of Pharmaceutics and Biopharmaceutics, 2011. **79**(1): p. 15-22.
237. Boge, L., et al., *Cubosomes post-loaded with antimicrobial peptides: characterization, bactericidal effect and proteolytic stability.* International journal of pharmaceutics, 2017. **526**(1-2): p. 400-412.
238. Cervin, C., et al., *A combined in vitro and in vivo study on the interactions between somatostatin and lipid-based liquid crystalline drug carriers and bilayers.* European journal of pharmaceutical sciences, 2009. **36**(4-5): p. 377-385.
239. Pan, X., et al., *Nanostructed cubosomes as advanced drug delivery system.* Current pharmaceutical design, 2013. **19**(35): p. 6290-6297.

240. Esposito, E., et al., *Cubosome dispersions as delivery systems for percutaneous administration of indomethacin.* Pharmaceutical research, 2005. **22**(12): p. 2163-2173.
241. Chung, H., et al., *Self-assembled "nanocubicle" as a carrier for peroral insulin delivery.* Diabetologia, 2002. **45**(3): p. 448-451.
242. Angelova, A., et al., *Self-assembled multicompartment liquid crystalline lipid carriers for protein, peptide, and nucleic acid drug delivery.* Accounts of chemical research, 2010. **44**(2): p. 147-156.
243. Landau, E.M., et al., *Crystallization of a polar protein and small molecules from the aqueous compartment of lipidic cubic phases.* The Journal of Physical Chemistry B, 1997. **101**(11): p. 1935-1937.
244. Lai, J., et al., *Pharmacokinetics and enhanced oral bioavailability in beagle dogs of cyclosporine A encapsulated in glyceryl monooleate/poloxamer 407 cubic nanoparticles.* International journal of nanomedicine, 2010. **5**: p. 13.
245. Diepold, R., et al., *Distribution of poly-hexyl-2-cyano-[3-14C] acrylate nanoparticles in healthy and chronically inflamed rabbit eyes.* International journal of pharmaceutics, 1989. **54**(2): p. 149-153.
246. Duncan, R., T.A. Connors, and H. Meada, *Drug targeting in cancer therapy: the magic bullet, what next?* 1996, Taylor & Francis.
247. Monsky, W.L., et al., *Augmentation of transvascular transport of macromolecules and nanoparticles in tumors using vascular endothelial growth factor.* Cancer Research, 1999. **59**(16): p. 4129-4135.
248. Boyd, B.J., *Characterisation of drug release from cubosomes using the pressure ultrafiltration method.* International journal of pharmaceutics, 2003. **260**(2): p. 239-247.
249. Kaasgaard, T. and C.J. Drummond, *Ordered 2-D and 3-D nanostructured amphiphile self-assembly materials stable in excess solvent.* Physical Chemistry Chemical Physics, 2006. **8**(43): p. 4957-4975.
250. Sagalowicz, L., R. Mezzenga, and M.E. Leser, *Investigating reversed liquid crystalline mesophases.* Current opinion in colloid & interface science, 2006. **11**(4): p. 224-229.
251. Milak, S., et al., *Vancomycin Loaded Glycerol Monooleate Liquid Crystalline Phases Modified with Surfactants.* Pharmaceutics, 2020. **12**(6): p. 521.
252. Boyd, B.J., et al., *Lyotropic liquid crystalline phases formed from glycerate surfactants as sustained release drug delivery systems.* International journal of pharmaceutics, 2006. **309**(1-2): p. 218-226.
253. Lopes, L.B., F.F. Speretta, and M.V.L. Bentley, *Enhancement of skin penetration of vitamin K using monoolein-based liquid crystalline systems.* European Journal of Pharmaceutical Sciences, 2007. **32**(3): p. 209-215.
254. Cohen-Avrahami, M., A. Aserin, and N. Garti, *HII mesophase and peptide cell-penetrating enhancers for improved transdermal delivery of sodium diclofenac.* Colloids and Surfaces B: Biointerfaces, 2010. **77**(2): p. 131-138.
255. Swarnakar, N.K., et al., *Enhanced oromucosal delivery of progesterone via hexosomes.* Pharmaceutical research, 2007. **24**(12): p. 2223-2230.
256. Li, Y., et al., *PH responsiveness of hexosomes and cubosomes for combined delivery of Brucea javanica oil and doxorubicin.* Langmuir, 2019. **35**(45): p. 14532-14542.
257. Borné, J., T. Nylander, and A. Khan, *Effect of lipase on different lipid liquid crystalline phases formed by oleic acid based acylglycerols in aqueous systems.* Langmuir, 2002. **18**(23): p. 8972-8981.
258. Wallin, R. and T. Arnebrant, *The activity of lipase at the cubic liquid-crystalline phase/water interface.* Journal of colloid and interface science, 1994. **164**(1): p. 16-20.
259. Campos, J., et al., *On the interaction between adsorbed layers of monoolein and the lipase action on the formed layers.* Colloids and Surfaces B: Biointerfaces, 2002. **26**(1-2): p. 172-182.
260. Verger, R. and G.H. De Haas, *Interfacial enzyme kinetics of lipolysis.* Annual review of biophysics and bioengineering, 1976. **5**(1): p. 77-117.

261. Maylie, M.-F., M. Charles, and P. Desnuelle, *Action of organophosphates and sulfonyl halides on porcine pancreatic lipase.* Biochimica et Biophysica Acta (BBA)-Enzymology, 1972. **276**(1): p. 162-175.
262. Winkler, F., A. d'Arcy, and W. Hunziker, *Structure of human pancreatic lipase.* Nature, 1990. **343**(6260): p. 771.
263. Chang, J.W., et al., *Highly selective inhibitors of monoacylglycerol lipase bearing a reactive group that is bioisosteric with endocannabinoid substrates.* Chemistry & biology, 2012. **19**(5): p. 579-588.
264. Borgström, B. and C. Erlanson, *Pancreatic juice co-lipase: physiological importance.* Biochimica et biophysica acta, 1971. **242**(2): p. 509.
265. Golding, M. and T.J. Wooster, *The influence of emulsion structure and stability on lipid digestion.* Current Opinion in Colloid & Interface Science, 2010. **15**(1-2): p. 90-101.
266. Patton, J.S., et al., *Binding of porcine pancreatic lipase and colipase in the absence of substrate studies by two-phase partition and affinity chromatography.* Journal of Biological Chemistry, 1978. **253**(12): p. 4195-4202.
267. Lowe, M.E., *Pancreatic triglyceride lipase and colipase: insights into dietary fat digestion.* Gastroenterology, 1994. **107**(5): p. 1524-1536.
268. Liao, T.H., P. Hamosh, and M. Hamosh, *Fat digestion by lingual lipase: mechanism of lipolysis in the stomach and upper small intestine.* Pediatric research, 1984. **18**(5): p. 402-409.
269. Hamosh, M., *Lingual and gastric lipases.* Nutrition (Burbank, Los Angeles County, Calif.), 1990. **6**(6): p. 421-428.
270. Borovicka, J., et al., *Regulation of gastric and pancreatic lipase secretion by CCK and cholinergic mechanisms in humans.* American Journal of Physiology-Gastrointestinal and Liver Physiology, 1997. **273**(2): p. G374-G380.
271. Fredenberg, S., et al., *The mechanisms of drug release in poly (lactic-co-glycolic acid)-based drug delivery systems—a review.* International journal of pharmaceutics, 2011. **415**(1-2): p. 34-52.
272. Frankel, E.N., *Lipid oxidation*. 2014: Elsevier.
273. Rhoades, R.A. and D.R. Bell, *Medical phisiology: Principles for clinical medicine*. 2012: Lippincott Williams & Wilkins.
274. Keller, P.J. and B.J. Allan, *The protein composition of human pancreatic juice.* Journal of Biological Chemistry, 1967. **242**(2): p. 281-287.
275. Embleton, J.K. and C.W. Pouton, *Structure and function of gastro-intestinal lipases.* Advanced Drug Delivery Reviews, 1997. **25**(1): p. 15-32.
276. Phan, C.T. and P. Tso, *Intestinal lipid absorption and transport.* Front Biosci, 2001. **6**(5): p. D299-D319.
277. Iqbal, J. and M.M. Hussain, *Intestinal lipid absorption.* American Journal of Physiology-Endocrinology and Metabolism, 2009. **296**(6): p. E1183-E1194.
278. Tso, P., A. Nauli, and C.-M. Lo, *Enterocyte fatty acid uptake and intestinal fatty acid-binding protein*. 2004, Portland Press Ltd.
279. Simmonds, W., *The role of micellar solubilization in lipid absorption.* Australian Journal Of Experimental Biology And Medical Science, 1972. **50**(4): p. 403-421.
280. Hofmann, A.F. and B. Borgström, *The intraluminal phase of fat digestion in man: the lipid content of the micellar and oil phases of intestinal content obtained during fat digestion and absorption.* The Journal of clinical investigation, 1964. **43**(2): p. 247-257.
281. Hoffman, N., *The relationship between uptake in vitro of oleic acid and micellar solubilization.* Biochimica et Biophysica Acta (BBA)-Biomembranes, 1970. **196**(2): p. 193-203.
282. Abumrad, N.A. and N.O. Davidson, *Role of the gut in lipid homeostasis.* Physiological reviews, 2012. **92**(3): p. 1061-1085.

283. Risovic, V., et al., *Effect of various lipid-based oral formulations on plasma and tissue concentrations and renal toxicity of amphotericin B within male rats.* Antimicrob Agents Chemother, 2003. **47**: p. 3339-3342.
284. Bogman, K., et al., *The role of surfactants in the reversal of active transport mediated by multidrug resistance proteins.* Journal of pharmaceutical sciences, 2003. **92**(6): p. 1250-1261.
285. Hugger, E.D., et al., *A comparison of commonly used polyethoxylated pharmaceutical excipients on their ability to inhibit P‐glycoprotein activity in vitro.* Journal of pharmaceutical sciences, 2002. **91**(9): p. 1991-2002.
286. Johnson, B.M., W.N. Charman, and C.J. Porter, *An in vitro examination of the impact of polyethylene glycol 400, pluronic P85, and vitamin E da-tocopheryl polyethylene glycol 1000 succinate on P-glycoprotein efflux and enterocyte-based metabolism in excised rat intestine.* AAPS pharmsci, 2002. **4**(4): p. 193-205.
287. Wandel, C., R.B. Kim, and C.M. Stein, *"Inactive" excipients such as Cremophor can affect in vivo drug disposition.* Clinical Pharmacology & Therapeutics, 2003. **73**(5): p. 394-396.
288. Risovic, V., et al., *Potential mechanisms by which Peceol® increases the gastrointestinal absorption of amphotericin B.* Drug development and industrial pharmacy, 2004. **30**(7): p. 767-774.
289. Agellon, L.B., M.J. Toth, and A.B. Thomson, *Intracellular lipid binding proteins of the small intestine*, in *Cellular Lipid Binding Proteins*. 2002, Springer. p. 79-82.
290. Thompson, J., et al., *The liver fatty acid binding protein-comparison of cavity properties of intracellular lipid-binding proteins.* Molecular and cellular biochemistry, 1999. **192**(1-2): p. 9-16.
291. Storch, J. and A.E. Thumser, *Tissue-specific functions in the fatty acid-binding protein family.* Journal of Biological Chemistry, 2010. **285**(43): p. 32679-32683.
292. Mansbach, C.M. and S.A. Siddiqi, *The biogenesis of chylomicrons.* Annual review of physiology, 2010. **72**: p. 315-333.
293. Pan, X. and M.M. Hussain, *Gut triglyceride production.* Biochimica et Biophysica Acta (BBA)-Molecular and Cell Biology of Lipids, 2012. **1821**(5): p. 727-735.
294. Demignot, S., F. Beilstein, and E. Morel, *Triglyceride-rich lipoproteins and cytosolic lipid droplets in enterocytes: key players in intestinal physiology and metabolic disorders.* Biochimie, 2014. **96**: p. 48-55.
295. Sturley, S.L. and M.M. Hussain, *Lipid droplet formation on opposing sides of the endoplasmic reticulum.* Journal of lipid research, 2012. **53**(9): p. 1800-1810.
296. Hernell, O., J.E. Staggers, and M.C. Carey, *Physical-chemical behavior of dietary and biliary lipids during intestinal digestion and absorption. 2. Phase analysis and aggregation states of luminal lipids during duodenal fat digestion in healthy adult human beings.* Biochemistry, 1990. **29**(8): p. 2041-2056.
297. Kaukonen, A.M., et al., *Drug solubilization behavior during in vitro digestion of suspension formulations of poorly water-soluble drugs in triglyceride lipids.* Pharmaceutical research, 2004. **21**(2): p. 254-260.
298. Kaukonen, A.M., et al., *Drug solubilization behavior during in vitro digestion of simple triglyceride lipid solution formulations.* Pharmaceutical research, 2004. **21**(2): p. 245-253.
299. Larsen, A., et al., *Lipid-based formulations for danazol containing a digestible surfactant, Labrafil M2125CS: in vivo bioavailability and dynamic in vitro lipolysis.* Pharmaceutical research, 2008. **25**(12): p. 2769-2777.
300. Porter, C.J., et al., *Enhancing intestinal drug solubilisation using lipid-based delivery systems.* Advanced drug delivery reviews, 2008. **60**(6): p. 673-691.
301. Caliph, S.M., W.N. Charman, and C.J. Porter, *Effect of short‐, medium‐, and long‐chain fatty acid‐based vehicles on the absolute oral bioavailability and intestinal lymphatic transport of*

halofantrine and assessment of mass balance in lymph‐cannulated and non‐cannulated rats. Journal of pharmaceutical sciences, 2000. **89**(8): p. 1073-1084.
302. Narangifard, A., et al., *Human skin barrier formation takes place via a cubic to lamellar lipid phase transition as analyzed by cryo-electron microscopy and EM-simulation.* Experimental cell research, 2018. **366**(2): p. 139-151.
303. Best, C.H., et al., *The nature of the vaso‐dilator constituents of certain tissue extracts.* The Journal of physiology, 1927. **62**(4): p. 397-417.
304. Loew, E.R. and O. Chickering, *Gastric secretion in dogs treated with histamine antagonist, thymoxyethyldiethylamine.* Proceedings of the Society for Experimental Biology and Medicine, 1941. **48**(1): p. 65-68.
305. Black, J., et al., *Definition and antagonism of histamine H2-receptors.* Nature, 1972. **236**: p. 385-390.
306. Wollenberg, A. and K. Feichtner, *Atopic dermatitis and skin allergies–update and outlook.* Allergy, 2013. **68**(12): p. 1509-1519.
307. Hide, M., et al., *Autoantibodies against the high-affinity IgE receptor as a cause of histamine release in chronic urticaria.* New England Journal of Medicine, 1993. **328**(22): p. 1599-1604.
308. Walch, H., *Topical application of cetirizine and loratadine*. 2004, Google Patents.
309. Heinrich, J., et al., *European health survey in adults (ECRHS).* Pneumologie, 2002. **56**(5): p. 297-303.
310. World Allergy Organization (WAO), *White book on allergy: update 2013*, W.a. organization, Editor. 2013: Milwaukee, WI.
311. Simons, F.E.R. and K.J. Simons, *Histamine and H1-antihistamines: celebrating a century of progress.* Journal of Allergy and Clinical Immunology, 2011. **128**(6): p. 1139-1150. e4.
312. Leurs, R., M. Church, and M. Taglialatela, *H1‐antihistamines: inverse agonism, anti‐inflammatory actions and cardiac effects.* Clinical & Experimental Allergy, 2002. **32**(4): p. 489-498.
313. Simons, F.E.R., *The antiallergic effects of antihistamines (H1-receptor antagonists).* Journal of allergy and clinical immunology, 1992. **90**(4): p. 705-715.
314. Simons, F.E.R., *Advances in H1-antihistamines.* New England Journal of Medicine, 2004. **351**(21): p. 2203-2217.
315. Bakker, R.A., et al., *Histamine H1-receptor activation of nuclear factor-κB: roles for Gβγ-and Gαq/11-subunits in constitutive and agonist-mediated signaling.* Molecular pharmacology, 2001. **60**(5): p. 1133-1142.
316. Weller, K. and M. Maurer, *Desloratadine inhibits human skin mast cell activation and histamine release.* The Journal of investigative dermatology, 2009. **129**(11): p. 2723.
317. Chishty, M., et al., *Affinity for the P-glycoprotein efflux pump at the blood-brain barrier may explain the lack of CNS side-effects of modern antihistamines.* Journal of drug targeting, 2001. **9**(3): p. 223-228.
318. Timmerman, H., *Factors involved in the absence of sedative effects by the second-generation antihistamines.* ALLERGY-COPENHAGEN-SUPPLEMENT-, 2000. **55**: p. 5-10.
319. Chen, C., et al., *P-glycoprotein limits the brain penetration of nonsedating but not sedating H1-antagonists.* Drug Metabolism and Disposition, 2003. **31**(3): p. 312-318.
320. Machado, O.L.T., D.M. de Campos‐Mesquita, and T. Pacheco‐Soares, *Antihistaminic Treatment, Allergen‐Specific Immunotherapy, and Blockade of IgE as Alternative Allergy Treatments.* Allergen, 2017: p. 67.
321. Church, M.K. and D.S. Church, *Pharmacology of antihistamines.* Indian journal of dermatology, 2013. **58**(3): p. 219.

322. Tashiro, M., et al., *Roles of histamine in regulation of arousal and cognition: functional neuroimaging of histamine H1 receptors in human brain.* Life sciences, 2002. **72**(4-5): p. 409-414.
323. Gelotte, C.K., B.A. Zimmerman, and G.A. Thompson, *Single‐Dose Pharmacokinetic Study of Diphenhydramine HCl in Children and Adolescents.* Clinical pharmacology in drug development, 2018. **7**(4): p. 400-407.
324. BD Simplist, *Diphenhydramine Hydrochloride Injection, USP.* 2010.
325. Banerji, A., A.A. Long, and C.A. Camargo Jr. *Diphenhydramine versus nonsedating antihistamines for acute allergic reactions: A literature review*. in *Allergy & Asthma Proceedings*. 2007.
326. Edwards, R.J., C.-T. Huang, and N.-M. Pui, *Long acting dual release product containing carbinoxamine and pseudoephedrine*. 2016, Google Patents.
327. Food and Drug Administration, *HIGHLIGHTS OF PRESCRIBING INFORMATION: Karbinal ER*. 2013.
328. FDA. *Arbinoxa Oral Solution*. 2020; Available from: https://www.drugs.com/pro/arbinoxa-oral-solution.html.
329. Goindi, S., B. Dhatt, and A. Kaur, *Ethosomes-based topical delivery system of antihistaminic drug for treatment of skin allergies.* Journal of microencapsulation, 2014. **31**(7): p. 716-724.
330. Zemtsov, A. and H. Hosier, *A Novel Vehicle Formulation for Treatment of Inflammatory Skin Diseases.* Journal of Cosmetics, Dermatological Sciences and Applications, 2013. **3**(01): p. 18.
331. Salib, R.J. and P.H. Howarth, *Safety and tolerability profiles of intranasal antihistamines and intranasal corticosteroids in the treatment of allergic rhinitis.* Drug Safety, 2003. **26**(12): p. 863-893.
332. Hampel, F.C., et al., *Double-blind, placebo-controlled study of azelastine and fluticasone in a single nasal spray delivery device.* Annals of Allergy, Asthma & Immunology, 2010. **105**(2): p. 168-173.
333. Food and Drug Administration, *ASTELIN - azelastine hydrochloride spray, metered* 2011.
334. Shin, S.-C. and M.-K. Yoon, *Application of TPX polymer membranes for the controlled release of triprolidine.* International journal of pharmaceutics, 2002. **232**(1-2): p. 131-137.
335. Hindmarch, I. and Z. Shamsi, *Antihistamines: models to assess sedative properties, assessment of sedation, safety and other side‐effects.* Clinical & Experimental Allergy, 1999. **29**: p. 133-142.
336. Jain, G.K., A. Rampal, and H. Sen, *Process for the preparation of a controlled drug delivery system containing pseudoephedrine and a long acting antihistamine*. 2001, Google Patents.
337. Rabinowitz, J.D. and A.C. Zaffaroni, *Delivery of antihistamines through an inhalation route*. 2004, Google Patents.
338. Gu, X., et al., *Evaluation and comparison of five matrix excipients for the controlled release of acrivastine and pseudoephedrine.* Drug development and industrial pharmacy, 2004. **30**(10): p. 1009-1017.
339. Rossi, A., et al., *A preliminary study on topical cetirizine in the therapeutic management of androgenetic alopecia.* Journal of Dermatological Treatment, 2018. **29**(2): p. 149-151.
340. Elzainy, A.A., et al., *Cetirizine from topical phosphatidylcholine-hydrogenated liposomes: evaluation of peripheral antihistaminic activity and systemic absorption in a rabbit model.* The AAPS journal, 2004. **6**(3): p. 7-12.
341. Shin, S.-C. and H.-J. Lee, *Controlled release of triprolidine using ethylene-vinyl acetate membrane and matrix systems.* European journal of pharmaceutics and biopharmaceutics, 2002. **54**(2): p. 201-206.
342. Ramachandran, S., S. Nandhakumar, and M.D. Dhanaraju, *Formulation and characterization of glutaraldehyde cross-linked chitosan biodegradable microspheres loaded with famotidine.* Tropical Journal of Pharmaceutical Research, 2011. **10**(3).

343. Bize, C., et al., *Bioactive Formulations with Sugar‐Derived Surfactants: A New Approach for Photoprotection and Controlled Release of Promethazine.* ChemPhysChem, 2013. **14**(6): p. 1126-1131.
344. Dian, L., et al., *Cubic phase nanoparticles for sustained release of ibuprofen: formulation, characterization, and enhanced bioavailability study.* International journal of nanomedicine, 2013. **8**: p. 845.
345. Hundekar, Y.R., et al., *Preparation and evaluation of diclofenac sodium cubosomes for percutaneous administration.* World journal of pharmacy and pharmaceutical sciences, 2014. **3**(1): p. 523-539.
346. Müller, R., E. Souto, and M. Radtke, *Medicament vehicle for the controlled administration of an active agent, produced from lipid matrix-medicament conjugates*, in *WO00/67800*. 2000.
347. Chang, C.-M. and R. Bodmeier, *Monoglyceride based liquid crystalline topical drug delivery systems.* Pharm. Res., 1994. **11**: p. S185.
348. Du Buske, L.M., *Clinical comparison of histamine H1–receptor antagonist drugs.* Journal of allergy and clinical immunology, 1996. **98**(6): p. S307-S318.
349. Wu, H., et al., *A novel small Odorranalectin-bearing cubosomes: Preparation, brain delivery and pharmacodynamic study on amyloid-β25–35-treated rats following intranasal administration.* European Journal of Pharmaceutics and Biopharmaceutics, 2012. **80**(2): p. 368-378.
350. Boge, L., *Lipid-based liquid crystals as drug delivery vehicles for antimicrobial peptides*. 2018: Department of Chemistry and Chemical Engineering, Chalmers University of ….
351. Filik, J., et al., *Processing two-dimensional X-ray diffraction and small-angle scattering data in DAWN 2.* Journal of applied crystallography, 2017. **50**(3): p. 959-966.
352. Briggs, J., H. Chung, and M. Caffrey, *The temperature-composition phase diagram and mesophase structure characterization of the monoolein/water system.* Journal de Physique II, 1996. **6**(5): p. 723-751.
353. Zhou, X.E., et al., *X-ray laser diffraction for structure determination of the rhodopsin-arrestin complex.* Scientific data, 2016. **3**: p. 160021.
354. Turner, D.C., et al., *Structural study of the inverted cubic phases of di-dodecyl alkyl-β-D-glucopyranosyl-rac-glycerol.* Journal de Physique II, 1992. **2**(11): p. 2039-2063.
355. Prosperi-Porta, G., et al., *Phenylboronic-acid-based polymeric micelles for mucoadhesive anterior segment ocular drug delivery.* Biomacromolecules, 2016. **17**(4): p. 1449-1457.
356. Martinac, A., et al., *Development and bioadhesive properties of chitosan-ethylcellulose microspheres for nasal delivery.* International journal of pharmaceutics, 2005. **291**(1-2): p. 69-77.
357. Farid, R.M., et al., *Formulation and in vitro evaluation of salbutamol sulphate in situ gelling nasal inserts.* Aaps Pharmscitech, 2013. **14**(2): p. 712-718.
358. Hasan, S., et al., *Controlled-release formulation of antihistamine based on cetirizine zinc-layered hydroxide nanocomposites and its effect on histamine release from basophilic leukemia (RBL-2H3) cells.* International Journal of Nanomedicine, 2012. **7**: p. 3351.
359. Nazaruk, E., et al., *Design and assembly of pH-sensitive lipidic cubic phase matrices for drug release.* Langmuir, 2014. **30**(5): p. 1383-1390.
360. Caboi, F., et al., *Structural effects, mobility, and redox behavior of vitamin K1 hosted in the monoolein/water liquid crystalline phases.* Langmuir, 1997. **13**(20): p. 5476-5483.
361. Yaghmur, A., et al., *Tuning curvature and stability of monoolein bilayers by designer lipid-like peptide surfactants.* PLoS One, 2007. **2**(5).
362. Borné, J., T. Nylander, and A. Khan, *Phase behavior and aggregate formation for the aqueous monoolein system mixed with sodium oleate and oleic acid.* Langmuir, 2001. **17**(25): p. 7742-7751.
363. Hyde, S., et al., *The language of shape: the role of curvature in condensed matter: physics, chemistry and biology*. 1996: Elsevier.

364. Kim, H., Z. Song, and C. Leal, *Super-swelled lyotropic single crystals.* Proceedings of the National Academy of Sciences, 2017. **114**(41): p. 10834-10839.
365. Larsson, K. and F. Tiberg, *Periodic minimal surface structures in bicontinuous lipid–water phases and nanoparticles.* Current opinion in colloid & interface science, 2005. **9**(6): p. 365-369.
366. Hyde, S.T., *Bicontinuous structures in lyotropic liquid crystals and crystalline hyperbolic surfaces.* Current Opinion in Solid State and Materials Science, 1996. **1**(5): p. 653-662.
367. Johnsson, M., J. Barauskas, and F. Tiberg, *Cubic phases and cubic phase dispersions in a phospholipid-based system.* Journal of the American Chemical Society, 2005. **127**(4): p. 1076-1077.
368. Tenchov, B., R. Koynova, and G. Rapp, *Accelerated formation of cubic phases in phosphatidylethanolamine dispersions.* Biophysical journal, 1998. **75**(2): p. 853-866.
369. Angelov, B., et al., *Long-living intermediates during a lamellar to a diamond-cubic lipid phase transition: a small-angle X-ray scattering investigation.* Langmuir, 2009. **25**(6): p. 3734-3742.
370. Nakano, M., et al., *Small-angle X-ray scattering and 13C NMR investigation on the internal structure of "cubosomes".* Langmuir, 2001. **17**(13): p. 3917-3922.
371. Yaghmur, A., et al., *Self-assembly in monoelaidin aqueous dispersions: direct vesicles to cubosomes transition.* PLoS One, 2008. **3**(11).
372. Nakano, M., et al., *Dispersions of liquid crystalline phases of the monoolein/oleic acid/Pluronic F127 system.* Langmuir, 2002. **18**(24): p. 9283-9288.
373. Sagalowicz, L., et al., *Crystallography of dispersed liquid crystalline phases studied by cryo‐transmission electron microscopy.* Journal of microscopy, 2006. **221**(2): p. 110-121.
374. Falchi, A.M., et al., *Effects of monoolein-based cubosome formulations on lipid droplets and mitochondria of HeLa cells.* Toxicology Research, 2015. **4**(4): p. 1025-1036.
375. Mozafari, M., *Nanoliposomes: preparation and analysis*, in *Liposomes*. 2010, Springer. p. 29-50.
376. Sou, K., *Electrostatics of carboxylated anionic vesicles for improving entrapment capacity.* Chemistry and physics of lipids, 2011. **164**(3): p. 211-215.
377. Han, S., et al., *Novel vehicle based on cubosomes for ophthalmic delivery of flurbiprofen with low irritancy and high bioavailability.* Acta Pharmacologica Sinica, 2010. **31**(8): p. 990-998.
378. Levy, M., et al., *Characterization of diazepam submicron emulsion interface: role of oleic acid.* Journal of microencapsulation, 1994. **11**(1): p. 79-92.
379. Freitas, C. and R.H. Müller, *Effect of light and temperature on zeta potential and physical stability in solid lipid nanoparticle (SLN™) dispersions.* International journal of pharmaceutics, 1998. **168**(2): p. 221-229.
380. Barriga, H.M., M.N. Holme, and M.M. Stevens, *Cubosomes: the next generation of smart lipid nanoparticles?* Angewandte Chemie International Edition, 2019. **58**(10): p. 2958-2978.
381. Tilley, A.J., C.J. Drummond, and B.J. Boyd, *Disposition and association of the steric stabilizer Pluronic® F127 in lyotropic liquid crystalline nanostructured particle dispersions.* Journal of colloid and interface science, 2013. **392**: p. 288-296.
382. Guo, C., et al., *Lyotropic liquid crystal systems in drug delivery.* Drug discovery today, 2010. **15**(23-24): p. 1032-1040.
383. Nafee, N., et al., *Relevance of the colloidal stability of chitosan/PLGA nanoparticles on their cytotoxicity profile.* International journal of pharmaceutics, 2009. **381**(2): p. 130-139.
384. Selvi, R.B., et al., *ATP driven clathrin dependent entry of carbon nanospheres prefer cells with glucose receptors.* Journal of nanobiotechnology, 2012. **10**(1): p. 35.
385. Chung, T.-H., et al., *The effect of surface charge on the uptake and biological function of mesoporous silica nanoparticles in 3T3-L1 cells and human mesenchymal stem cells.* Biomaterials, 2007. **28**(19): p. 2959-2966.

386. Zhang, D., et al., *The morphology and surface charge-dependent cellular uptake efficiency of upconversion nanostructures revealed by single-particle optical microscopy.* Chemical science, 2018. **9**(23): p. 5260-5269.
387. Wilhelm, C., et al., *Intracellular uptake of anionic superparamagnetic nanoparticles as a function of their surface coating.* Biomaterials, 2003. **24**(6): p. 1001-1011.
388. Lorenz, M.R., et al., *Uptake of functionalized, fluorescent-labeled polymeric particles in different cell lines and stem cells.* Biomaterials, 2006. **27**(14): p. 2820-2828.
389. Sahay, G., D.Y. Alakhova, and A.V. Kabanov, *Endocytosis of nanomedicines.* Journal of controlled release, 2010. **145**(3): p. 182-195.
390. Martins, S., et al., *Solid lipid nanoparticles as intracellular drug transporters: an investigation of the uptake mechanism and pathway.* International journal of pharmaceutics, 2012. **430**(1-2): p. 216-227.
391. Ravi, P.R., et al., *Lipid nanoparticles for oral delivery of raloxifene: optimization, stability, in vivo evaluation and uptake mechanism.* European journal of pharmaceutics and biopharmaceutics, 2014. **87**(1): p. 114-124.
392. Kam, N.W.S., Z. Liu, and H. Dai, *Carbon nanotubes as intracellular transporters for proteins and DNA: an investigation of the uptake mechanism and pathway.* Angewandte Chemie International Edition, 2006. **45**(4): p. 577-581.
393. Thurn, K.T., et al., *Endocytosis of titanium dioxide nanoparticles in prostate cancer PC-3M cells.* Nanomedicine: Nanotechnology, Biology and Medicine, 2011. **7**(2): p. 123-130.
394. Yang, Z., et al., *Evaluating the potential of cubosomal nanoparticles for oral delivery of amphotericin B in treating fungal infection.* International journal of nanomedicine, 2014. **9**: p. 327.
395. Prange, J.A., et al., *Overcoming endocytosis deficiency by cubosome nanocarriers.* ACS Applied Bio Materials, 2019. **2**(6): p. 2490-2499.
396. Luo, Q., et al., *A novel glyceryl monoolein-bearing cubosomes for gambogenic acid: preparation, cytotoxicity and intracellular uptake.* International journal of pharmaceutics, 2015. **493**(1-2): p. 30-39.
397. Fröhlich, E., *The role of surface charge in cellular uptake and cytotoxicity of medical nanoparticles.* International journal of nanomedicine, 2012. **7**: p. 5577.
398. Pelle, E., et al., *Identification of histamine receptors and reduction of squalene levels by an antihistamine in sebocytes.* Journal of investigative dermatology, 2008. **128**(5): p. 1280-1285.
399. Snyder, R.D. and J.W. Green, *A review of the genotoxicity of marketed pharmaceuticals.* Mutation Research/Reviews in Mutation Research, 2001. **488**(2): p. 151-169.
400. Ellegaard, A.-M., et al., *Repurposing cationic amphiphilic antihistamines for cancer treatment.* EBioMedicine, 2016. **9**: p. 130-139.
401. Salimi, A., M. Razian, and J. Pourahmad, *Analysis of toxicity effects of buspirone, cetirizine and olanzapine on human blood lymphocytes: in vitro model.* Current clinical pharmacology, 2018. **13**(2): p. 120-127.
402. Rosa, A., et al., *Monoolein-based cubosomes affect lipid profile in HeLa cells.* Chemistry and physics of lipids, 2015. **191**: p. 96-105.
403. Eldem, T. and P. Speiser, *Intestinal fat absorption and its relevance in lipid drug delivery systems.* Pharmazie, 1989. **44**(7): p. 444-447.
404. Illum, L., *Nasal drug delivery—possibilities, problems and solutions.* Journal of controlled release, 2003. **87**(1-3): p. 187-198.
405. Mura, P., et al., *In situ mucoadhesive-thermosensitive liposomal gel as a novel vehicle for nasal extended delivery of opiorphin.* European Journal of Pharmaceutics and Biopharmaceutics, 2018. **122**: p. 54-61.

406. Campbell, C., et al., *Drug development of intranasally delivered peptides.* Therapeutic Delivery, 2012. **3**(4): p. 557-568.
407. Ghori, M.U., et al., *Nasal drug delivery systems: an overview.* American Journal of Pharmacological Sciences, 2015. **3**(5): p. 110-119.
408. Lochhead, J.J. and R.G. Thorne, *Intranasal delivery of biologics to the central nervous system.* Advanced drug delivery reviews, 2012. **64**(7): p. 614-628.
409. Kim, Y.S. and S.B. Ho, *Intestinal goblet cells and mucins in health and disease: recent insights and progress.* Current gastroenterology reports, 2010. **12**(5): p. 319-330.
410. Bøgh, M., et al., *Mucosal drug delivery: barriers, in vitro models and formulation strategies.* Journal of Drug Delivery Science and Technology, 2013. **23**(4): p. 383-391.
411. Thornton, D.J. and J.K. Sheehan, *From mucins to mucus: toward a more coherent understanding of this essential barrier.* Proceedings of the American Thoracic Society, 2004. **1**(1): p. 54-61.
412. Li, L.D., et al., *Spatial configuration and composition of charge modulates transport into a mucin hydrogel barrier.* Biophysical journal, 2013. **105**(6): p. 1357-1365.
413. Bravo-Osuna, I., et al., *Interfacial interaction between transmembrane ocular mucins and adhesive polymers and dendrimers analyzed by surface plasmon resonance.* Pharmaceutical research, 2012. **29**(8): p. 2329-2340.
414. Joergensen, L., et al., *New insights into the mucoadhesion of pectins by AFM roughness parameters in combination with SPR.* International journal of pharmaceutics, 2011. **411**(1-2): p. 162-168.
415. Zeng, W., et al., *Hyaluronic acid-coated niosomes facilitate tacrolimus ocular delivery: Mucoadhesion, precorneal retention, aqueous humor pharmacokinetics, and transcorneal permeability.* Colloids and Surfaces B: Biointerfaces, 2016. **141**: p. 28-35.
416. Bansil, R., E. Stanley, and J.T. LaMont, *Mucin biophysics.* Annual review of physiology, 1995. **57**(1): p. 635-657.
417. Bhaskar, K.R., et al., *Viscous fingering of HCI through gastric mucin.* Nature, 1992. **360**(6403): p. 458-461.
418. Ugwoke, M.I., et al., *Nasal mucoadhesive drug delivery: background, applications, trends and future perspectives.* Advanced drug delivery reviews, 2005. **57**(11): p. 1640-1665.
419. Jiang, L., et al., *The application of mucoadhesive polymers in nasal drug delivery.* Drug development and industrial pharmacy, 2010. **36**(3): p. 323-336.
420. Morita, Y., N. Koyama, and S. Ohsawa, *Methods employing stable preparation containing azelastine hydrochloride*. 2000, Google Patents.
421. Wang, C., S. Hu, and C.C. Sun, *Expedited development of diphenhydramine orally disintegrating tablet through integrated crystal and particle engineering.* Molecular pharmaceutics, 2017. **14**(10): p. 3399-3408.
422. Van Eeckhaut, A., et al., *Influence of methanol on the enantioresolution of antihistamines with carboxymethyl - β - cyclodextrin in capillary electrophoresis.* Electrophoresis, 2004. **25**(16): p. 2838-2847.
423. Bajerski, L., et al., *Determination of cetirizine in tablets and compounded capsules: comparative study between CE and HPLC.* Química Nova, 2010. **33**(1): p. 114-118.
424. Wang, C., et al., *Relationships among crystal structures, mechanical properties, and tableting performance probed using four salts of diphenhydramine.* Crystal Growth & Design, 2017. **17**(11): p. 6030-6040.
425. Reddy, M., et al., *Polymorphic forms of dihydrochloride salts of cetirizine and processes for preparation thereof*. 2004, Google Patents.
426. Maccaroni, E., et al., *Azelastine hydrochloride: A powder diffraction and 13C CPMAS NMR study of its anhydrous and solvated forms.* Crystal Growth and Design, 2009. **9**(1): p. 517-524.

427. Deng, Y., et al., *Studies on the in vitro ion exchange kinetics and thermodynamics and in vivo pharmacokinetics of the carbinoxamine-resin complex.* International Journal of Pharmaceutics, 2020. **588**: p. 119779.
428. Dully, M., et al., *Modulating the Release of Pharmaceuticals from Lipid Cubic Phases using a Lipase Inhibitor.* Journal of Colloid and Interface Science, 2020(573): p. 176-192.
429. Hatefi, Y. and W. Hanstein, *Destabilization of membranes with chaotropic ions*, in *Methods in enzymology*. 1974, Elsevier. p. 770-790.
430. Hyde, A.M., et al., *General principles and strategies for salting-out informed by the Hofmeister series.* Organic Process Research & Development, 2017. **21**(9): p. 1355-1370.
431. Lo Nostro, P. and B.W. Ninham, *Hofmeister phenomena: an update on ion specificity in biology.* Chemical reviews, 2012. **112**(4): p. 2286-2322.
432. Brasnett, C., et al., *Effects of cations on the behaviour of lipid cubic phases.* Scientific reports, 2017. **7**(1): p. 1-7.
433. Nguyen, T.-H., et al., *Nanostructured liquid crystalline particles provide long duration sustained-release effect for a poorly water soluble drug after oral administration.* Journal of controlled release, 2011. **153**(2): p. 180-186.
434. Vervaeck, A., et al., *Prilling of fatty acids as a continuous process for the development of controlled release multiparticulate dosage forms.* European journal of pharmaceutics and biopharmaceutics, 2013. **85**(3): p. 587-596.
435. Clogston, J., et al., *Controlling release from the lipidic cubic phase by selective alkylation.* Journal of controlled release, 2005. **102**(2): p. 441-461.
436. Togias, A.G., et al., *Demonstration of inhibition of mediator release from human mast cells by azatadine base: in vivo and in vitro evaluation.* JAMA, 1986. **255**(2): p. 225-229.
437. Lichtenstein, L.M. and E. Gillespie, *The effects of the H1 and H2 antihistamines on" allergic" histamine release and its inhibition by histamine.* Journal of Pharmacology and Experimental Therapeutics, 1975. **192**(2): p. 441-450.
438. Nadler, M., et al., *Signal transduction by the high-affinity immunoglobulin E receptor FcRI: coupling form to function.* Adv. Immunol, 2000. **76**: p. 325-355.
439. Kitani, S., et al., *Inhibition of IgE-mediated histamine release by myosin light chain kinase inhibitors.* Biochemical and biophysical research communications, 1992. **183**(1): p. 48-54.
440. Hanifin, J.M., *The role of antihistamines in atopic dermatitis.* Journal of allergy and clinical immunology, 1990. **86**(4): p. 666-669.
441. Michel, L., C. De Vos, and L. Dubertret, *Cetirizine effects on the cutaneous allergic reaction in humans.* Annals of allergy, 1990. **65**(6): p. 512.
442. Church, M.K. and C.F. GRADIDGE, *Inhibition of histamine release from human lung in vitro by antihistamines and related drugs.* British journal of pharmacology, 1980. **69**(4): p. 663-667.
443. Vannieuwenhuyse, E., et al., *Double-blind placebo-controlled clinical evaluation of oxatimide (R 35443). A novel potent anti-allergic drug in the treatment of hay fever.* Acta allergologica, 1977. **32**(4): p. 278-289.
444. De Clerck, F., et al., *Oxatomide protectsTrichinella spiralis infected mice from lethal anaphylaxis.* Agents and actions, 1978. **8**(6): p. 568-571.
445. Little, M.M. and T.B. Casale, *Azelastine inhibits IgE-mediated human basophil histamine release.* Journal of allergy and clinical immunology, 1989. **83**(5): p. 862-865.
446. Katayama, S., *Anti-allergic effect of azelastine hydrochloride on immediate type hypersensitivity reactions in vivo and in vitro.* 1981.
447. Chand, N., et al., *Inhibition of IgE-mediated allergic histamine release from rat peritoneal mast cells by azelastine and selected antiallergic drugs.* Agents and actions, 1985. **16**(5): p. 318-322.

448. Fischer, B. and W. Schmutzler, *Inhibition by azelastine of the immunologically induced histamine release from isolated guinea pig mast cells.* Arzneimittel-forschung, 1981. **31**(8): p. 1193-1195.
449. Seddon, J., *Inverse cubic phases of membrane-lipids, and their relevance to the static and dynamic structure of biomembranes.* Acta Pharm, 1992. **42**(4): p. 255-62.
450. Blijleven, J.S., et al. *Mechanisms of influenza viral membrane fusion*. in *Seminars in cell & developmental biology*. 2016. Elsevier.
451. Michaelsen, M.H., et al., *The effect of digestion and drug load on halofantrine absorption from self-nanoemulsifying drug delivery system (SNEDDS).* The AAPS journal, 2016. **18**(1): p. 180-186.
452. Feeney, O.M., et al., *'Stealth'lipid-based formulations: poly (ethylene glycol)-mediated digestion inhibition improves oral bioavailability of a model poorly water soluble drug.* Journal of Controlled Release, 2014. **192**: p. 219-227.
453. Tran, T., et al., *In vitro and in vivo performance of monoacyl phospholipid-based self-emulsifying drug delivery systems.* Journal of Controlled Release, 2017. **255**: p. 45-53.
454. Li, Y. and D.J. McClements, *Inhibition of lipase-catalyzed hydrolysis of emulsified triglyceride oils by low-molecular weight surfactants under simulated gastrointestinal conditions.* European journal of pharmaceutics and biopharmaceutics, 2011. **79**(2): p. 423-431.
455. Wulff-Pérez, M., et al., *Controlling lipolysis through steric surfactants: new insights on the controlled degradation of submicron emulsions after oral and intravenous administration.* International journal of pharmaceutics, 2012. **423**(2): p. 161-166.
456. Hadvary, P., H. Lengsfeld, and H. Wolfer, *Inhibition of pancreatic lipase in vitro by the covalent inhibitor tetrahydrolipstatin.* Biochemical Journal, 1988. **256**(2): p. 357-361.
457. Gargouri, Y., et al., *Inactivation of pancreatic and gastric lipases by THL and C12: 0-TNB: a kinetic study with emulsified tributyrin.* Biochimica et Biophysica Acta (BBA)-Lipids and Lipid Metabolism, 1991. **1085**(3): p. 322-328.
458. Heck, A.M., J.A. Yanovski, and K.A. Calis, *Orlistat, a new lipase inhibitor for the management of obesity.* Pharmacotherapy: The Journal of Human Pharmacology and Drug Therapy, 2000. **20**(3): p. 270-279.
459. Drent, M.L. and E.A. van der Veen, *First clinical studies with orlistat: a short review.* Obesity research, 1995. **3**(S4): p. 623S-625S.
460. Lee, M.W., F.B. Kraemer, and D.L. Severson, *Characterization of a partially purified diacylglycerol lipase from bovine aorta.* Biochimica et Biophysica Acta (BBA)-Lipids and Lipid Metabolism, 1995. **1254**(3): p. 311-318.
461. McNeely, W. and P. Benfield, *Orlistat.* Drugs, 1998. **56**(2): p. 241-9; discussion 250.
462. Lookene, A., N. Skottova, and G. Olivecrona, *Interactions of lipoprotein lipase with the active-site inhibitor tetrahydrolipstatin (Orlistat) R.* European journal of biochemistry, 1994. **222**(2): p. 395-403.
463. Lawson, D., A. Brzozowski, and G. Dodson, *Lifting the lid off lipases.* Curr. Biol, 1992. **2**: p. 473-475.
464. Hadvary, P., et al., *The lipase inhibitor tetrahydrolipstatin binds covalently to the putative active site serine of pancreatic lipase.* Journal of Biological Chemistry, 1991. **266**(4): p. 2021-2027.
465. Lüthi-Peng, Q., H.P. Märki, and P. Hadváry, *Identification of the active-site serine in human pancreatic lipase by chemical modification with tetrahydrolipstatin.* FEBS letters, 1992. **299**(1): p. 111-115.
466. Borgström, B., *Mode of action of tetrahydrolipstatin: a derivative of the naturally occurring lipase inhibitor lipstatin.* Biochimica et Biophysica Acta (BBA)-Lipids and Lipid Metabolism, 1988. **962**(3): p. 308-316.
467. Carrière, F., et al., *Inhibition of gastrointestinal lipolysis by Orlistat during digestion of test meals in healthy volunteers.* American Journal of Physiology-Gastrointestinal and Liver Physiology, 2001. **281**(1): p. G16-G28.

468. Human Metabolome Database (HMDB). *Orlistat*. Available from: http://www.hmdb.ca/metabolites/HMDB0015215.
469. Tiss, A., et al., *Transfer of orlistat through oil–water interfaces.* Chemistry and physics of lipids, 2002. **119**(1-2): p. 41-49.
470. Tiss, A., et al., *Surface behaviour of bile salts and tetrahydrolipstatin at air/water and oil/water interfaces.* Chemistry and physics of lipids, 2001. **111**(1): p. 73-85.
471. Bannigan, P., et al., *Role of biorelevant dissolution media in the selection of optimal Salt forms of oral drugs: maximizing the gastrointestinal solubility and in vitro activity of the antimicrobial molecule, clofazimine.* ACS omega, 2017. **2**(12): p. 8969-8981.
472. Shakeel, F. and W. Ramadan, *Transdermal delivery of anticancer drug caffeine from water-in-oil nanoemulsions.* Colloids and Surfaces B: Biointerfaces, 2010. **75**(1): p. 356-362.
473. Azhari, H., et al., *Stabilising cubosomes with Tween 80 as a step towards targeting lipid nanocarriers to the blood–brain barrier.* European Journal of Pharmaceutics and Biopharmaceutics, 2016. **104**: p. 148-155.
474. Dombrowski, R., *Microscopy techniques for analyzing the phase nature and morphology of biomaterials*, in *Characterization of Biomaterials*. 2013, Elsevier. p. 1-33.
475. Lutton, E., *Phase behavior of aqueous systems of monoglycerides.* Journal of the American Oil Chemists Society, 1965. **42**(12): p. 1068-1070.
476. Conn, C.E., et al., *High-throughput analysis of the structural evolution of the monoolein cubic phase in situ under crystallogenesis conditions.* Soft Matter, 2012. **8**(7): p. 2310-2321.
477. Cherezov, V., K.M. Riedl, and M. Caffrey, *Too hot to handle? Synchrotron X-ray damage of lipid membranes and mesophases.* Journal of synchrotron radiation, 2002. **9**(6): p. 333-341.
478. van't Hag, L., et al., *Lyotropic liquid crystal engineering moving beyond binary compositional space–ordered nanostructured amphiphile self-assembly materials by design.* Chemical society reviews, 2017. **46**(10): p. 2705-2731.
479. Rand, R., et al., *Membrane curvature, lipid segregation, and structural transitions for phospholipids under dual-solvent stress.* Biochemistry, 1990. **29**(1): p. 76-87.
480. Templer, R.H., B.J. Khoo, and J.M. Seddon, *Gaussian curvature modulus of an amphiphilic monolayer.* Langmuir, 1998. **14**(26): p. 7427-7434.
481. Edwards, H.G., et al., *Metamorphosis of caffeine hydrate and anhydrous caffeine.* Journal of the Chemical Society, Perkin Transactions 2, 1997(10): p. 1985-1990.
482. Patton, J.S., et al., *The light microscopy of triglyceride digestion.* Food Structure, 1985. **4**(1): p. 5.
483. Kirchgessner, T.G., et al., *Organization of the human lipoprotein lipase gene and evolution of the lipase gene family.* Proceedings of the National Academy of Sciences, 1989. **86**(24): p. 9647-9651.
484. Mukherjee, M., *Human digestive and metabolic lipases—a brief review.* Journal of Molecular Catalysis B: Enzymatic, 2003. **22**(5-6): p. 369-376.
485. Warren, D.B., et al., *Real time evolution of liquid crystalline nanostructure during the digestion of formulation lipids using synchrotron small-angle X-ray scattering.* Langmuir, 2011. **27**(15): p. 9528-9534.
486. Lynch, M.L., et al., *Enhanced loading of water-soluble actives into bicontinuous cubic phase liquid crystals using cationic surfactants.* Journal of colloid and interface science, 2003. **260**(2): p. 404-413.
487. Lindell, K., et al., *Influence of a charged phospholipid on the release pattern of timolol maleate from cubic liquid crystalline phases.* The Colloid Science of Lipids, 1998. **108**: p. 111-118.
488. Patel, V. and A. Misra, *Encapsulation and stability of clofazimine liposomes.* Journal of microencapsulation, 1999. **16**(3): p. 357-367.

489. O'Reilly, J.R., O.I. Corrigan, and C.M. O'Driscoll, *The effect of simple micellar systems on the solubility and intestinal absorption of clofazimine (B663) in the anaesthetised rat.* International journal of pharmaceutics, 1994. **105**(2): p. 137-146.
490. Azhari, H., *Surface modified cubosomes for drug delivery across the blood-brain barrier*. 2018, University of Otago.
491. Stegemann, S., et al., *When poor solubility becomes an issue: from early stage to proof of concept.* European journal of pharmaceutical sciences, 2007. **31**(5): p. 249-261.
492. Kerns, E.H. and L. Di, *Pharmaceutical profiling in drug discovery.* Drug discovery today, 2003. **8**(7): p. 316-323.
493. Takagi, T., et al., *A provisional biopharmaceutical classification of the top 200 oral drug products in the United States, Great Britain, Spain, and Japan.* Molecular pharmaceutics, 2006. **3**(6): p. 631-643.
494. Lipinski, C.A., et al., *Experimental and computational approaches to estimate solubility and permeability in drug discovery and development settings.* Advanced drug delivery reviews, 1997. **23**(1-3): p. 3-25.
495. Di, L., P.V. Fish, and T. Mano, *Bridging solubility between drug discovery and development.* Drug discovery today, 2012. **17**(9-10): p. 486-495.
496. Di, L., E.H. Kerns, and G.T. Carter, *Drug-like property concepts in pharmaceutical design.* Current pharmaceutical design, 2009. **15**(19): p. 2184-2194.
497. Vo, C.L.-N., C. Park, and B.-J. Lee, *Current trends and future perspectives of solid dispersions containing poorly water-soluble drugs.* European journal of pharmaceutics and biopharmaceutics, 2013. **85**(3): p. 799-813.
498. Fong, W.-K., T. Hanley, and B.J. Boyd, *Stimuli responsive liquid crystals provide 'on-demand'drug delivery in vitro and in vivo.* Journal of Controlled Release, 2009. **135**(3): p. 218-226.
499. Fong, W.-K., et al., *Plasmonic nanorods provide reversible control over nanostructure of self-assembled drug delivery materials.* Langmuir, 2010. **26**(9): p. 6136-6139.
500. Kwon, T.K. and J.-C. Kim, *Monoolein cubic phase containing acidic proteinoid: pH-dependent release.* Drug development and industrial pharmacy, 2011. **37**(1): p. 56-61.
501. Angelov, B., et al., *Small-angle neutron and X-ray scattering from amphiphilic stimuli-responsive diamond-type bicontinuous cubic phase.* Journal of the American Chemical Society, 2007. **129**(44): p. 13474-13479.
502. Liu, Z., et al., *Cytotoxic and anti-angiogenic paclitaxel solubilized and permeation-enhanced by natural product nanoparticles.* Anti-cancer drugs, 2015. **26**(2): p. 167.
503. Kavallaris, M., *Microtubules and resistance to tubulin-binding agents.* Nature Reviews Cancer, 2010. **10**(3): p. 194-204.
504. Liggins, R.T., W. Hunter, and H.M. Burt, *Solid-state characterization of paclitaxel.* Journal of pharmaceutical sciences, 1997. **86**(12): p. 1458-1463.
505. Yao, H.-J., et al., *The antitumor efficacy of functional paclitaxel nanomicelles in treating resistant breast cancers by oral delivery.* Biomaterials, 2011. **32**(12): p. 3285-3302.
506. Chae, S.W., et al., *Intestinal P‐glycoprotein inhibitors, benzoxanthone analogues.* Journal of Pharmacy and Pharmacology, 2018. **70**(2): p. 234-241.
507. Amin, M.L., *P-glycoprotein inhibition for optimal drug delivery.* Drug target insights, 2013. **7**: p. DTI. S12519.
508. Zeng, N., et al., *Preparation and characterization of paclitaxel-loaded DSPE-PEG-liquid crystalline nanoparticles (LCNPs) for improved bioavailability.* International journal of pharmaceutics, 2012. **424**(1-2): p. 58-66.

509. Zeng, N., et al., *Lipid-based liquid crystalline nanoparticles as oral drug delivery vehicles for poorly water-soluble drugs: cellular interaction and in vivo absorption.* International journal of nanomedicine, 2012. **7**: p. 3703.
510. Green, M., et al., *Abraxane®, a novel Cremophor®-free, albumin-bound particle form of paclitaxel for the treatment of advanced non-small-cell lung cancer.* Annals of Oncology, 2006. **17**(8): p. 1263-1268.
511. Zhang, J., et al., *Polymeric nanoparticles based on chitooligosaccharide as drug carriers for co-delivery of all-trans-retinoic acid and paclitaxel.* Carbohydrate polymers, 2015. **129**: p. 25-34.
512. He, Y., et al., *Mesoporous silica nanoparticles as potential carriers for enhanced drug solubility of paclitaxel.* Materials Science and Engineering: C, 2017. **78**: p. 12-17.
513. Lundberg, B., et al., *A lipophilic paclitaxel derivative incorporated in a lipid emulsion for parenteral administration.* Journal of Controlled Release, 2003. **86**(1): p. 93-100.
514. Yang, X.-y., et al., *Hyaluronic acid-coated nanostructured lipid carriers for targeting paclitaxel to cancer.* Cancer letters, 2013. **334**(2): p. 338-345.
515. Yuan, H., et al., *Cellular uptake of solid lipid nanoparticles and cytotoxicity of encapsulated paclitaxel in A549 cancer cells.* International journal of pharmaceutics, 2008. **348**(1-2): p. 137-145.
516. Zhai, J., et al., *Paclitaxel-loaded self-assembled lipid nanoparticles as targeted drug delivery systems for the treatment of aggressive ovarian cancer.* ACS applied materials & interfaces, 2018. **10**(30): p. 25174-25185.
517. Briggs, J., *The phase behavior of hydrated monoacylglycerols and the design of an X-ray compatible scanning calorimeter*. 1994, The Ohio State University.
518. Lairon, D., et al., *Effects of bile lipids on the adsorption and activity of pancreatic lipase on triacylglycerol emulsions.* Biochimica et Biophysica Acta (BBA)-Lipids and Lipid Metabolism, 1980. **618**(1): p. 119-128.
519. Kimura, H., et al., *Activation of human pancreatic lipase activity by calcium and bile salts.* The Journal of Biochemistry, 1982. **92**(1): p. 243-251.
520. Alvarez, F.J. and V.J. Stella, *The role of calcium ions and bile salts on the pancreatic lipase-catalyzed hydrolysis of triglyceride emulsions stabilized with lecithin.* Pharmaceutical research, 1989. **6**(6): p. 449-457.
521. Bläckberg, L., et al., *Colipase enhances hydrolysis of dietary triglycerides in the absence of bile salts.* The Journal of clinical investigation, 1979. **64**(5): p. 1303-1308.
522. Borgstrom, B., *Binding of pancreatic colipase to interfaces: effects of detergents.* FEBS Lett, 1976. **71**: p. 201-204.
523. Vandermeers, A., et al., *Effect of colipase on adsorption and activity of rat pancreatic lipase on emulsified tributyrin in the presence of bile salt.* FEBS letters, 1975. **49**(3): p. 334-337.
524. Nilsson, C., et al., *SPECT/CT imaging of radiolabeled cubosomes and hexosomes for potential theranostic applications.* Biomaterials, 2013. **34**(33): p. 8491-8503.
525. Mealey, D., et al., *Influence of solvent on crystal nucleation of risperidone.* Faraday discussions, 2015. **179**: p. 309-328.
526. Zeglinski, J., et al., *Crystal nucleation of tolbutamide in solution: Relationship to solvent, solute conformation, and solution structure.* Chemistry–A European Journal, 2018. **24**(19): p. 4916-4926.
527. Padrela, L., J. Zeglinski, and K.M. Ryan, *Insight into the role of additives in controlling polymorphic outcome: A CO2-antisolvent crystallization process of carbamazepine.* Crystal Growth & Design, 2017. **17**(9): p. 4544-4553.
528. Grimme, S., S. Ehrlich, and L. Goerigk, *Effect of the damping function in dispersion corrected density functional theory.* Journal of computational chemistry, 2011. **32**(7): p. 1456-1465.
529. Rassolov, V.A., et al., *6‐31G* basis set for third‐row atoms.* Journal of Computational Chemistry, 2001. **22**(9): p. 976-984.

530. Goerigk, L. and S. Grimme, *Efficient and Accurate Double-Hybrid-Meta-GGA Density Functionals ☒ Evaluation with the Extended GMTKN30 Database for General Main Group Thermochemistry, Kinetics, and Noncovalent Interactions.* Journal of chemical theory and computation, 2011. **7**(2): p. 291-309.
531. Weigend, F. and R. Ahlrichs, *Balanced basis sets of split valence, triple zeta valence and quadruple zeta valence quality for H to Rn: Design and assessment of accuracy.* Physical Chemistry Chemical Physics, 2005. **7**(18): p. 3297-3305.
532. Hermoso, J., et al., *Lipase activation by nonionic detergents. The crystal structure of the porcine lipase-colipase-tetraethylene glycol monooctyl ether complex.* J Biol Chem, 1996. **271**(30): p. 18007-16.
533. Khan, F.I., et al., *The Lid Domain in Lipases: Structural and Functional Determinant of Enzymatic Properties.* Front Bioeng Biotechnol, 2017. **5**: p. 16.
534. Lowe, M.E., *Colipase stabilizes the lid domain of pancreatic triglyceride lipase.* J Biol Chem, 1997. **272**(1): p. 9-12.
535. Lowe, M.E., *The catalytic site residues and interfacial binding of human pancreatic lipase.* J Biol Chem, 1992. **267**(24): p. 17069-73.
536. Morris, G.M., et al., *AutoDock4 and AutoDockTools4: Automated docking with selective receptor flexibility.* J Comput Chem, 2009. **30**(16): p. 2785-91.
537. *Editorial: ChemSpider--a tool for Natural Products research.* Nat Prod Rep, 2015. **32**(8): p. 1163-4.
538. Morris, G.M., et al., *Automated docking using a Lamarckian genetic algorithm and an empirical binding free energy function.* Journal of computational chemistry, 1998. **19**(14): p. 1639-1662.
539. Huang, J., et al., *CHARMM36m: an improved force field for folded and intrinsically disordered proteins.* Nat Methods, 2017. **14**(1): p. 71-73.
540. Vanommeslaeghe, K., et al., *CHARMM general force field: A force field for drug-like molecules compatible with the CHARMM all-atom additive biological force fields.* J Comput Chem, 2010. **31**(4): p. 671-90.
541. Yu, W., et al., *Extension of the CHARMM General Force Field to sulfonyl-containing compounds and its utility in biomolecular simulations.* J Comput Chem, 2012. **33**(31): p. 2451-68.
542. MacKerell, A.D., et al., *All-atom empirical potential for molecular modeling and dynamics studies of proteins.* J Phys Chem B, 1998. **102**(18): p. 3586-616.
543. Berendsen, H.J., D. van der Spoel, and R. van Drunen, *GROMACS: a message-passing parallel molecular dynamics implementation.* Computer physics communications, 1995. **91**(1-3): p. 43-56.
544. Van Der Spoel, D., et al., *GROMACS: fast, flexible, and free.* J Comput Chem, 2005. **26**(16): p. 1701-18.
545. Hockney, R.W., *The potential calculation and some applications.* Methods Comput. Phys., 1970. **9**: p. 136.
546. Hess, B., et al., *LINCS: A linear constraint solver for molecular simulations.* Journal of Computational Chemistry, 1997. **18**(12): p. 1463-1472.
547. Miyamoto, S. and P.A. Kollman, *Settle: An analytical version of the SHAKE and RATTLE algorithm for rigid water models.* Journal of Computational Chemistry, 1992. **13**(8): p. 952-962.
548. Darden, T., D. York, and L. Pedersen, *Particle mesh Ewald: An N·log (N) method for Ewald sums in large systems.* The Journal of chemical physics, 1993. **98**(12): p. 10089-10092.
549. Bussi, G., D. Donadio, and M. Parrinello, *Canonical sampling through velocity rescaling.* J Chem Phys, 2007. **126**(1): p. 014101.
550. Berendsen, H.J., et al., *Molecular dynamics with coupling to an external bath.* The Journal of chemical physics, 1984. **81**(8): p. 3684-3690.
551. Parrinello, M. and A. Rahman, *Polymorphic transitions in single crystals: A new molecular dynamics method.* Journal of Applied Physics, 1981. **52**(12): p. 7182-7190.

552. Humphrey, W., A. Dalke, and K. Schulten, *VMD: visual molecular dynamics.* J Mol Graph, 1996. **14**(1): p. 33-38.
553. Pettersen, E.F., et al., *UCSF Chimera--a visualization system for exploratory research and analysis.* J Comput Chem, 2004. **25**(13): p. 1605-12.
554. Kollman, P.A., et al., *Calculating structures and free energies of complex molecules: combining molecular mechanics and continuum models.* Acc Chem Res, 2000. **33**(12): p. 889-97.
555. Kumari, R., et al., *g_mmpbsa--a GROMACS tool for high-throughput MM-PBSA calculations.* J Chem Inf Model, 2014. **54**(7): p. 1951-62.
556. Aleksandrov, A., D. Thompson, and T. Simonson, *Alchemical free energy simulations for biological complexes: powerful but temperamental.* J Mol Recognit, 2010. **23**(2): p. 117-27.
557. Reyes, P., et al., *Taxane coatings for implantable medical devices*. 2012, Google Patents.
558. Caboi, F., et al., *NMR investigation on Melaleuca alternifolia essential oil dispersed in the monoolein aqueous system: phase behavior and dynamics.* Langmuir, 2002. **18**(21): p. 7916-7922.
559. Bernstein, J., *Polymorphism in Molecular Crystals 2e*. Vol. 30. 2020: International Union of Crystal.
560. Hilfiker, R., *Polymorphism in the pharmaceutical industry*. Vol. 308. 2006: Wiley Online Library.
561. Yu, K., et al., *Role of four different kinds of polyethylenimines (PEIs) in preparation of polymeric lipid nanoparticles and their anticancer activity study.* Journal of Cancer, 2016. **7**(7): p. 872.
562. Pyo, S.-H., et al., *Preparation and dissolution profiles of the amorphous, dihydrated crystalline, and anhydrous crystalline forms of paclitaxel.* Drying Technology, 2007. **25**(10): p. 1759-1767.
563. Lv, Q., et al., *Development and evaluation of penciclovir-loaded solid lipid nanoparticles for topical delivery.* International journal of pharmaceutics, 2009. **372**(1-2): p. 191-198.
564. Liu, M., et al., *Characterization and release of triptolide-loaded poly (D, L-lactic acid) nanoparticles.* European polymer journal, 2005. **41**(2): p. 375-382.
565. Venkateswarlu, V. and K. Manjunath, *Preparation, characterization and in vitro release kinetics of clozapine solid lipid nanoparticles.* Journal of controlled release, 2004. **95**(3): p. 627-638.
566. Lee, J.H., et al., *Preparation and characterization of solvent induced dihydrated, anhydrous, and amorphous paclitaxel.* Bulletin of the Korean Chemical Society, 2001. **22**(8): p. 925-928.
567. Aleandri, S., et al., *Biotinylated cubosomes: a versatile tool for active targeting and codelivery of paclitaxel and a fluorescein-based lipid dye.* Langmuir, 2015. **31**(46): p. 12770-12776.
568. Yaghmur, A., et al., *Emulsified microemulsions and oil-containing liquid crystalline phases.* Langmuir, 2005. **21**(2): p. 569-577.
569. Barauskas, J., et al., *Cubic phase nanoparticles (cubosome): principles for controlling size, structure, and stability.* Langmuir, 2005. **21**(6): p. 2569-2577.
570. Sagalowicz, L., et al., *Study of liquid crystal space groups using controlled tilting with cryogenic transmission electron microscopy.* Langmuir, 2007. **23**(24): p. 12003-12009.
571. van Tilbeurgh, H., et al., *Interfacial activation of the lipase-procolipase complex by mixed micelles revealed by X-ray crystallography.* Nature, 1993. **362**(6423): p. 814-20.
572. Kratz, A., et al., *Normal reference laboratory values.* New England Journal of Medicine, 2004. **351**(15): p. 1548-1563.
573. Olbrich, W.M. and R. Müller. *Development of an in vitro degradation assay for solid lipid nanoparticles*. in *Proceeding 2 th world Meeting APGI/APV, Paris*. 1998.
574. Olbrich, C. and R. Müller, *Enzymatic degradation of SLN—effect of surfactant and surfactant mixtures.* International journal of pharmaceutics, 1999. **180**(1): p. 31-39.
575. Scow, R.O., *Effect of sodium taurodeoxycholate, CaCl2 and albumin on the action of pancreatic lipase on droplets of trioleoylglycerol and the release of lipolytic products into aqueous media.* Biochimie, 1988. **70**(9): p. 1251-1261.

576. Zangenberg, N.H., et al., *A dynamic in vitro lipolysis model: I. Controlling the rate of lipolysis by continuous addition of calcium.* European Journal of Pharmaceutical Sciences, 2001. **14**(2): p. 115-122.
577. Hu, M., et al., *Role of calcium and calcium-binding agents on the lipase digestibility of emulsified lipids using an in vitro digestion model.* Food Hydrocolloids, 2010. **24**(8): p. 719-725.
578. Benzonana, G. and P. Desnuelle, *Action of some effectors on the hydrolysis of long-chain triglycerides by pancreatic lipase.* Biochimica et Biophysica Acta (BBA)-Lipids and Lipid Metabolism, 1968. **164**(1): p. 47-58.
579. Wenk, M.R., et al., *Paclitaxel partitioning into lipid bilayers.* Journal of pharmaceutical sciences, 1996. **85**(2): p. 228-231.
580. Alani, A.W., et al., *Polymeric micelles for the pH-dependent controlled, continuous low dose release of paclitaxel.* Biomaterials, 2010. **31**(7): p. 1765-1772.
581. Abouelmagd, S.A., et al., *Release kinetics study of poorly water-soluble drugs from nanoparticles: are we doing it right?* Molecular pharmaceutics, 2015. **12**(3): p. 997-1003.
582. Kulkarni, C.V., et al., *Self-assembled lipid cubic phase and cubosomes for the delivery of aspirin as a model drug.* Langmuir, 2017. **33**(38): p. 9907-9915.
583. Nazaruk, E., et al., *Lyotropic cubic phases for drug delivery: diffusion and sustained release from the mesophase evaluated by electrochemical methods.* Langmuir, 2015. **31**(46): p. 12753-12761.
584. Bender, J., et al., *Lipid cubic phases in topical drug delivery: visualization of skin distribution using two-photon microscopy.* Journal of Controlled Release, 2008. **129**(3): p. 163-169.
585. Lopes, L.B., et al., *Liquid crystalline phases of monoolein and water for topical delivery of cyclosporin A: characterization and study of in vitro and in vivo delivery.* European Journal of Pharmaceutics and Biopharmaceutics, 2006. **63**(2): p. 146-155.
586. Kar, M., et al., *Current Developments in Excipient Science: Implication of Quantitative Selection of Each Excipient in Product Development*, in *Basic Fundamentals of Drug Delivery*. 2019, Elsevier. p. 29-83.
587. Cheng, A., et al., *A simple mechanical mixer for small viscous lipid-containing samples.* Chemistry and Physics of Lipids, 1998. **95**(1): p. 11-21.
588. Caffrey, M. and C. Porter, *Crystallizing membrane proteins for structure determination using lipidic mesophases.* JoVE (Journal of Visualized Experiments), 2010(45): p. e1712-e1712.
589. Nunes, K.M., et al., *The Monoglyceride Content Affects the Self-Assembly Behavior, Rheological Properties, Syringeability, and Mucoadhesion of In Situ–Gelling Liquid Crystalline Phase.* Journal of pharmaceutical sciences, 2016. **105**(8): p. 2355-2364.
590. Pham, A.C., et al., *In vivo formation of cubic phase in situ after oral administration of cubic phase precursor formulation provides long duration gastric retention and absorption for poorly water-soluble drugs.* Molecular pharmaceutics, 2016. **13**(1): p. 280-286.
591. Esposito, E., et al., *Comparative analysis of tetracycline-containing dental gels: poloxamer-and monoglyceride-based formulations.* International journal of pharmaceutics, 1996. **142**(1): p. 9-23.
592. Geraghty, P.B., et al., *The in vitro release of some antimuscarinic drugs from monoolein/water lyotropic liquid crystalline gels.* Pharmaceutical research, 1996. **13**(8): p. 1265-1271.
593. Takahashi, H., A. Matsuo, and I. Hatta, *Effects of chaotropic and kosmotropic solutes on the structure of lipid cubic phase: Monoolein-water systems.* Molecular Crystals and Liquid Crystals Science and Technology. Section A. Molecular Crystals and Liquid Crystals, 2000. **347**(1): p. 231-238.
594. Clogston, J., et al., *Phase behavior of a monoacylglycerol:(myverol 18-99K)/water system.* Chemistry and physics of lipids, 2000. **107**(2): p. 191-220.
595. Collins, K.D. and M.W. Washabaugh, *The Hofmeister effect and the behaviour of water at interfaces.* Quarterly reviews of biophysics, 1985. **18**(4): p. 323-422.

596. Sanderson, P.W., et al., *The Hofmeister effect in relation to membrane lipid phase stability.* Biochimica et Biophysica Acta (BBA)-Biomembranes, 1991. **1067**(1): p. 43-50.
597. Takahashi, H., H. Ohmae, and I. Hatta, *Trehalose-induced destabilization of interdigitated gel phase in dihexadecylphosphatidylcholine.* Biophysical journal, 1997. **73**(6): p. 3030-3038.
598. Hyde, S., *Microstructure of bicontinuous surfactant aggregates.* The Journal of physical chemistry, 1989. **93**(4): p. 1458-1464.
599. Rapp, G., et al., *X-ray diffraction studies on the effect of additives on the phase behaviour of lipids*, in *Lipid Bilayers*. 2001, Springer. p. 165-187.
600. Marcus, Y., *Ions in Solution and their Solvation*. 2015: John Wiley & Sons.
601. Moelbert, S., B. Normand, and P. De Los Rios, *Kosmotropes and chaotropes: modelling preferential exclusion, binding and aggregate stability.* Biophysical chemistry, 2004. **112**(1): p. 45-57.
602. Gater, D.L., et al., *Hydrogen bonding of cholesterol in the lipidic cubic phase.* Langmuir, 2013. **29**(25): p. 8031-8038.
603. Shojaei, A.H., B. Berner, and X. Li, *Transbuccal delivery of acyclovir: I. In vitro determination of routes of buccal transport.* Pharmaceutical research, 1998. **15**(8): p. 1182-1188.
604. Kanda, T., et al., *Inhibitory effects of apple polyphenol on induced histamine release from RBL-2H3 cells and rat mast cells.* Bioscience, biotechnology, and biochemistry, 1998. **62**(7): p. 1284-1289.
605. Caltagirone, C., et al., *Cancer-cell-targeted theranostic cubosomes.* Langmuir, 2014. **30**(21): p. 6228-6236.

Appendices

Appendix A

Appendix A

A.1. Calibration Curves

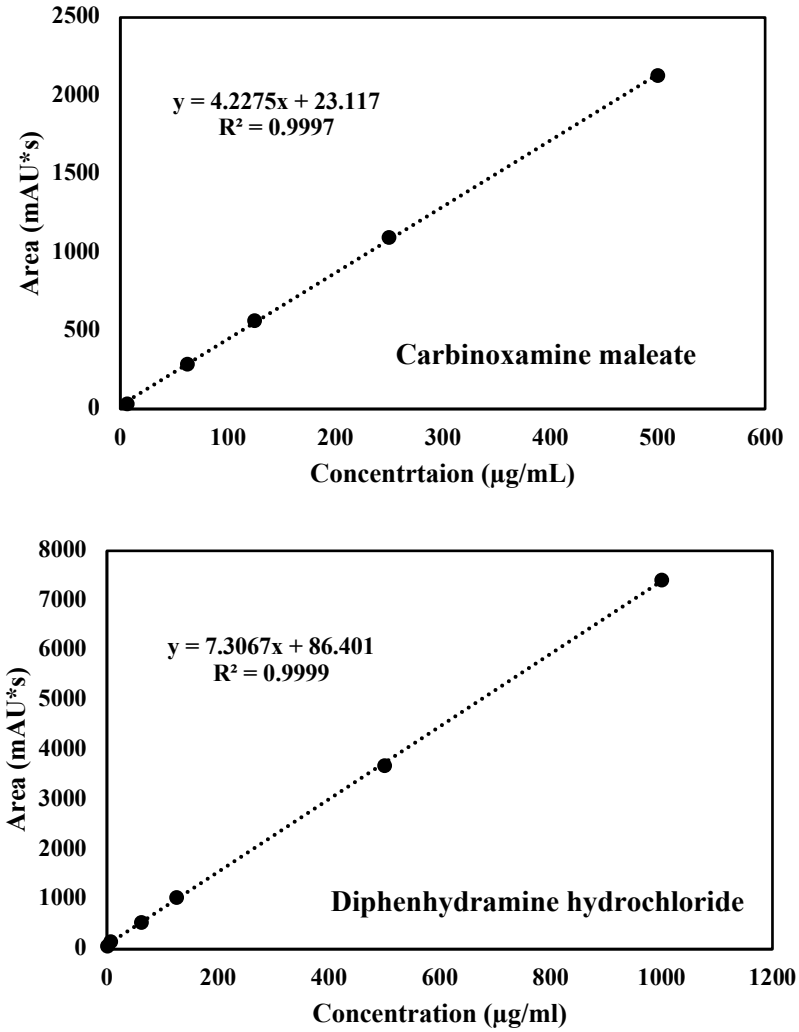

Figure A.1.1. Calibration curves for 1st generation antihistamines Carbinoxamine maleate (CBX) and Diphenhydramine hydrochloride (DPH) obtained by HPLC

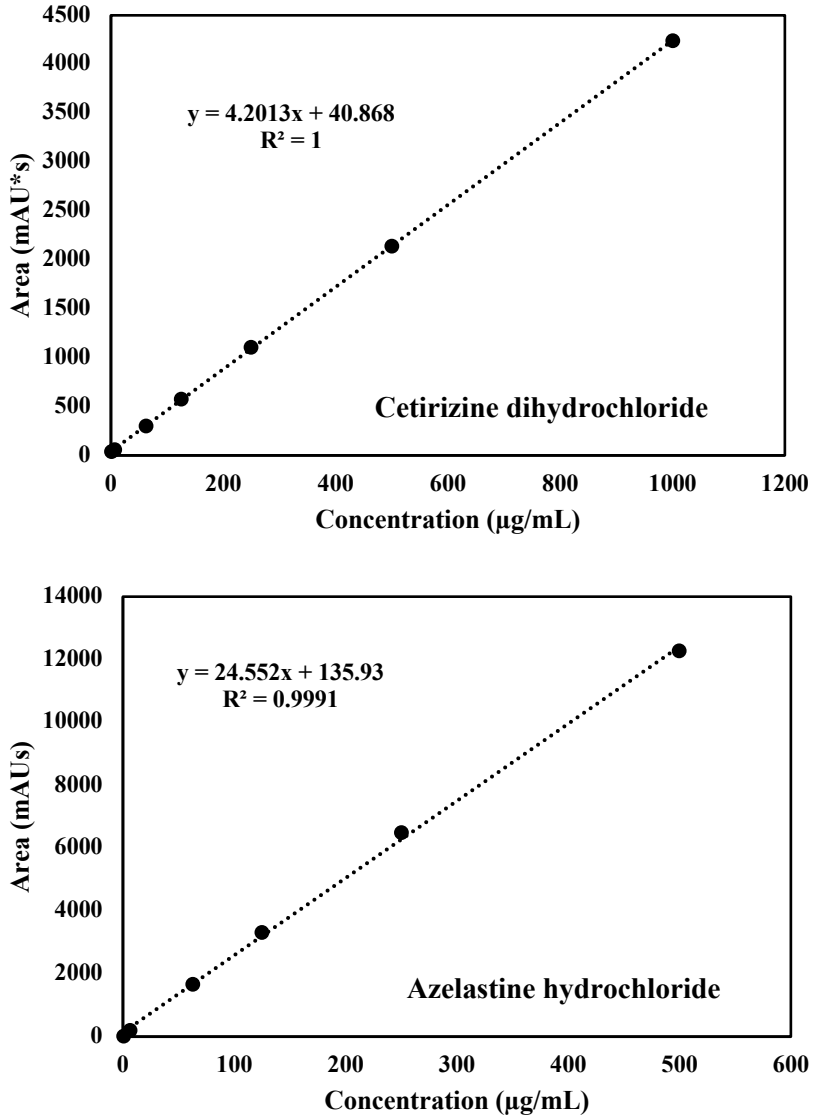

Figure A.1.2. Calibration curves for 2nd generation antihistamines Cetirizine dihydrochloride (CZH) and Azelastine hydrochloride (AZL) obtained by HPLC

A.2. Host lipid selection

A number of different monoacylglyerols were investigated for their ability to form the cubic phase in the presence of water. 8 lipids were selected and a range of water-lipid ratios under selected conditions of temperature were investigated. The lipid phases were prepared in accordance with the bulk preparation method. The lipids were weighed in their molten state and known volumes of water were carefully layered on top to allow for the diffusion of water and assembly of the lyotropic liquid crystals.

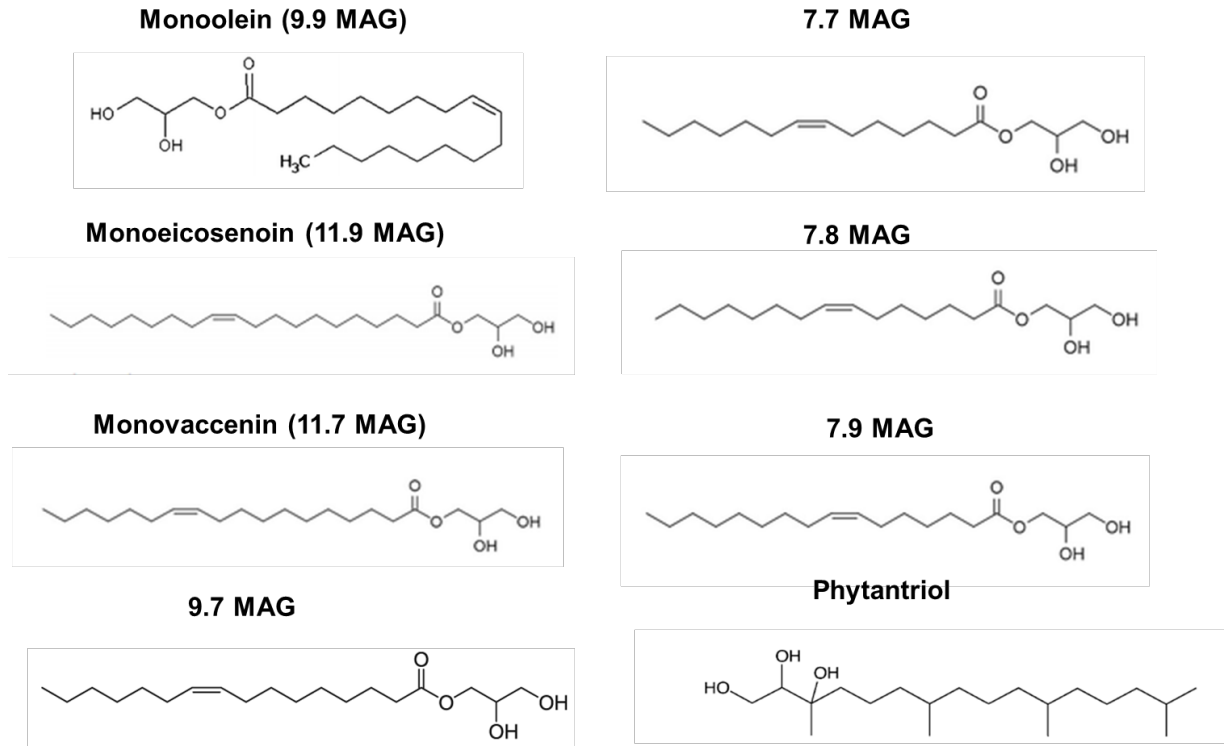

Figure A.2.1 *Chemical structures of the lipids used in this investigation*

The 8 lipids selected, whose structures are shown in figure A.2.1 were as follows: Phytantriol (3,7,11,15-Tetramethyl-1,2,3-hexadecanetriol); 7.7 MAG (1-(7Z-tetradecenoyl)-rac-glycerol), 7.8 MAG (1-(7Z-pentadecenoyl)-rac-glycerol) and 7.9 MAG (1-(7Z-hexadecenoyl)-rac-glycerol); Monoolein 9.9 MAG (1-(9Z-octadecenoyl)-rac-glycerol), Monopalmitolein 9.7 MAG (1-(9Z-hexadecenoyl)-rac-glycerol), Monovaccenin 11.7 MAG (1-(11Z-octadecenoyl)-rac-glycerol) and Monoeicosenoin 11.9 MAG (1-(11Z-eicosenoyl)-rac-glycerol).

Table A.2.1. Experimental conditions trialled for accessing the lipid cubic phase of various MAG lipids

Lipid Characteristics			Experimental Conditions				
Lipid	**Chain Length (MAGs)**	**Consist-ency at RT**	**Temperat-ure (°C)**	**Water Content %**	**Appearance**	**Birefringent**	**Cubic Phase**
Monopalmitolein	9.7	Oil	RT	45	Clear/Viscous	N	Y
			RT	55	Clear/Viscous	N	Y
			RT	65	Clear/Viscous	N	Y
Monovaccenin	11.7	Wax	RT	55	Clear/Viscous	N	Y
			37	48	Clear/Viscous	N	Y
Monoeicosenoin	11.9	Wax	RT	45	Crystals	Y	N
			RT	55	Crystals	Y	N
			RT	65	Crystals	Y	N
1-(7Z-tetradecenoyl)-rac-glycerol	7.7	Oil	37	60	Kaleidoscope effect	Y	N
			37	65	Kaleidoscope effect	Y	N
			37	70	Kaleidoscope effect	Y	N
-(7Z-pentadecenoyl)-rac-glycerol	7.8	Oil	37	60	Clear/Viscous	N	Y
			37	55	Clear/Viscous	N	Y
			RT	50	Clear/Viscous	N	Y
1-(7Z-hexadecenoyl)-rac-glycerol	7.9	Oil	RT	50	Kaleidoscope effect	Y	N
			37	40	Kaleidoscope effect	Y	N
Monoolein	9.9	Wax	40	40	Clear/Viscous	N	Y
			RT	40	Clear/Viscous	N	Y
Phytantriol	N/A	Wax	RT	27	Clear/Viscous	N	Y

A kaleidoscope effect was observed on the microscope for 7.7 and 7.9 MAG which would indicate the formation of the hexagonal phase. 11.9 MAG is a very waxy lipid at room temperature, with a relatively high melting point compared to the others on the list. The transportation of water into more waxy lipids when solid is much slower. The lipid began to solidify much more rapidly

and this may have impeded the movement of water within the membrane even further and would require much higher temperatures for cubic phase formation. Those processes that would demand extended hold time at high temperatures to prepare cubic phases would be very costly, and from an economical perspective would be highly impractical. For this reason 11.9 MAG was ruled out as a primary host lipid for stent coating applications.

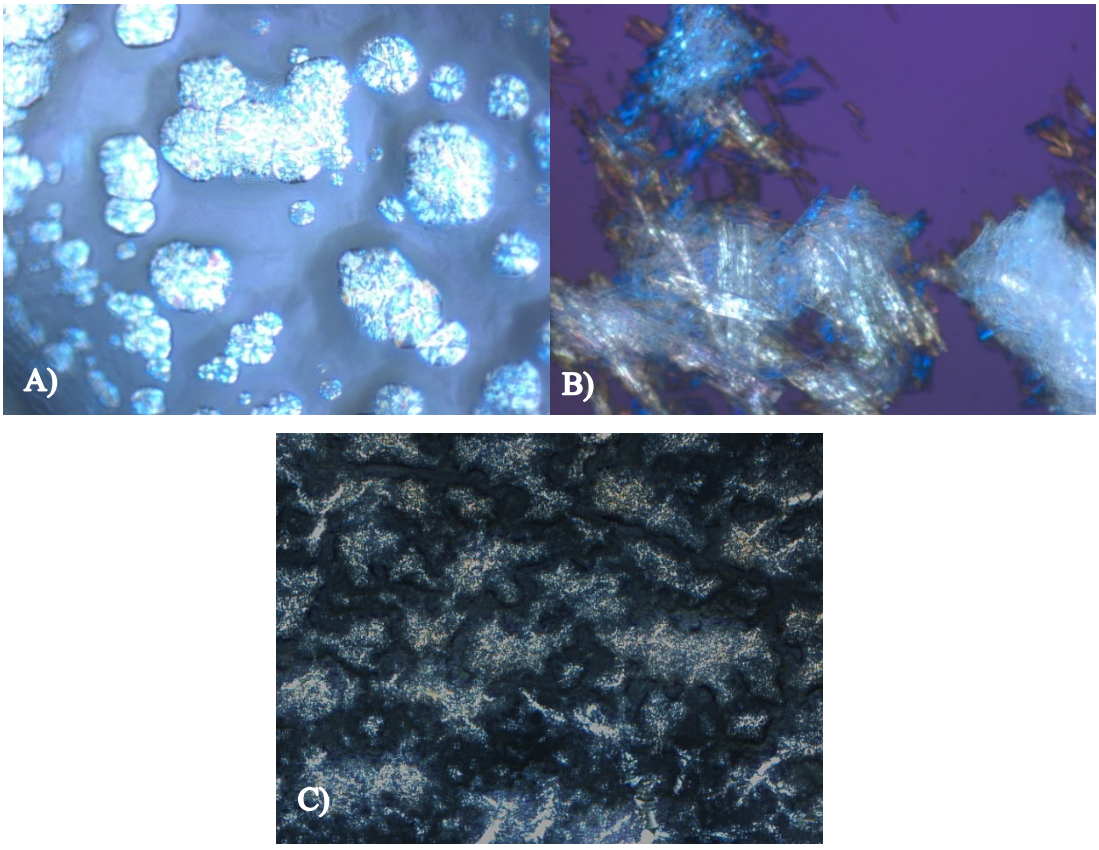

Figure A.2.2. example CPLM images aquired on the Zeiss AxioScope Optical microscope at 10x magnification showing different phases of liquid crystalline systems: Hexagonal phase for 7.9 MAG (A); non-ordered phase crystals for 11.9 MAG (B), and watery lamellar phase for Phytantriol (C)

A.3. Cell Culture

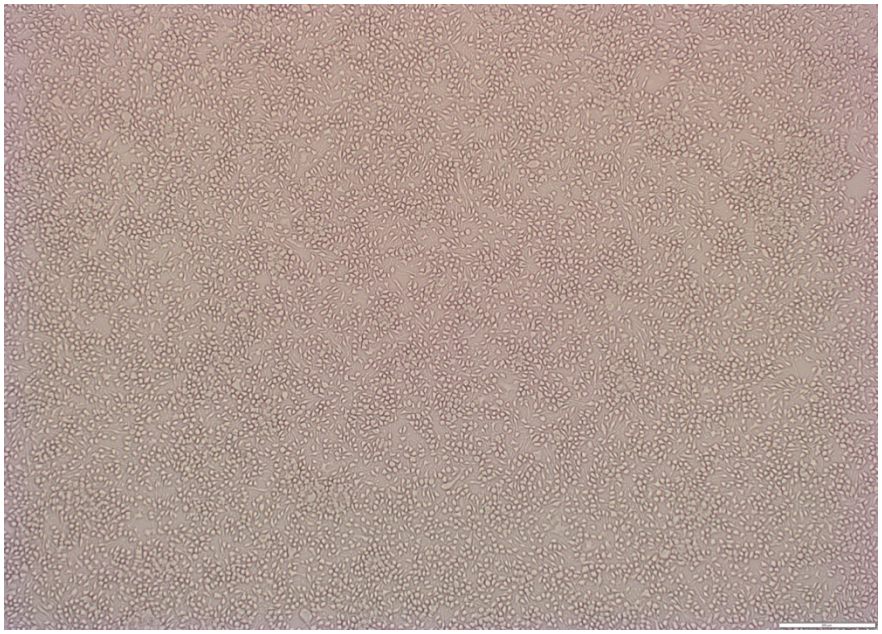

Figure A.3.1. Micrograph of RBL-2H3 cells cultured in Eagle's Minimum Essential Medium (EMEM)

A.4. Mucoadhesion Studies: MP-SPR investigation

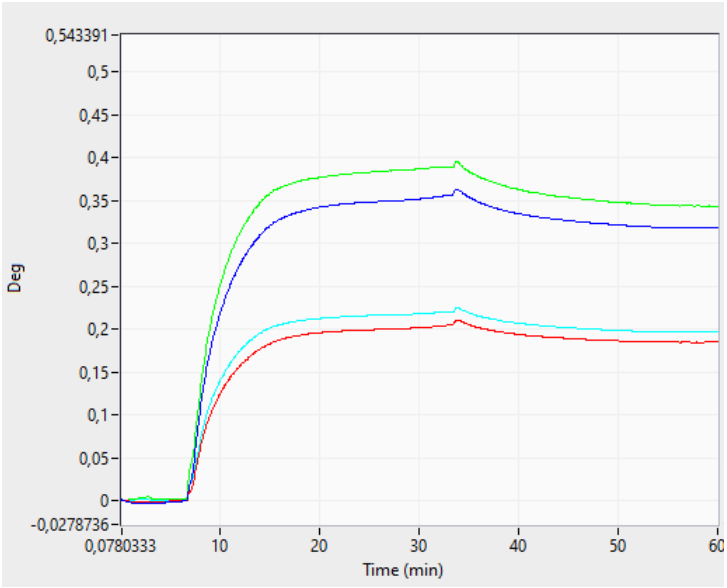

Figure A.4.1. MP-SPR sensogram from adsorption of mucin onto clean Au sensor registered at two wavelengths (670 and 785 nm). Mucin (100 ug/ml in PBS) was injected into 2 channels at a flow rate of 30ul/min.

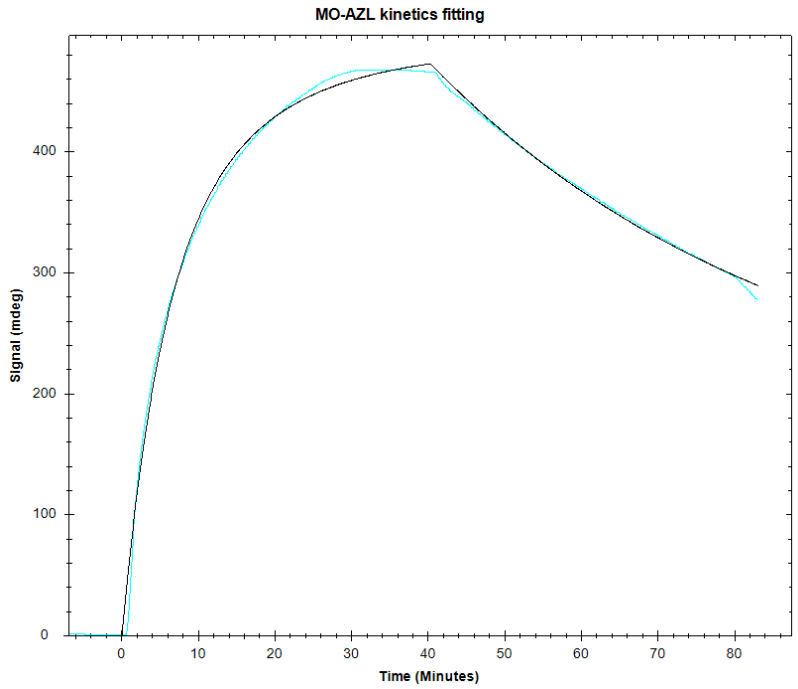

Figure A.4.2. Typical kinetics fitting resulted obtained for MO-AZL from TraceDrawer™ software according to One-to-Two interaction model. Blue curve is the measured data while black curve represents the resulting fitting curve.

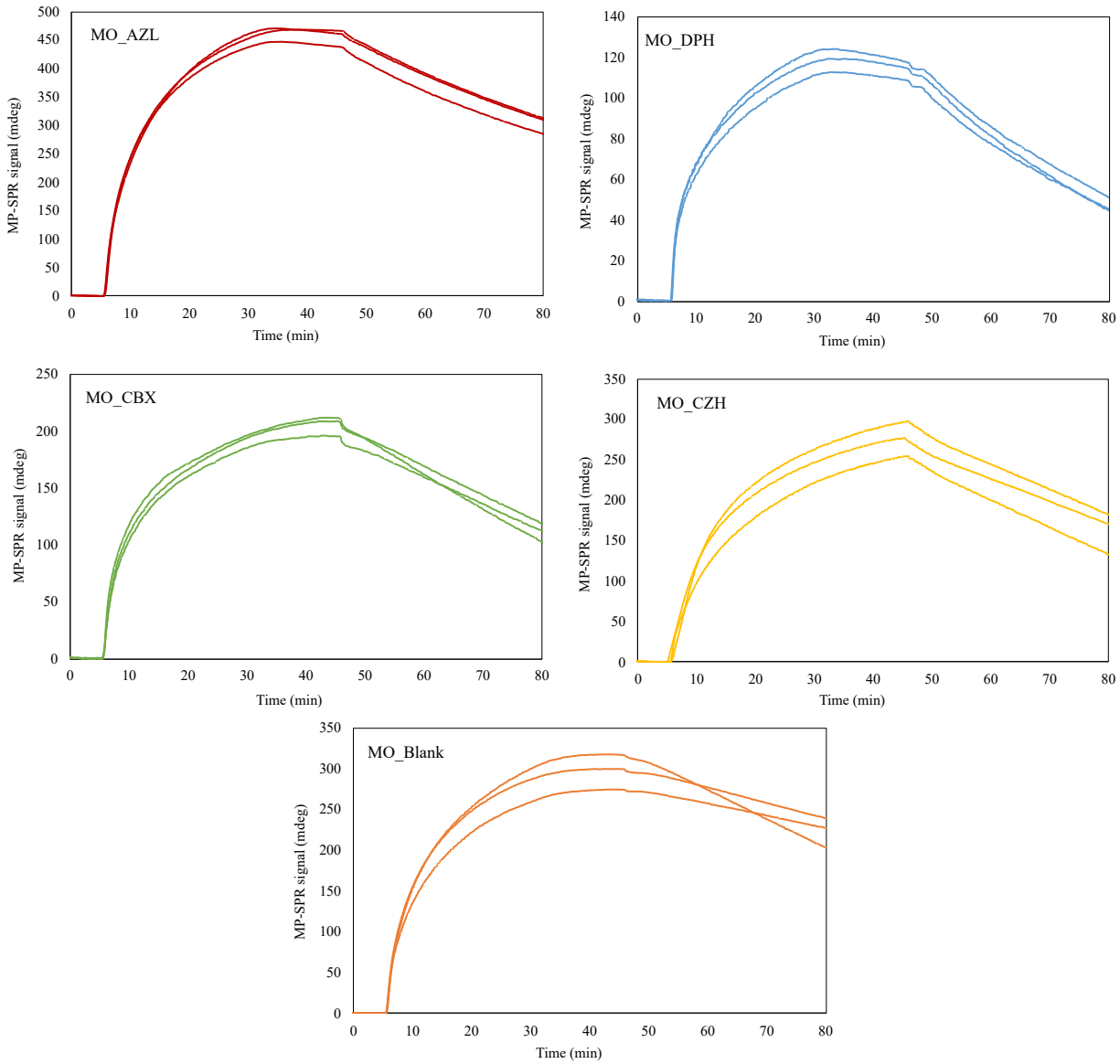

Figure A.4.3. Kinetics of adsorption to mucin as measured by MP-SPR: overlay of triplicate injection for each tested lipid analyte.

A.5. PXRD of antihistamine drugs

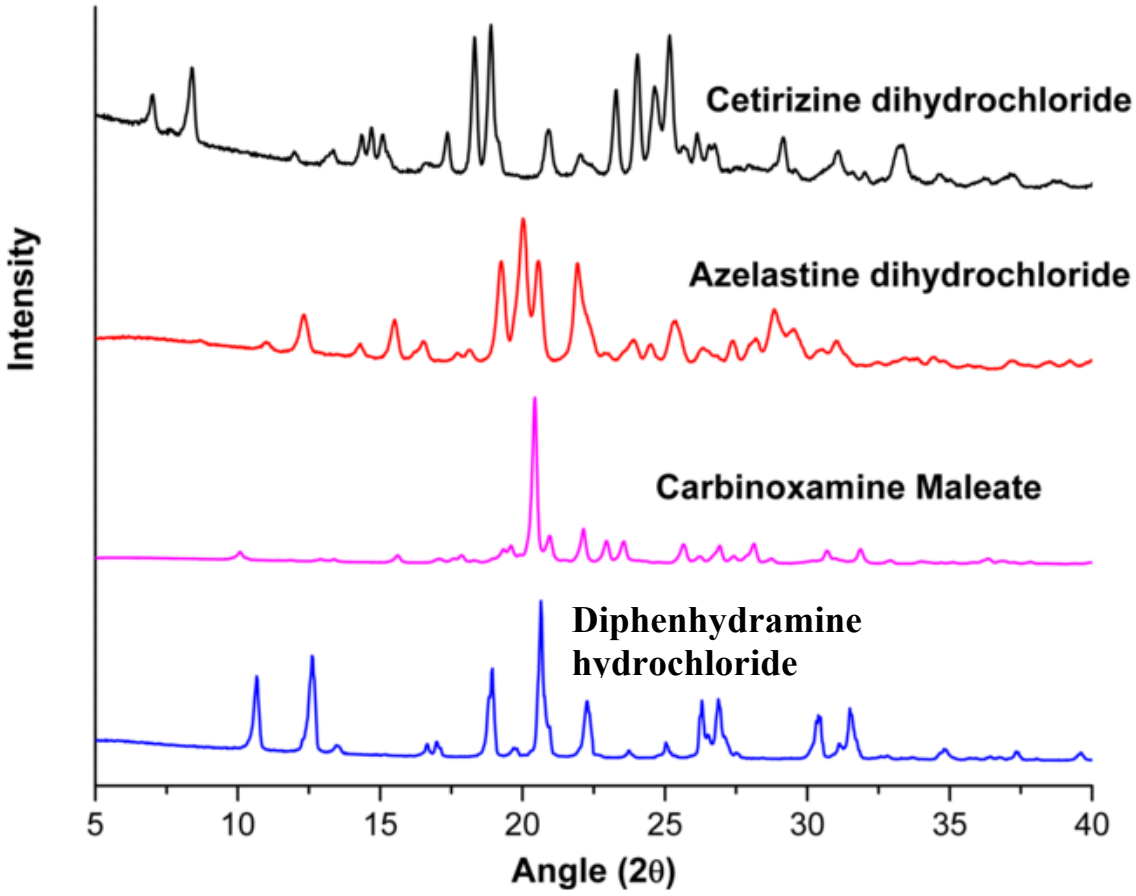

Figure A.5.1. Diffractograms of the as-received antihistamine molecules

A.6. SAXS patterns of antihistamine-loaded LCP

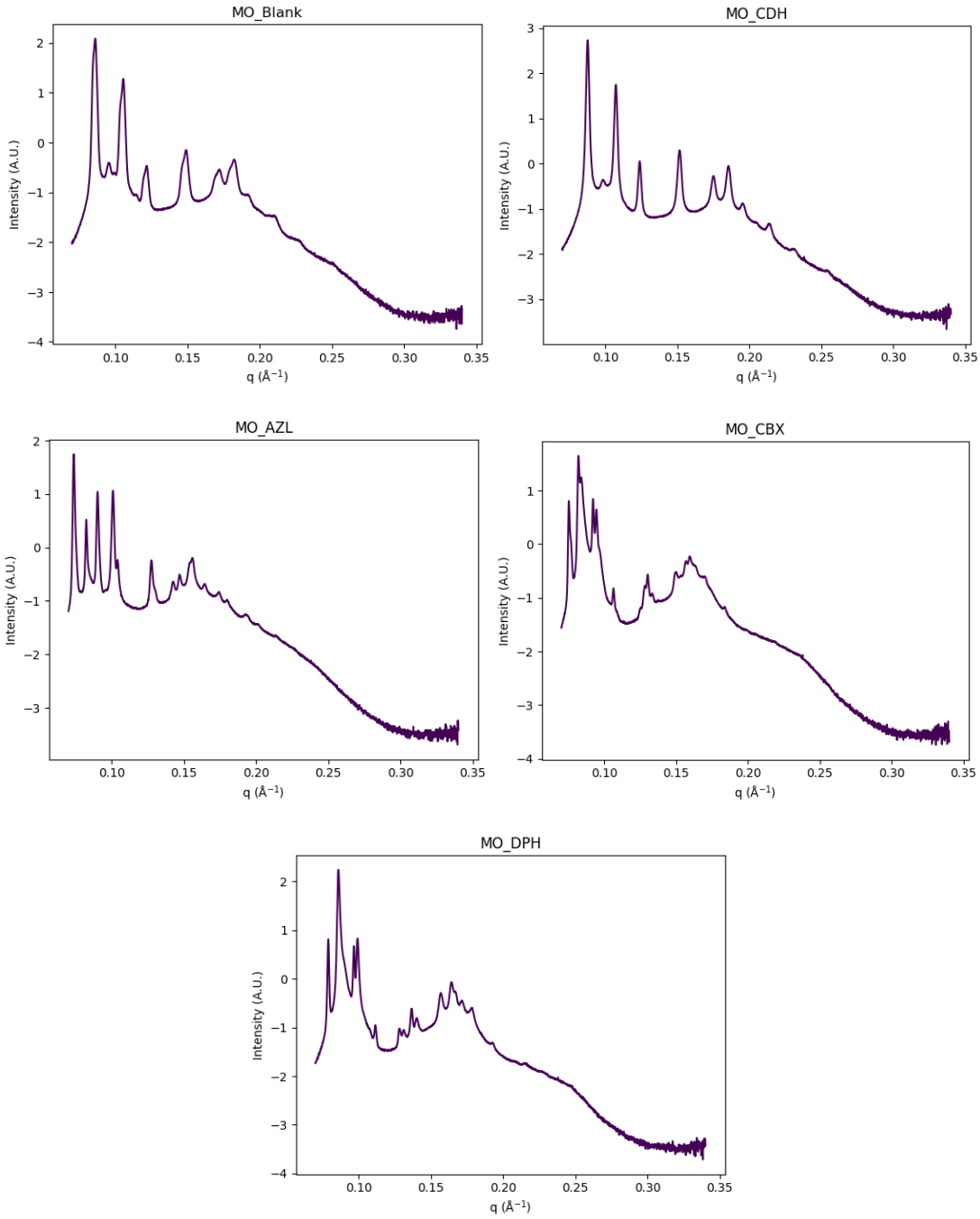

Figure A.6.1. 1D azimuthally integrated SAXS patterns of monoolein (MO) cubic mesophases formulated with or without antihistamines. The peaks of the patterns have been indexed according to the Q_{II}^{D} mesophase.

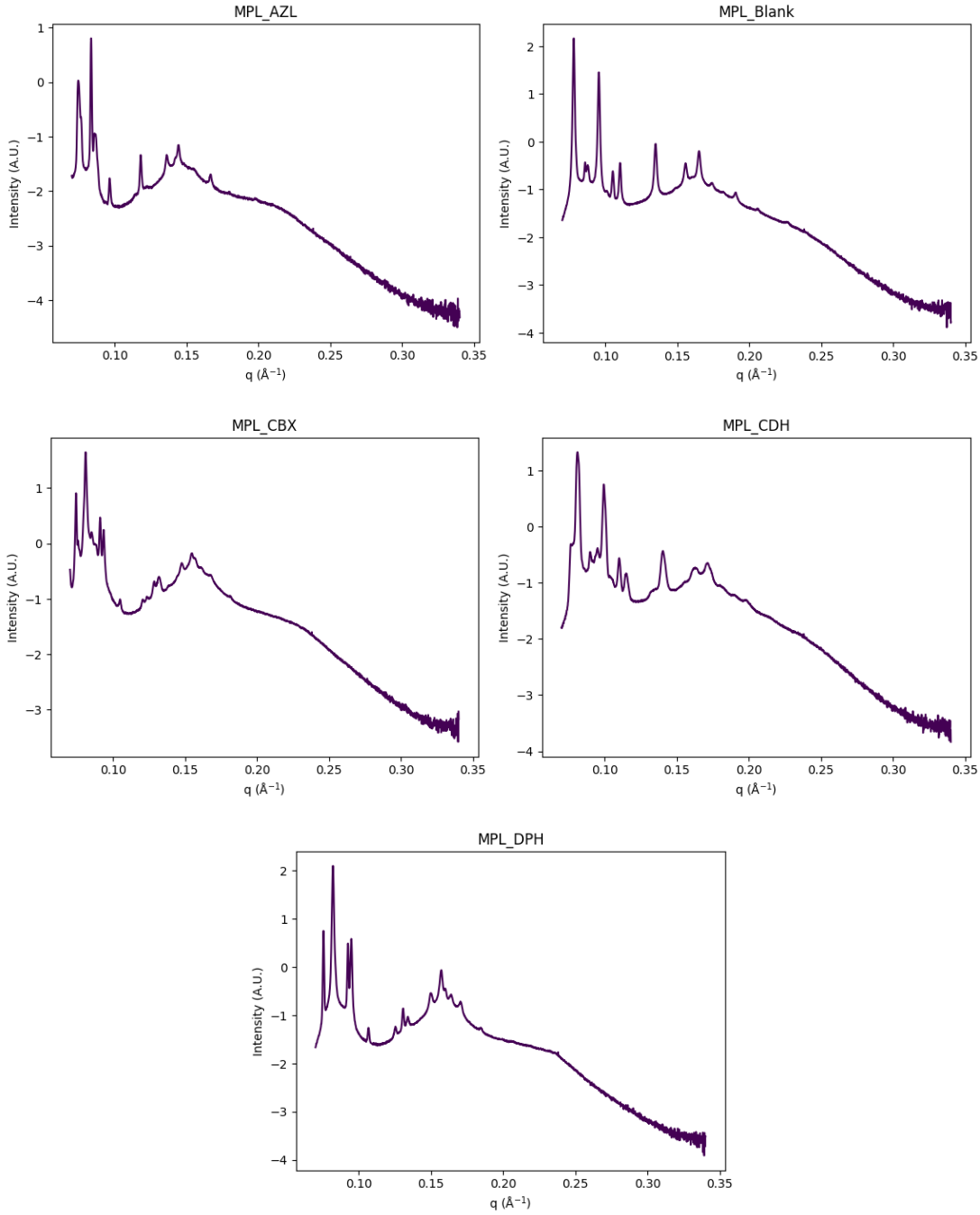

Figure A.6.2. 1D azimuthally integrated SAXS patterns of monopalmitolein (MPL) cubic mesophases formulated with or without antihistamines. The peaks of the patterns have been indexed according to the Q_{II}^{D} mesophase.

Appendix B

Appendix B

Modulating the Release of Pharmaceuticals from Lipid Cubic Phases using a Lipase Inhibitor

Supplementary Information

Chemical interaction schematics

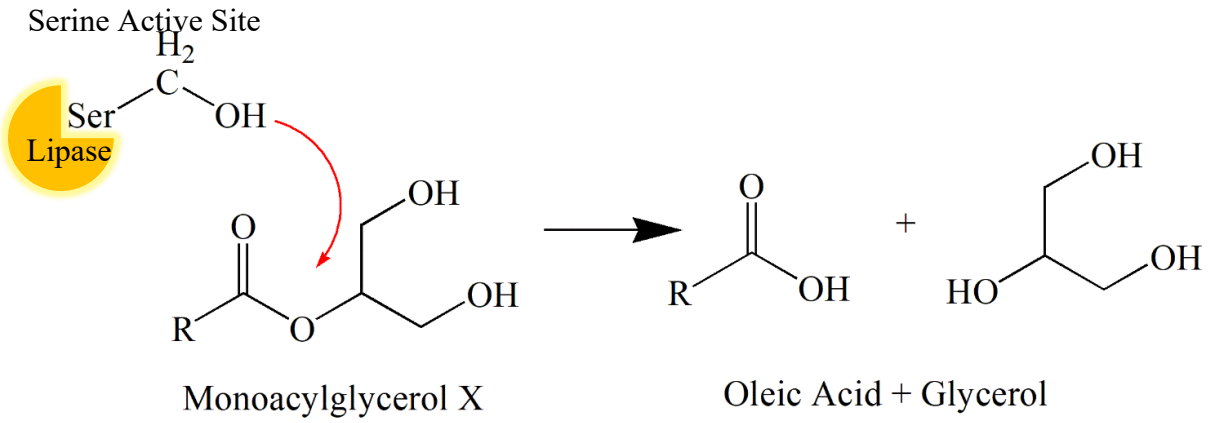

Scheme B.1. Lipase attack on the ester bond present on the Monoacylglycerol lipid chain bridging the oleic acid component to the glycerol backbone breaking the lipid down into its constituents. Adapted from [1].

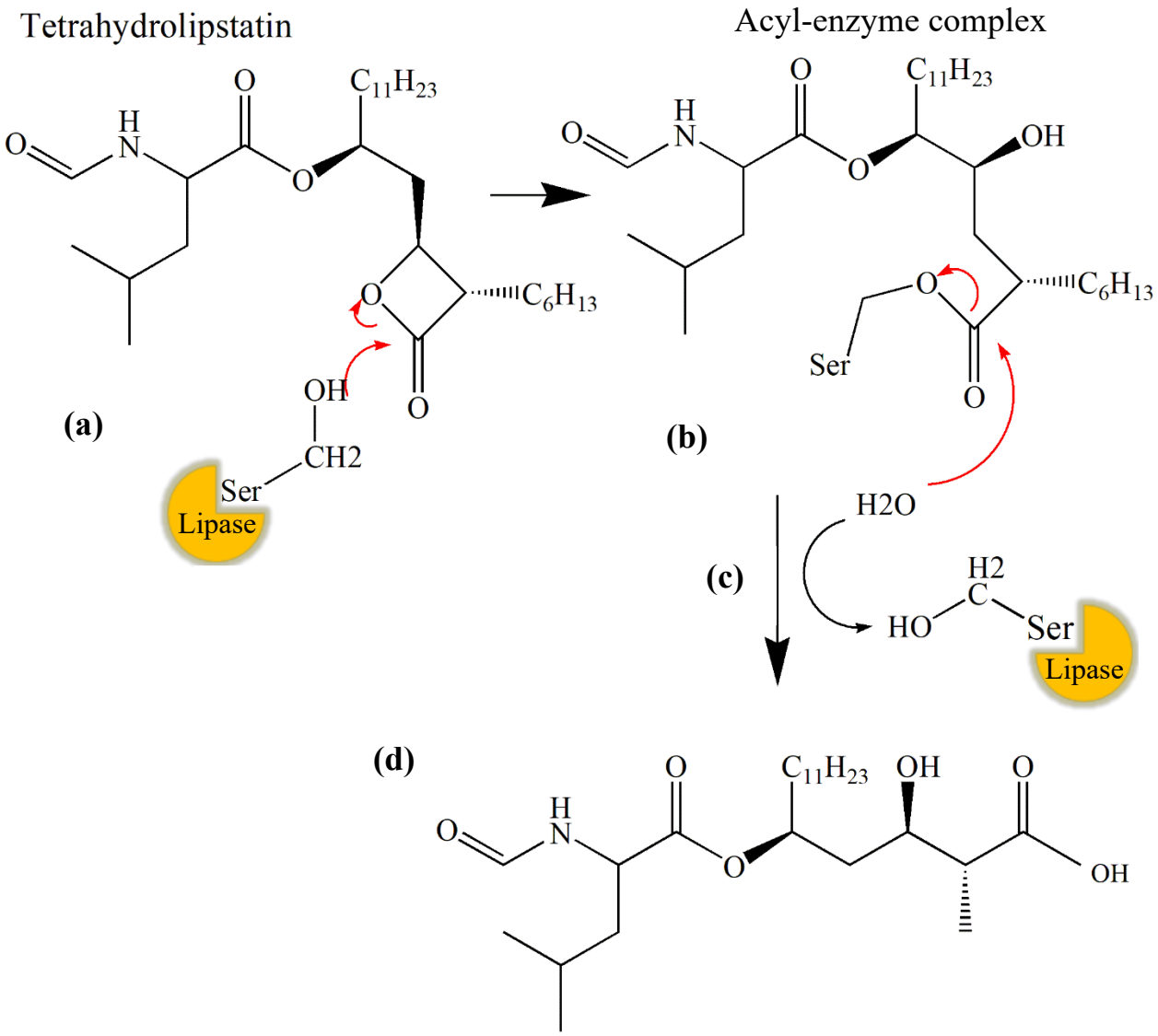

Scheme B.2. Schematic of Tetrahydrolipstatin's reversible inhibitory action on the lipase demonstrating a nucleophilic attack of the β-lactone ring of THL by the serine residue at the lipase active site (a) producing an inactive acyl-enzyme complex product (b). Ultimately, hydrolysis of this covalent linkage frees the active enzyme (c) resulting in a carboxylic acid which may then be isomerised into various isomers (d) [2]. Adapted from [2-5].

Scattering Patterns

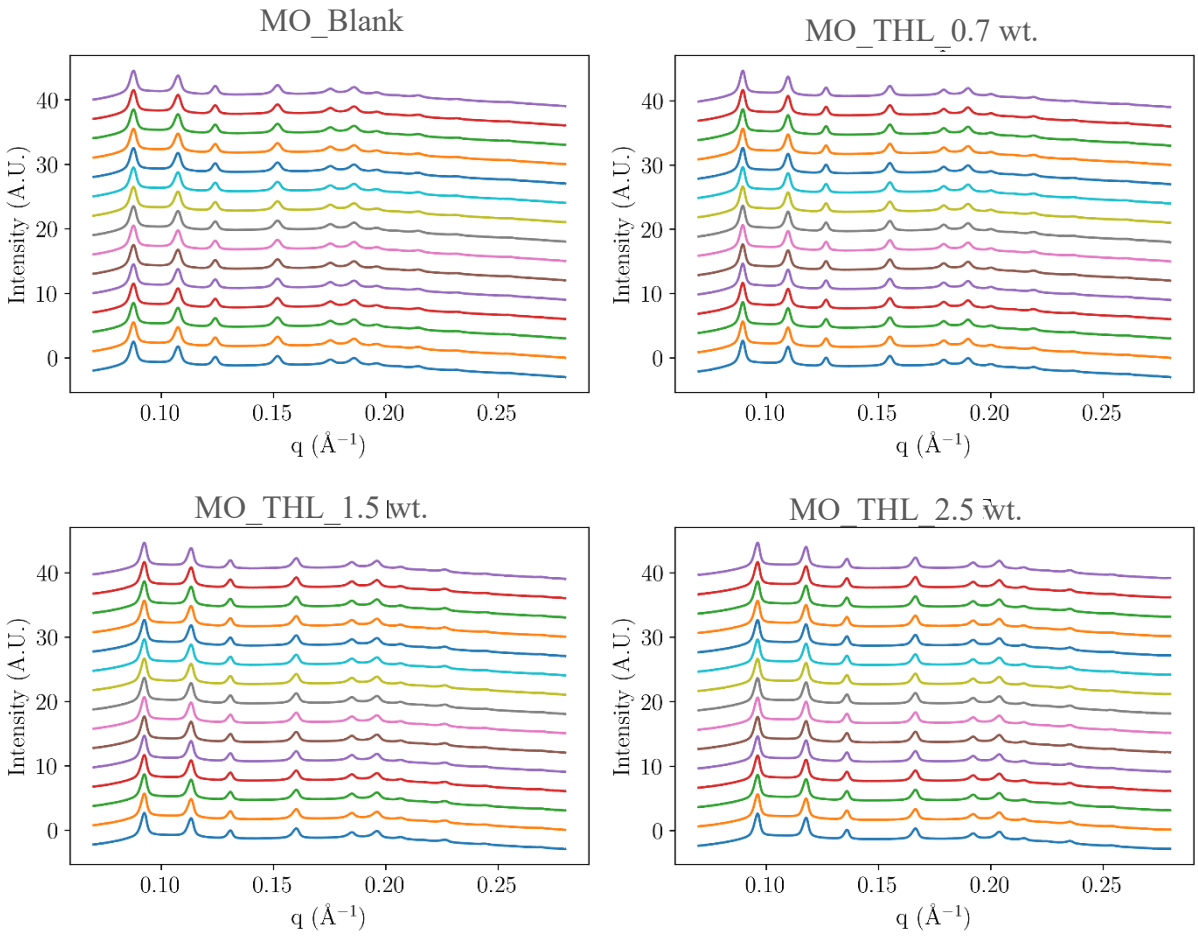

Figure B.1. 1D azimuthally integrated SAXS patterns of fresh monoolein blank/THL loaded cubic mesophases. Repetitions recorded sequentially demonstrate no impact on the phase from radiation exposure at a single location. Patterns are plotted from first scan at the bottom to last scan at the top.

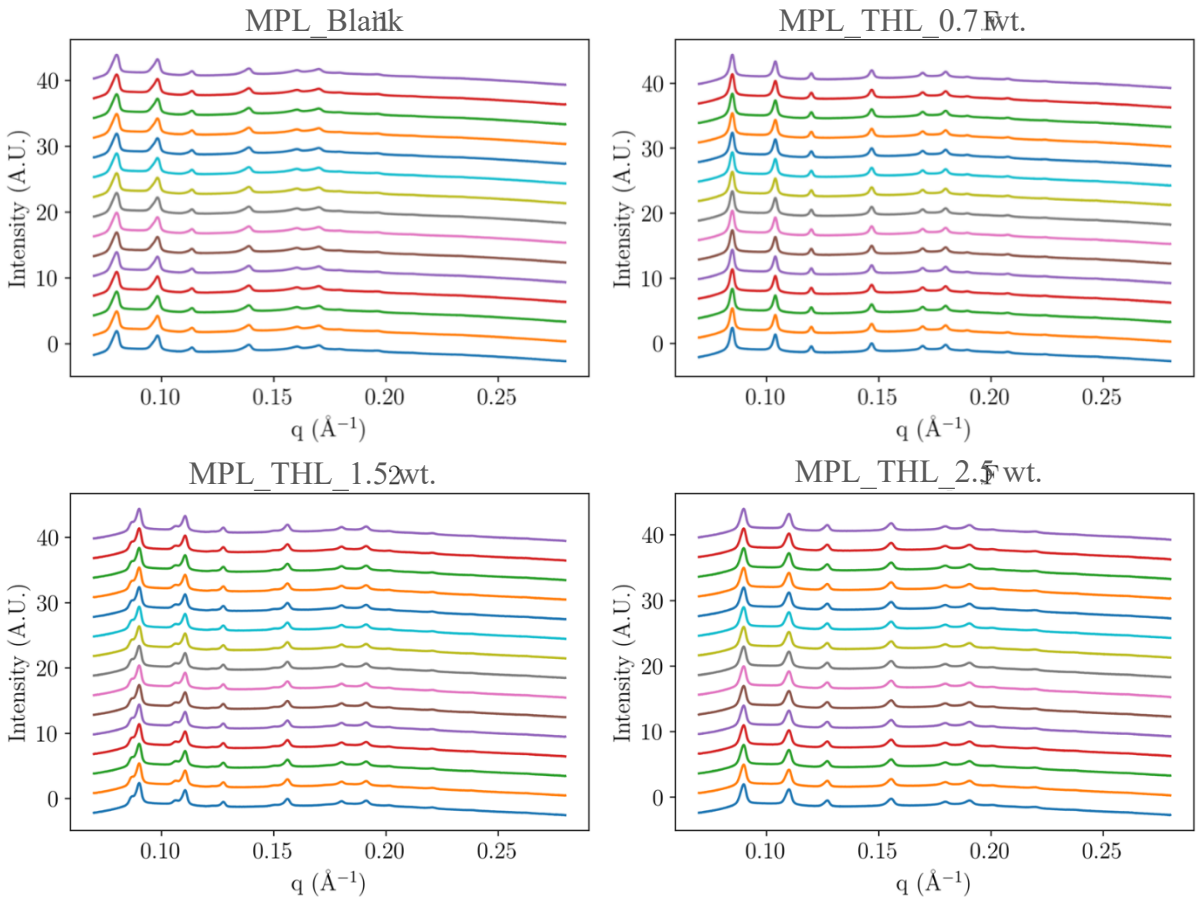

Figure B.2. 1D azimuthally integrated SAXS patterns of fresh monopalmitolein blank/THL loaded cubic mesophases. Repetitions recorded sequentially demonstrate no impact on the phase from radiation exposure at a single location. Patterns are plotted from first scan at the bottom to last scan at the top.

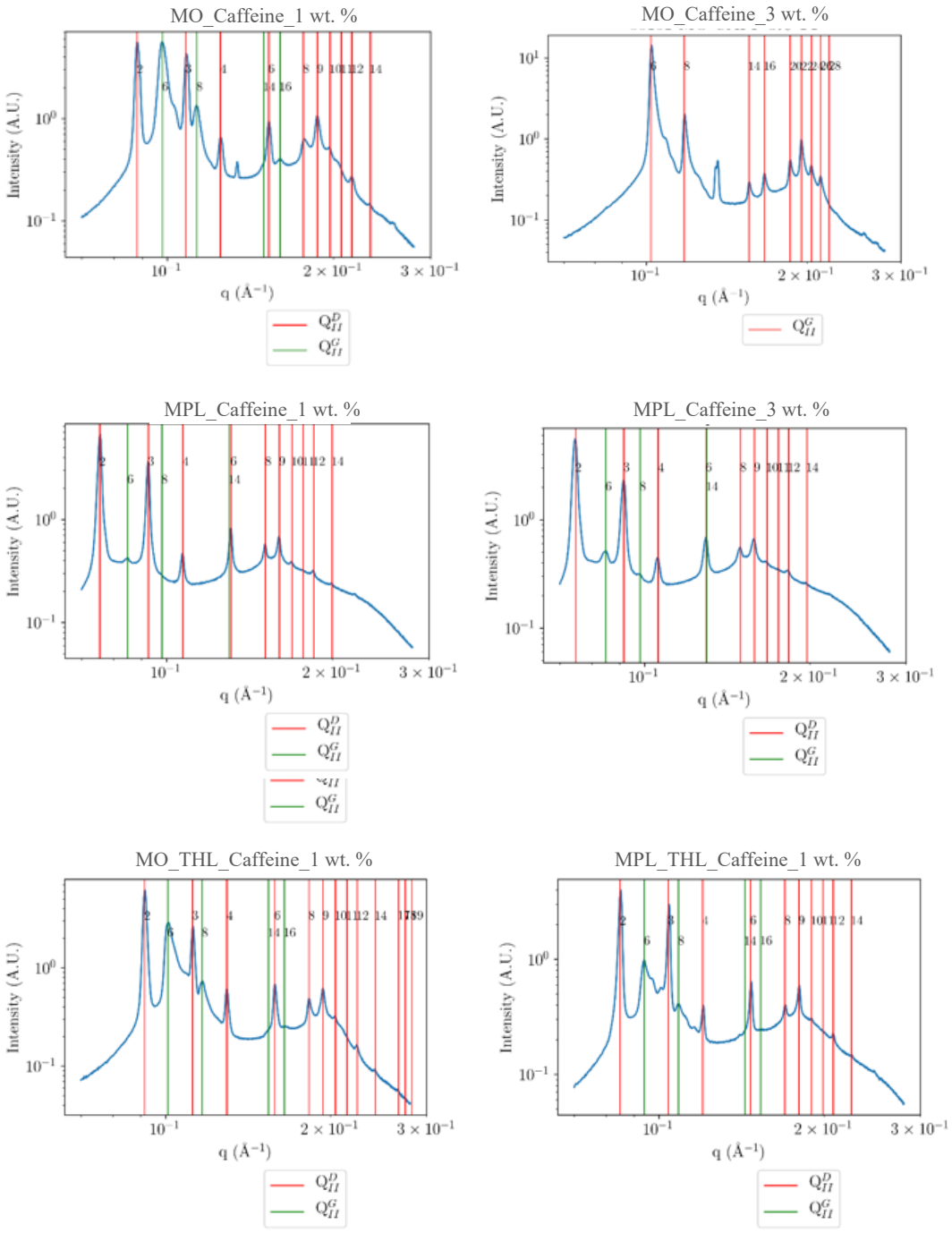

Figure B.3. 1D azimuthally integrated SAXS patterns of fresh monoolein and monopalmitolein caffeine loaded cubic mesophases with/without THL. Vertical lines indicate the position of the peaks of the mesophase(s) present in the system as detailed in the legend, with the squares of the

indices at each line corresponding to a Miller plane from the space group. Q_{II}^{D} indicates a Diamond cubic phase and Q_{II}^{G} the Gyroid phase.

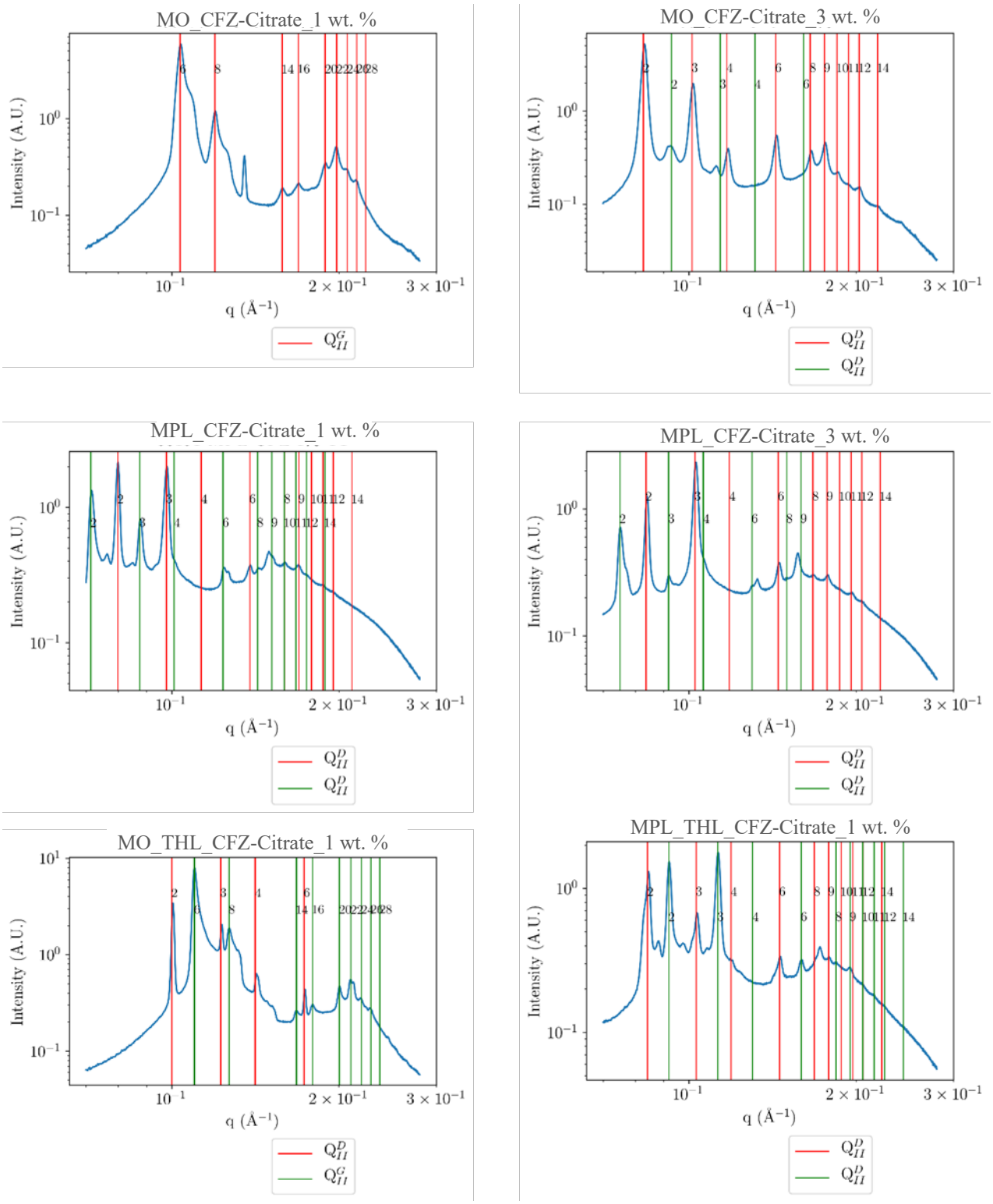

Figure B.4. 1D azimuthally integrated SAXS patterns of fresh monoolein and monopalmitolein clofazimine citrate loaded cubic mesophases with/without THL. Vertical lines indicate the position of the peaks of the mesophase(s) present in the system as detailed in the legend, with the squares

of the indices at each line corresponding to a Miller plane from the space group. Q_{II}^{D} indicates a Diamond cubic phase and Q_{II}^{G} the Gyroid phase.

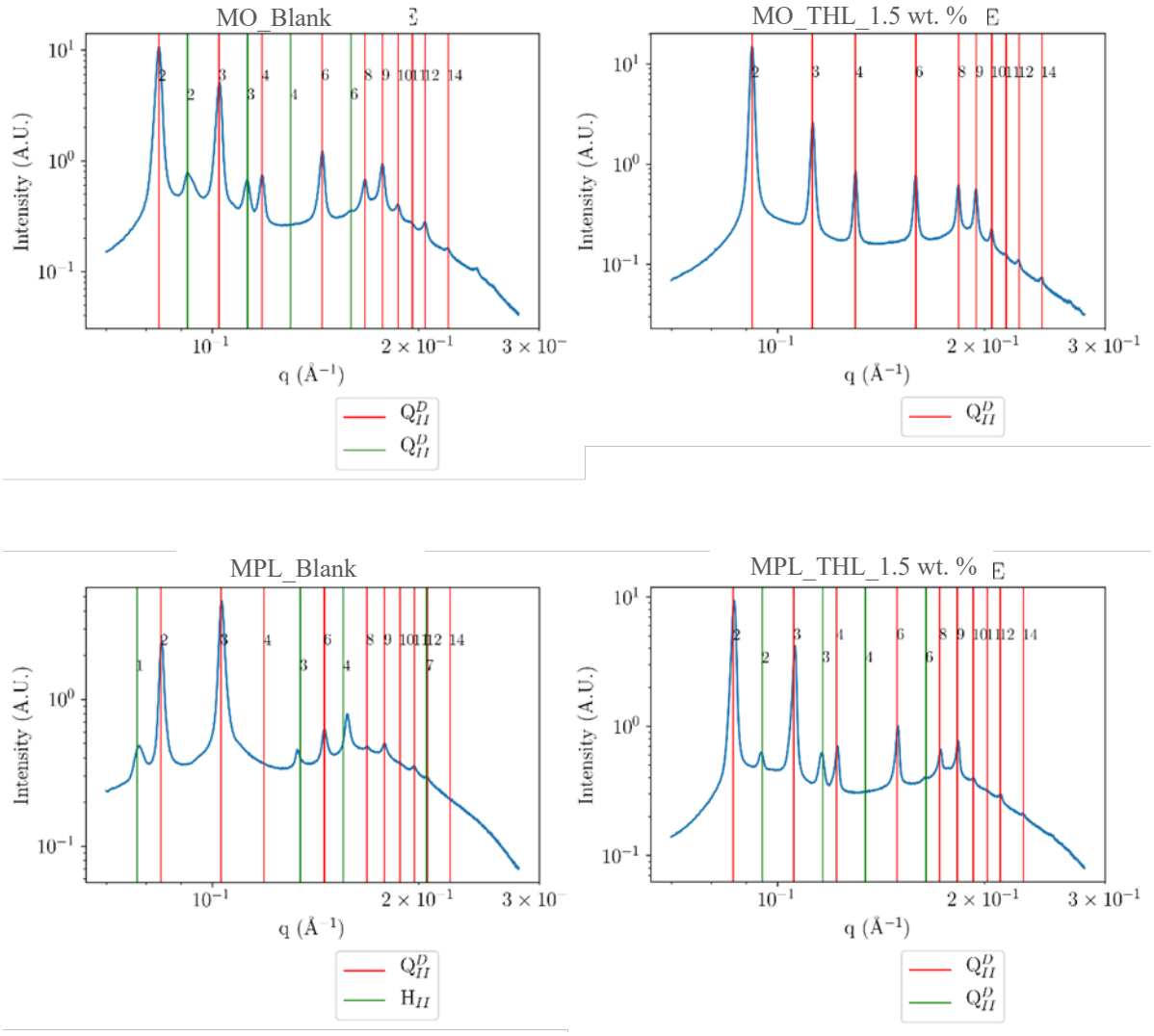

Figure B.5. 1D azimuthally integrated SAXS patterns of fresh monoolein and monopalmitolein cubic mesophases with/without THL showing the impact of lipase exposure on the phase. Vertical lines indicate the position of the peaks of the mesophase(s) present in the system as detailed in the legend, with the squares of the indices at each line corresponding to a Miller plane from the space group. Q_{II}^{D} indicates a Diamond cubic phase and Q_{II}^{G} the Gyroid phase.

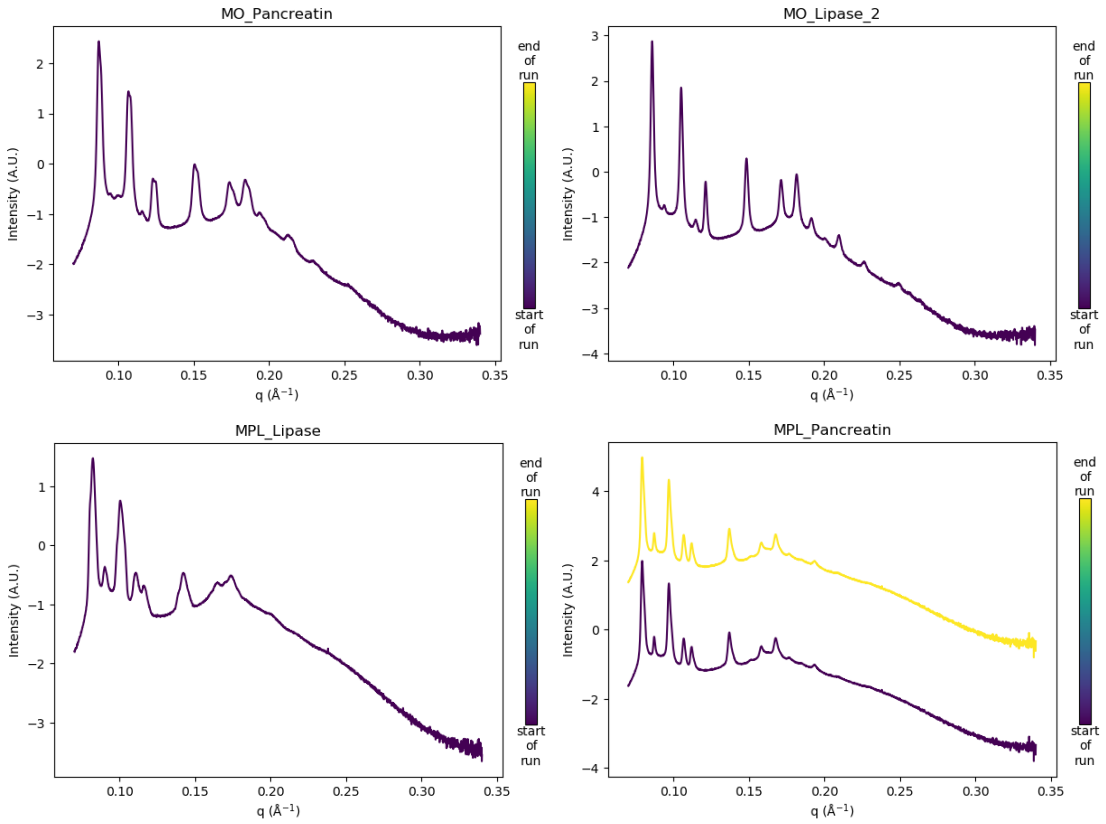

Figure B.6. 1D azimuthally integrated SAXS patterns of monoolein (MO) and monopalmitolein (MPL) cubic mesophases swelled in a variety of bio-relevant media of varied pH. The peaks of the patterns have been indexed according to the Q_{II}^{D} mesophase

Drug release studies

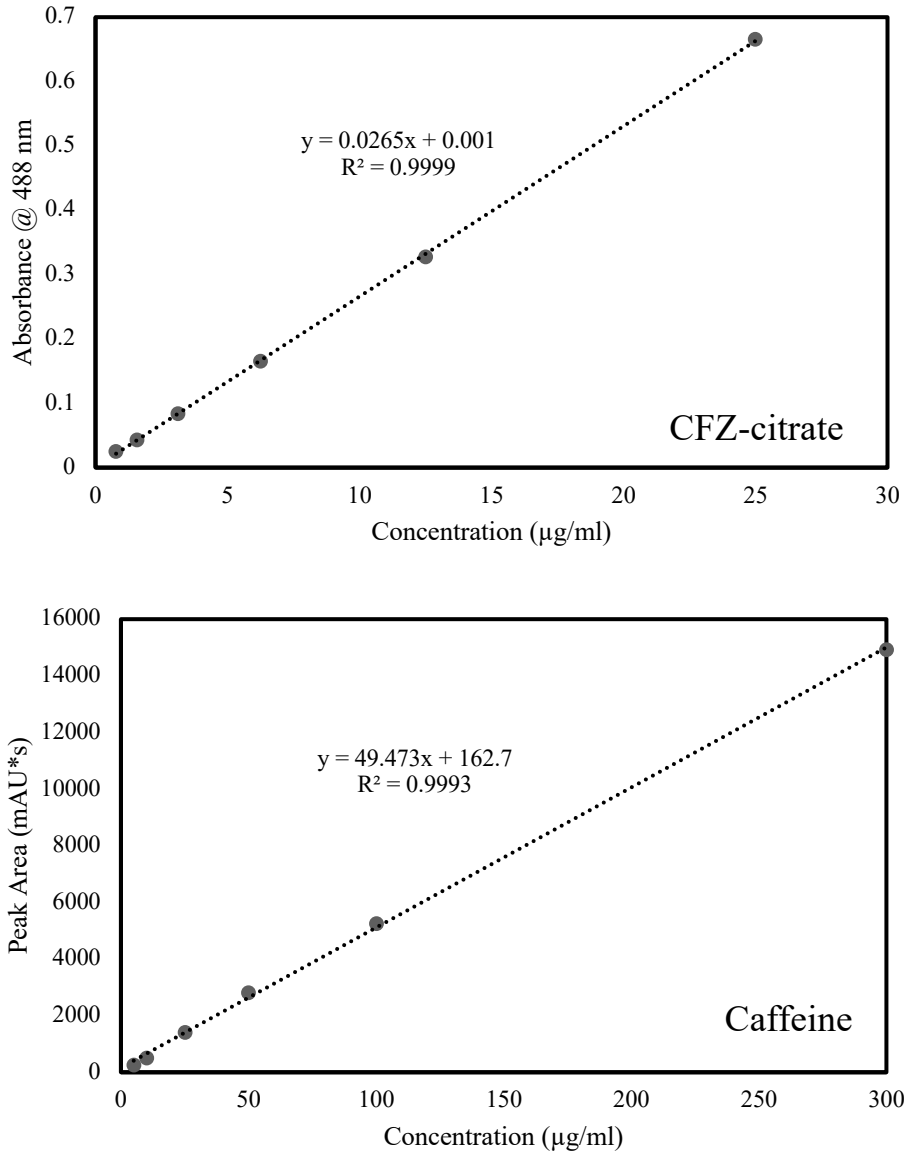

Figure B.7. Calibration curves for CFZ-citrate and caffeine obtained by UV-Vis spectroscopy and HPLC respectively

Mathematical model plots for kinetics of release of CFZ-citrate

Table B.1. Release kinetic modelling of CFZ-citrate from LCP gels

Gel Sample	Calculated R^2 Values for CFZ-citrate Release					
	Zero Order	First Order	Higuchi	Hixson Crowell	Korsmeyer-Peppas	Diffusion Coefficient for Korsmeyer-Peppas (n)
MO	0.949	0.778	0.827	0.851	0.938	0.641
MO_THL	0.885	0.896	0.955	0.893	0.945	0.517
MPL	0.905	0.724	0.792	0.804	0.976	0.783
MPL_THL	0.97	0.951	0.897	0.959	0.971	0.58

Drug release from the cubic phase is usually diffusion-controlled and follows square root of time kinetics. This is shown by a linear relationship between the cumulative % of drug released and the square root of time (Higuchi model) for all of the LCP formulations. This is indicated by the relatively high correlation coefficient values. The linear relationship was stronger in the case of those samples prepared with the enzyme inhibitor where the correlation coefficient was closer to unity (0.897 and 0.955). The method describes a rate of release in a case where the drug loading in the matrix exceeds that of its solubility in a given media.

Carrier systems that obey zero-order kinetics are considered gold-star in terms of their prolonged release capabilities. When the release data was fitted to the zero-order kinetic equation (cumulative % of drug released versus time), the relatively high r2 values suggested that the release kinetics from the system followed the zero-order model releasing CFZ-citrate at a constant rate per unit time, while the dissolution results were found not to fit as well with first order kinetics in the case of the gels in the absence of THL. This highlights the potential of the THL as a controlled release mediator underpinned of course by its ability to maintain an in-tact matrix for a greatly extended period of time.

Furthermore, to reiterate the hypothesis that erosion of the gels had a part to play in the release kinetics, and could be controlled by the introduction of THL, the data was fitted to the Hixson-Crowell model (cube root % total drug - cube root of % unreleased drug v time (min)) which describes diffusion controlled release that is partly influenced by the change in size of the matrix system. The correlation coefficients were relatively high in the cases of all formulations (0.8 to 0.96), again slightly higher in those containing THL. The linear relationships observed confirm that the digestion of the gels likely influenced the release of the CFZ-citrate salt from the phase.

The data was then fitted to a Korsemeyer-Peppas model. The diffusion coefficients for all formulations was estimated from the linear regression of the Korsmeyer-Peppas model. This allows for further confirmation of the contribution of gel erosion to the release of CFZ-citrate upon determination of the diffusion coefficient (n). All formulations, showed coefficient values larger than 0.45. This would indicate an anomalous non-fickian diffusion transport that is both diffusion and swelling/erosion controlled. In this case, an $n \leq 0.45$ indicates a Fickian diffusion mechanism and $0.45 < n < 0.89$ corresponds to non-Fickian transport [6]. The diffusion coefficient is generally larger for those release systems driven by the erosion of the matrix, compared to the observed n values less than 0.89 indicative of diffusive release ([7]. Incorporating THL resulted in a decrease of the averaged diffusion coefficient of CFZ embedded in the LCP systems as expected, as the degradation of the phase was slow and thus it was possible for the drug to penetrate the aqueous channels and be released into the sink.

MO_THL_CFZ-citrate

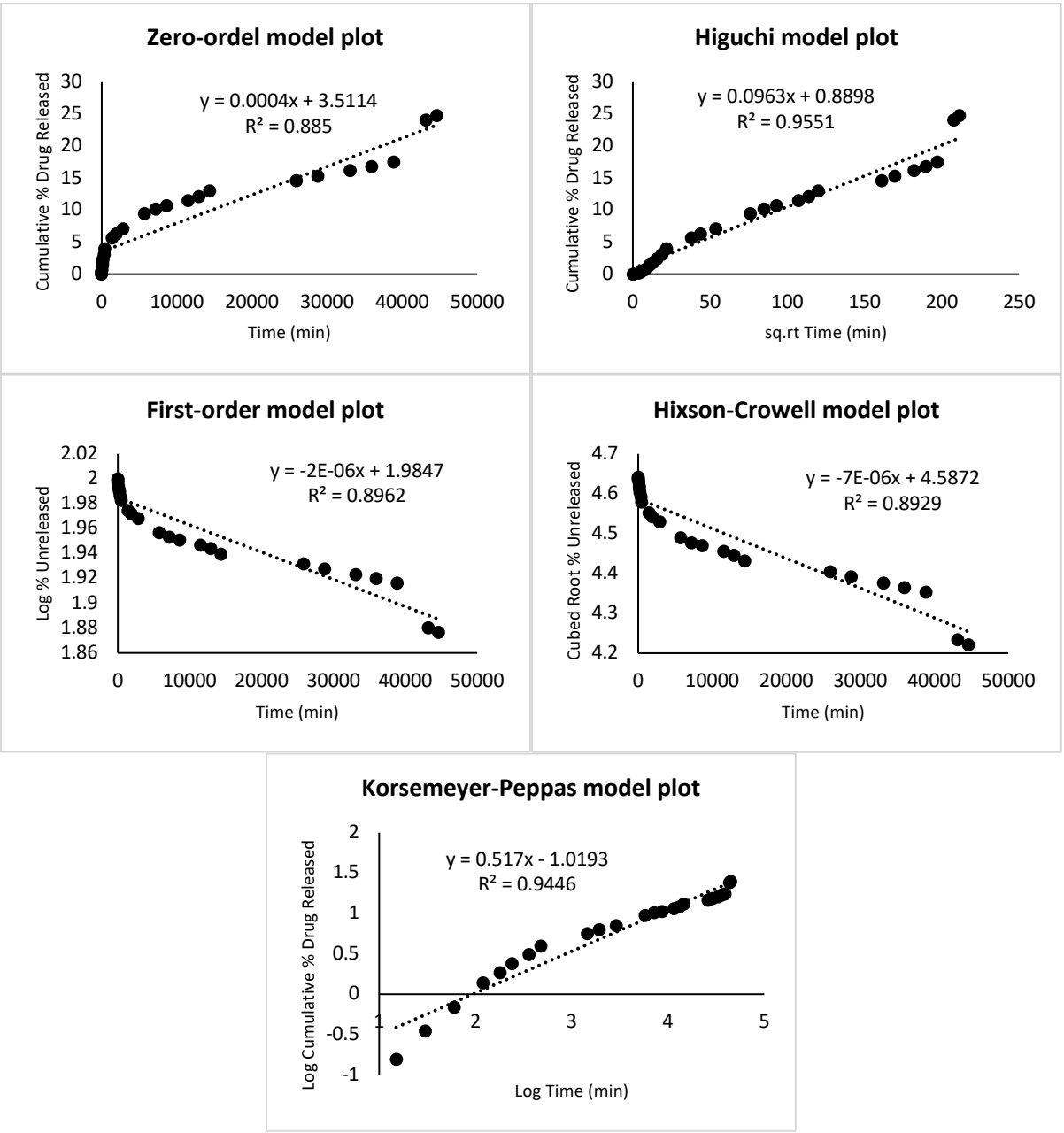

Figure B.8. Kinetic model plots for the release of CFZ-citrate from monoolein LCP formulated with 1.5 wt. % THL in the presence of Lipase fitted to different mathematical models

MO_CFZ-citrate

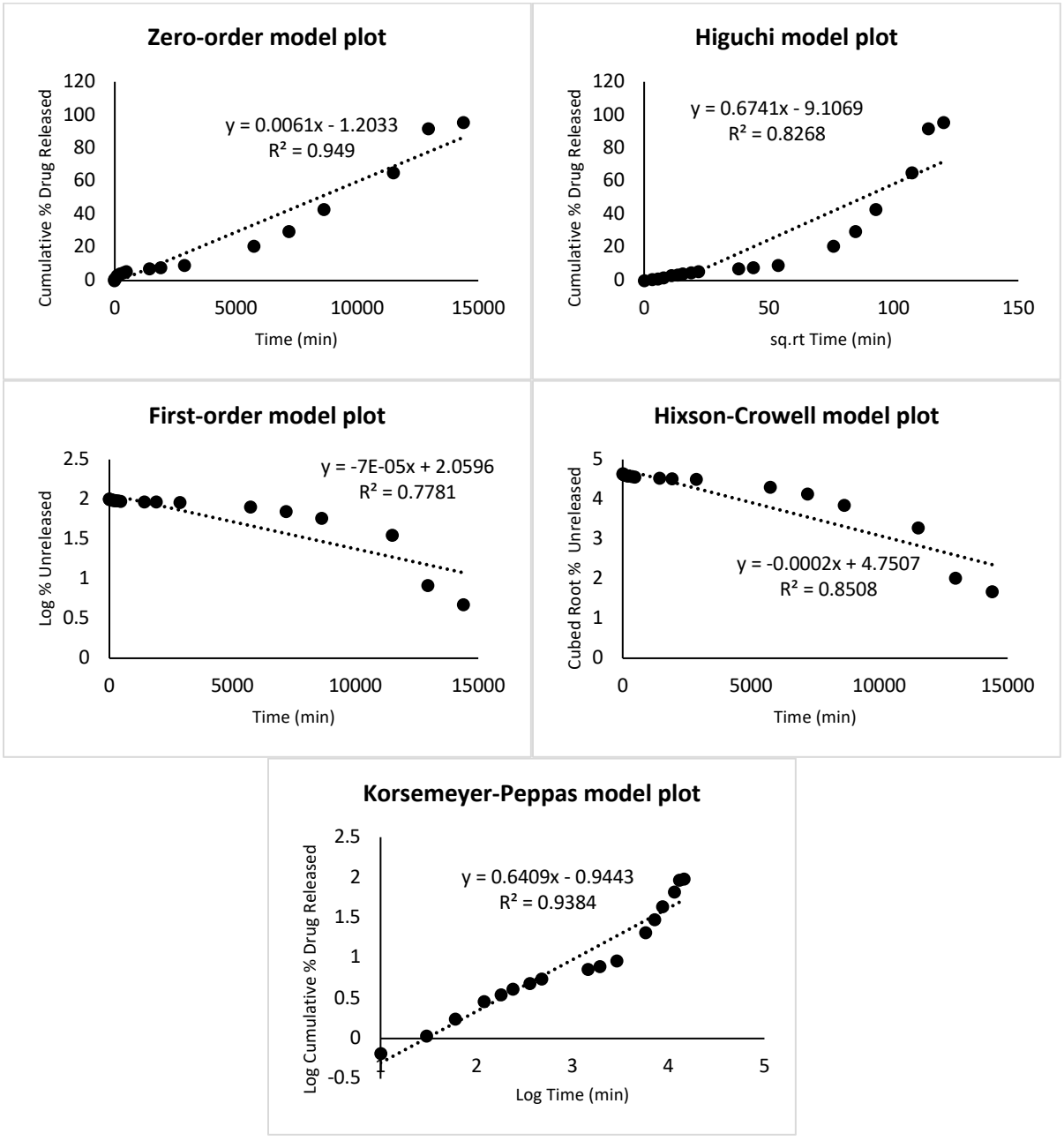

Figure B.9. Kinetic model plots for the release of CFZ-citrate from monoolein LCP in the presence of Lipase fitted to different mathematical models

MPL_THL_CFZ-citrate

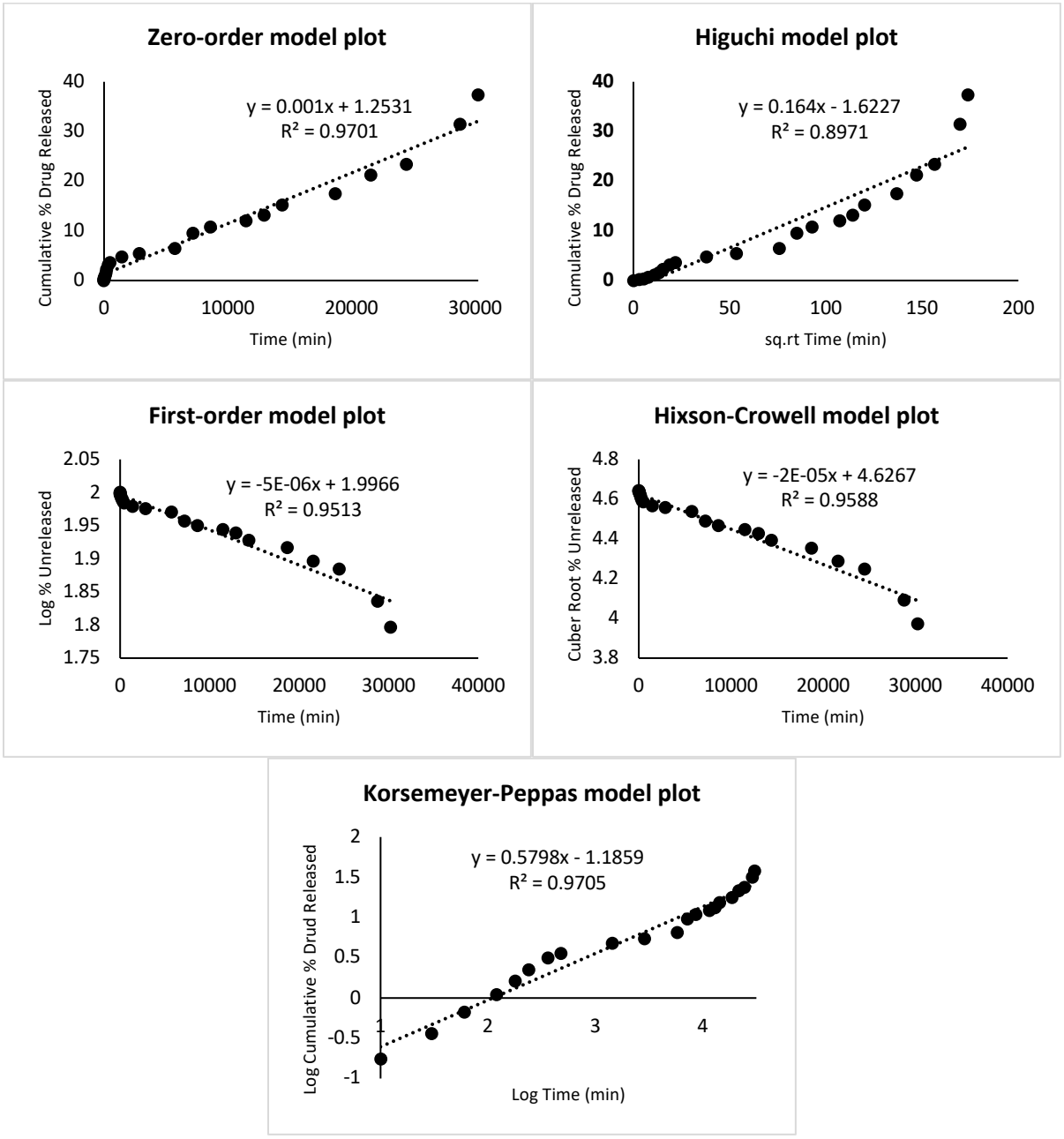

Figure B.10. Kinetic model plots for the release of CFZ-citrate from monopalmitolein LCP formulated with 1.5 wt. % THL in the presence of Lipase fitted to different mathematical models

MPL_CFZ-citrate

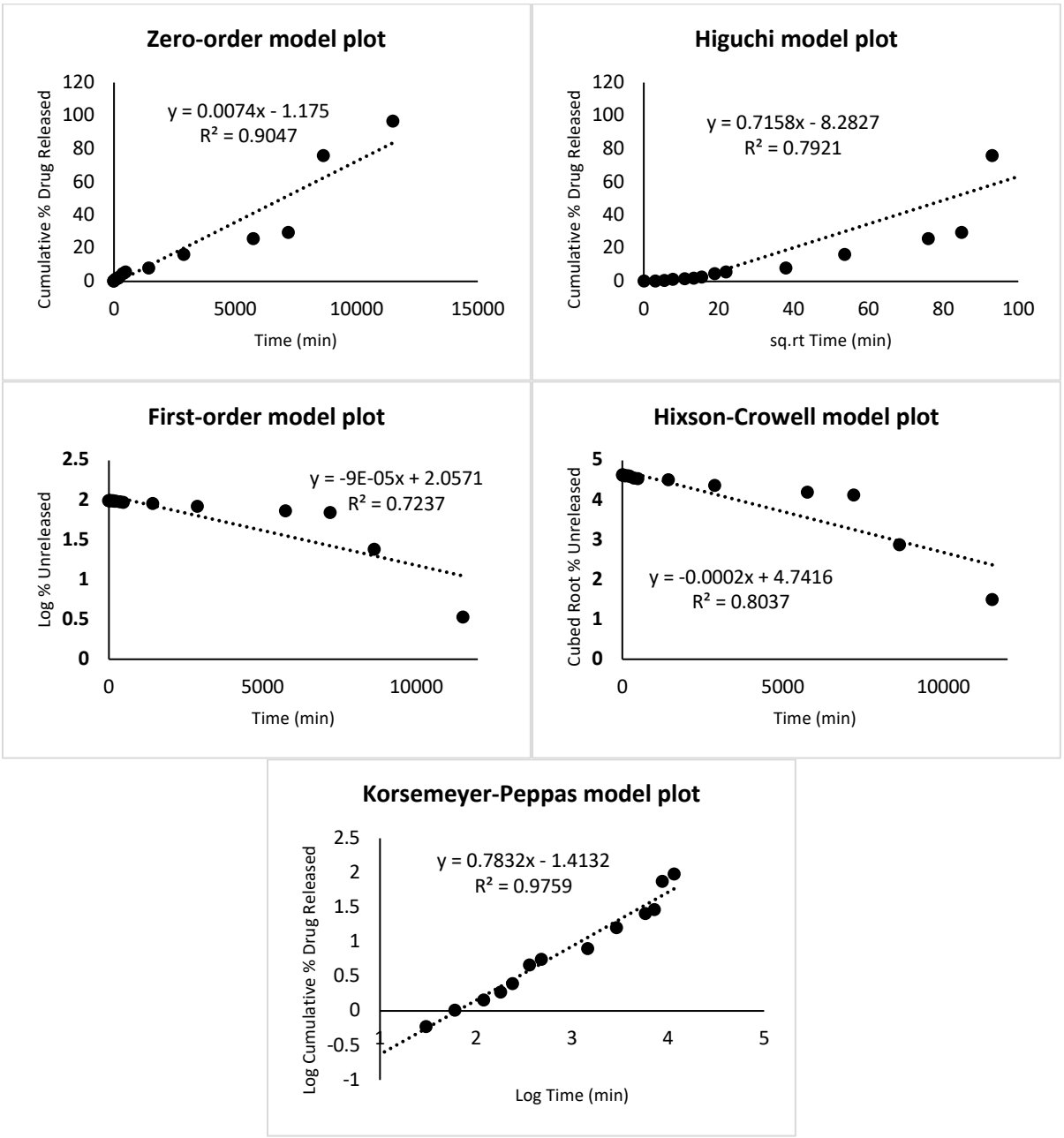

Figure B.11. Kinetic model plots for the release of CFZ-citrate from monopalmitolein LCP THL in the presence of Lipase fitted to different mathematical models

Mathematical model plots for kinetics of release of caffeine

Table B.2. Release kinetic modelling of caffeine from LCP gels

Gel Sample	Calculated R^2 Values for Caffeine Release from T_0 to T_8 (h)					
	Zero Order	First Order	Higuchi	Hixson Crowell	Korsmeyer -Peppas	Diffusion Coefficient for Korsmeyer-Peppas (n)
MO	0.761	0.96	0.955	0.905	0.917	0.44
MO_THL	0.3961	0.952	0.901	0.875	0.943	0.274
MPL	0.508	0.341	0.805	0.79	0.75	0.208
MPL_THL	0.495	0.903	0.797	0.762	0.894	0.163

The Higuchi square root of time release kinetics defines the release of pharmaceuticals from the cubic phase [8]. The Higuchi equation is based on a pseudo-steady-state approach and provides a mathematical means of demonstrating a direct proportionality between the total quantity of released drug and the square root of time, allowing one to understand the release mechanism of a material [9]. An exchange of water from the media into the internal matrix and simultaneous transfer of incorporated drug and water from the matrix to the external environment are the proposed events occurring during hydrophilic drug release from the cubic phase [8]. The calculated r2 values shown here present strong linear relationships between the cumulative % of drug released in the first 8 hours and the square root of time. These results indicate that the caffeine does indeed partitions predominantly into the aqueous channel network from which it diffuses into the media with little influence from the swelling and breakdown of the matrix itself. This data was complemented by fitting the release to a Korsemeyer-Peppas model as previously described. The various formulations yielded n values of ≤ 0.45. This is indicative of the simplest diffusion-controlled process that is a Fickian diffusion mechanism corresponding to Fick's law [6].

In contrast to the kinetics of CFZ release, when the release data from the various Caffeine systems were fitted to the zero-order kinetic equation, the relatively small regression values suggested that the system did not obey the model. However, the dissolution results were found to

have a better fit with first order kinetics. The correlation coefficient in this case was closest to unity suggesting that the release of caffeine from LCP most likely follows first order kinetics. This data strongly confirms the expected diffusion-controlled kinetics. In first-order release, the rate of drug diffusion is dependent on the concentration of the API incorporated in the formulation.

MO_THL_Caffeine

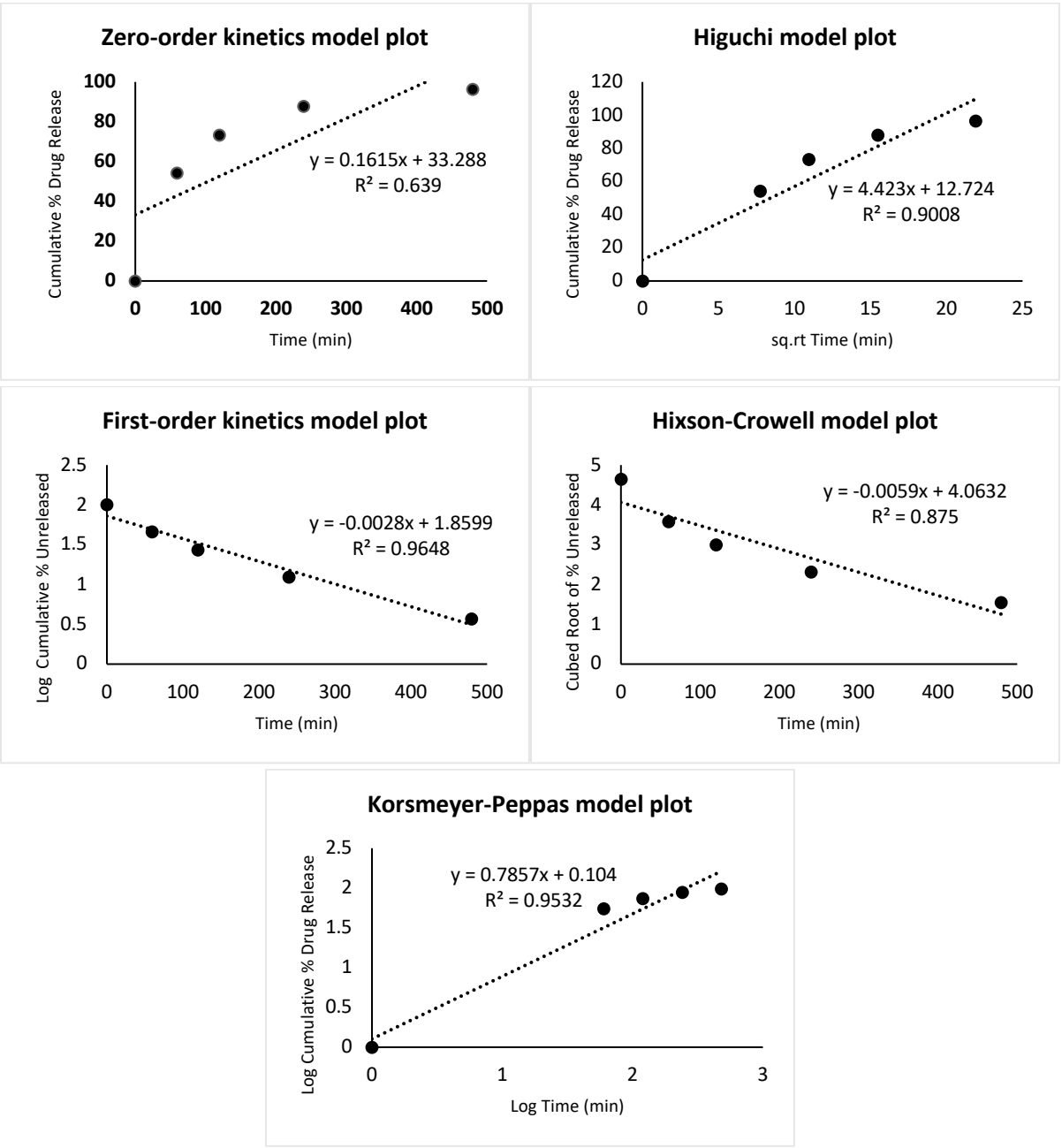

Figure B.12. Kinetic model plots for the release of caffeine from monoolein LCP formulated with 1.5 wt. % THL in the presence of Lipase fitted to different mathematical models

MO_Caffeine

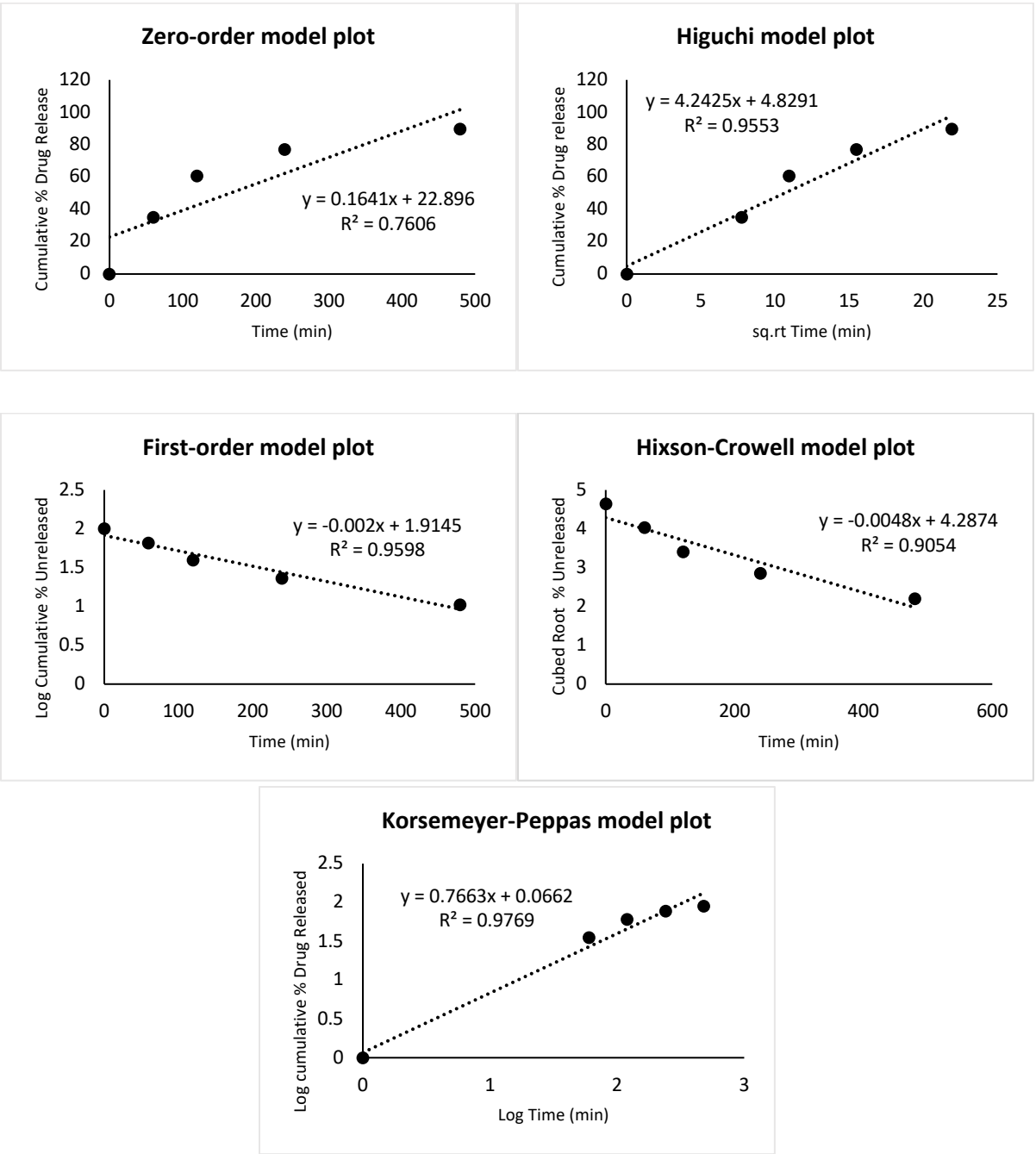

Figure B.13. Kinetic model plots for the release of caffeine from monoolein LCP in the presence of Lipase fitted to different mathematical models

MPL_THL_Caffeine

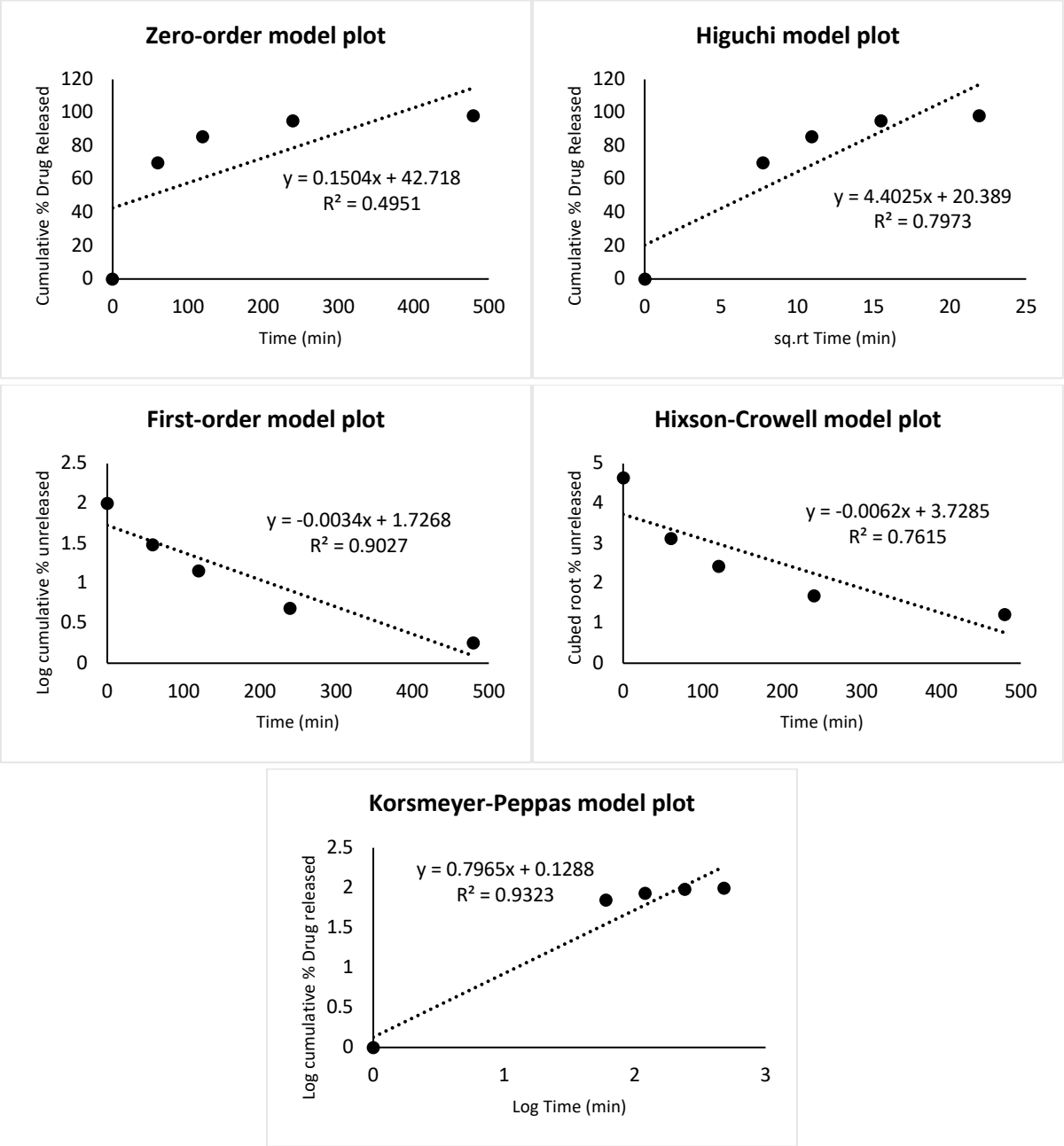

Figure B.14. Kinetic model plots for the release of caffeine from monopalmitolein LCP formulated with 1.5 wt. % THL in the presence of Lipase fitted to different mathematical models

MPL_B_Caffeine

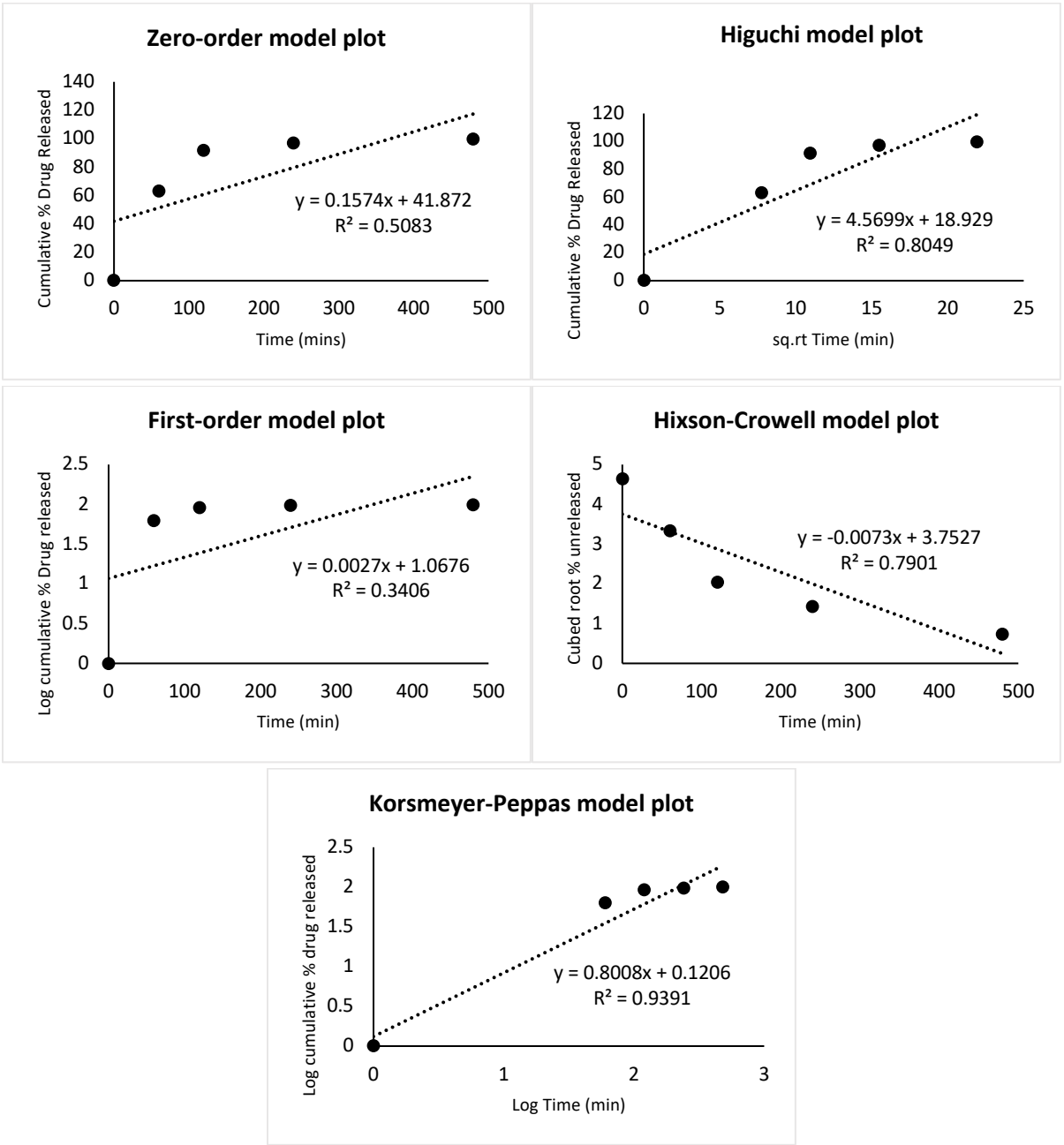

Figure B.15. Kinetic model plots for the release of caffeine from monopalmitolein LCP in the presence of Lipase fitted to different mathematical models

Appendix B references

1. Chang, J.W., et al., Highly selective inhibitors of monoacylglycerol lipase bearing a reactive group that is bioisosteric with endocannabinoid substrates. Chemistry & biology, 2012. 19(5): p. 579-588.

2. Bénarouche, A., et al., Using the reversible inhibition of gastric lipase by Orlistat for investigating simultaneously lipase adsorption and substrate hydrolysis at the lipid–water interface. Biochimie, 2014. 101: p. 221-231.

3. Borgström, B., Mode of action of tetrahydrolipstatin: a derivative of the naturally occurring lipase inhibitor lipstatin. Biochimica et Biophysica Acta (BBA)-Lipids and Lipid Metabolism, 1988. 962(3): p. 308-316.

4. Stalder, H., G. Oesterhelt, and B. Borgström, Tetrahydrolipstatin: Degradation products produced by human carboxyl-ester lipase. Helvetica chimica acta, 1992. 75(5): p. 1593-1603.

5. Stalder, H., P.R. Schneider, and G. Oesterhelt, Tetrahydrolipstatin: thermal and hydrolytic degradation. Helvetica Chimica Acta, 1990. 73(4): p. 1022-1036.

6. Nazaruk, E., et al., Design and assembly of pH-sensitive lipidic cubic phase matrices for drug release. Langmuir, 2014. 30(5): p. 1383-1390.

7. Siepmann, J. and N. Peppas, Modelling of drug release from delivery systems based on hydroxypropyl methylcellulose (HPMC). Advanced drug delivery reviews, 2012. 64: p. 163-174.

8. Shah, J.C., Y. Sadhale, and D.M. Chilukuri, Cubic phase gels as drug delivery systems. Advanced Drug Delivery Reviews, 2001. 47(2-3): p. 229-250.

9. Siepmann, J. and N.A. Peppas, Higuchi equation: derivation, applications, use and misuse. International journal of pharmaceutics, 2011. 418(1): p. 6-12.

Appendix C

Appendix C

Probing the mechanism behind inhibitor-controlled degradation of lipid cubic formulations

Supplementary Information

Michele Dully[1], Shayon Bhattacharya[2], Vivek Verma[1], Damien Thompson[2], Tewfik Soulimane[1], Sarah P. Hudson[1,*]

[1] Department of Chemical Sciences, Faculty of Science & Engineering, Bernal Institute, University of Limerick, Castletroy, Co. Limerick, Ireland

[2] Department of Physics, Faculty of Science & Engineering, Bernal Institute, University of Limerick, Castletroy, Co. Limerick, Ireland

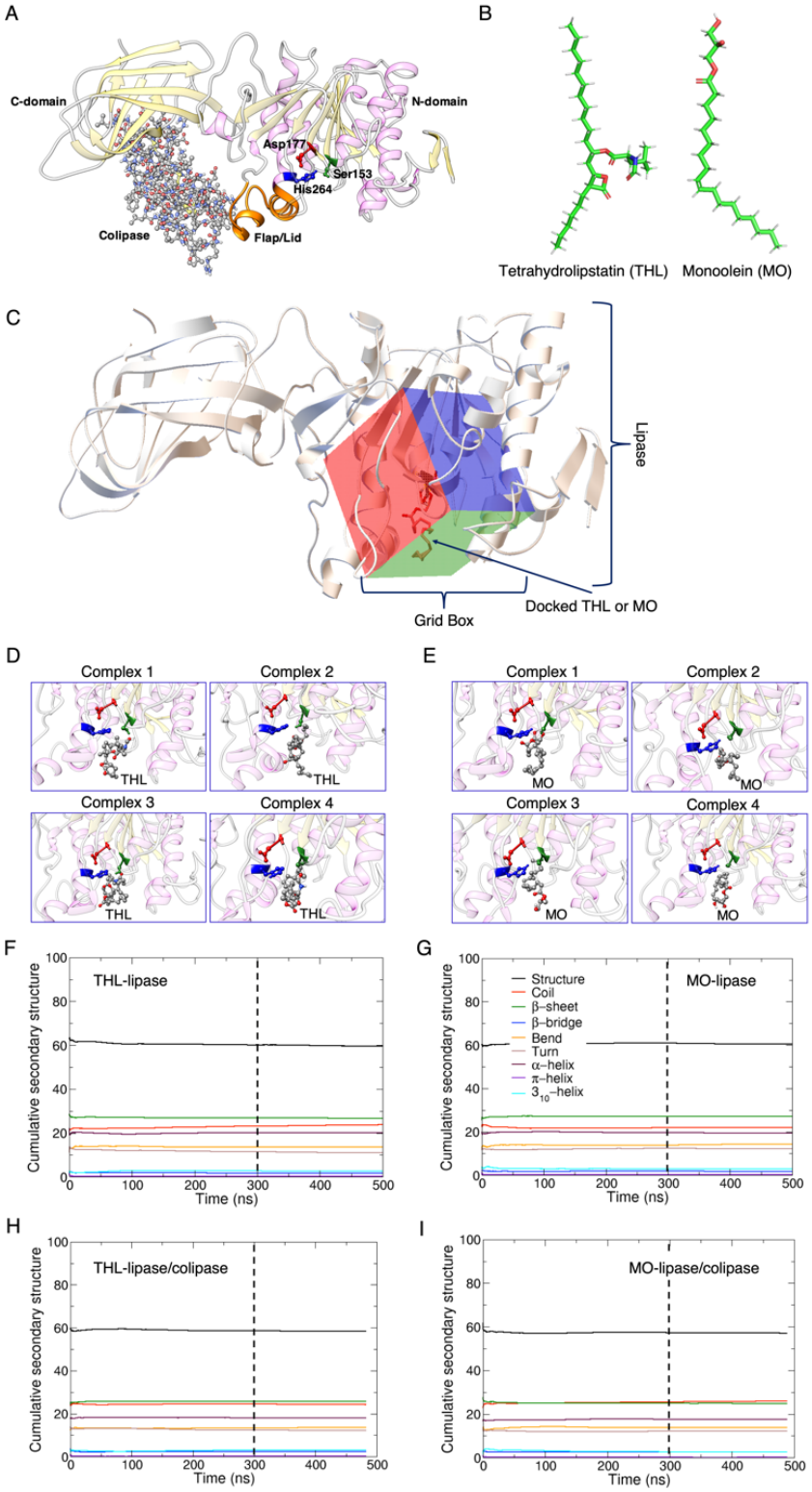

Figure C.1. (A) 2.8 Å resolution crystal structure (PDB code 1ETH [524]) of porcine pancreatic lipase showing one subunit out of the two identical subunits used for computation. The catalytic triad in the active site are shown in ball and stick representation coloured green for Ser153, red for

Asp177 and blue for His264. The colipase is shown in ball and stick which controls the opening and closing of the flap/lid shown in orange (Cys238-Cys262). The secondary structures are represented as violet – a-helix, yellow – b-sheet/strand and grey – random coil. (B) 3D structures of the inhibitor Tetrahydrolipstatin (THL) and MAG lipid substrate Monoolein (MO). (C) Initial setup for docking with AutoDock 4.2 [528] with the grid box of dimensions 50 nm X 50 nm X 50 nm around the catalytic residue Asp153 at the centre. (D) Four best docked THL-lipase complex poses ranked according to their binding energies (see Table C1). The same colour coding for the catalytic triad is followed. (E) Four best docked MO-lipase complex poses (Table C2). (F-I) Time evolution of cumulative average secondary structure content of lipase as a test of convergence for different systems.

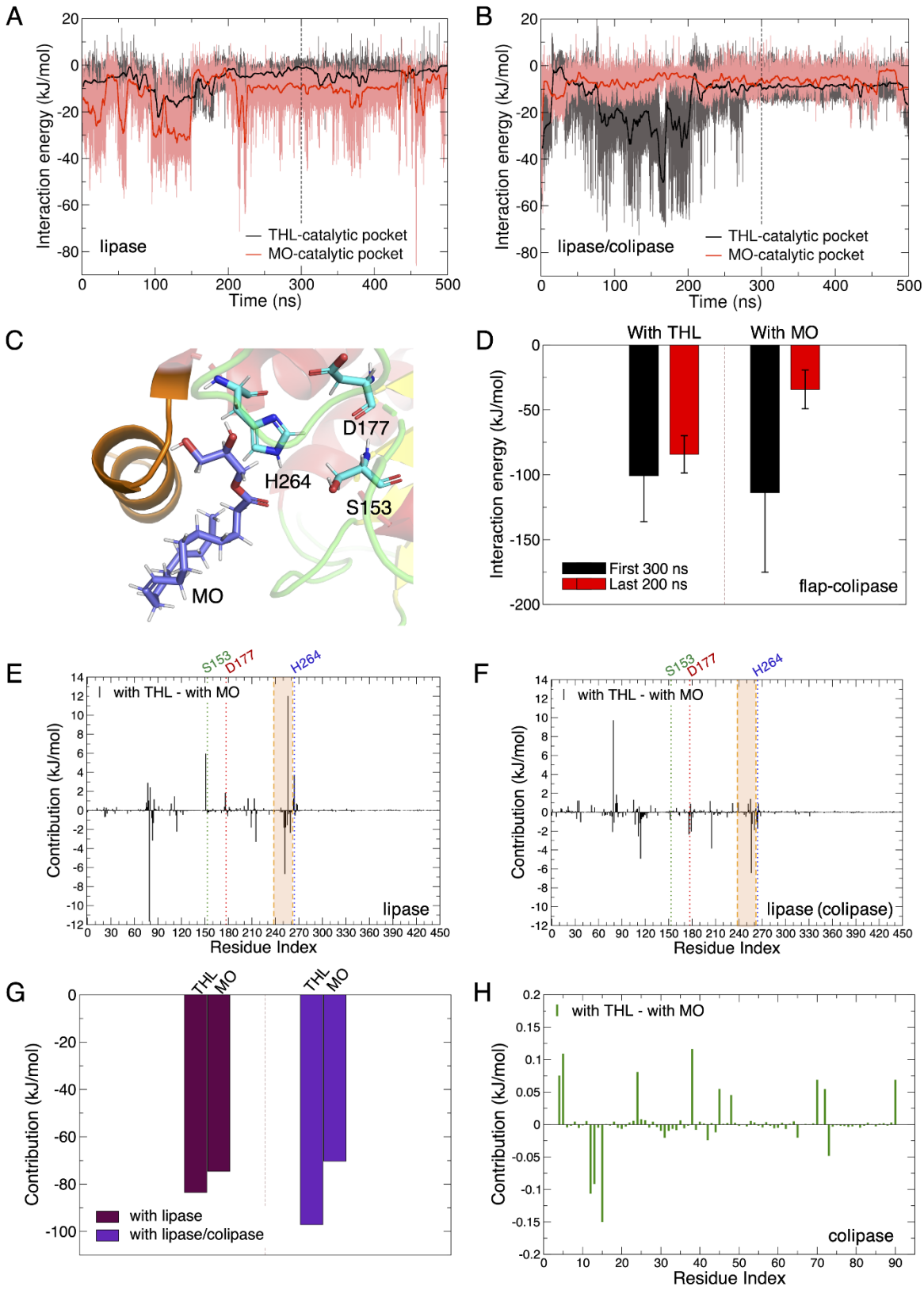

Figure C.2. Time evolution of the total interaction energies (Coulomb electrostatics + vdW) of THL-catalytic pocket and MO-catalytic pocket **(A)** without colipase and **(B)** with colipase. The

running average traces of energies are computed over every 2000 time points. **(C)** Representative snapshot of MO interacting with His264 of the lipase catalytic pocket *via* electrostatic interactions. **(D)** Interaction energies of the mobile flap domain with colipase. Residue-wise energy contributions towards the total binding energy of inhibitor and lipid substrate with lipase. Difference in energy contributions between THL and MO binding from residues of **(E)** lipase without colipase and **(F)** lipase with colipase. The residues forming the catalytic triad are annotated as green for S153, red for D177 and blue for His264, and residues encompassing the mobile flap (Cys238-Cys262) domain is shaded in orange. **(G)** Contributions from THL and MO towards the total binding energy. **(H)** Difference in energy contributions between THL and MO binding from residues in colipase.

Table C.1. Docked complexes of THL-lipase and their corresponding binding energies obtained from docking

Docked Complexes ranked	Binding energy (kJ/mol)
1	**-21.97**
2	-18.12
3	-15.94
4	-11.09

Table C.2. MO-lipase docked complexes and their corresponding binding energies obtained from docking

Docked Complexes ranked	Binding energy (kJ/mol)
1	**-24.48**
2	-21.05
3	-18.16
4	-16.61

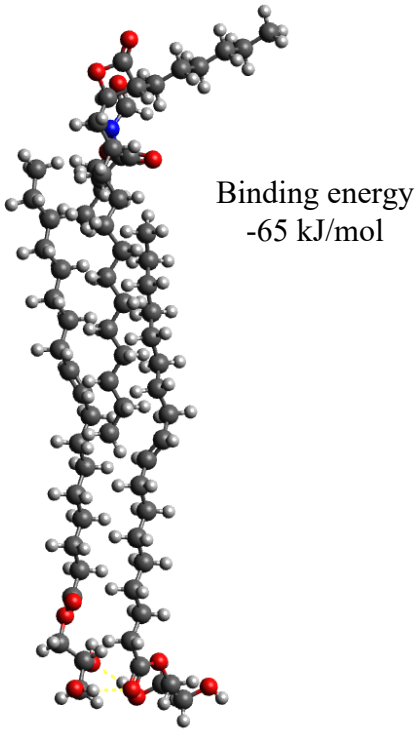

Figure C.3. Optimized geometry of MO-THL-MO. Binding energy in kJ mol-1. Hydrogen – white, carbon – grey, oxygen – red, nitrogen – blue; intra and inter molecular hydrogen bonds are shown with dotted green lines

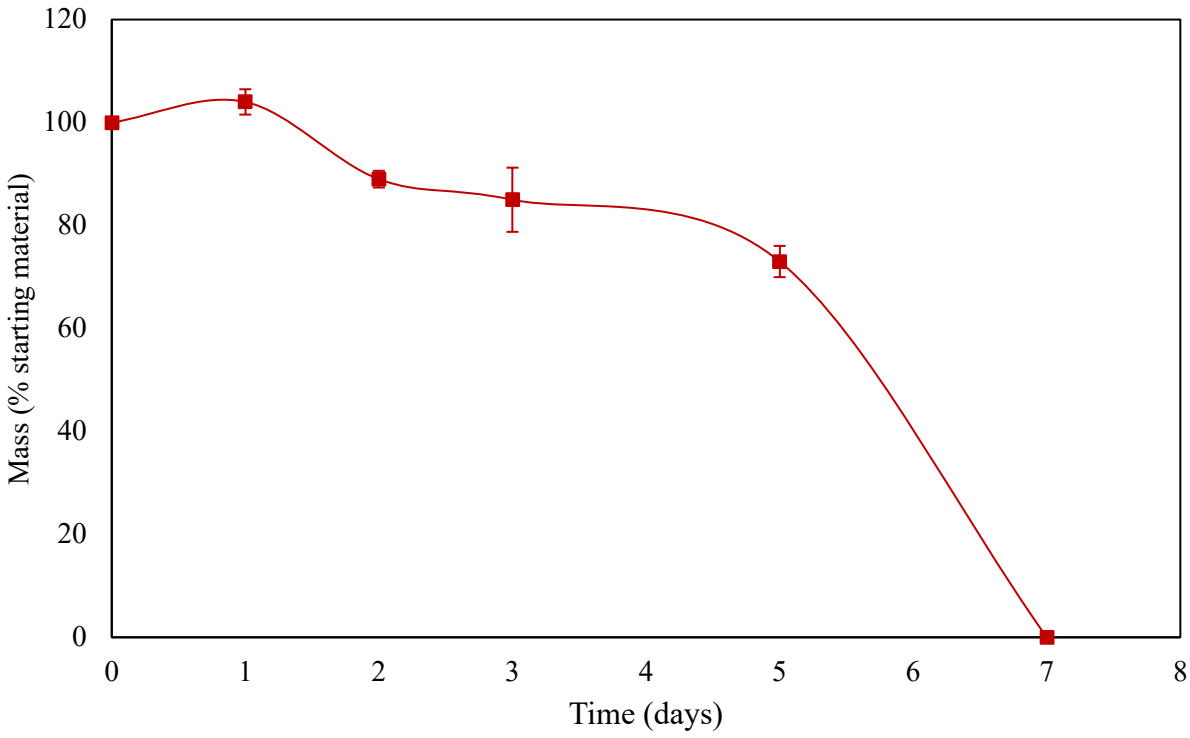

Figure C.4. Degradation behaviour of blank monoolein lipid controlled-release formulations in lipase-containing PBS at 37°C and 200 rpm.

Table C.3. Calculated solubility of PTX in dissolution media through HPLC analysis (N=3)

Dissolution Media	**Calculated Concentration (mg/mL)**
1X PBS pH 7.4	TLTD
1X PBS pH 5.8	TLTD
10X PBS pH 5.8	TLTD
Deionised water	TLTD
Acetonitrile	48.2
2 % HCD (Heptakis(2,6-di-*O*-methyl)-β-cyclodextrin)	71.5
Ethanol	31.5
Methanol	28.3

TLTD is "too low to detect"

Appendix D

Volume 574, August 15, 2020

ISSN 0021-9797

ELSEVIER

Journal of COLLOID AND INTERFACE SCIENCE

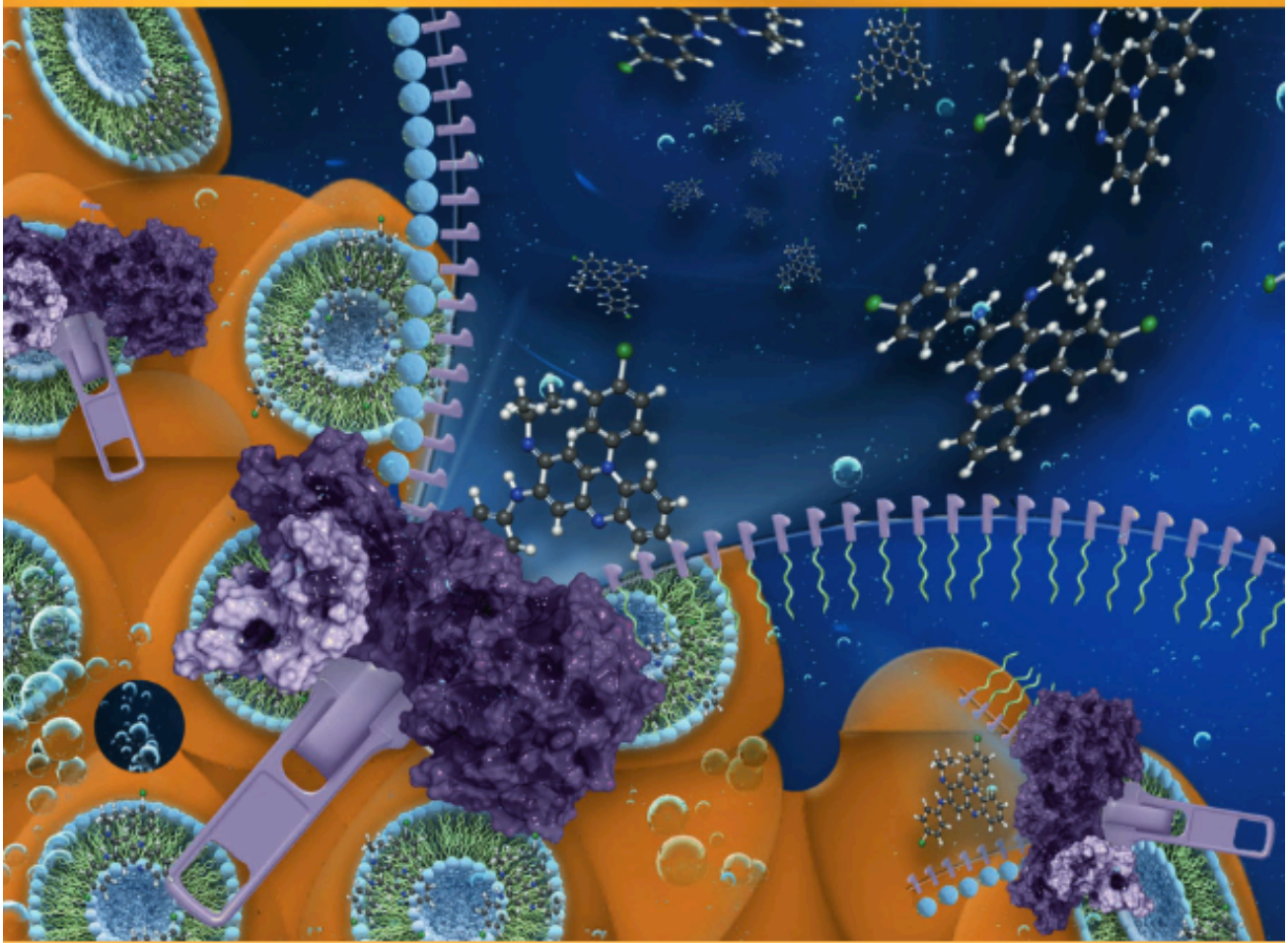

Hydrophobic pharmaceuticals embed within the framework of the lipid cubic phase, and release is limited by a matrix effect. The rate of degradation of the matrix is tuned by addition of an enzyme inhibitor. Here, the release of poorly-soluble clofazimine is shown, driven by modulated enzymatic degradation of the lipid-matrix.

Modulating the release of pharmaceuticals from lipid cubic phases using a lipase inhibitor.

(M. Dully et al., Volume 573 (2020) 176–192).

www.elsevier.com/locate/jcis

Appendix E

diamond

Drug Development

CASE STUDY

Modulating API release with a tuneable lipid carrier

The ability to modulate drug delivery at therapeutically effective doses over a sustained period of time, *in vivo*, is very challenging. In the case of poorly water-soluble drugs this requires a carefully designed matrix to manage and maintain their controlled release.

Lipid cubic phase carriers offer an effective way to transport both small molecules and larger proteins through oral and parenteral routes (those outside of the digestive tract), as well as local delivery via subcutaneous and intramuscular routes. Complex interactions between the drug and the lipid matrix govern the release profile; for hydrophilic drugs, release can be very fast. The carriers can also be compromised by naturally occurring lipolytic enzymes which act to break down the lipid microstructure.

COOK MEDICAL

UNIVERSITY OF LIMERICK
OLLSCOIL LUIMNIGH

The Challenge

A team from the University of Limerick, the University of Bristol and COOK Ireland Ltd have developed an approach in which an enzyme inhibitor is incorporated into the lipid network forming the carrier system to regulate carrier degradation and thereby control the release profile. Polarising optical microscopy has been used to detect the presence of liquid crystalline structures; however, a more advanced analytical technique was necessary to distinguish between different mesophases.

The Solution

The scientific team used small angle X-ray scattering (SAXS) on beamline B21 to analyse the lipid microstructures. A series of experiments were designed to investigate the microstructures formed and how these varied with inhibitor and API loading and to track changes over a period of ageing from 1 hour to 30 days. The high intensity of the synchrotron X-rays allowed rapid measurements, essential for ageing experiments, and enabled the team to establish which mesophases were present.

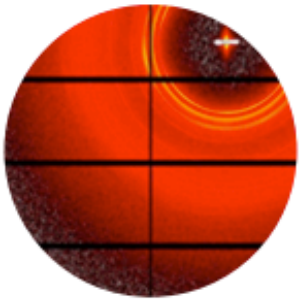

The Benefits

SAXS investigations showed exactly which lipid mesophase(s) were present in each sample. The measurements showed that the addition of inhibitor and API did not negatively affect the microstructure of the matrix. The release kinetics are governed by the particular mesophase formed so a detailed understanding of the microstructure allowed the team to create a tuneable lipid release system.

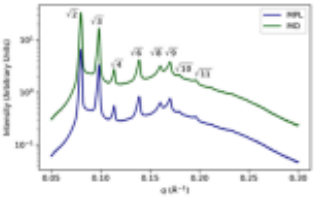

> "Cook Medical New Ventures focuses on transforming patient care through technology generation. In our collaboration with University of Limerick to develop lipid based carrier systems we needed a sensitive measurement technique to characterize the lipid microstructures over time. Gaining access to the world-leading facilities and staff at Diamond Light Source was key in completing this work and advancing our understanding of this technology for future patient treatments."
> David Murray, COOK Medical

> "The high resolution data collected at the B21 beamline helped us to properly characterise our lipid drug delivery formulations which will enable their development as stable delivery vehicles for drug candidates that exhibit challenging solution behaviours. The custom viscous sample holders designed by the Diamond scientists made analysis of our sticky, tacky, lipid formulations straight forward and simple. We are very grateful for the attentive support and assistance from the Diamond staff and scientists." Michele Dully, Dept. Chemical Sciences, Bernal Institute at the University of Limerick

For further information

Diamond Industrial Liaison Team

+44 1235 778797
industry@diamond.ac.uk
diamond.ac.uk/industry
@DiamondILO

CS-DDV-ULIM-062-1